

UCLA

UCLA Electronic Theses and Dissertations

Title

Experimental Study on Lap Splice Nonlinear Fatigue Behavior under Wind-Loading Protocol

Permalink

<https://escholarship.org/uc/item/3gk840h8>

Author

Halim, Samuel Dwima

Publication Date

2024

Peer reviewed|Thesis/dissertation

UNIVERSITY OF CALIFORNIA

Los Angeles

Experimental Study on Lap Splice Nonlinear Fatigue Behavior
under Wind-Loading Protocol

A thesis submitted in partial satisfaction
of the requirements for the degree Master of Science
in Civil Engineering

by

Samuel Dwima Halim

2024

© Copyright by
Samuel Dwima Halim
2024

ABSTRACT OF THE THESIS

Experimental Study on Lap Splice Nonlinear Fatigue Behavior under Wind-Loading Protocol

by

Samuel Dwima Halim

Master of Science in Civil Engineering

University of California, Los Angeles, 2024

Professor John Wright Wallace, Chair

Current US building codes require the Lateral-Force Resisting System (LFRS) of reinforced concrete structures resisting wind loads to be designed for elastic response. Imposing the requirement of elastic behavior may produce an overly conservative design if the lateral system has some inherent ductility and may also have unintended adverse effects on structural performance under seismic loading. Performance-Based Wind Design (PBWD), which would allow limited nonlinear behavior in key components, has been introduced by the American Society of Civil Engineers (ASCE) Structural Engineering Institute (SEI) and the American Concrete Institute (ACI) to address these issues. A critical aspect of PBWD involves an assessment of the strength and detailing requirements needed to allow limited nonlinear demands in critical components. Of particular interest is the behavior at critical sections subjected to high-cycle

fatigue loading, which is common for wind loading. If detailing commonly used for special seismic systems is used, then it is reasonable to assume that behavior under high-cycle fatigue loading will be acceptable, although the importance of stiffness degradation under wind loading requires investigation. The need for improved detailing for nonlinear responses under wind loading, in addition to that required of ordinary or intermediate structural systems, requires additional study.

This thesis focuses on the behavior of lap splices at critical sections in ordinary structural walls under wind loading. A detailed literature review was conducted and it was revealed that the existing information in the literature is insufficient to develop recommendations; therefore, an experimental program was developed. Lap splice behavior was initially investigated by testing T-beams subjected to 4-point loading, which are cheaper to construct and easier to test than walls, followed by testing of C-shaped walls.

The T-beam tests were conducted in two phases: Phase I involved three smaller scale beams with #4 Grade 80 longitudinal reinforcement to provide the information needed to develop the wall test program; Phase II was conducted on two larger T-beams with #8 Grade 80 longitudinal reinforcement to address potential issues associated with the use of larger bar sizes. The beams were designed to reproduce the strain demands expected in the test wall longitudinal reinforcement under a prescribed wind-loading protocol.

Two main variables were considered to evaluate the lap splice behavior: lap splice length and transverse reinforcement spacing in the splice region. The longitudinal bars were spliced according to ACI 318-19 provisions. For the initial small beam tests, splice failure was observed prior to reaching bar yield. Therefore, in subsequent tests, a multiplier of 1.25 was used to account for strain hardening behavior of the longitudinal reinforcement; this approach is consistent with provisions for special walls (ACI 318-19 Chapter 18.10.2.3). The small beam tests, with tie

spacings of 2, 3, and 6 in., revealed that tight spacing (2 in.) was required to resist the entire wind loading protocol without strength loss. To enable comparisons between the small and large beam tests, a parameter a_{sp} , which is the ratio of the total confining force provided by the transverse reinforcements along the splice length to the total yield strength of the spliced bars, was used. The performance of the small and large beams with comparable a_{sp} factors was similar, indicating no bar size effect between #4 and #8 spliced longitudinal reinforcement. For the given loading protocol, minimum a_{sp} values of 1.25 and 2.0 are recommended for lap splices if strain ductility demands are ≤ 6 or ≥ 10 , respectively.

The thesis of Samuel Dwima Halim is approved.

Henry V. Burton

Thomas A. Sabol

Sofia Gavridou

John W. Wallace, Committee Chair

University of California, Los Angeles

2024

Pa, Ma, and Bram,

Thank you for your abundant prayers and
reminders of what is truly important in life.

Love you guys always.



Table of Contents

Abstract of the Thesis	ii
Table of Contents	vii
List of Tables.....	x
List of Figures	xi
Acknowledgments.....	xviii
1. Introduction.....	1
1.1. Background.....	1
1.2. Objectives	2
1.3. Thesis Organization	3
2. Literature Review.....	4
2.1. Lap Splice Failure and Governing Factors	4
2.2. Fatigue Failure	6
2.2.1. Fatigue Behavior of Plain Concrete.....	7
2.2.2. Fatigue Behavior of Steel Reinforcement.....	8
2.3. Lap Splice Experiments.....	10
2.3.1. Monotonic and Elastic Unidirectional Cyclic Experiments	10
2.3.2. Inelastic Reverse Cyclic Experiments	18
2.4. Transverse Reinforcement Requirements in Lap Splice	24
2.5. Summary of Lap Splice Experiments.....	25
2.5.1. Elastic Range of Loading.....	25
2.5.2. Inelastic Range of Loading	26
3. Experimental Program	28

3.1.	Naming Convention.....	30
3.2.	Design of Test Specimens.....	30
3.3.	Loading Protocol	35
3.4.	Test Setup	38
3.5.	Material Properties	41
	3.5.1. Concrete.....	41
	3.5.2. Steel Reinforcements	44
3.6.	Fabrication of Test Specimens.....	46
3.7.	Instrumentation.....	49
	3.7.1. Average Concrete Longitudinal Strains: LVDTs	49
	3.7.2. Beam Vertical Displacements: Wire Potentiometers (WPs)	50
	3.7.3. Beam Axial Elongation: Wire Potentiometers (WPs).....	51
	3.7.4. Digital Image Correlation (DIC).....	52
	3.7.5. Additional Instrumentations/Documentations	52
4.	Results and Discussions	54
4.1.	Observed Damage and Cracking	56
4.2.	Load-Deformation Responses	66
4.3.	Moment-Curvature Responses	70
4.4.	Axial Growth	77
4.5.	Digital Image Correlation (DIC) Results	78
5.	Comparison of Beam Specimens	81
5.1.	Rebar Diameter Size Factor in Lap Splice	81
5.2.	Recommendation of Transverse Reinforcement based on Confining Force	82

6.	Summary and Conclusions	84
Appendix A.	Strength Calculation	86
Appendix B.	Concrete Mix Design.....	92
Appendix C.	Steel Reinforcements Certified Mill Test Report	98
Appendix D.	LVDTs and Wire Potentiometers Readings	105
Appendix E.	Digital Image Correlation (DIC) Results	123
References.....	157

List of Tables

Table 2-1: Zaccaruk's stress range variation in the specimens (Zaccaruk, 1990).....	14
Table 2-2: Comparison between repeated and reversed loading	20
Table 2-3: Series 1 and Series 2 comparison (MacKay et al., 1989)	23
Table 2-4: Lap splice parameter comparison for elastic tests	25
Table 2-5: Lap splice parameter comparison for inelastic tests	27
Table 3-1: Small and large beam properties comparison	34
Table 3-2: Applied strain demands in walls and small beams	36
Table 3-3: Strain demands comparison between small and large beams	37
Table 3-4: Concrete compressive strength results from supplier.....	42
Table 3-5: Small beam concrete compressive strength results	42
Table 3-6: Large beam concrete compressive strength results	43
Table 3-7: Steel reinforcement properties in the beam specimens	44
Table 3-8: Trilinear fit of rebar stress-strain curve	44
Table 3-9: Summary of #4 and #8 Grade 80 rebar tests	45
Table 4-1: Sectional strength properties - analytical v. experiment.....	54
Table 4-2: Experiments summary and results for SB-S6-16	54
Table 4-3: Experiments summary and results for SB-S3-20	55
Table 4-4: Experiments summary and results for SB-S2-20	55
Table 4-5: Experiments summary and results for LB-S7.5-50	55
Table 4-6: Experiments summary and results for LB-S5-50	56
Table 5-1: a_{sp} values of beam test specimens.....	82

List of Figures

Figure 2-1: Idealized bond load-transfer mechanism (ACI 408.2R, 2012)	4
Figure 2-2: Pullout failure diagram (ACI 408.2R, 2012)	5
Figure 2-3: Splitting failure diagram (Eligehausen et al., 1983)	5
Figure 2-4: S-N diagram example (Hibbeler, 2017 Fig.3-28)	6
Figure 2-5: Fatigue loading spectra in structures (Khatri, 2016).....	7
Figure 2-6: Fatigue strength of plain concrete (ACI 215R, 1974).....	7
Figure 2-7: Steel reinforcement fatigue fracture (ACI 215R, 1974)	8
Figure 2-8: S_r -N curve of steel reinforcement (Moss, 1980)	9
Figure 2-9: Typical S-N curve for steel rebar (ACI 215R, 1974).....	9
Figure 2-10: Tepfers's proposed spiral reinforcement at lap splice (Tepfers, 1973)	11
Figure 2-11: Bond stresses distribution at failure (Tepfers, 1973).....	11
Figure 2-12: Zaccaruk's beam specimens configuration (Zaccaruk, 1990).....	13
Figure 2-13: Afseth's beam specimens configuration (Afseth, 1993)	15
Figure 2-14: S-N curve of Afseth's experiments (Afseth, 1993).....	16
Figure 2-15: Alyousef's beam specimen configuration (Alyousef, 2016).....	17
Figure 2-16: Alyousef's unwrapped specimen's S-N curve	18
Figure 2-17: Beam specimens sizes in mm (Lukose et al., 1982)	19
Figure 2-18: Splices in constant moment v. in shear region (Lukose et al., 1982).....	19
Figure 2-19: Beam specimens detail (Sparling & Rezansoff, 1986)	21
Figure 2-20: Stress-strain curves of steel reinforcement in MacKay's experiment (MacKay et al., 1989)	22
Figure 2-21: MacKay's beam specimens and loading diagram (MacKay et al., 1989).....	23

Figure 2-22: Envelope S-N curves for elastic tests.....	26
Figure 3-1: Ordinary wall cross-section (Unal et al., 2024)	28
Figure 3-2: Ordinary wall elevation view (Unal et al., 2024).....	29
Figure 3-3: Naming convention of beam specimens	30
Figure 3-4: Small beam tests: (a) elevation view; (b) cross section (Unal et al., 2024).....	31
Figure 3-5: Elevation view of the beam specimens	33
Figure 3-6: Cross-section of the beam specimens	33
Figure 3-7: Loading protocol for ordinary wall (Unal et al., 2024).....	35
Figure 3-8: Loading protocol for small beams (Unal et al., 2024)	37
Figure 3-9: Loading protocol for large beams	38
Figure 3-10: Small beam test setup schematic (not drawn to scale).....	38
Figure 3-11: Large beam test setup schematic (not drawn to scale).....	39
Figure 3-12: Small beam test setup photo.....	39
Figure 3-13: Large beam test setup photo.....	40
Figure 3-14: (a) Pin and (b) Roller support mechanism	41
Figure 3-15: Unconfined concrete stress-strain curve: (a) small beams; (b) large beams.....	43
Figure 3-16: Rebar stress-strain relations: (a) #4 Grade 80; (b) #8 Grade 80	45
Figure 3-17: Rebar cage assembly of large beam specimens	46
Figure 3-18: Beam construction: (a) rebar chairs and threaded rods in large beams; (b) concrete placement and pouring of large beams; (c) small beam rebar cages in formwork	47
Figure 3-19: Formwork removal of large beams	48
Figure 3-20: Finished large beam specimens with paint for DIC	48
Figure 3-21: Small beam LVDTs and WPs locations	49

Figure 3-22: Large beam LVDTs and WPs locations	50
Figure 3-23: (a) LVDTs and (b) Attachment to the beam specimens	50
Figure 3-24: Vertical WPs attachment to the beam specimens	51
Figure 3-25: Horizontal WPs attachment to the beam specimens	51
Figure 3-26: Digital Image Correlation (DIC): (a) speckle pattern; (b) camera field of view	52
Figure 3-27: Force and displacement measurement: (a) small beam test setup; (b) large beam test setup	53
Figure 4-1: Horizontal cracks in the splice region of SB-S6-16.....	57
Figure 4-2: SB-S6-16 at the end of test	57
Figure 4-3: Slip at the end of spliced bars (SB-S6-16).....	58
Figure 4-4: Horizontal cracks in the splice region of SB-S3-20.....	58
Figure 4-5: Slip at the end of splice bars (SB-S3-20).....	59
Figure 4-6: SB-S3-20 at the end of the test.....	59
Figure 4-7: SB-S2-20 at the end of the wind-loading protocol	60
Figure 4-8: Minor horizontal cracks at ends of splice (SB-S2-20).....	60
Figure 4-9: Large vertical cracks at splice ends of SB-S2-20	61
Figure 4-10: Bar fracture failure on SB-S2-20	61
Figure 4-11: SB-S2-20 at the end of the test.....	61
Figure 4-12: LB-S7.5-50 splice failure @4 th cycle of 2.5 Θ_y	62
Figure 4-13: LB-S7.5-50 failure detail	62
Figure 4-14: LB-S7.5-50 at the end of each loading stage (WLP)	63
Figure 4-15: LB-S5-50 at the end of the wind-loading protocol	64
Figure 4-16: LB-S5-50 at the end of the monotonic push	64

Figure 4-17: LB-S5-50 at the end of each loading stage (WLP)	65
Figure 4-18: Load-Deformation responses of small beam test specimens	66
Figure 4-19: Load-Deformation responses of large beam test specimens	68
Figure 4-20: Custom link roller support issue	69
Figure 4-21: SB-S6-16 moment-curvature for each LVDT pair	71
Figure 4-22: SB-S3-20 moment-curvature for each LVDT pair	72
Figure 4-23: SB-S2-20 moment-curvature for each LVDT pair	73
Figure 4-24: LB-S7.5-50 moment-curvature for each LVDT pair	74
Figure 4-25: LB-S5-50 moment-curvature for each LVDT pair	75
Figure 4-26: LB-S5-50 crack detail (LVDT: Pair 3 and 4)	76
Figure 4-27: Axial growth on large beam test specimens	77
Figure 4-28: Y-Y surface strain at 0.75 wall M_{pr} demand (LB-S7.5-50)	78
Figure 4-29: LB-S7.5-50 Surface strain and crack pattern from DIC (LB-S7.5-50)	79
Figure 4-30: LB-S5-50 Surface strain and crack pattern from DIC (LB-S5-50)	80
Figure 5-1: Small versus large beams normalized load-displacement curve	81
Figure 5-2: a_{sp} and μ_{ϵ} correlation for small and large beams	83
Figure A-1: Small beam positive bending analytical moment-curvature	86
Figure A-2: Small beam negative bending analytical moment-curvature	86
Figure A-3: Large beam positive bending analytical moment-curvature	87
Figure A-4: Large beam negative bending analytical moment-curvature	87
Figure D-1: 01 and 02 LVDT readings (SB-S6-16)	105
Figure D-2: 03 and 03R LVDT readings (SB-S6-16)	106
Figure D-3: 04 and 05 LVDT readings (SB-S6-16)	107

Figure D-4: Wire potentiometers readings (SB-S6-16)	108
Figure D-5: 01 and 02 LVDT readings (SB-S3-20).....	109
Figure D-6: 03 and 03R LVDT readings (SB-S3-20).....	110
Figure D-7: 04 and 05 LVDT readings (SB-S3-20).....	111
Figure D-8: Wire potentiometers readings (SB-S3-20)	112
Figure D-9: 01 and 02 LVDT readings (SB-S2-20).....	113
Figure D-10: 03 and 03R LVDT readings (SB-S3-20).....	114
Figure D-11: 04 and 05 LVDT readings (SB-S2-20).....	115
Figure D-12: Wire potentiometers readings (SB-S2-20)	116
Figure D-13: West side LVTD readings (LB-S7.5-50).....	117
Figure D-14: East side LVTD readings (LB-S7.5-50).....	118
Figure D-15: Wire potentiometers readings (LB-S7.5-50).....	119
Figure D-16: West side LVTD readings (LB-S5-50).....	120
Figure D-17: East side LVTD readings (LB-S5-50).....	121
Figure D-18: Wire potentiometers readings (LB-S5-50)	122
Figure E-1: (LB-S7.5-50) Stage 1-100 th cycle @0.18M _{pr} ⁺ DIC results	123
Figure E-2: (LB-S7.5-50) Stage 1-100 th cycle @0.32M _{pr} ⁻ DIC results	124
Figure E-3: (LB-S7.5-50) Stage 1-200 th cycle @0.18M _{pr} ⁺ DIC results	125
Figure E-4: (LB-S7.5-50) Stage 1-200 th cycle @0.32M _{pr} ⁻ DIC results	126
Figure E-5: (LB-S7.5-50) Stage 1-500 th cycle @0.18M _{pr} ⁺ DIC results	127
Figure E-6: (LB-S7.5-50) Stage 1-500 th cycle @0.32M _{pr} ⁻ DIC results	128
Figure E-7: (LB-S7.5-50) Stage 2-40 th cycle @0.79M _{pr} ⁺ DIC results	129
Figure E-8: (LB-S7.5-50) Stage 2-40 th cycle @0.63M _{pr} ⁻ DIC results	130

Figure E-9: (LB-S7.5-50) Stage 3-10 th cycle @1.38 δ_y^+ DIC results	131
Figure E-10: (LB-S7.5-50) Stage 3-10 th cycle @0.63M _{pr} ⁻ DIC results	132
Figure E-11: (LB-S7.5-50) Stage 4-6 th cycle @1.77 δ_y^+ DIC results	133
Figure E-12: (LB-S7.5-50) Stage 4-6 th cycle @0.63M _{pr} ⁻ DIC results	134
Figure E-13: (LB-S7.5-50) Stage 5-4 th cycle @2.55 δ_y^+ DIC results	135
Figure E-14: (LB-S7.5-50) Stage 5-4 th cycle @0.63M _{pr} ⁻ DIC results	136
Figure E-15: (LB-S7.5-50) Stage 6-4 th cycle @3.81 δ_y^+ DIC results	137
Figure E-16: (LB-S7.5-50) Stage 6-4 th cycle @0.63M _{pr} ⁻ DIC results	138
Figure E-17: (LB-S5-50) Stage 1-100 th cycle @0.18M _{pr} ⁺ DIC results.....	139
Figure E-18: (LB-S5-50) Stage 1-100 th cycle @0.32M _{pr} ⁻ DIC results	140
Figure E-19: (LB-S5-50) Stage 1-200 th cycle @0.18M _{pr} ⁺ DIC results.....	141
Figure E-20: (LB-S5-50) Stage 1-200 th cycle @0.32M _{pr} ⁻ DIC results	142
Figure E-21: (LB-S5-50) Stage 1-500 th cycle @0.18M _{pr} ⁺ DIC results.....	143
Figure E-22: (LB-S5-50) Stage 1-500 th cycle @0.32M _{pr} ⁻ DIC results	144
Figure E-23: (LB-S5-50) Stage 2-75 th cycle @0.79M _{pr} ⁺ DIC results.....	145
Figure E-24: (LB-S5-50) Stage 2-75 th cycle @0.63M _{pr} ⁻ DIC results	146
Figure E-25: (LB-S5-50) Stage 3-10 th cycle @1.38 δ_y^+ DIC results	147
Figure E-26: (LB-S5-50) Stage 3-10 th cycle @0.63M _{pr} ⁻ DIC results	148
Figure E-27: (LB-S5-50) Stage 4-6 th cycle @1.77 δ_y^+ DIC results	149
Figure E-28: (LB-S5-50) Stage 4-6 th cycle @0.63M _{pr} ⁻ DIC results	150
Figure E-29: (LB-S5-50) Stage 5-4 th cycle @2.55 δ_y^+ DIC results	151
Figure E-30: (LB-S5-50) Stage 5-4 th cycle @0.63M _{pr} ⁻ DIC results	152
Figure E-31: (LB-S5-50) Stage 6-4 th cycle @3.81 δ_y^+ DIC results	153

Figure E-32: (LB-S5-50) Stage 6-4th cycle @0.63M_{pr}⁻ DIC results 154

Figure E-33: (LB-S5-50) Stage 7-2nd cycle @4.71δ_y⁺ DIC results 155

Figure E-34: (LB-S5-50) Stage 7-2nd cycle @0.63M_{pr}⁻ DIC results..... 156

Acknowledgments

I would like to express my greatest gratitude to Professor John W. Wallace, my academic advisor, for the invaluable insights and experience he has shared throughout my time at UCLA. His knowledge, trust, and support have developed a creative and thorough mindset for me to become a better engineer and a better individual.

I would also like to thank Professor Henry V. Burton, Professor Thomas A. Sabol, and Dr. Sofia Gavridou for their commitment to serve on my thesis committee and for their valuable comments. Moreover, I thank the faculty and staff of the Department of Civil and Environmental Engineering at UCLA, especially to Student Affairs Officers, Mimi Baik, and Management Services Officer, Stacey Fong, for providing information, helping me, and keeping me on schedule during my time at UCLA.

This research project would not be possible without the funding contribution of the American Concrete Institute (ACI), Charles Pankow, and Magnusson Klemencic Associates (MKA) Foundations. The donation of materials and workforce from Pacific Steel Group (PSG) and Webcor are also deeply appreciated.

I am grateful to have Mehmet Emre Unal and Santiago Rodriguez Sanchez as my friends and mentors during the research project. Their presence, knowledge, and humor have made working in the laboratory enjoyable. I am also grateful for Dr. Eric Ahlberg for his guidance and willingness to introduce me to the laboratory working environment, also for his expertise in developing the test setup and in setting up the sensors and the data acquisition.

My master's study journey has been delightful through the presence of the friends I made along the way. I thank the students I assisted as a Teaching Assistant for their passion and desire to learn which encouraged me to deepen my understanding in the field of structural engineering. I also thank my friends and cohorts in Los Angeles and Indonesia who have always reminded me to have some fun in life.

Finally, I am forever blessed for the chance of continuing my study with the support from the Republic of Indonesia through the Indonesia Endowment Fund for Education / *Lembaga Pengelola Dana Pendidikan* (LPDP) which relieved my parents of any financial responsibility for my study. It is time to show Indonesia that their trust is in good hands.

“If we have a strong desire from within our hearts, then the entire universe will work together to make it happen” – Ir. Soekarno



1. Introduction

1.1. Background

Reinforced concrete (RC) structures are commonly used as lateral force-resisting systems (LFRS) to resist earthquake and wind loads in the U.S. and around the world. In buildings taller than 8 to 10 stories, the use of RC walls is common. Since steel reinforcement is produced in finite lengths, lap splices are required to achieve strength continuity, i.e., force transfer from one bar to another. Provisions exist in ACI 318 that define required lap splice lengths and detailing requirements (transverse reinforcement) to achieve continuity for gravity and wind loads for elastic behavior, as well as for seismic loading where yield of spliced reinforcement at critical sections is expected. However, similar guidance does not exist for lap splices in walls subjected to minor nonlinear demands on wind loading.

In this thesis, lap splice behavior at critical (yielding) sections of RC walls is studied. For seismic design, wall lap splices are designed according to Section 18.10 of ACI 318 for special structural walls. Section 18.10.2 includes provisions that require longer lap splice lengths at yielding critical sections, closely spaced transverse reinforcement for boundary longitudinal reinforcement, and limits on where splices can be located. However, other than the requirements for Ordinary Walls in ACI 318-19 Chapter 11, no additional limits on lap splices for walls designed to resist wind loads exist. Observed performance of existing buildings, designed to remain elastic under the design wind loads, justifies this approach.

Currently, the approaches used for seismic design and wind design are different; that is, seismic design is based on expected nonlinear behavior whereas wind design is based on linear behavior. Seismic design is based on using R-factors that reduce design loads from expected mean elastic demands; therefore, inelastic behavior is expected, and the design provisions address this

expectation. However, wind design still relies on proportioning the structural components such that linear responses are expected (American Society of Civil Engineers, 2021). The primary reason for this limitation for wind loading is due to the lack of information related to the lateral system responses beyond yield. Imposing the requirement of elastic behavior may produce an overly conservative design if the lateral system has some inherent ductility and may also have unintended adverse effects on structural performance under seismic loading. (Abdullah et al., 2020; Unal et al., 2024).

Performance-Based Wind Design (PBWD) has been proposed to address these issues. The primary reference documents for PBWD are published by ASCE (American Society of Civil Engineers, 2019), NIST (Scott, 2023), and ACI (ACI 318-25, Appendix W). The current approach for PBWD is to allow limited nonlinearity at specified critical sections of the LFRS. In the case of core walls, limited yielding is expected to occur in coupling beams and in wall piers. Experimental studies are needed to assess whether current strength and detailing requirements are adequate to achieve the expected nonlinear demands and, if not, what changes are needed. As noted previously, this study focuses on addressing this need for ordinary structural wall systems; prior studies have addressed these issues for coupling beams.

1.2. Objectives

The primary objective of this study is to support the implementation of Performance-Based Wind Design by conducting an experimental study to investigate the nonlinear fatigue behavior of lap spliced wall longitudinal reinforcement and to develop strength and detailing provisions that achieve a prescribed level of ductility without strength loss. The primary variables of the test program are the lap splice length, detailing (amount and spacing of transverse reinforcement), and lap splice bar diameter.

1.3. Thesis Organization

This thesis is organized into six chapters. The first chapter provides a brief introduction and background, as well as the research objectives and the thesis organization. The second chapter includes a review of relevant research. The third chapter details the experimental program of the small and large beam tests. The fourth chapter includes results of the small and large beam experiments. The fifth chapter includes comparisons of the experimental results with predicted results and previously conducted tests. Lastly, the sixth chapter summarizes the research and provides important conclusions and recommendations. Possible future work is also included.

In addition to the six chapters, five appendices are also included which contain: (1) important strength calculations, (2) concrete material properties, (3) reinforcement properties, (4) results from LVDTs and wire potentiometers, and (5) results from Digital Image Correlation (DIC).

2. Literature Review

2.1. Lap Splice Failure and Governing Factors

Lap splices, as discussed previously, are intended to provide stress transfer from one bar to another bar. The load-transfer mechanism over the lap length, for both tension or compression stresses, is needed. In reinforced concrete structures, bond between steel reinforcement and concrete enables load-transfer. There are three idealized components for bond force transfer mechanisms: 1) mechanical adhesion (V_a), 2) mechanical anchorage due to rib bearing (V_b), and 3) frictional resistance (V_c) as visualized in Figure 2-1. Adhesion and friction forces are effective at lower load levels; whereas, rib bearing is the dominant load-transfer mechanism at higher load levels (ACI 408.2R, 2012).

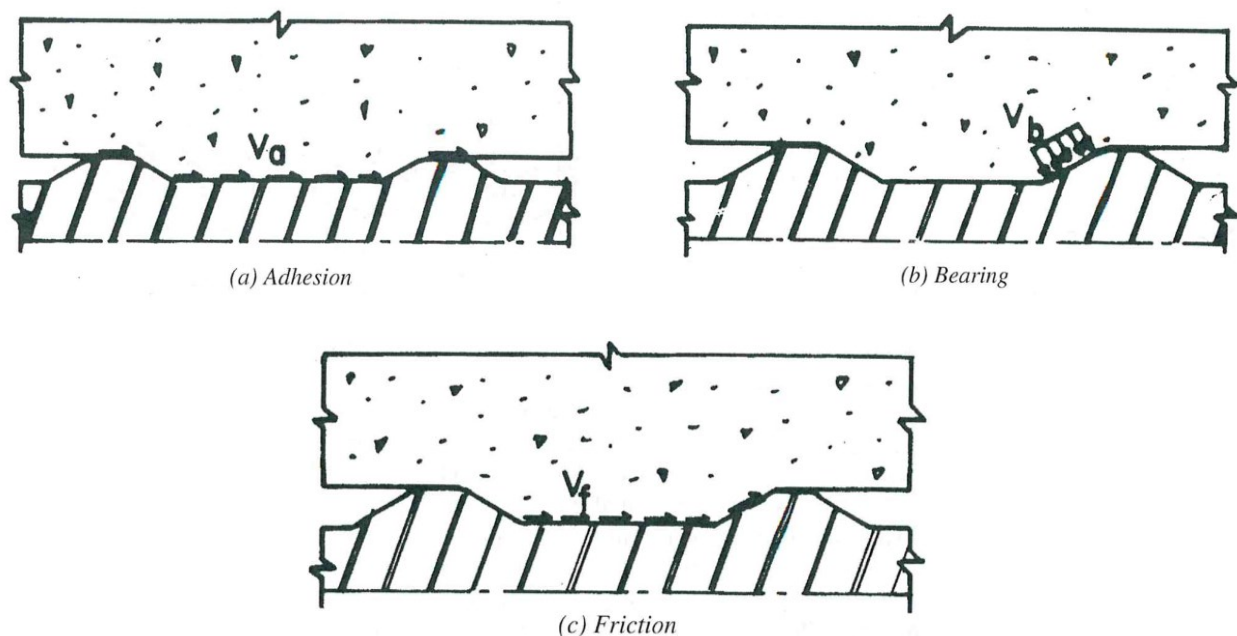


Figure 2-1: Idealized bond load-transfer mechanism (ACI 408.2R, 2012)

Lap splices have different failure modes depending on the loading type. Under monotonic and low-cycle loading, the typical failure modes are pullout and splitting of the concrete cover. The pullout failure, depicted in Figure 2-2, is due to the shearing of the concrete where the concrete

cover or transverse reinforcement is sufficient to prevent splitting. On the other hand, splitting failure occurs due to radial tensile stresses that create cracks that propagate to the concrete surfaces (See Figure 2-3). Under high-cycle loading, these failure modes can still occur; however, fatigue failure may also be present.

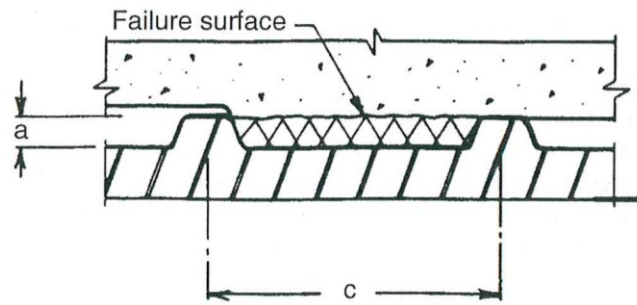


Figure 2-2: Pullout failure diagram (ACI 408.2R, 2012)

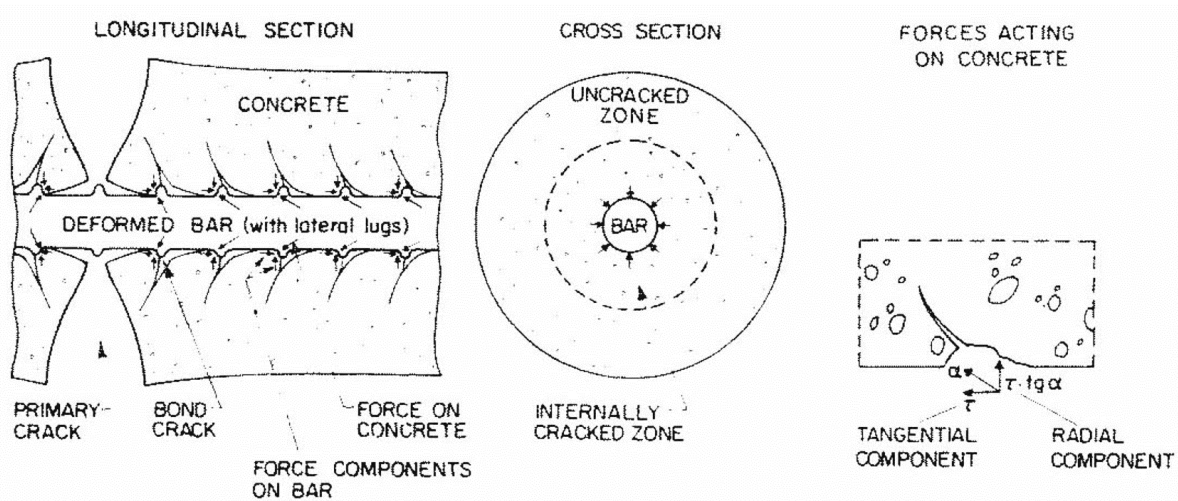


Figure 2-3: Splitting failure diagram (Eligehausen et al., 1983)

There are several factors that affect the behavior of lap splices, including the amount of transverse reinforcements providing confinement to the splice, the type (monotonic, repeated, reversed cyclic) and rate of loading, the magnitude and range of the applied strain or stress, moment gradient along the splice length, concrete cover over and the distance between spliced rebars, and concrete strength. Other factors are correlated to the construction of the component, e.g., casting position, concrete vibration, coatings, and corrosion (ACI 408.2R, 2012).

2.2. Fatigue Failure

Fatigue is a mechanism induced by repetitive loadings (tensile and/or compressive stresses), either reverse cyclic or unidirectional, that creates an initial crack at the weak area of a material due to microscopic imperfections which propagates as additional cycles are applied. The increasing crack size of the material reduces the cross-sectional area, which leads to sudden fracture; this mechanism triggers a brittle failure even for ductile material (Hibbeler, 2017).

In terms of the magnitude of loading, most materials will fail under fatigue at load levels less than the yield strength of the material. However, some materials have a fatigue or endurance limit, defined as the stress level that a material can resist without experiencing fatigue failure. This limit is defined using tests with a specified stress and number of cycles where the test results can be plotted as a graph with stress (S) as the Y-axis and number of cycles (N) as the X-axis, or S-N diagram (See Figure 2-4).

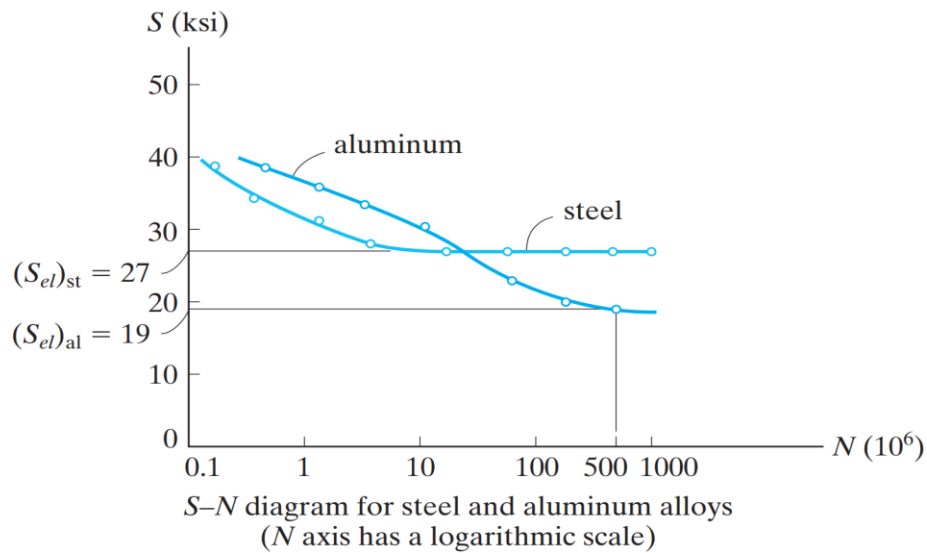


Figure 2-4: S-N diagram example (Hibbeler, 2017 Fig.3-28)

In Figure 2-4, the endurance limit (S_{el}) is shown with a horizontal line on the Y-axis, and the stresses below this limit are commonly assumed to not induce any fatigue failure. Some materials have a distinct endurance limit; however, other materials may not.

Fatigue loading is also classified based on the number of cycles performed. Figure 2-5 shows the spectra of fatigue loading that is commonly experienced in structures (Khatri, 2016) where it is noted that the load intensity decreases as the number of cycles increases.

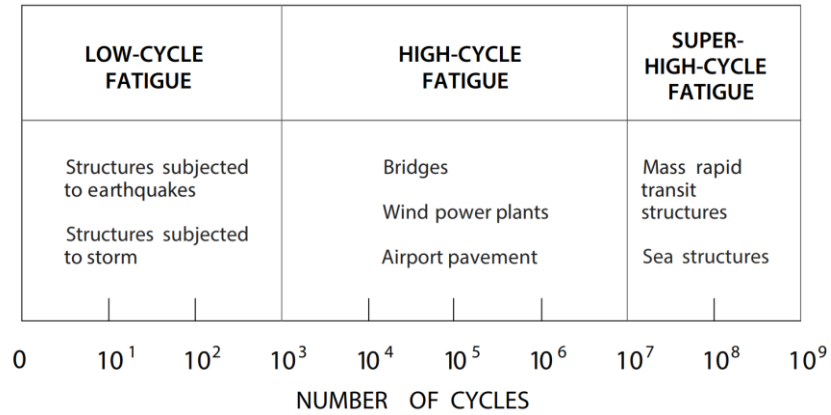


Figure 2-5: Fatigue loading spectra in structures (Khatri, 2016)

2.2.1. Fatigue Behavior of Plain Concrete

Concrete commonly fails in fatigue due to propagation of microcracks at a load level lower than the static strength. A plain concrete four-point bending test is commonly performed to develop typical S-N curves for plain concrete (Figure 2-6 (ACI 215R, 1974)).

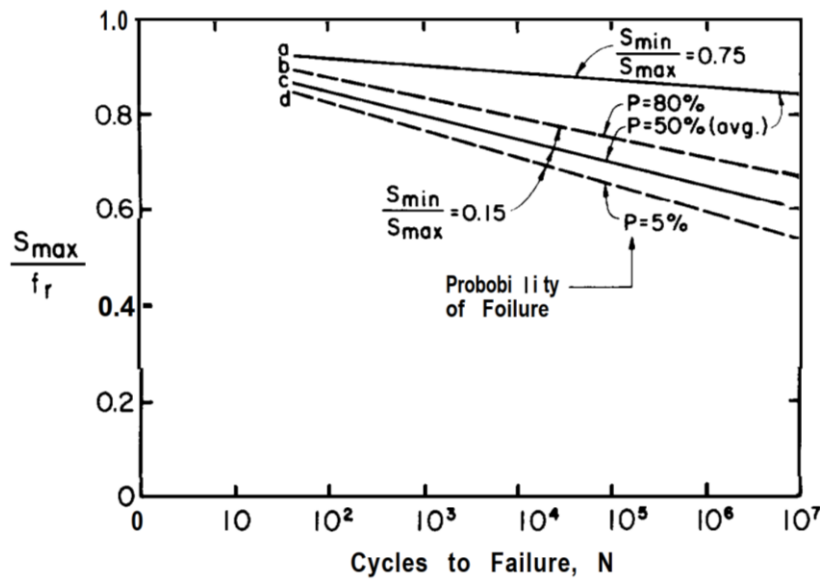


Figure 2-6: Fatigue strength of plain concrete (ACI 215R, 1974)

In Figure 2-6, S_{max} is the maximum stress applied, S_{min} is the minimum stress applied, f_r is the concrete modulus of rupture, and P is the probability of failure. Curve “a” represents specimens with an applied loading ratio of 0.75, and curve “c” is for specimens with a loading ratio of 0.15. Both curves are for a 50% probability of failure. Curve “b” and “d” were developed for 80% and 5% probability of failure, respectively, for specimens with S_{min}/S_{max} values of 0.15. A general trend, observed for all tests, is decreasing maximum stress with increasing number of cycles. However, a larger stress range (curve “c”) results in a decrease of the maximum stress for the same number of cycles.

2.2.2. Fatigue Behavior of Steel Reinforcement

Failure of steel reinforcement in fatigue is depicted in Figure 2-7 where the smooth surface is the fatigue crack that propagated until the reduced cross-sectional area of the steel is insufficient to resist the applied stress. Subsequently, brittle fracture is observed, producing the rough fracture surface.

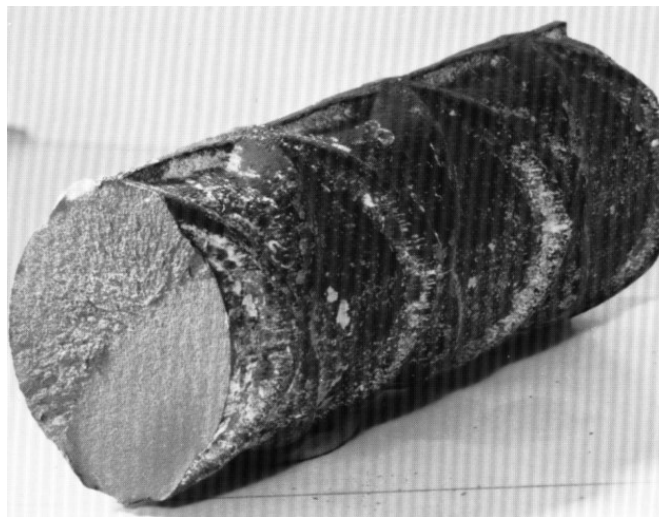


Figure 2-7: Steel reinforcement fatigue fracture (ACI 215R, 1974)

Several types of fatigue experiments have been performed to develop S-N curves of reinforcing steel. The tests involved either testing the steel reinforcement in air or embedded in

concrete. A comparison between the fatigue strength of the reinforcing steel in air and embedded in concrete was performed by Moss (1980), which showed slightly higher values for the embedded bars (See Figure 2-8). However, this behavior was not observed in previously conducted experiments (MacGregor et al., 1971; Wascheidt, 1965). Hence, it was concluded that there are small differences in fatigue strength of bars in air or embedded in concrete (ACI 215R, 1974).

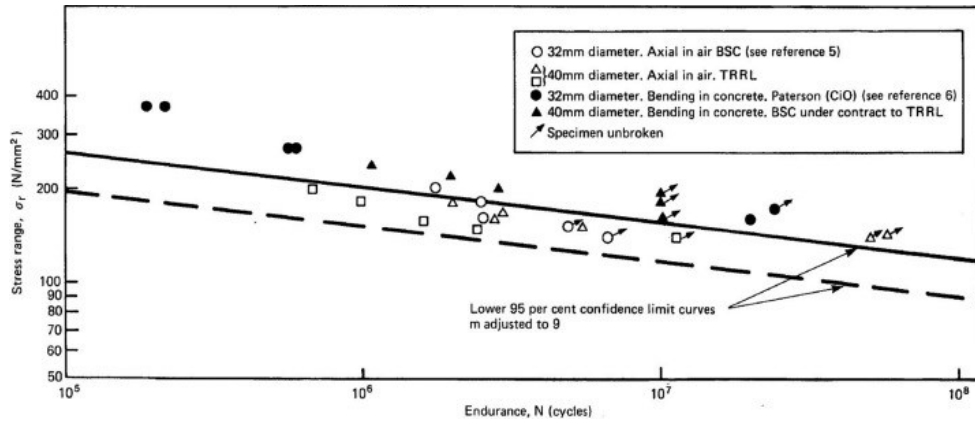


Figure 2-8: S_r - N curve of steel reinforcement (Moss, 1980)

Several experiments on concrete beams with straight deformed bars performed in North America were used to develop S_r - N curves displayed in Figure 2-9. Most of the curves showed their fatigue limit value after 1 million cycles. A typical value for the fatigue limit of steel reinforcement is a stress of about 0.5 of the ultimate tensile strength.

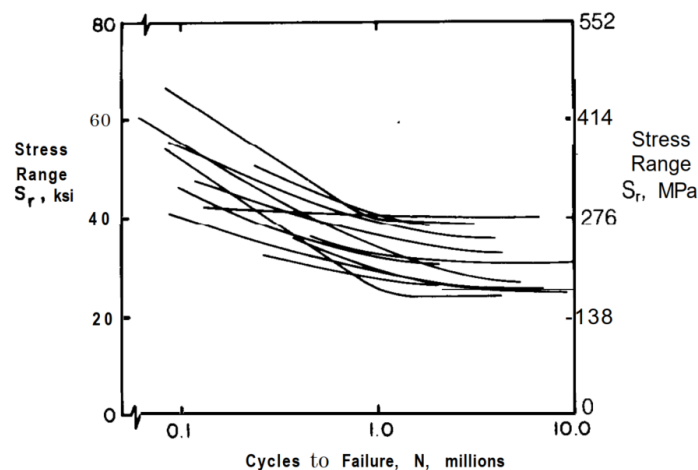


Figure 2-9: Typical S - N curve for steel rebar (ACI 215R, 1974)

Based on testing, it was determined that the main factors affecting steel fatigue behavior are related to the physical properties, which are minimum stress, bar size, geometry of the bar deformations, yield and tensile strengths, and bending or welding of a bar (ACI 215R, 1974).

2.3. Lap Splice Experiments

Fatigue behavior of lap splices has been evaluated using different testing methods. The methods discussed in this literature review are divided into two subcategories: unidirectional cyclic loading under elastic demands (stresses below yield stress of the steel reinforcement), and reverse cyclic experiments with inelastic demands (stresses higher than the yield stress of the steel reinforcement). Lap splice experiments under monotonic loading were typically performed within the literature reviewed as a control variable.

2.3.1. Monotonic and Elastic Unidirectional Cyclic Experiments

2.3.1.1. Tepfers (1973)

Tepfers conducted six different series of experiments to study various aspects of lap splice behavior on a total of 288 beam experiments. Tepfers evaluated the behavior of contact lap splices without stirrups, non-contact lap splices without stirrups, layered lap splices, and the effect of spiral confinement along the splice length. Tepfers divided the specimens into static and cyclic (fatigue) loading with different test variables for each group. For static tests, the significant parameters were splice length, reinforcing bar roughness or deformations, bar steel grade, bar diameter, concrete strength, concrete cover, presence and amount of stirrups, and presence of spiral reinforcement along the spliced bars. Subsequently, the cyclic (fatigue) experiments were limited to four parameters: roughness or deformation of reinforcing bars, steel grade, concrete strength, and the utilization of spiral reinforcement. Tepfers did not evaluate the use of stirrups on splice

behavior, but instead considered the use of spiral reinforcement along the lapped bars to resist the radial concrete tensile stresses along the lap splice (See Figure 2-10).

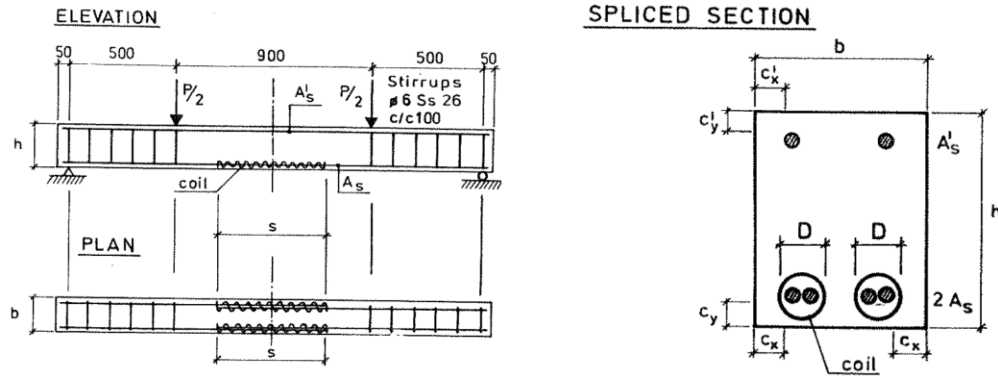


Figure 2-10: Teffers's proposed spiral reinforcement at lap splice (Teffers, 1973)

Based on the tests, Teffers concluded that lap splice failures resulted from longitudinal concrete cracking along the splice. Several different failure modes were defined: A) cover cracks along the entire length of the splice, B) cover cracks start at the end and propagate to the middle of splice, C) no cover cracks with a zipper-like failure depicted in Figure 2-11.

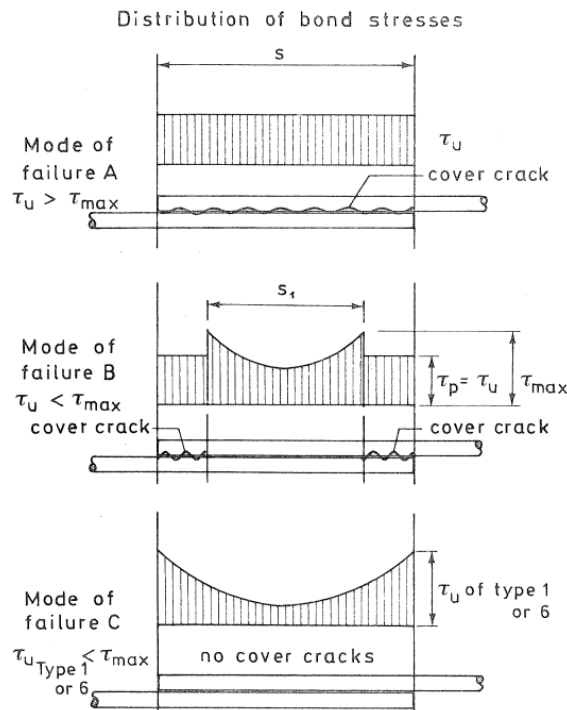


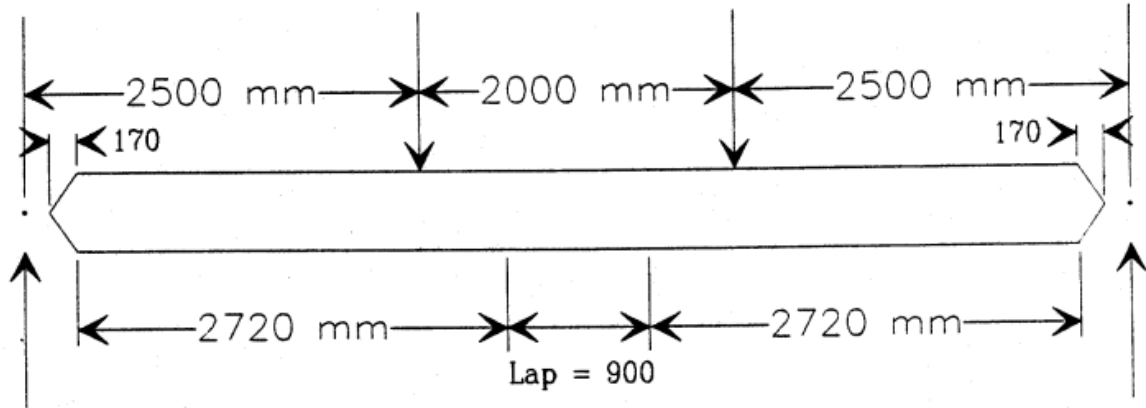
Figure 2-11: Bond stresses distribution at failure (Teffers, 1973)

From the static loading tests, 23 beams failed with mode of failure A and 6 beams failed with mode of failure B. Mode of failure C was not present in this series and was expected to occur only if very specific parameter combinations existed. From the fatigue loading tests, 17 beams failed in lap splice fatigue, 4 beams failed in lap splice fatigue after an increase in the repeating loads, 5 beams failed in fatigue outside of splice, and 7 beams were loaded to static failure after completing the repeating loading; 33 beams failed with mode of failure A, and 8 beams failed with mode of failure B. It was noted that fatigue failure occurred at loads as low as 60% of the ultimate static load.

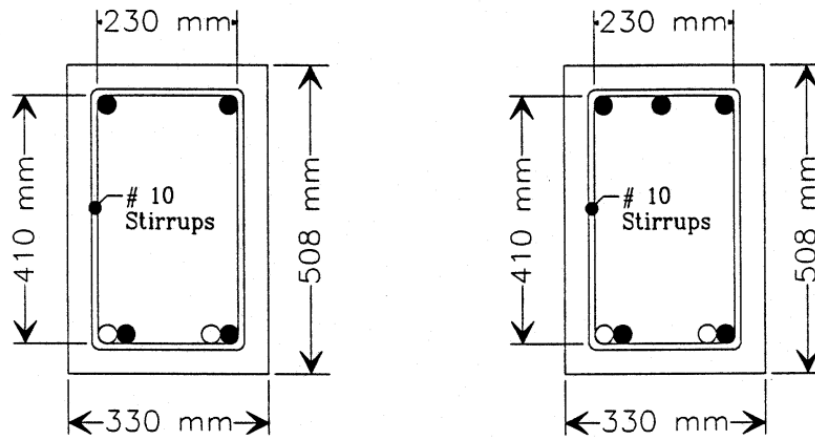
Tepfers's experiments included a wide range of test parameters. The tests were filtered to obtain the tests only with conditions similar to the experiments conducted as a part of this thesis and are evaluated later in Section 2.5.

2.3.1.2. Zacaruk (1990)

Zacaruk prepared seven beams with 90mm long lap splices that were tested under monotonic or unidirectional cyclic loading. The specimens were 7 m (23 ft) long, with a 330 mm x 508 mm (13 in. x 20 in.) cross-section. The spliced longitudinal reinforcement consisted of 2-No. 30 mm Grade 400 (MPa) bars with either 2-No. 30 mm or 3-No. 25 mm Grade 400 bars as compression reinforcement. Transverse reinforcement along the splice consisted of No. 10 mm Grade 300 bars spaced at 129 mm on center in accordance with ACI 408 recommendations. The applied stress range was varied for six of the tests (See Table 2-1), one beam was tested under monotonic loading, and one beam (F1-CONT) was tested with continuous top and bottom bars.



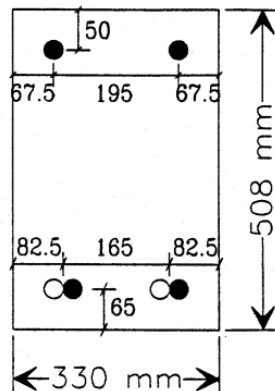
Longitudinal Details - Side View



2 No. 30 Compression Reinforcement

3 No. 25 Compression Reinforcement

Typical Beam Cross-Section Details



Typical Reinforcement Clear Covers

(Stirrups and Additional Compression Bar Not Shown)

Figure 2-12: Zaccaruk's beam specimens configuration (Zaccaruk, 1990)

Table 2-1: Zaccaruk's stress range variation in the specimens (Zaccaruk, 1990)

Specimen	f_{max} (MPa)	f_{min} (MPa)	f_r (MPa)
900-ST1-T129	472.9	0.0	472.9
900-F1-T129	354.9	114.3	240.6
900-F2-T129	301.7	114.7	186.9
900-F3-T129	244.7	71.7	172.6
900-F4S-T129	189.2	48.6	140.7
900-F5-T129	360.9	194.3	166.6
900-F6-T129	352.6	114.7	237.8
F1-CONT	353.5	112.9	240.6

Out of the seven beams tested using cyclic loading, six failed during the cyclic loading due to fatigue failure of the primary reinforcement. The rest of the beams completed the cyclic loading protocol and were subsequently loaded monotonically until failure. However, none of the test beams failed in fatigue bond as observed by Tepfers. A comparison between these two experimental programs showed that the additional confinement provided by the transverse reinforcement can change the mode of failure from concrete bond fatigue to steel reinforcement fatigue. Moreover, the comparison between specimens with lap splice and the continuous bars (similar steel and concrete properties) produced a nearly identical number of cycles to reach failure. This showed that the fatigue life of the specimen was not affected by the severe flexural cracks at the end of the lap splices. Zaccaruk's experimental results are compared to results from other experiments in Section 2.5.

2.3.1.3. Afseth (1993)

Afseth's experiments were an extension of Zacaruk's tests, i.e., (7 m long; 330 mm x 508 mm cross-section; 2-No. 30 mm Grade 400 bars for top and bottom; No. 10 mm transverse reinforcement). Ten beam specimens were constructed and divided into two beam configurations: 1) 975 mm lap splice length with either five stirrups at 195 mm or four stirrups at 244 mm; 2) 900 mm lap splice length with 7 stirrups at 129 mm. One specimen was loaded monotonically as a control test.

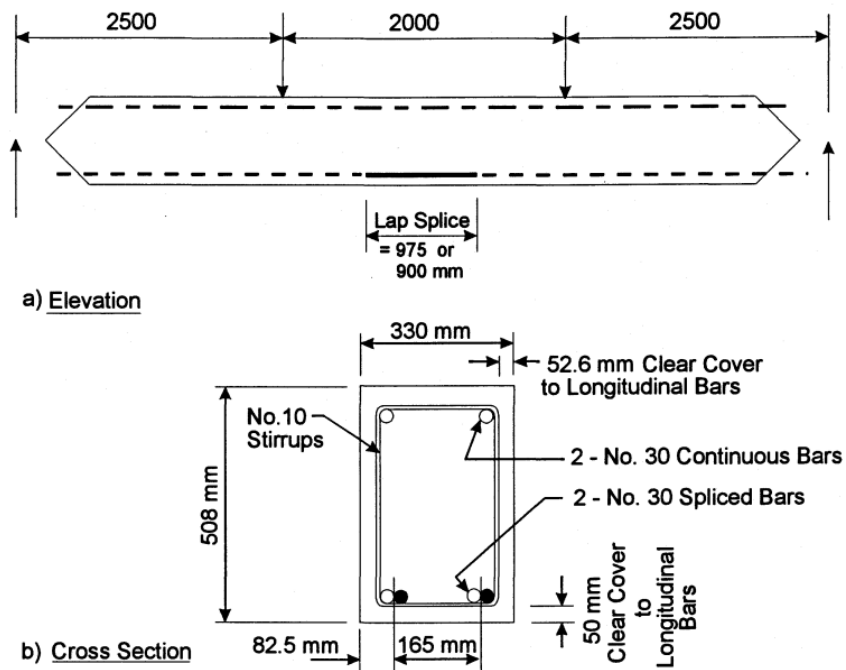


Figure 2-13: Afseth's beam specimens configuration (Afseth, 1993)

From the experiments, Afseth concluded that the specimens with heavy confinement ($s = 129$ mm) and shorter lap splice length ($l_s = 900$ mm) did not fail due to lap splice fatigue. These results were comparable to Zacaruk's test results with similar stress ranges. However, the specimens with nominally confined lap splices failed due to bond fatigue. These tests again supported the observation that transverse reinforcement along the lap splice influenced fatigue behavior.

Afseth modified the regression line formula proposed by Aas-Jakobsen (1970) by changing the maximum stress applied to the concrete strength ratio to the maximum stress in the steel to predicted static strength ratio:

$$\frac{\sigma_{s \max}}{\sigma_{static}} = 1 - \beta(1 - R) \log(N) \quad (2.1)$$

where $\sigma_{s \max}$ is the maximum stress the steel reinforcement experienced, σ_{static} is the predicted static strength, β is the regression constant, R is the ratio of minimum and maximum stress applied, and N is the number of cycles to failure.

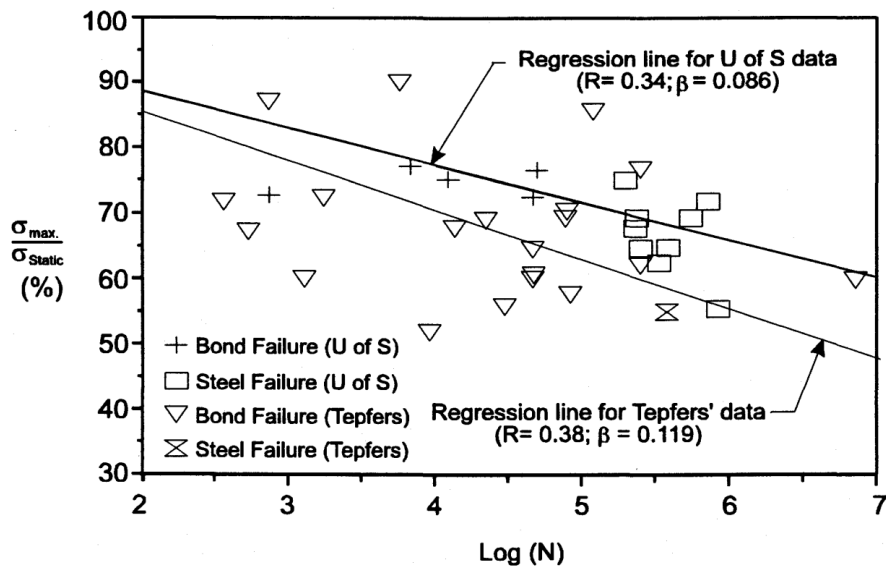


Figure 2-14: S-N curve of Afseth's experiments (Afseth, 1993)

Afseth's experimental results are compared to results from other experiments in Section 2.5.

2.3.1.4. Alyousef (2016)

Alyousef's primary objective was to evaluate the effect of FRP on the bond strength of lap splices with different concrete cover thickness under monotonic and fatigue loading. Hence, a comparison of unwrapped and wrapped specimens with different concrete cover values was

produced. The specimens were divided into three categories, with 20 mm, 30 mm, and 50 mm concrete cover. A set loading range was used for each category of the test specimens.

The beam test configuration utilized in Alyousef’s experiments was a 2.2-m-long beam with a 250 mm x 350 mm cross-section (See Figure 2-15). The beams were designed to fail in bond rather than in flexure. The bottom spliced reinforcement included 2-No. 20 mm Grade 400 and the top reinforcement considered of 2-No. 10 mm Grade 400 bars outside of the splice region. There were no stirrups used within the splice region to clearly evaluate the effect of FRP confinement on the bond behavior. The splice length used was 300 mm.

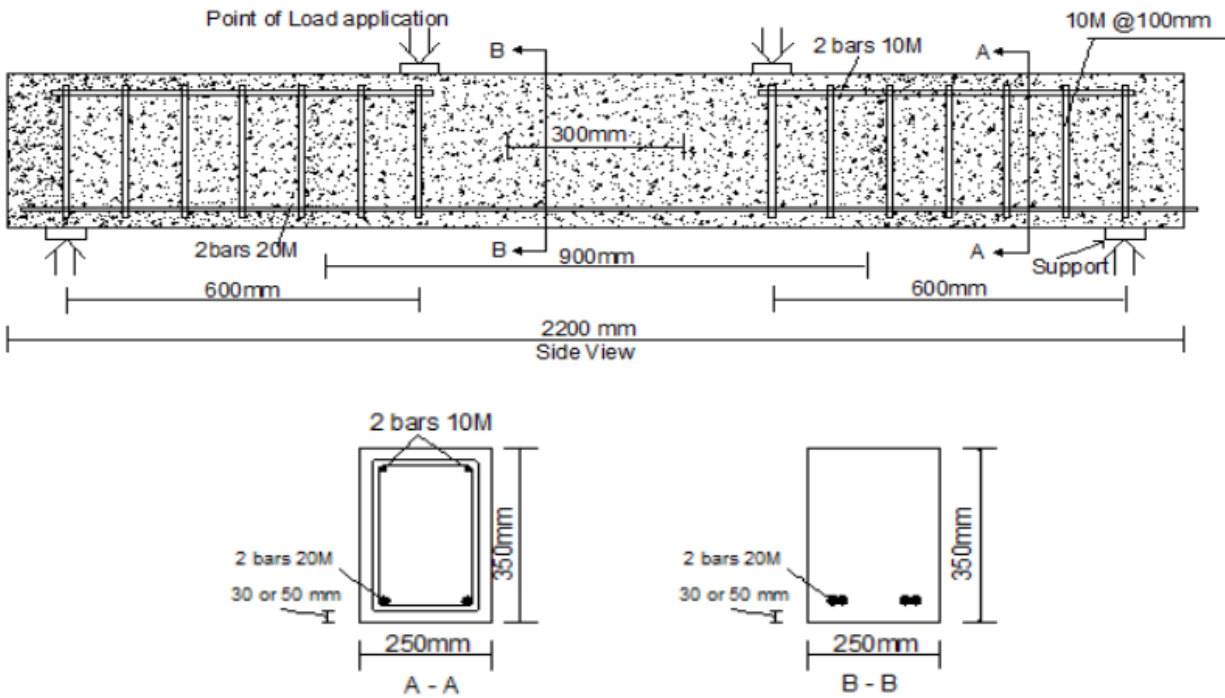


Figure 2-15: Alyousef’s beam specimen configuration (Alyousef, 2016)

Even though FRP is not considered in this thesis, Alyousef’s experiments evaluated several test specimens with lap splices and without FRP, which can be used in this study.

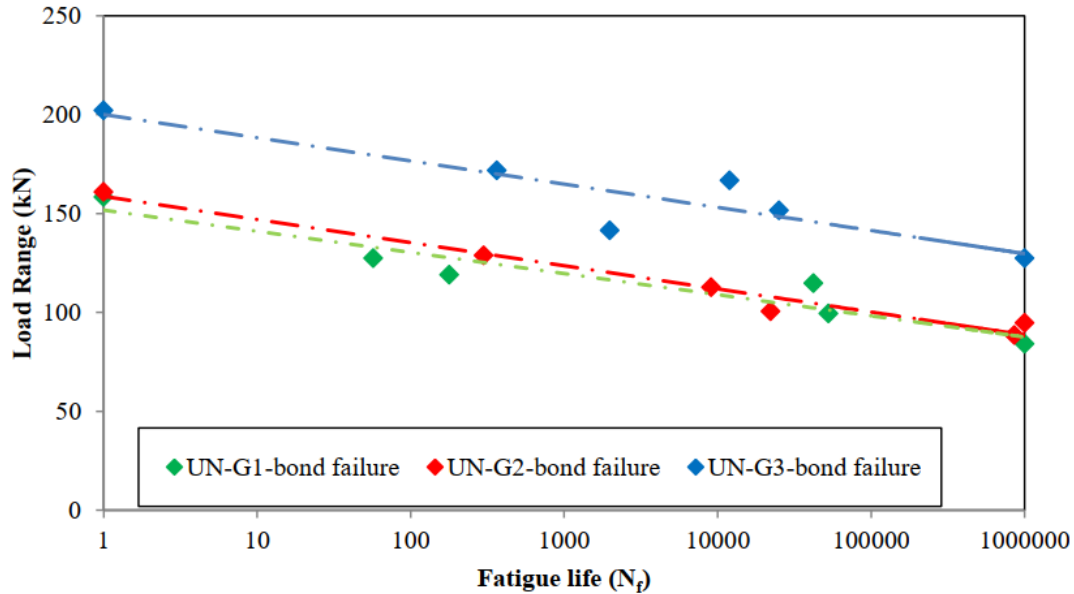


Figure 2-16: Alyousef's unwrapped specimen's S-N curve

Figure 2-16 shows that different concrete cover, e.g., specimens G1, G2, and G3 with 20 mm, 30 mm, and 50 mm of concrete cover, can affect the fatigue bond behavior. As the beams were designed to fail in bond, the unwrapped beams failed in fatigue bond failure. These experimental results are compared to results from other experiments in Section 2.5.

2.3.2. Inelastic Reverse Cyclic Experiments

2.3.2.1. Lukose et al. (1982)

These experiments were divided into four phases where the first two phases were beam-type tests with splices subjected to reverse cyclic loading, and the last two phases were column-type tests with splices subjected to reverse cyclic loadings (not discussed in this literature review). Sixty-eight beams were tested in the first two phases; eight half-scale and fourteen full-scale beams were tested in the first phase, and twenty-two full-scale beams were tested in the second phase. The half-scale beams were 6-feet-long, and the full-scale beams were 21-feet-long. The dimensions of each beam and spliced reinforcements (67 ksi nominal yield stress) are given in Figure 2-17. The concrete compressive strength was between 3.8 to 4.2 ksi.

accelerates the deterioration of bond. Furthermore, the number of cycles performed at loading above yield governed the splice behavior.

Table 2-2: Comparison between repeated and reversed loading

Beam	Bar size	Load history	Transverse steel*	Number of cycles above 90 percent yield	Number of cycles at highest displacement
1a	#10	rep	1.2	36	6 at 90 mm
1b		rev		10	6 at 46 mm
2a	# 8	rep	1.1	12	6 at 177 mm
2b		rev		11	5 at 90 mm
2c [†]		rev		21	12 at 76 mm
3a	#10	rep	2.1	45	9 at 90 mm
3b		rev		20	10 at 58 mm

*Transverse steel is expressed as a multiple of the amount given by Eq. (1).
[†]Beam 2c was subjected to a greater number of cycles at a lower level ($0.9M_y$) than beams 2a and 2b, which were cycled only above M_y .
 Bar size: #8 = 25 mm; #10 = 32 mm.

Results presented in Table 2-2 (refer to Lukose et al. (1982)) show that reversed loading decreases the number of cycles that could be performed on the beams with lap spliced bars, even though the mode of failures were the same. The theory was that reversed loading caused alternating directions of bond stresses and cracking, and loss of cover in both the top and bottom sides of the beams reduced the number of cycles until failure. Splice behavior was affected more for beams with larger diameter bars.

These experiments also emphasized the role of transverse reinforcement on lap splice behavior. Specimens with provided transverse reinforcement according to ACI Committee 408 (1979) could withstand several repeated cycles near yield. However, by providing twice the amount of transverse reinforcement, beam specimens could sustain inelastic behavior up to a displacement ductility of 2 before bond failure. The results indicated that the splice confinement near the ends of the splice was only effective for beams subjected to monotonic loading. The distribution of the transverse reinforcement also indicated that better performance was observed for small diameter and closely-spaced stirrups rather than for larger diameter and widely-spaced stirrups.

2.3.2.2. Sparling and Rezansoff (1986)

These experiments focused on evaluating the role of confinement, i.e., how the amount and type of transverse reinforcement affected splice strength and ductility. Three types of transverse reinforcement were considered: (1) ACI 408 recommended stirrups for static loading; (2) Stirrups spaced according to Tocci et al. (1981), or 72% more than required for ACI 408 in item (1); and (3) Spiral reinforcement along the splice (similar to Tepfers's (1973) spiral reinforcement) with similar transverse steel area per unit length of splice as in configuration (2). Eleven beams were constructed and tested; the details of the specimens are shown in Figure 2-19.

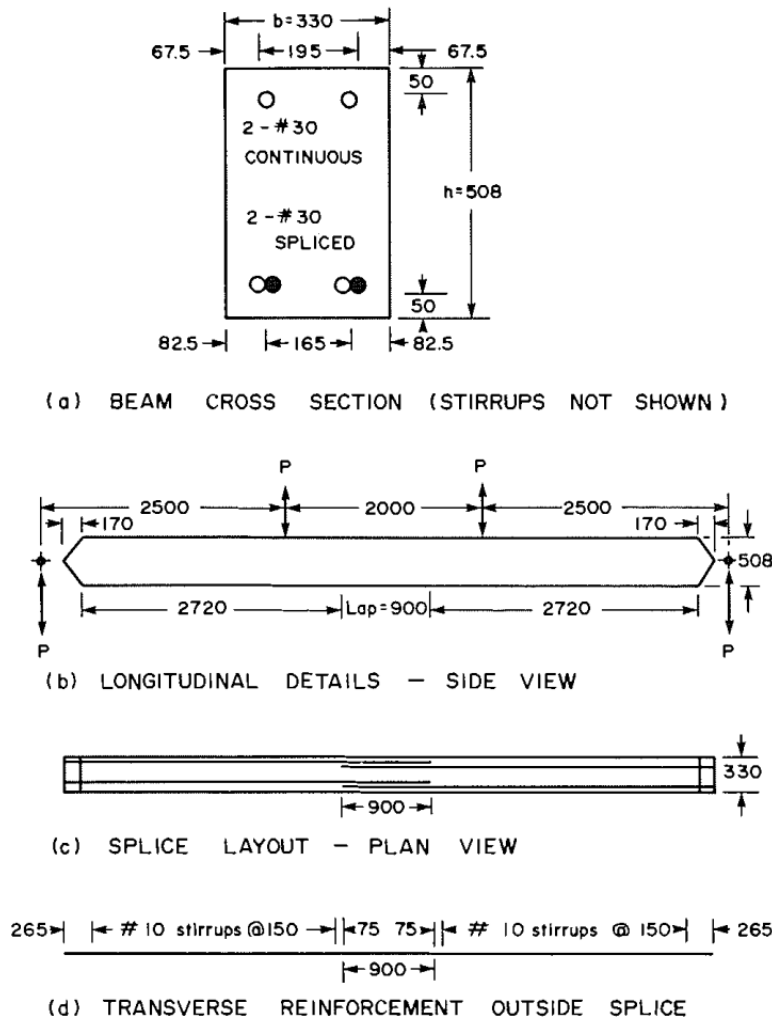


Figure 2-19: Beam specimens detail (Sparling & Rezansoff, 1986)

The loading protocols for this experiment were monotonic, repeated unidirectional cyclic, and reverse cyclic with loading above yield. However, the primary focus was on splice behavior for inelastic reverse cyclic loading. From these loading patterns and transverse reinforcement configurations, it was shown that the reverse cyclic loading and a poorly confined splice produced the worst damage. Cyclic loading also generated stiffness degradation, which produced higher deflections. Under fully reverse cyclic loading, the amount of displacement ductility achieved from configurations (2) and (3) were around 2.6 to 3.0, respectively, and 1.55 to 2.08 for configuration (1).

2.3.2.3. MacKay et al. (1988)

The beams in this experiment were constructed in two series with varying lap splice lengths and steel reinforcement grades. Series one included beams with steel reinforcement (f_y of 412 MPa) with splice lengths of $25d_b$, $35d_b$, and $45d_b$. Series two consisted of beams with steel reinforcement (f_y of 494 MPa) with splice lengths of $30d_b$, $40d_b$, and $50d_b$. The steel reinforcement had distinct stress-strain characteristics depicted in Figure 2-20.

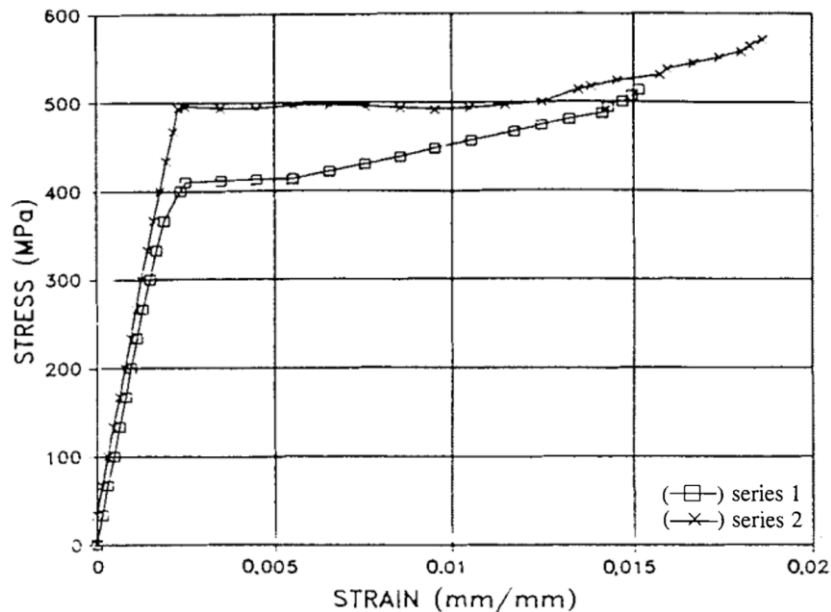


Figure 2-20: Stress-strain curves of steel reinforcement in MacKay's experiment (MacKay et al., 1989)

The transverse reinforcement (f_y of 400 MPa) was designed based on an equation from Sivakumar et al. (1983), which translated to 8 stirrups in series one and 10 stirrups in series two tests. The main objective of this experiment was to evaluate the confining effect of concrete on the lap splice behavior for inelastic demands; prior testing (Lukose et al., 1982) assumed that the confining effect in the splice region was only from the transverse reinforcement .

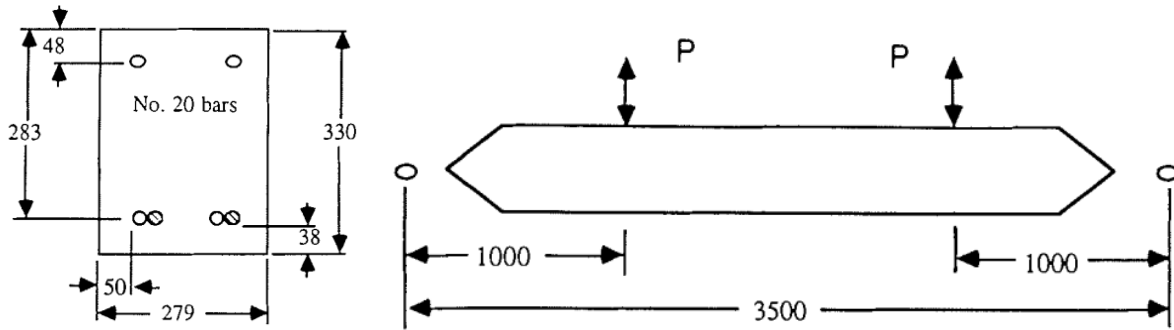


Figure 2-21: MacKay's beam specimens and loading diagram (MacKay et al., 1989)

The specimens were loaded with high-intensity reverse cyclic loading; the specimens with the shortest lap splice length for each series is the control specimen to assess any strength gain achieved due to the use of a longer lap splice length.

Table 2-3: Series 1 and Series 2 comparison (MacKay et al., 1989)

Specimen splice length (mm)	f_y (MPa)	f'_c (MPa)	Completed cycles	Ultimate moment (kN·m)	Relative strength	Peak midspan deflection*	Ductility ratio	Peak midspan deflection range† (mm)	Relative deflection range
Series 1									
500	412	26.6	13	68.8	1.00	48.3	2.62	86.6	1.00
700	412	26.6	20	72.5	1.05	59.3	3.21	103.6	1.20
900	412	26.6	28	73.8	1.07	70.3	3.81	120.8	1.39
Series 2									
600	494	27.7	21	78.3	1.00	63.5	3.00	115.7	1.00
800	494	27.7	24	81.5	1.04	63.4	2.99	108.1	0.93
1000	494	27.7	40	82.0	1.05	67.7	3.19	150.2	1.30

*Splice in tension.

†Total travel from peak load with compression on splice to peak load with tension on splice.

The results presented in Table 2-3 indicate that the number of cycles prior to failure increased with the increases in lap splice length. As more cycles were performed, larger

longitudinal reinforcement strains were present resulting in an increase in the ultimate strength. Due to strain-hardening, on average, a seven percent increase was observed for Series One tests and a five percent increase was observed for Series Two tests. MacKay et al. (1989) concluded that additional confinement effect to the lap splice can be provided by the concrete when longer lap splice lengths were used. Furthermore, the results indicated that lap splices can withstand inelastic reverse cyclic demands if detailed properly.

2.4. Transverse Reinforcement Requirements in Lap Splice

Test results reported in the literature clearly indicate that transverse reinforcement (amount and configuration) is required to achieve the yield strength or ductile response for lap spliced bars. To achieve yield strength for static loading, ACI 408 recommends a maximum stirrup spacing of:

$$s = \frac{A_{tr} f_y}{1500 d_{b,l}} \text{ [psi, in]} \quad (2.2)$$

where s is the stirrup spacing, A_{tr} is the transverse reinforcement area, f_y is the yield stress, and $d_{b,l}$ is the diameter of the spliced longitudinal bar. Subsequently, Lukose et al. (1982) recommended to double the transverse reinforcement specified by ACI 408 for loading above yield. More information regarding Lukose et al. (1982) tests can be found in Section 2.3.2.1.

Sivakumar et al. (1983) also proposed a relationship to determine the required spacing of transverse reinforcement along a lap splice to withstand 15 to 20 cycles reversed loading with a minimum strain demand in splice of at least $2.5\varepsilon_y$:

$$s = k \frac{A_{tr} l_s}{d_b^2} \leq 6 \text{ in}; \quad k = \frac{3/8}{\text{stirrup diameter}} \quad (2.3)$$

where k is a stirrup diameter size factor, A_{tr} is the transverse reinforcement area, l_s is the splice length, and d_b is the spliced steel reinforcement diameter. MacKay et al. (1988) then proposed to modify the spacing based on the ratio of $f_{y,\text{design}}/f_{y,\text{measured}}$.

Tocci's (1981) recommended spacing of transverse reinforcement for lap splices subjected to inelastic demands is:

$$s = \frac{0.28\alpha d_{b,t} l_s}{d_{b,l}^2}; \quad \alpha = \frac{60}{f_y} \quad (2.4)$$

where α is steel reinforcement grade factor, $d_{b,t}$ is the transverse reinforcement diameter, $d_{b,l}$ is the spliced bar diameter, and l_s is the splice length. This equation was also used by Sparling and Rezansoff (1986) to achieve a displacement ductility ratio of around 2.0-2.5 for their beam tests.

2.5. Summary of Lap Splice Experiments

2.5.1. Elastic Range of Loading

Specimens from Tepfers (1973), Zacaruk (1990), Afseth (1993), and Alyousef (2016) are categorized based on the lap splice parameters and the maximum stress achieved for the corresponding number of cycles performed in each test.

Table 2-4: Lap splice parameter comparison for elastic tests

Experiments	Parameters						
	c_b (in)	d_t (in)	d_b (in)	f_y (ksi)	f_c (psi)	l_d (in)	l_s/l_d
R. Tepfers (1973)	1.02	0.00	0.63	56.9-85.3	4641	35.6	0.6-1.4
J. A. Zacaruk (1990)	2.56	0.44	1.18	66.7	5802	35.6	0.9
J. G. Afseth (1993)	2.56	0.44	1.18	66.7	4351	41.1	0.9
R. Alyousef (2016)	1.62-2.81	0.44	0.79	63.1	6382	20.5-23.1	0.5-0.6

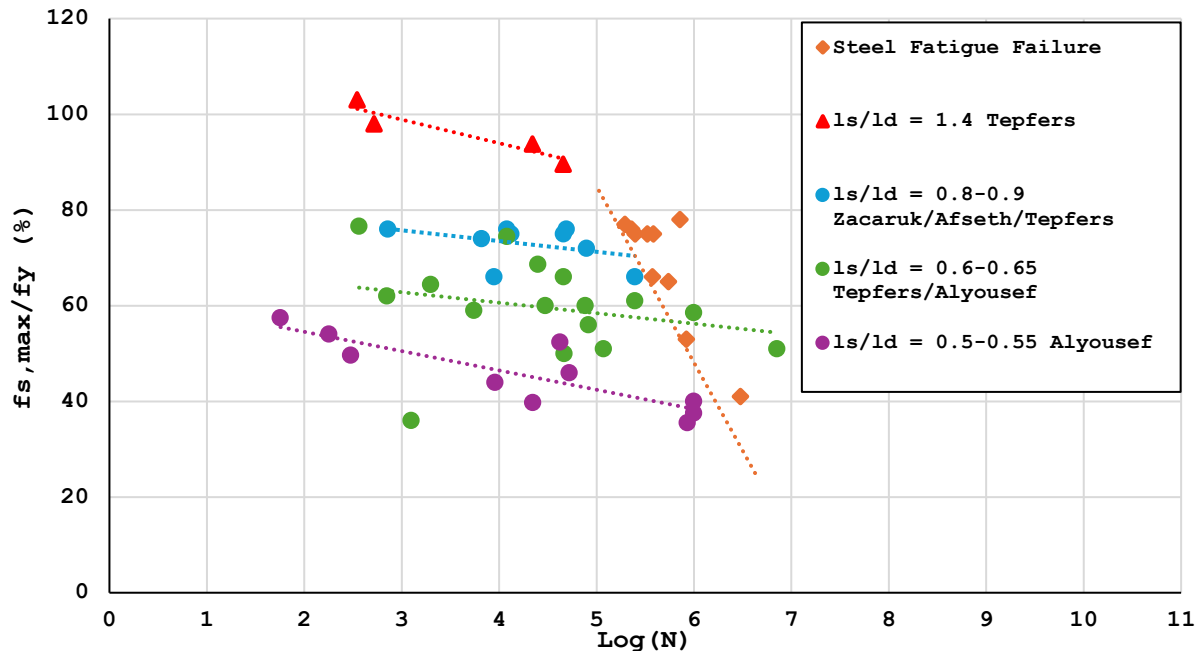


Figure 2-22: Envelope S-N curves for elastic tests

Figure 2-22 presents the results of regression analyses for each category of test specimens. It is noted that the specimens with splice lengths similar to those used in this program ($l_s/l_d = 1.625$), which are based on ACI 318-19, are those from Tepfers's tests ($l_s/l_{d,ACI} = 1.3$ to 1.4). Tepfers's beam specimens did not have stirrups over the splice length and have a value of $c_b/d_b = 1.5$; therefore, Tepfer's tests would be expected to provide a lower-bound to what would be expected for the beams tested in this study. However, the beams tested by Tepfers's were subjected to unidirectional cyclic loading, whereas the beams tested in this study were subjected to reverse cyclic loading, which would be expected to result in less favorable lap splice performance.

2.5.2. Inelastic Range of Loading

The behavior of lap splices subjected to inelastic loading is affected by the provided transverse reinforcement and concrete properties as identified in Section 2.3.2. Lukose et al. (1982), Sparling and Rezansoff (1986), and MacKay et al. (1988) all investigated lap splice behavior for bar stress demands beyond the yield stress.

Table 2-5: Lap splice parameter comparison for inelastic tests

Experiments	Parameters							
	c_b (in)	d_t (in)	d_b (in)	f_y (ksi)	f'_c (psi)	l_d (in)	l_s/l_d	s
Lukose et al. (1982)	1.36	0.37	0.51	67.4	3916	13.2- 50.9	0.8- 1.2	$3d_b$ - $7d_b$
Sparling and Rezansoff (1986)	2.56	0.00	1.18	60.3	3626	41	0.9	$2.5d_b$
MacKay et al. (1988)	1.89	0.31	0.79	59.8	3916	23.5- 28.2	1.0- 1.2	$4d_b$ - $5d_b$

Detailing recommendations to achieve inelastic responses for lap splices resulted from these studies; however, the maximum ductility achieved for the different test programs varied due to parameters considered in each test program.

The review of the lap splice experiments reported in the literature indicates that insufficient information exists to adequately represent the lap splice behavior at wall critical sections for the strain demands and loading histories expected for wall design utilizing Performance-Based Wind Design approach described in the ASCE Prestandard for Performance-Based Wind Design (2019). The beam tests carried out as part of this thesis were focused on addressing the gaps identified to support further development of PBWD as described in ASCE (2019) and ACI 318-25.

3. Experimental Program

The beam experiments were developed to support of a research study related to the performance of ordinary c-shaped walls subjected to wind-loading protocols (See Figure 3-1 and Figure 3-2). The wall specimens were representative of one-third scale prototype walls from several example buildings designed and constructed in wind-prone cities in the U.S. (e.g., Austin, Miami, Chicago). The wall experiments were designed to study elastic and inelastic responses when subjected to wind loading demands. An important issue related to the test specimen design was whether to include splices of longitudinal reinforcement at the critical section at the wall-foundation interface. Splicing wall longitudinal reinforcement at the critical section is common construction practice; however, splice performance under wind loading protocols that include nonlinear cycles, as noted in the literature review in Chapter 2, have not been thoroughly investigated. Hence, a study was undertaken to develop recommendations for splice requirements (i.e., length and detailing) that could be used for the wall test program.

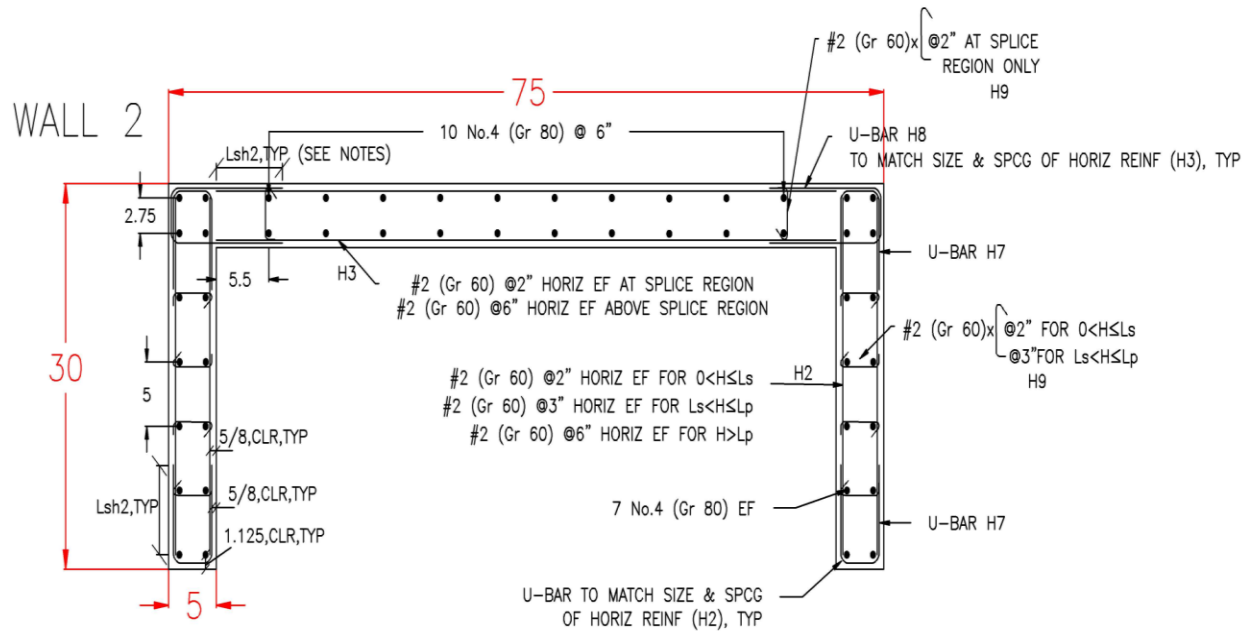


Figure 3-1: Ordinary wall cross-section (Unal et al., 2024)

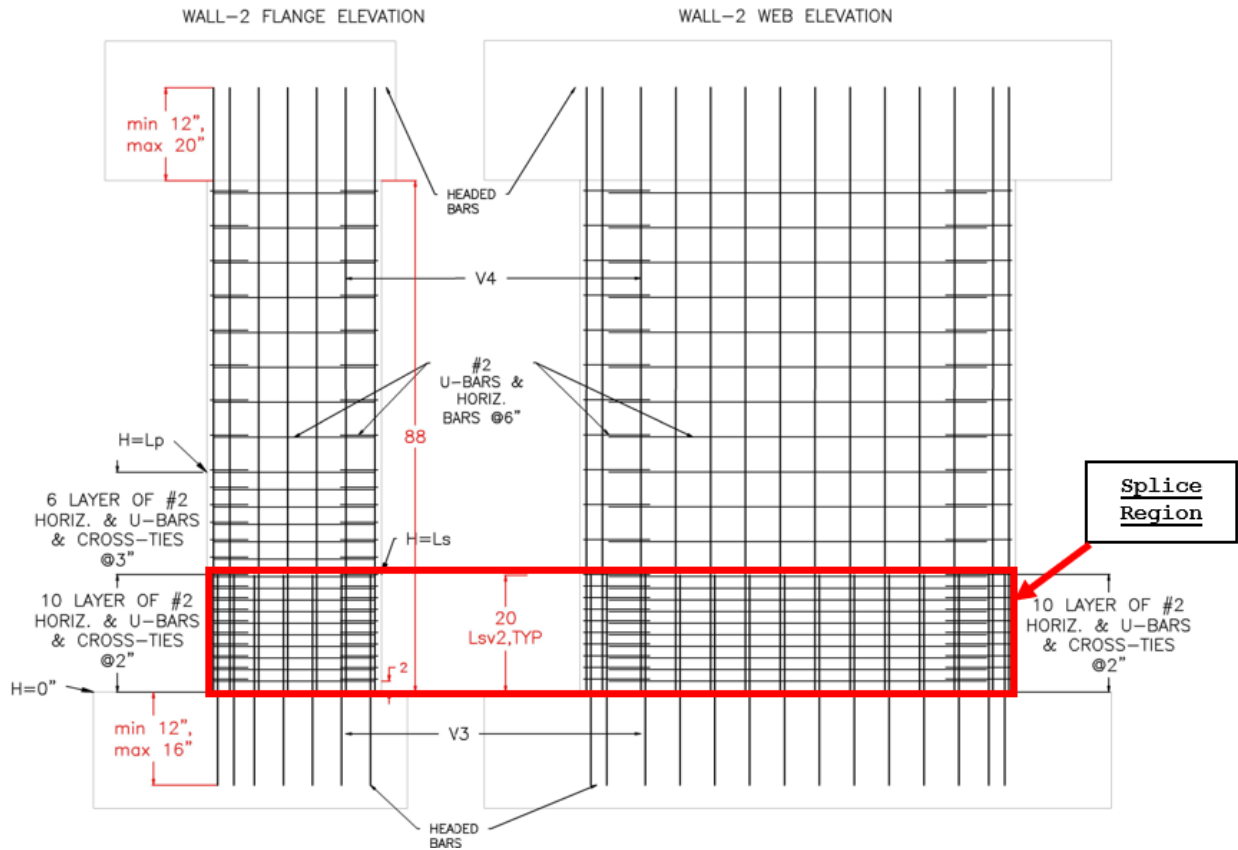


Figure 3-2: Ordinary wall elevation view (Unal et al., 2024)

The proposed wall test specimens are relatively expensive to construct and test; therefore, a beam test program was developed that could adequately represent the demands on the wall splice (Figure 3-4). The beams were designed to use the same rebar size, web width, cover, and transverse reinforcement that would be used in the wall test specimens (See Section 3.2) and a loading protocol was developed for the beams to match the wall strain demands under the given wind-loading protocol (See Section 3.3). The small beam tests, with #2 Grade 60 tie spacing of 2, 3, and 6 in., were tested first because the results were needed to finalize the design of the wall test specimens. However, due to concerns related to splice behavior for larger bars sizes, i.e., bar sizes used in typical building construction, additional, larger beams were tested with larger longitudinal bar sizes.

3.1. Naming Convention

The beam specimens were given a naming convention (See Figure 3-3) to identify the corresponding test parameters used for each test. The first code is either SB (small beam) or LB (large beam), followed by SX (where X is the transverse reinforcement spacing in the splice region) and YY (where YY is the splice length).

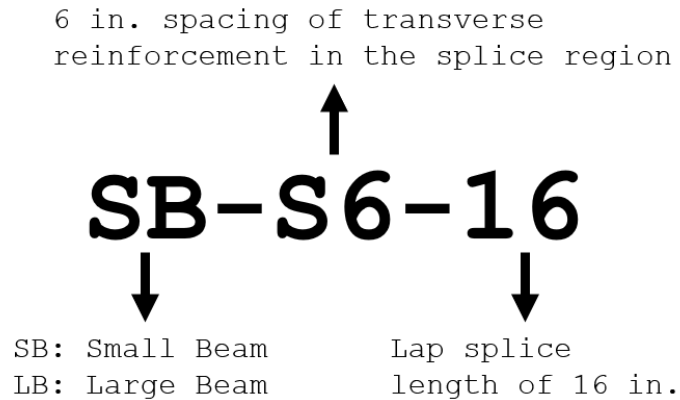


Figure 3-3: Naming convention of beam specimens

3.2. Design of Test Specimens

In the first phase of the beam test program, three small beams were designed to evaluate the lap splice behavior of #4 Grade 80 bars with different lap splice lengths and different spacing of transverse reinforcement over the splice length. The beam cross-section was selected to produce strain gradients under the wind loading protocol that would be representative of the strain gradients in the wall tests (e.g., neutral axis depth over the wall web length, c/l_w ; neutral axis depth over the beam depth, c/h). To accomplish this goal, a T-shaped beam cross section was used (Figure 3-4).

Tension reinforcement consisted of 2#4 spliced bars at the bottom of the beam and compression reinforcement consisted of 2#8 continuous bars at the top of the beam. A larger bar size (#8) was used for top reinforcement to enable higher compressive strain demands in the spliced #4 bars under negative moment without yielding the #8 continuous top bars.

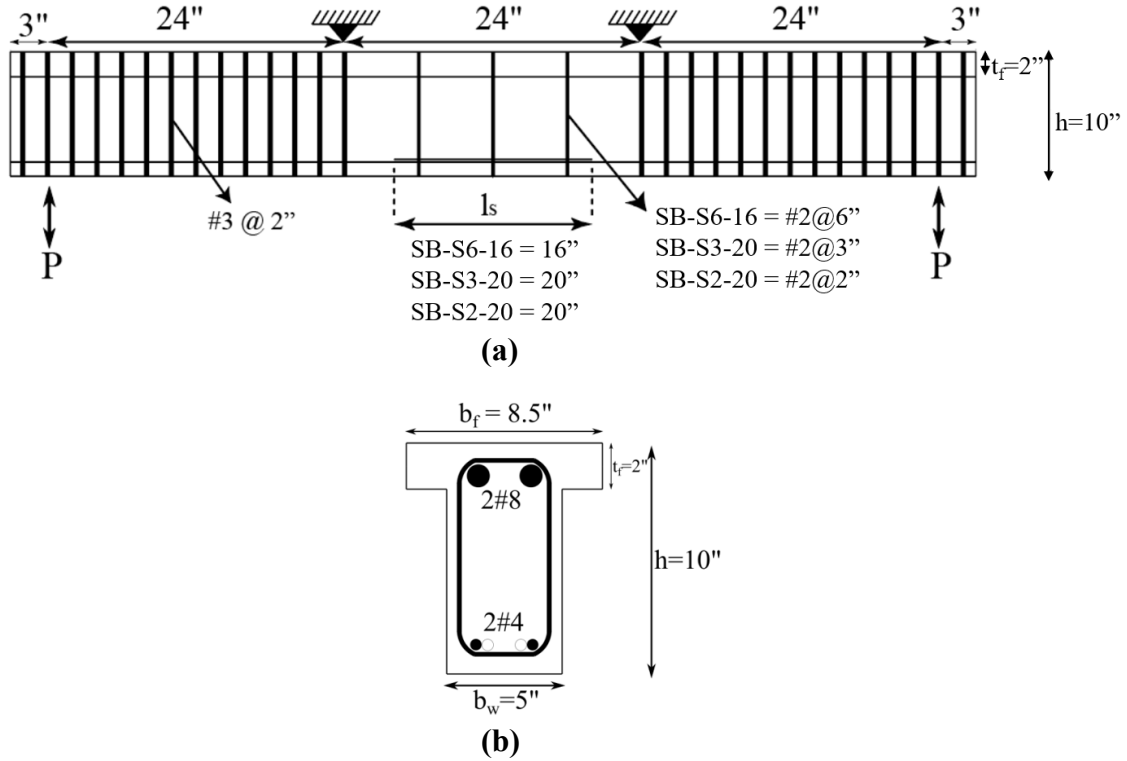


Figure 3-4: Small beam tests: (a) elevation view; (b) cross section (Unal et al., 2024)

Since all #4 longitudinal bars were spliced at the critical section, the splice length required is determined as 1.3 times the development length (l_d) calculated according to ACI 318-19 section 25.4.2.4. Initial tests were performed for beams with a lap splice length of $1.3l_d$ which did not perform adequately (described later). For subsequent beam tests, the required splice length was multiplied by 1.25 to account for overstrength and strain hardening of the longitudinal reinforcement, i.e., consistent with provisions at critical yielding sections for special walls (ACI 318-19 Section 18.10.2.3).

$$l_{s1} = 1.3 \times l_d; \text{ Minimum ACI 318-19 lap splice length} \quad (3.1)$$

$$l_{s2} = 1.25 \times 1.3 \times l_d; \text{ ACI 318-19 splice length for special walls} \quad (3.2)$$

$$l_d = \left[\frac{3}{40} \frac{f_y}{\lambda \sqrt{f'_c}} \frac{\Psi_t \Psi_e \Psi_s \Psi_g}{\left(\frac{c_b + K_{tr}}{d_b} \right)} \right] d_b \quad (3.3)$$

where l_s is the splice length, l_d is the development length, f_y is the yield strength of the reinforcement, λ is the lightweight concrete modification factor, f_c' is the concrete compressive strength (expected properties for this experiment), c_b is the lesser of the distance from the center of the spliced reinforcement to the nearest concrete surface and one-half of the center-to-center spacing between longitudinal reinforcement in the same layer, K_{tr} is the transverse reinforcement index, d_b is the diameter of the spliced reinforcement, and $\Psi_t, \Psi_e, \Psi_s, \Psi_g$ are modification factors according to ACI 318-19 Table 25.4.2.5. For the spliced #4 bars with $c_b=1.125$ in. and $K_{tr}=0.33$, a 12.3 in. development length results. Therefore, the minimum required splice length was $1.3 \times 12.3'' = 16$ inches (SB-S6-16). Initial tests with 16 in. splice lengths did not perform adequately (as described later); therefore, for subsequent tests, this length was then multiplied by 1.25 for the other two small beams (SB-S3-20; SB-S2-20).

Transverse reinforcement along the splice region was provided by #2 Grade 60 stirrups. As there are no requirements for transverse reinforcement spacing in the splice region for ordinary walls in ACI 318-19, the spacing was based on the minimum spacing of 18 in. for wall web horizontal reinforcement (ACI 318-19 Chapter 11.7.2.1). The beam stirrups represent the U-shaped bars that are lapped at the wall edge with the web horizontal reinforcement. The minimum spacing of ACI 318-19 was then scaled from 18 in. to 6 in. because of the scale factor used for the wall test specimens. However, initial testing of beams with 6-in. stirrup spacing did not perform adequately. Stirrup spacing was reduced to 3 in. and 2 in. in subsequent small beam test specimens. The stirrups between the support and the applied load at the end of the beam (See Figure 3-4(a)) were designed to provide enough shear capacity to resist expected shear demands assuming the probable moment (M_{pr}) strength of the beam would be reached during the test (i.e., to avoid shear failure).

Phase II of the test program involved tests on two large beams to evaluate the effect of spliced bar diameter on lap splice behavior for wind loading. The beam cross sections for the large beams were 20 in. deep and 10 in. wide (See Figure 3-6), i.e., twice the dimensions of the small beam tests; however, spliced longitudinal reinforcement consisted of 2#8 Grade 80 bars at the beam bottom and 2#8 continuous bars at the beam top (See Figure 3-6). For the large beams, with $c_b = 2.25$ in. and for a #4 stirrup spaced at 7.5 in., the resulting development length is 30.9 inches. Again, based on initial small beam tests (See Equation (3.2)), this length was multiplied by 1.3 and 1.25 to produce a splice length of 50 in. for both beam tests.

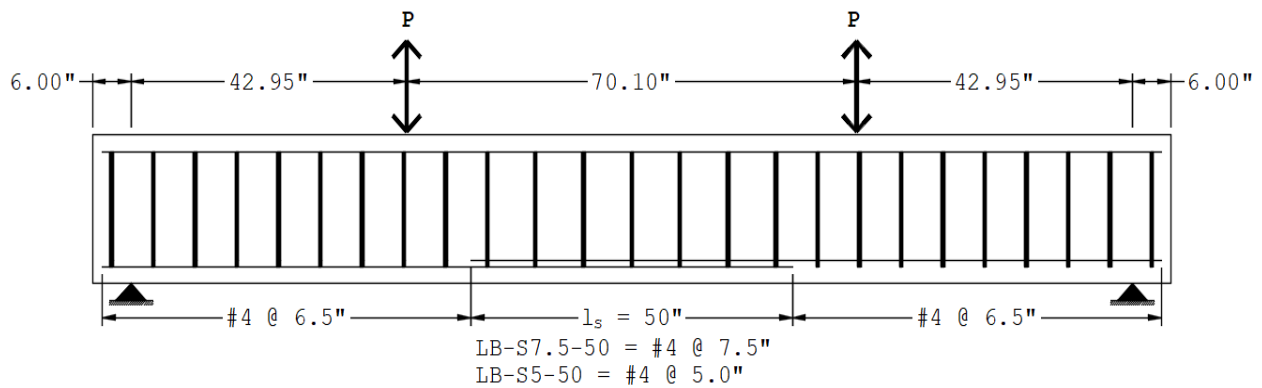


Figure 3-5: Elevation view of the beam specimens

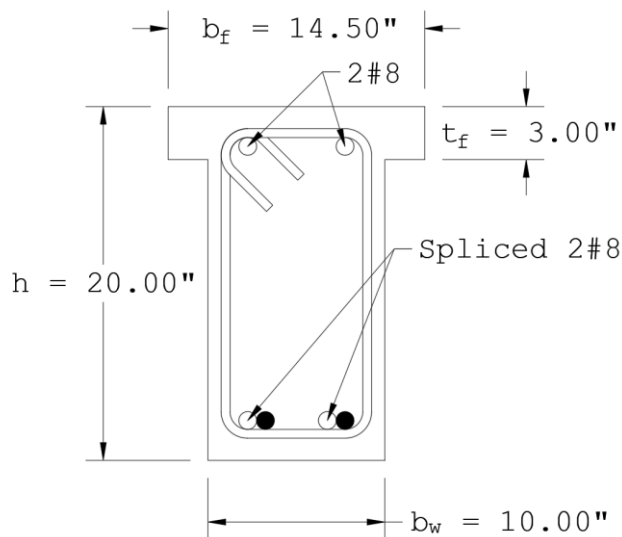


Figure 3-6: Cross-section of the beam specimens

The transverse reinforcement spacing in the large beam tests was related to that of the small beam tests using the parameter, a_{sp} , which is the ratio of the confining force along the splice to the yield force of the spliced bars:

$$a_{sp} = \frac{A_{vsp} \times f_{yt}}{A_{sl} \times f_{yl}} \quad (3.4)$$

where a_{sp} is the spacing parameter in splice region, A_{vsp} is the total transverse reinforcement area in the splice region, A_{sl} is the total spliced longitudinal reinforcement area, f_{yt} is the yield strength of transverse reinforcement, and f_{yl} is the yield strength of spliced longitudinal reinforcement. The small beam test specimens with 6, 3, and 2 in. stirrup spacings have a_{sp} values of 0.46, 1.15, and 1.73, respectively. For the large beam tests, stirrup spacing was selected to provide values of a_{sp} that were similar to the values provided in the small beam tests for stirrup spacing of 3 and 2 inches. Therefore, the stirrup spacings used in the large beam tests were 7.5 in. and 5 in., which produced a_{sp} values of 1.25 and 1.88, respectively. The comparison of the small and large beam test properties is provided in Table 3-1.

Table 3-1: Small and large beam properties comparison

Variable	Small Beam			Large Beam	
	SB-S6-16	SB-S3-20	SB-S2-20	LB-S7.5-50	LB-S5-50
b_f	8.5 in	8.5 in	8.5 in	14.5 in	14.5 in
b_w	5.0 in	5.0 in	5.0 in	10.0 in	10.0 in
t_f	2.0 in	2.0 in	2.0 in	3.0 in	3.0 in
h	10.0 in	10.0 in	10.0 in	20.0 in	20.0 in
A_s bot	2#4	2#4	2#4	2#8	2#8
A_s top	2#8	2#8	2#8	2#8	2#8
f_{yl}	80 ksi	80 ksi	80 ksi	80 ksi	80 ksi
f_{yt}	60 ksi	60 ksi	60 ksi	60 ksi	60 ksi
l_s	16.0 in	20.0 in	20.0 in	50.0 in	50.0 in
s	6.0 in	3.0 in	2.0 in	7.5 in	5.0 in
A_t	#2	#2	#2	#4	#4
a_{sp}	0.46	1.15	1.73	1.25	1.88

In Table 3-1, b_f is the beam flange width, b_w is the beam web width, t_f is the beam flange thickness, h is the beam total height, A_s is the longitudinal reinforcement area (top or bottom), f_{yl}

is the longitudinal reinforcement yield stress, f_{yt} is the transverse reinforcement yield stress, l_s is the splice length, s is the stirrup spacing, d_t is the transverse reinforcement diameter, and a_{sp} is the confining effect factor provided over the lap splice length.

3.3. Loading Protocol

A wind-loading protocol (See Figure 3-7) was developed for the ordinary wall test program that consisted of force-controlled loading (elastic behavior in the steel reinforcement) and displacement-controlled loading (inelastic behavior in the steel reinforcement). The loading protocol used was similar to the protocol used in the coupling beam experiments conducted by Abdullah et al. (2020). The loading protocol includes ramp-up cycles starting at $0.4M_{pr}$ and eventually reaching a rotation demand of $3.0\Theta_y$, where Θ_y is the estimated wall yield rotation, and then a symmetrical ramp-down. The value of Θ_y for the wall experiments was the estimated in-plane (parallel to the web) rotation over an assumed plastic hinge length of one-half the wall length (37.5 in.). For the wall tests, the loading protocol is the same for positive and negative directions due to the symmetry of wall cross section and reinforcements for loading in the plane of the web.

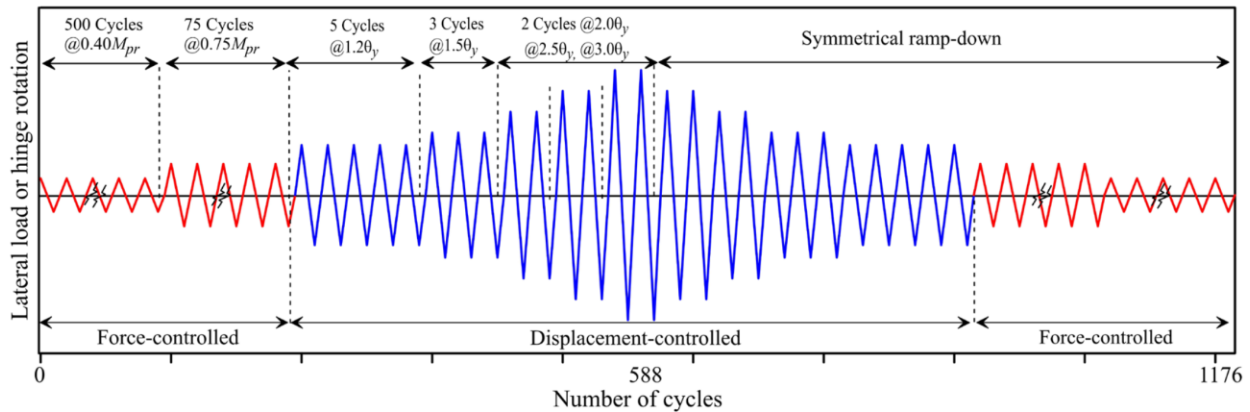


Figure 3-7: Loading protocol for ordinary wall (Unal et al., 2024)

The loading protocol for the small beam tests was modified from the wall test based on calculated strain demands in vertical reinforcement at the wall critical section (where lap splices

were present) located closest to the wall edge for compression and tension. These wall strain demands were then normalized by the expected yield strain of the longitudinal reinforcement to obtain target values for the small beam experiments for each load or displacement level of the wall loading protocol (Table 3-2; Unal et al., 2024). Therefore, the loading protocol for the beam experiment was based on target strain demands from the wall experiment, versus yield rotation, which is not relevant for the beam experiment because the lap splices were located in a region of constant moment. These strain demands were then translated to target beam displacements for the small beam loading protocol (e.g., $1.2\Theta_y$ wall demand and $1.6\delta_{y,b}^+$ for the small beam produced a tensile strain demand of $1.86\epsilon_y$ in the reinforcement; See Table 3-2). The yield displacement was based on the experimental yield displacement measured during the test (versus a predicted value).

However, due to the asymmetric wall strain demands in the lap splice in tension and compression, i.e., tensile strain demands eventually exceeded yield strain whereas compressive strain demands were less than yield strain, the load applied in the small beams loading protocol is not symmetric in the positive and negative bending to produce the same strains in the wall tests (See Figure 3-8). In addition, due to limitations and/or differences between the wall and beam test setups, the ramp-down cycles for the displacement-controlled portion of the beam loading protocol were combined with the ramp-up cycles.

Table 3-2: Applied strain demands in walls and small beams

Wall Wind Loading Protocol	Strain Demands		Beam Wind Loading Protocol		Number of Cycles
	Tension	Compression	Tension	Compression	
$0.4M_{pr}$	$0.2\epsilon_y$	$-0.14\epsilon_y$	$0.31M_{pr,b}^+$	$0.28M_{pr,b}^-$	500
$0.75M_{pr}$	$0.93\epsilon_y$	$-0.27\epsilon_y$	$0.79M_{pr,b}^+$	$0.51M_{pr,b}^-$	75
$1.2\Theta_y$	$1.86\epsilon_y$	$-0.36\epsilon_y$	$1.6\delta_{y,b}^+$	$0.64M_{pr,b}^-$	10
$1.5\Theta_y$	$2.55\epsilon_y$	$-0.4\epsilon_y$	$2.0\delta_{y,b}^+$	$0.72M_{pr,b}^-$	6
$2.0\Theta_y$	$3.87\epsilon_y$	$-0.4\epsilon_y$	$3.0\delta_{y,b}^+$	$0.72M_{pr,b}^-$	4
$2.5\Theta_y$	$5.46\epsilon_y$	$-0.4\epsilon_y$	$4.0\delta_{y,b}^+$	$0.72M_{pr,b}^-$	4
$3.0\Theta_y$	$6.82\epsilon_y$	$-0.4\epsilon_y$	$5.0\delta_{y,b}^+$	$0.72M_{pr,b}^-$	2

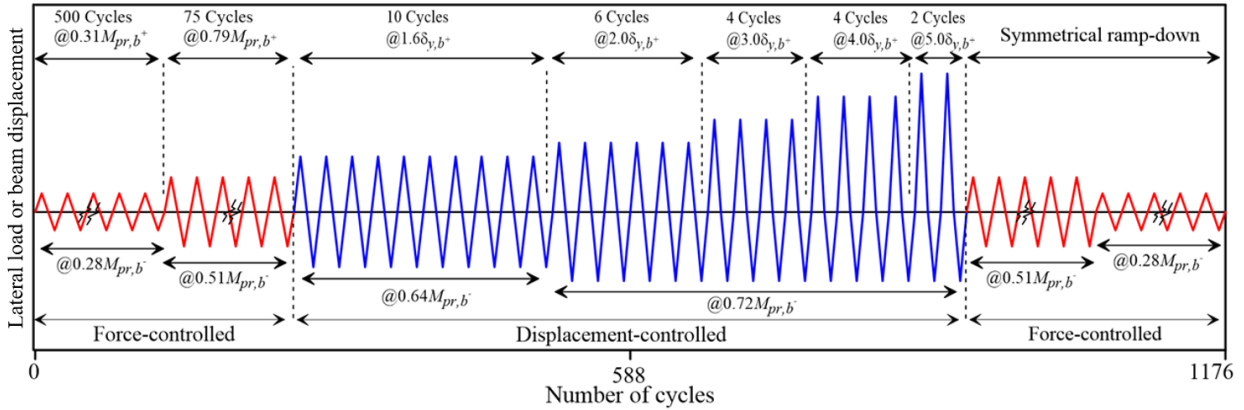


Figure 3-8: Loading protocol for small beams (Unal et al., 2024)

An additional modification of the loading protocol was required for the large beam tests. For practical reasons, it was not possible to provide sufficient beam compression (top) reinforcement to match the strain demands in the small beam tests (and the wall tests). Therefore, to avoid yielding the top reinforcement in the large beams, the compressive strain demands were limited to $0.1\epsilon_y$. As was done for the small beam tests, the ramp-down portion of the displacement-controlled portion of the loading protocol was combined with the ramp-up portion (See Figure 3-9). Table 3-3 provides a summary and a comparison of the strain demands applied to the small and large beam tests.

Table 3-3: Strain demands comparison between small and large beams

Wall Wind Loading Protocol	Small Beams - Strain Demands		Large Beams - Strain Demands		Number of Cycles
	Tension	Compression	Tension	Compression	
0.4 M_{pr}	$0.2\epsilon_y$	$-0.14\epsilon_y$	$0.2\epsilon_y$	$-0.05\epsilon_y$	500
0.75 M_{pr}	$0.93\epsilon_y$	$-0.27\epsilon_y$	$0.93\epsilon_y$	$-0.1\epsilon_y$	75
1.2 Θ_y	$1.86\epsilon_y$	$-0.36\epsilon_y$	$1.86\epsilon_y$	$-0.1\epsilon_y$	10
1.5 Θ_y	$2.55\epsilon_y$	$-0.4\epsilon_y$	$2.55\epsilon_y$	$-0.1\epsilon_y$	6
2.0 Θ_y	$3.87\epsilon_y$	$-0.4\epsilon_y$	$3.87\epsilon_y$	$-0.1\epsilon_y$	4
2.5 Θ_y	$5.46\epsilon_y$	$-0.4\epsilon_y$	$5.46\epsilon_y$	$-0.1\epsilon_y$	4
3.0 Θ_y	$6.82\epsilon_y$	$-0.4\epsilon_y$	$6.82\epsilon_y$	$-0.1\epsilon_y$	2

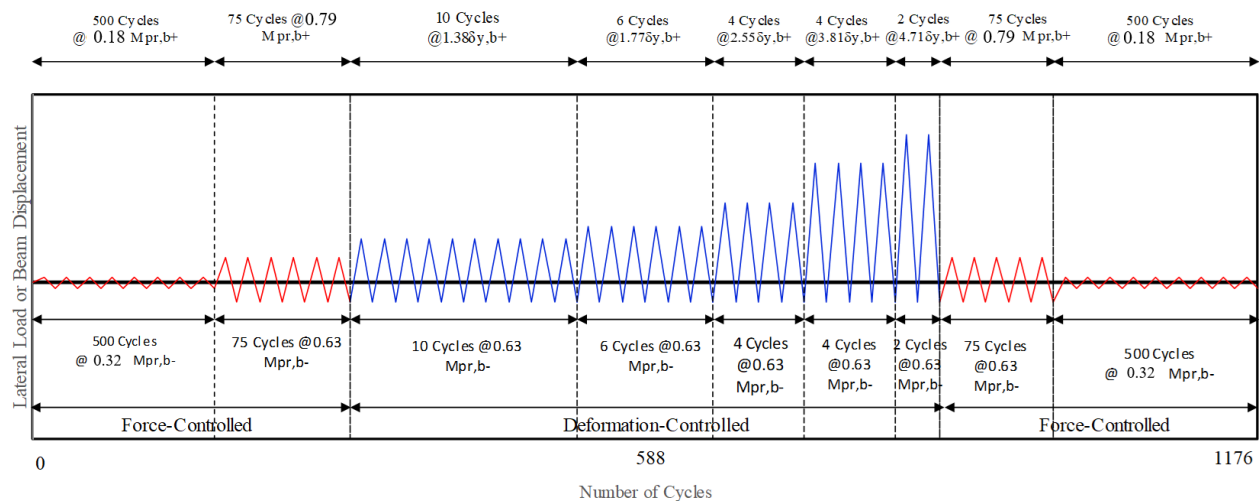


Figure 3-9: Loading protocol for large beams

3.4. Test Setup

A four-point loading test setup was fabricated to generate a constant moment region and zero shear (excluding beam self-weight) between the applied loads (See Figure 3-10, Figure 3-11, Figure 3-12, and Figure 3-13). The test setup supports were designed to enable the application of reversed cyclic loading to the beam (i.e., develop positive moment (tension in splice) and negative moment (compression in splice)).

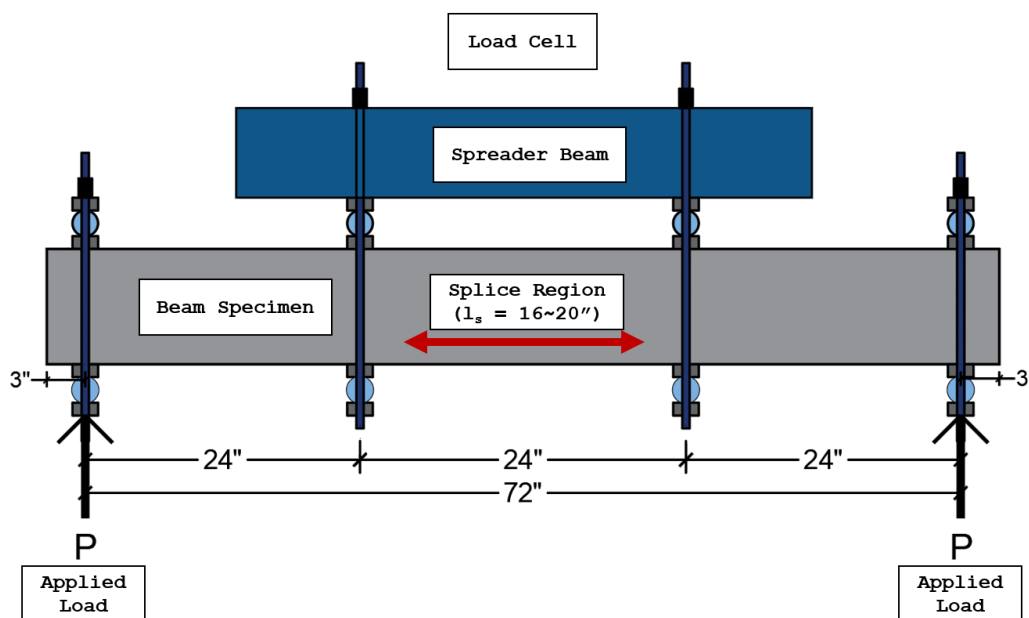


Figure 3-10: Small beam test setup schematic (not drawn to scale)

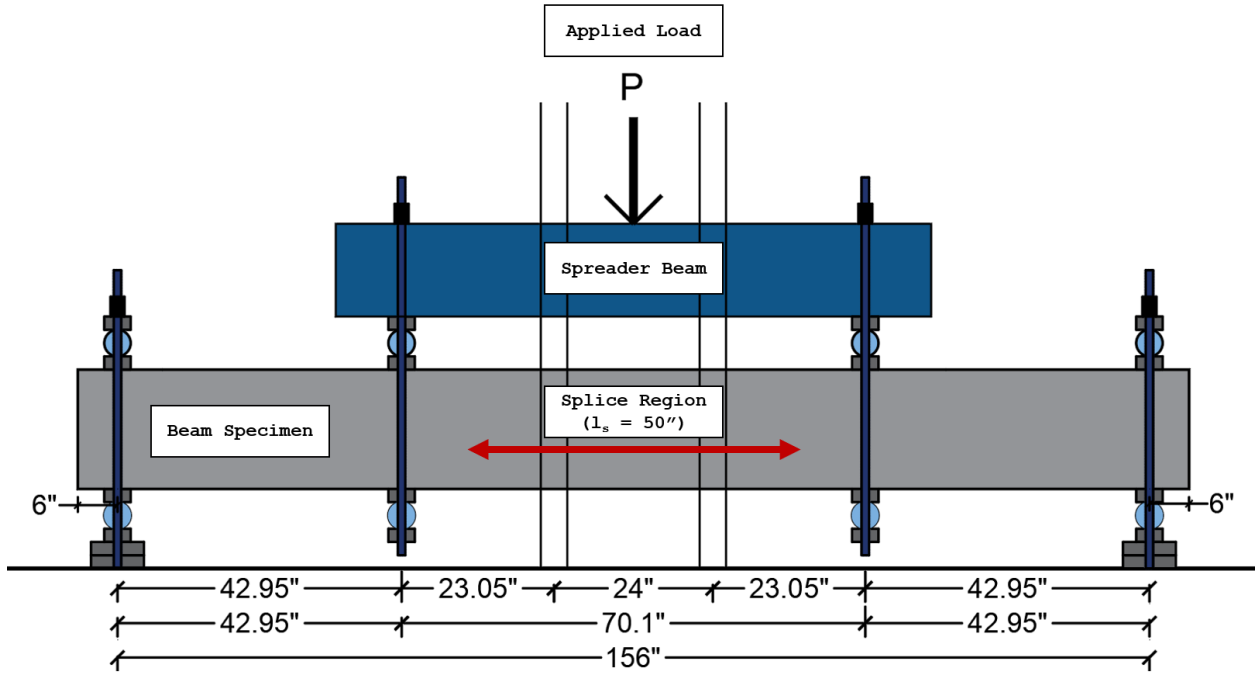


Figure 3-11: Large beam test setup schematic (not drawn to scale)

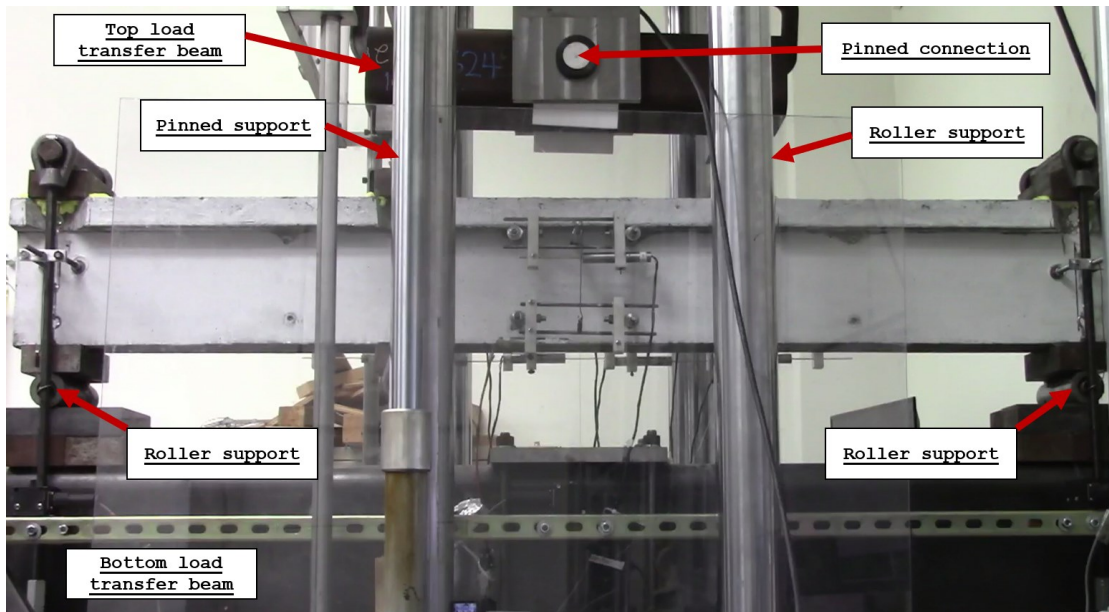


Figure 3-12: Small beam test setup photo

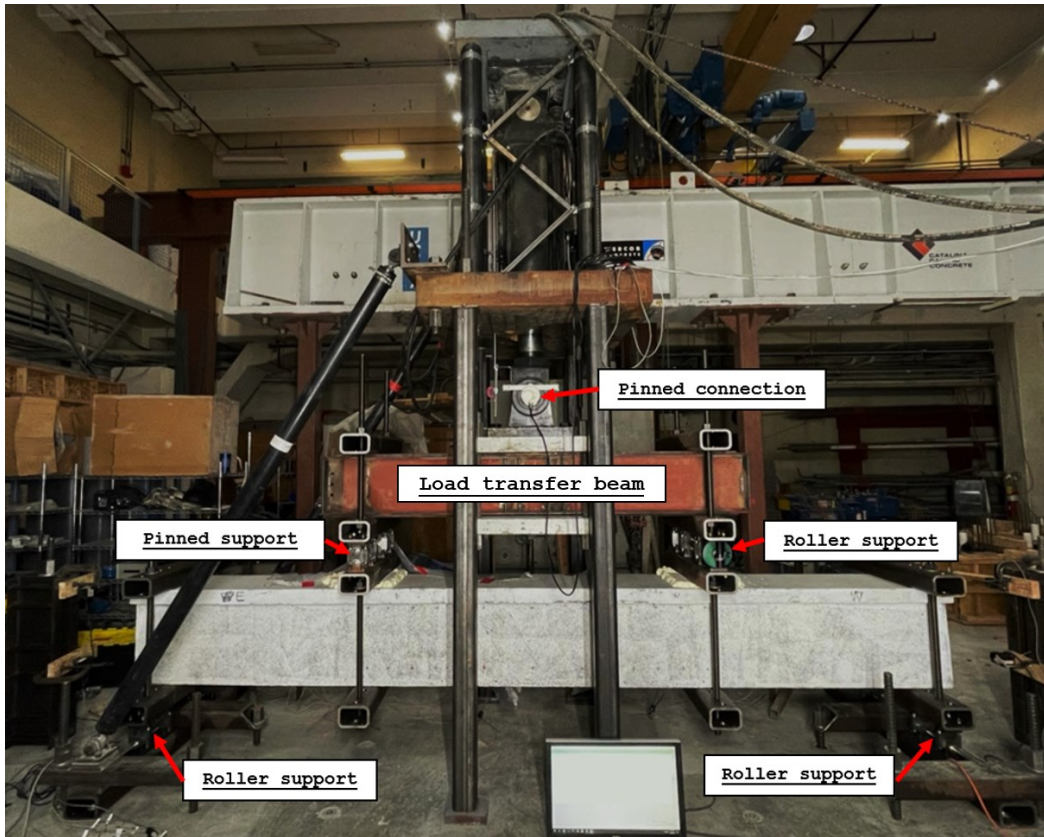


Figure 3-13: Large beam test setup photo

In the small beam test setup, the vertical load was applied from the bottom with a single actuator which was fixed to a bottom spreader (load transfer) beam. The bottom spreader beam transferred the vertical load through two rollers to the beam specimen which then was transferred to a top spreader beam through a pin support and a roller support. The top spreader beam was pin-connected to the load cell which measured the actuator load. The loads on the test beam were assumed to be equal to one-half of the measured actuator load.

In the large beam test setup, vertical loading was applied with a single actuator, pin-connected with a load cell to a spreader (load transfer) beam, which was simply supported on the test beam. The test beam specimens were supported on two rollers, and the spreader beam was supported on a pin support and a roller support. As in the small beam test, the loads on the test beam were assumed to be equal to one-half of the measured actuator load.

The support systems in both small and large beams were designed to allow beam axial growth during loading (due to cracking and damage) without generating axial forces in the beams. The roller supports consisted of a steel cylinder clamped between two steel plates whereas the pinned support consisted of a custom link that allowed rotation at one end with lateral (axial) movement restrained at both ends (see Figure 3-14).

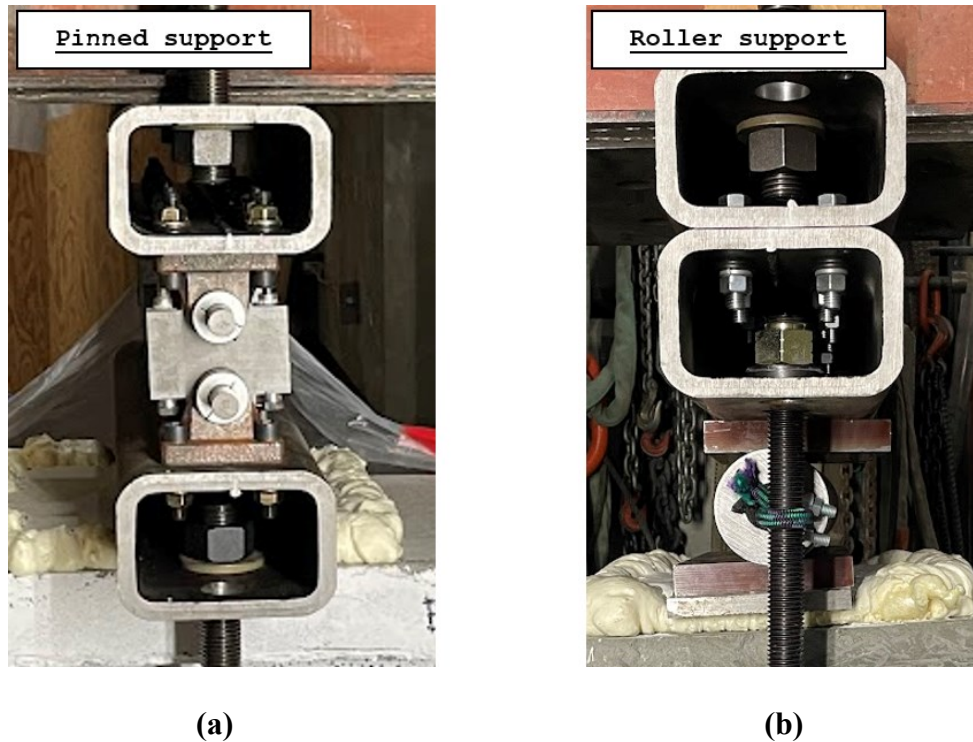


Figure 3-14: (a) Pin and (b) Roller support mechanism

3.5. Material Properties

3.5.1. Concrete

The specified compressive strength of normal weight concrete for the beam tests was 6,000 psi at 28 days. However, based on data provided by the supplier (See Table 3-4), the expected average strength at 28 and 56 days were 7,780 psi and 8,340 psi, respectively. This mix design was used to achieve the target concrete compressive strength of 8,000 psi. The complete concrete mix design details are provided in Appendix B.

Table 3-4: Concrete compressive strength results from supplier

COMPRESSIVE STRENGTH RESULTS (ASTM) C 39)

<u>Number</u>	<u>3 Days</u>	<u>7 Days</u>	<u>28 Days</u>	<u>56 Days</u>
1	5430 psi	6490 psi	7880 psi	8430 psi
2	5400 psi	6430 psi	7770 psi	8360 psi
3	5340 psi	6210 psi	7690 psi	8240 psi
Average	5390 psi	6380 psi	7780 psi	8340 psi

In the small beam tests, four-inch diameter concrete test cylinders were created for testing at 7 (2 samples), 14 (2 samples), 21 (3 samples), and 28 days (4 samples), and at test date (3 samples). The small beam tests were cast in late 2021 and tested in mid-2022. Concrete compressive strength test results for the small beam are provided in Table 3-5.

Table 3-5: Small beam concrete compressive strength results

Sample	7 Days	14 Days	21 Days	28 Days	Test Day
1	6,980 psi	7,760 psi	7,800 psi	7,938 psi	8,870 psi
2	6,830 psi	7,280 psi	8,050 psi	7,696 psi	7,610 psi
3	-	-	7,560 psi	7,267 psi	8,280 psi
Average	6,905 psi	7,520 psi	7,803 psi	7,634 psi	8,253 psi

Results of the cylinder tests for the small beam test specimens indicated average compressive strengths of 7,634 psi at 28 days and 8,253 psi at test date (8% higher). The strength gain was considered marginal and not expected to bias the test results.

In the large beam tests, four-inch diameter concrete test cylinders were also created for testing at 7 (2 samples), 15 (3 samples), and 28 days (4 samples), and at test date (3 samples). The large beams were cast in February 2023 and tested in February 2024. Concrete compressive strength test results for the large beam tests are provided in Table 3-6.

Table 3-6: Large beam concrete compressive strength results

Sample	7 Days	15 Days	28 Days	Test Day
1	6,968 psi	8,635 psi	6,987 psi	11,080 psi
2	6,828 psi	8,165 psi	8,002 psi	8,610 psi
3	-	8,176 psi	9,068 psi	11,093 psi
4	-	-	7,942 psi	-
Average	6,898 psi	8,325 psi	7,999 psi	10,261 psi

Results of the cylinder tests indicated average compressive strengths of 7,999 psi at 28 days and 10,261 psi at test date (28% higher). The higher compressive strength at test date was due to the long delay in testing (Phase I wall tests were prioritized over the large beam tests). The higher test date strength was deemed acceptable because the development length in ACI 318-19 is proportional to the square root of f'_c ($\sqrt{10,261/7,999} = 1.13$), and thus, results in only a modest decrease in development length. As well, for PBWD, use of expected material properties at approximately one year or longer are typically recommended (LATBSDC, 2023)

The stress versus strain relations for the cylinder tests at 28 days and at test date for both small and large beam tests are shown in Figure 3-15.

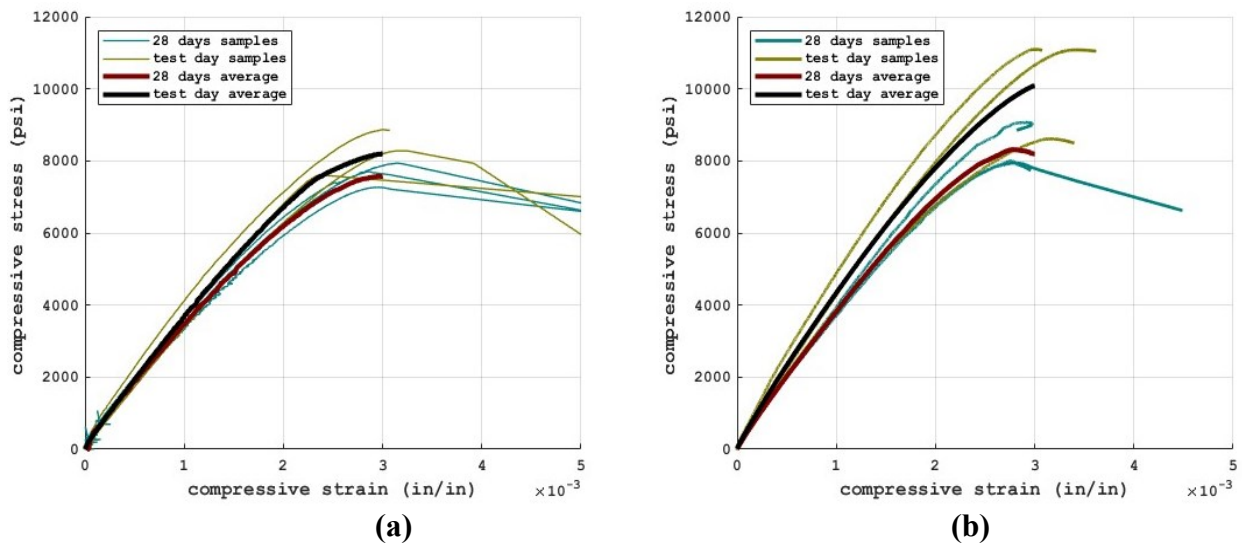


Figure 3-15: Unconfined concrete stress-strain curve: (a) small beams; (b) large beams

3.5.2. Steel Reinforcements

A summary of the properties for steel reinforcement is provided in Table 3-7.

Table 3-7: Steel reinforcement properties in the beam specimens

Steel Reinforcement		Rebar Properties	
		Small beam	Large beam
Longitudinal		#4 Grade 80	#8 Grade 80
Transverse	In Splice Region	#2 Grade 60	#4 Grade 60
	Outside of Splice	#4 Grade 80	#4 Grade 80

A total of seven samples of three #4 (small beam) and four #8 (large beam) Grade 80 rebars were tested to obtain stress versus strain relations. For subsequent calculations, a trilinear fit to the average of the test results was used (See Table 3-8 and Figure 3-16); the relevant strain range for the beam tests is also shown on Figure 3-16.

Table 3-8: Trilinear fit of rebar stress-strain curve

Strain (in/in)	Stress (ksi)
0	0
0.0043	88.1
0.0125	88.1
0.048	111.975
0.15	111.975

The maximum expected steel strain was calculated based on the maximum strain demands in the wind-loading protocol at $3\Theta_y$ wall demand ($6.82\varepsilon_y$; See Table 3-2) which corresponded to a strain value of 0.0207 ($\varepsilon_y = 88.1 \text{ ksi} / 29,000 \text{ ksi} = 0.00304$). A trilinear fit of the measured rebar stress-strain curve was adjusted so that the fit was representative of the test results up until the maximum expected steel strain expected from the wind-loading protocol (See Figure 3-16).

The summary of the #4 and #8 Grade 80 rebar test results is provided in Table 3-9.

Table 3-9: Summary of #4 and #8 Grade 80 rebar tests

Size	Sample	f_y (ksi)	f_u (ksi)	E_s (ksi)	ϵ_y (in/in)
#4	1	89.1	111.5	29000	0.00307
	2	87.7	110.1	29000	0.00302
	3	87.5	110.2	29000	0.00302
#8	1	88.7	112.3	29000	0.00306
	2	88.2	111.7	29000	0.00304
	3	88.5	112.0	29000	0.00305
	4	88.4	111.9	29000	0.00305

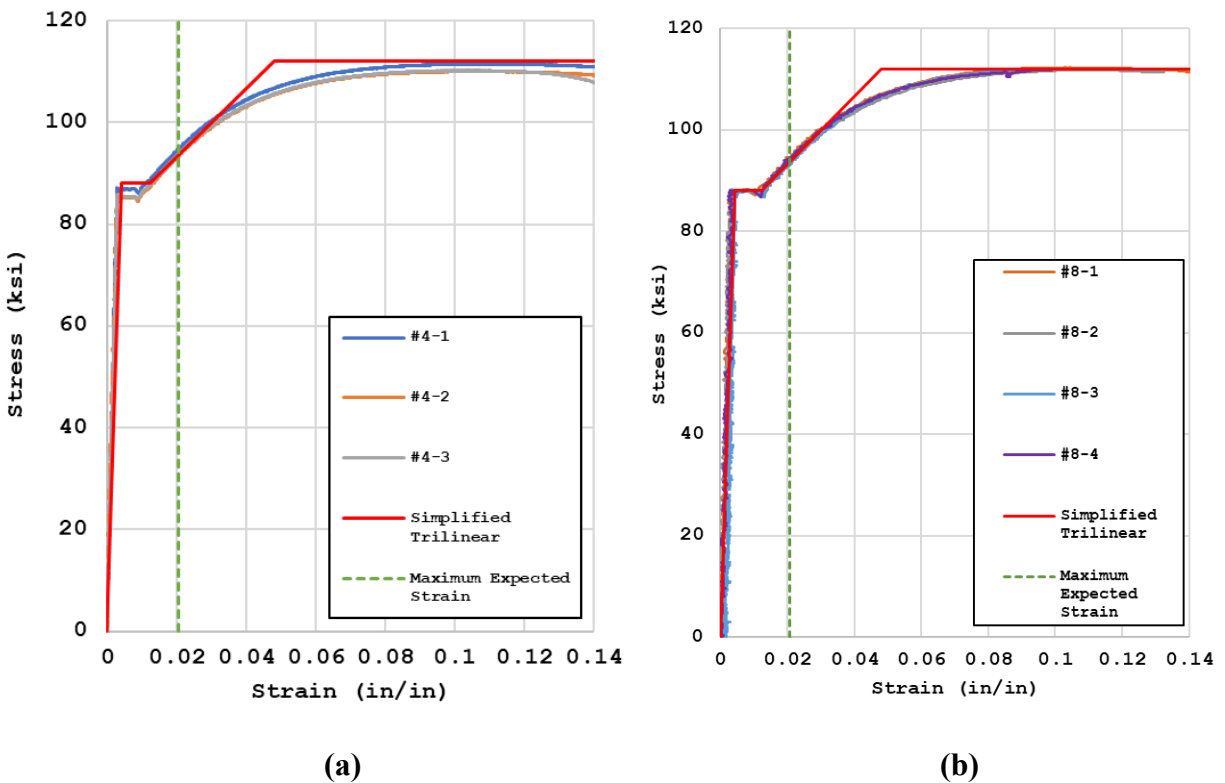


Figure 3-16: Rebar stress-strain relations: (a) #4 Grade 80; (b) #8 Grade 80

Stirrups in the splice region were #2 (small beam) and #4 (large beam) Grade 60 bars. As the splice was in a region of constant moment (zero shear), stirrups were only used to provide confinement to the splice length. Outside of the constant moment region, #4 Grade 80 stirrups were used to (conservatively) prevent shear failure in this region. As stirrups were expected to remain elastic, coupon tests of these bars to determine stress–strain relations were not performed.

3.6. Fabrication of Test Specimens

The fabrication of the beam specimens started with rebar cage assembly using two sawhorses to elevate the top longitudinal rebars. Next, several stirrups were slid into the splice region and tied in place. These stirrups helped to maintain the stability and shape of the beam reinforcement when the splice bottom longitudinal rebars were set into place. After the bottom rebars were tied to the stirrups, the rest of the stirrups were slid into place and tied in place. Photos of the finished rebar cages are shown in Figure 3-17.



Figure 3-17: Rebar cage assembly of large beam specimens

The finished rebar cages were then placed inside the formwork with rebar chairs attached to the bottom stirrups to provide the prescribed value of concrete cover (See Figure 3-18(a)). A series of threaded rods were also inserted through the formwork and beam, perpendicular to the longitudinal axes of the beam (See Figure 3-18(a)), to be used as the anchorages for LVDTs and wire potentiometers (WPs) used to measure average strains in the splice region (See Section 3.7). Subsequently, concrete was placed in the forms for both beams (See Figure 3-18(b)) and removed after the concrete has hardened (See Figure 3-19).



(a)



(b)



(c)

Figure 3-18: Beam construction: (a) rebar chairs and threaded rods in large beams; (b) concrete placement and pouring of large beams; (c) small beam rebar cages in formwork



Figure 3-19: Formwork removal of large beams

Finally, the beams were painted white using a watered-down paint. In the large beam specimens, a roller was used to apply a random black speckle pattern to one beam web surface to allow for use of digital image correlation (DIC) analysis (See Figure 3-20).



Figure 3-20: Finished large beam specimens with paint for DIC

3.7. Instrumentation

3.7.1. Average Concrete Longitudinal Strains: LVDTs

For the small beam test, twelve linear variable differential transformers (LVDT), with ± 1 in. of linear range, were used to measure the average concrete strains within the constant moment region of the beam test specimens. The LVDTs were installed in pairs, at the top and bottom beam surfaces over a length of 8 inches and with perpendicular distance of 8 inches between the LVDT pairs (See Figure 3-21).

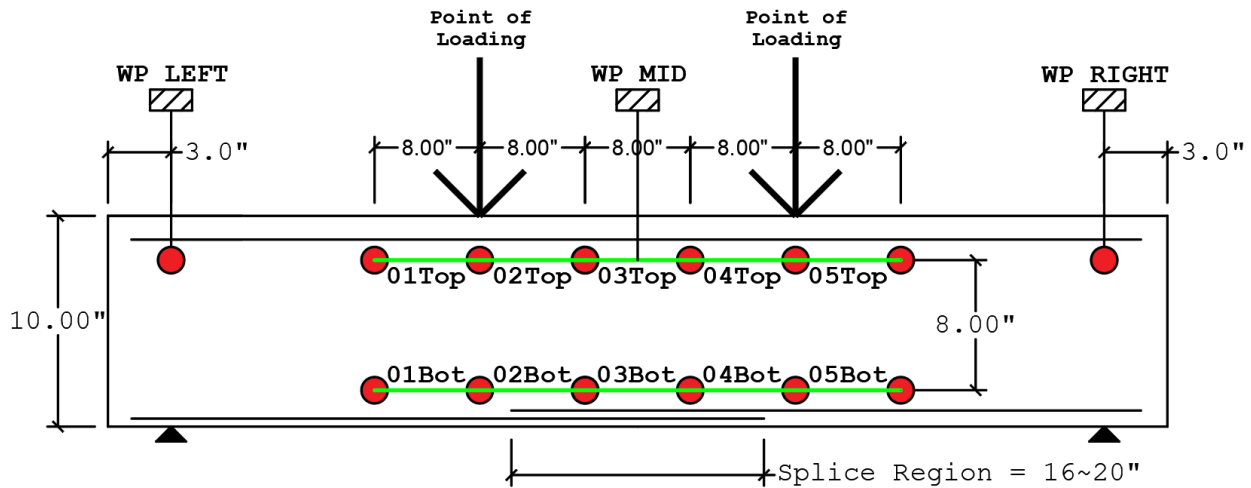


Figure 3-21: Small beam LVDTs and WPs locations

In the large beam tests, eight linear variable differential transformers (LVDT), with ± 1 in. of linear range, were used to measure the average concrete strains within the constant moment region of the beam test specimens. The LVDTs were installed in pairs, at the top and bottom beam surfaces over a length of 10 inches and with perpendicular distance of 12 inches between the LVDT pairs (See Figure 3-22). A 0.5-inch offset was applied to the bottom LVDTs cores to accommodate larger elongation due to higher tensile strain demands in the splice (0.5-inch contraction capacity, 1.5-inch elongation capacity).

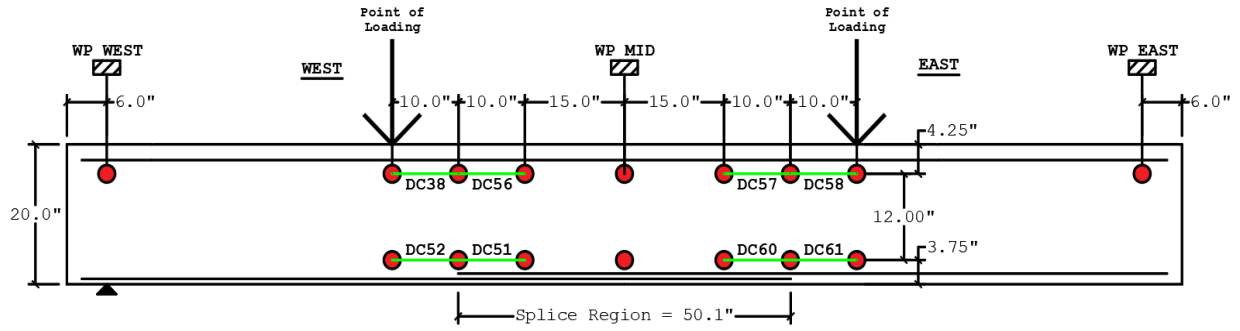


Figure 3-22: Large beam LVDTs and WPs locations



(a)



(b)

Figure 3-23: (a) LVDTs and (b) Attachment to the beam specimens

3.7.2. Beam Vertical Displacements: Wire Potentiometers (WPs)

Three WPs were also used for both small and large beam test programs; two were installed at the beam specimen supports and one was installed at the middle span to measure beam vertical displacements (See Figure 3-22 and Figure 3-24).



Figure 3-24: Vertical WPs attachment to the beam specimens

3.7.3. Beam Axial Elongation: Wire Potentiometers (WPs)

In the large beam specimens, additional WPs were used at the beam ends to measure axial elongations (See Figure 3-25).

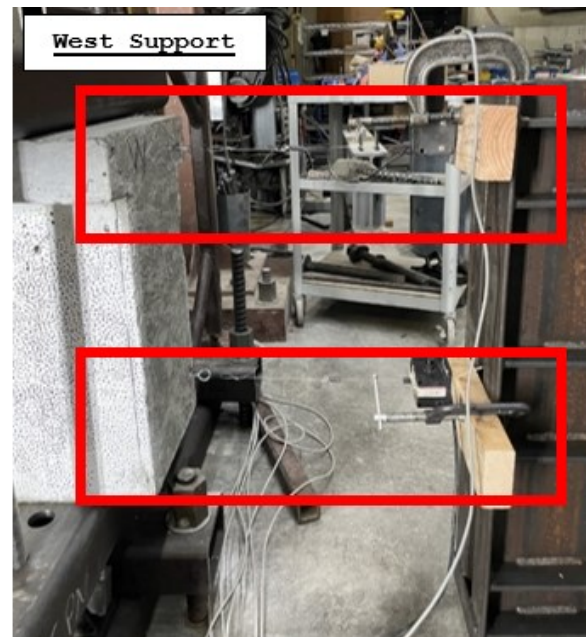


Figure 3-25: Horizontal WPs attachment to the beam specimens

3.7.4. Digital Image Correlation (DIC)

In the large beam test program, DIC was also used during testing with results post-processed to determine to measure strains along the vertical face (web) of the beam and to assess crack patterns, particularly at small loading amplitudes. The beams were painted white, and a random black speckle pattern was applied with a paint roller (See Figure 3-26(a)). During testing, cameras were placed to capture the deformations within the splice region (See Figure 3-26(b)).

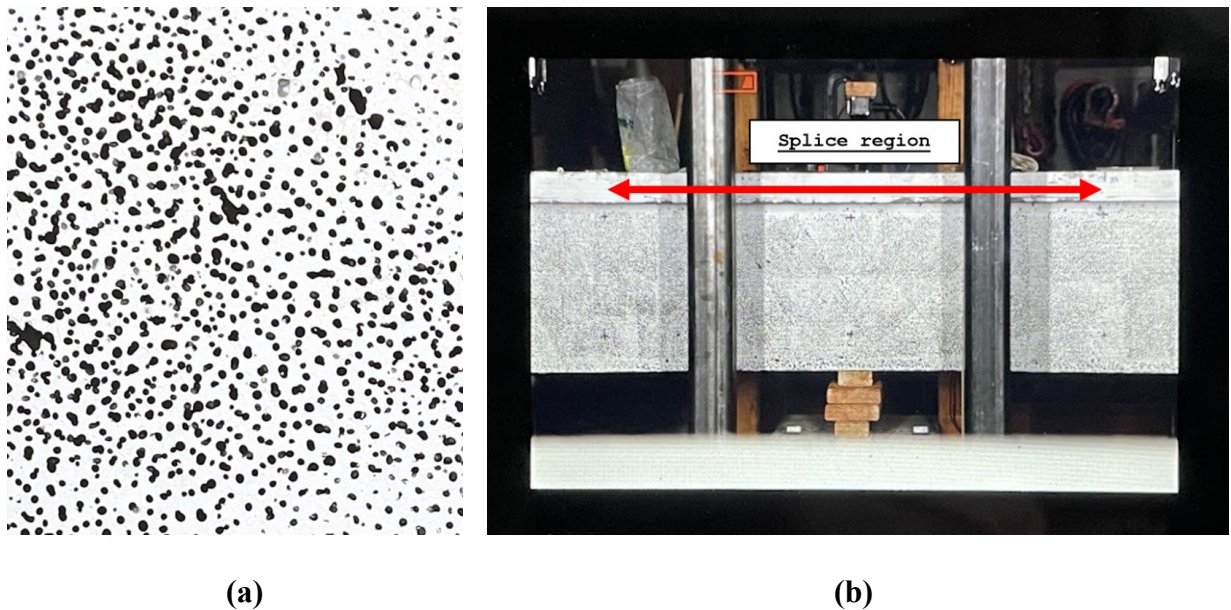


Figure 3-26: Digital Image Correlation (DIC): (a) speckle pattern; (b) camera field of view

Photos were taken at zero load, peak positive bending load (tensile strain demands in the splice), and peak negative bending load (compressive strain demands in the splice) during the application of the loading protocol. These pictures were then post-processed using Digital Image Correlation Engine (DICE) and Paraview 5.9.1 to provide strain fields and crack patterns.

3.7.5. Additional Instrumentations/Documentations

In the small beam test setup, the measurement of displacement and force of the actuator was integrated in the testing device using axial-force based load cell (See Figure 3-27(a)). In the large beam test setup, an AC LVDT was installed to measure the actuator displacement and shear-

force based load cell was installed to measure the actuator force (See Figure 3-27(b)). This measurement helped to automate the loading procedures, especially given the large number cycles (500 and 75 cycles) associated with the wind loading protocol. During the inelastic cycles of the loading protocol of the large beam test program, video documentation was used to help identify failure modes.

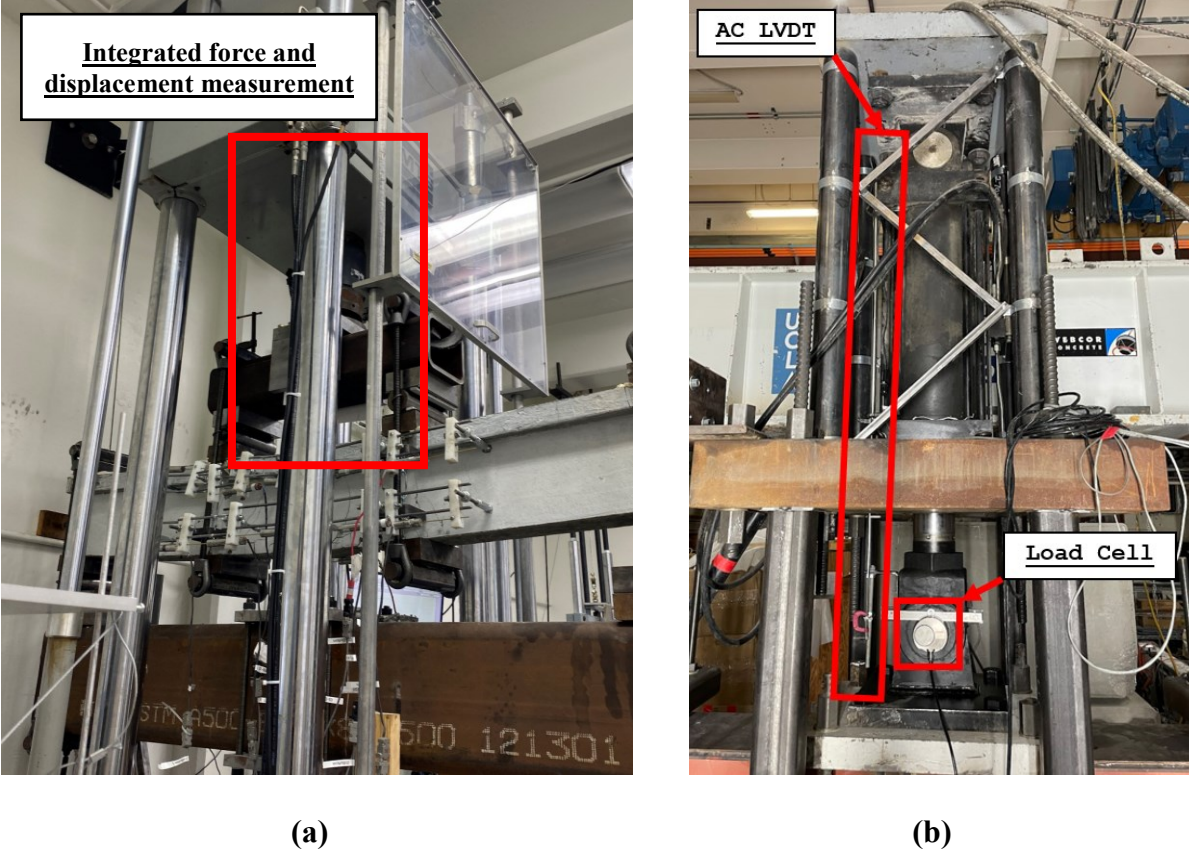


Figure 3-27: Force and displacement measurement: (a) small beam test setup; (b) large beam test setup

4. Results and Discussions

This section presents results for the three small beam and two large beam tests. SB-S3-20 is a companion test to LB-S7.5-50 (a_{sp} values of 1.15 and 1.25), and SB-S2-20 is a companion test to LB-S5-50 (a_{sp} values of 1.73 and 1.88). Table 4-1 provides a summary of predicted and measured beam yield and nominal flexural strengths, and yield displacement.

Table 4-1: Sectional strength properties - analytical v. experiment

Parameters	Small Beam Test Specimens				Large Beam Test Specimens		
	Analytical	Experiment			Analytical	Experiment	
		SB-S6-16	SB-S3-20	SB-S2-20		LB-S7.5-50	LB-S5-50
M_y^+ (kip-ft)	24.4	failed before yield	24.8	24.8	190.4	179.0	181.2
δ_y^+ (in)	0.26	failed before yield	0.32	0.33	0.71	0.97	1.02
M_n^+ (kip-ft)	26.1	failed before yield	30.7	31.5	216.0	206.4	210.0

In Table 4-1, M_y is the yield moment, δ_y is the yield displacement, and M_n is the nominal moment. Analytical values for M_y and M_n are based on an assumed linear concrete stress-strain relation and a Whitney Stress Block (ACI 318-19 Chapter 22.2.2.1), respectively; the experimental values are estimated based on a multilinear fit to the test backbone relation. In this case, M_n is the maximum moment observed in the test. Table 4-2 through Table 4-6 present summaries of the experiment results for each beam test.

Table 4-2: Experiments summary and results for SB-S6-16

Wall Wind Loading Protocol	Small Beam Wind Loading Protocol		SB-S6-16			
			Number of Cycles	Peak Load (Downwards)	Peak Load (Upwards)	Peak Downwards Displacements
0.4 M_{pr}	0.31 M_{pr}^+	0.28 M_{pr-}	500 cycles	9.4 kips	25.1 kips	0.17 inch
0.75 M_{pr}	0.79 M_{pr}^+	0.51 M_{pr-}	6 cycles (failed at 3rd)	22.6 kips	46.0 kips	0.33 inch
1.2 Θ_y	1.6 δ_y	0.64 M_{pr-}	-	-	-	-
1.5 Θ_y	2.0 δ_y	0.72 M_{pr-}	-	-	-	-
2.0 Θ_y	3.0 δ_y	0.72 M_{pr-}	-	-	-	-
2.5 Θ_y	4.0 δ_y	0.72 M_{pr-}	-	-	-	-
3.0 Θ_y	5.0 δ_y	0.72 M_{pr-}	-	-	-	-

Table 4-3: Experiments summary and results for SB-S3-20

Wall Wind Loading Protocol	Small Beam Wind Loading Protocol		SB-S3-20			
			Number of Cycles	Peak Load (Downwards)	Peak Load (Upwards)	Peak Downwards Displacements
0.4 M_{pr}	0.31 M_{pr+}	0.28 M_{pr-}	500 cycles	9.7 kips	25.0 kips	0.11 inch
0.75 M_{pr}	0.79 M_{pr+}	0.51 M_{pr-}	75 cycles	22.5 kips	46.0 kips	0.31 inch
1.2 Θ_y	1.6 δ_y	0.64 M_{pr-}	10 cycles	26.2 kips	57.4 kips	0.50 inch
1.5 Θ_y	2.0 δ_y	0.72 M_{pr-}	6 cycles	27.5 kips	65.0 kips	0.66 inch
2.0 Θ_y	3.0 δ_y	0.72 M_{pr-}	4 cycles	30.2 kips	65.0 kips	0.97 inch
2.5 Θ_y	4.0 δ_y	0.72 M_{pr-}	2 cycles (failed at 2nd)	30.5 kips	65.0 kips	1.29 inch
3.0 Θ_y	5.0 δ_y	0.72 M_{pr-}	-	-	-	-

Table 4-4: Experiments summary and results for SB-S2-20

Wall Wind Loading Protocol	Small Beam Wind Loading Protocol		SB-S2-20			
			Number of Cycles	Peak Load (Downwards)	Peak Load (Upwards)	Peak Downwards Displacements
0.4 M_{pr}	0.31 M_{pr+}	0.28 M_{pr-}	500 cycles	9.0 kips	24.0 kips	test setup error
0.75 M_{pr}	0.79 M_{pr+}	0.51 M_{pr-}	75 cycles	24.8 kips	46.0 kips	test setup error
1.2 Θ_y	1.6 δ_y	0.64 M_{pr-}	10 cycles	26.2 kips	57.9 kips	0.54 inch
1.5 Θ_y	2.0 δ_y	0.72 M_{pr-}	6 cycles	27.4 kips	65.0 kips	0.73 inch
2.0 Θ_y	3.0 δ_y	0.72 M_{pr-}	4 cycles	29.1 kips	65.0 kips	1.00 inch
2.5 Θ_y	4.0 δ_y	0.72 M_{pr-}	4 cycles	30.9 kips	65.0 kips	1.33 inch
3.0 Θ_y	5.0 δ_y	0.72 M_{pr-}	2 cycles	31.0 kips	65.0 kips	1.67 inch

Table 4-5: Experiments summary and results for LB-S7.5-50

Wall Wind Loading Protocol	Large Beam Wind Loading Protocol		LB-S7.5-50			
			Number of Cycles	Peak Load (Downwards)	Peak Load (Upwards)	Peak Downwards Displacements
0.4 M_{pr}	0.18 M_{pr+}	0.32 M_{pr-}	500 cycles	20.0 kips	41.1 kips	0.14 inch
0.75 M_{pr}	0.79 M_{pr+}	0.63 M_{pr-}	40 cycles	96.4 kips	78.9 kips	0.92 inch
1.2 Θ_y	1.38 δ_y	0.63 M_{pr-}	10 cycles	99.2 kips	78.9 kips	1.40 inch
1.5 Θ_y	1.77 δ_y	0.63 M_{pr-}	6 cycles	108.4 kips	78.9 kips	1.77 inch
2.0 Θ_y	2.53 δ_y	0.63 M_{pr-}	4 cycles	110.8 kips	78.9 kips	2.58 inch
2.5 Θ_y	3.81 δ_y	0.63 M_{pr-}	4 cycles (failed at 4th)	115.3 kips	78.9 kips	3.83 inch
3.0 Θ_y	4.71 δ_y	0.63 M_{pr-}	-	-	-	-

Table 4-6: Experiments summary and results for LB-S5-50

Wall Wind Loading Protocol	Large Beam Wind Loading Protocol		LB-S5-50			
			Number of Cycles	Peak Load (Downwards)	Peak Load (Upwards)	Peak Downwards Displacements
0.4 M_{pr}	0.18 M_{pr+}	0.32 M_{pr-}	500 cycles	20.0 kips	41.1 kips	0.17 inch
0.75 M_{pr}	0.79 M_{pr+}	0.63 M_{pr-}	40 cycles	96.4 kips	78.9 kips	1.01 inch
1.2 Θ_y	1.38 δ_y	0.63 M_{pr-}	10 cycles	99.5 kips	78.9 kips	1.42 inch
1.5 Θ_y	1.77 δ_y	0.63 M_{pr-}	6 cycles	106.3 kips	78.9 kips	1.85 inch
2.0 Θ_y	2.53 δ_y	0.63 M_{pr-}	4 cycles	111.0 kips	78.9 kips	2.59 inch
2.5 Θ_y	3.81 δ_y	0.63 M_{pr-}	4 cycles	111.1 kips	78.9 kips	3.85 inch
3.0 Θ_y	4.71 δ_y	0.63 M_{pr-}	2 cycles	117.8 kips	78.9 kips	4.78 inch

The small beam specimen, SB-S6-16 (a_{sp} value of 0.46), with minimum ACI 318-19 splice length (16 in., see Section 3.2) and transverse reinforcement spaced at 6 in. displayed splice failure at the 3rd cycle of 0.75 wall M_{pr} , which was below the expected yield strength (93% M_y). Strength loss was observed for LB-S7.5-50 during the 4th cycle to 2.5 Θ_y (prior to completing the wind loading protocol). This result was similar to small beam test (SB-S3-20); a_{sp} values were 1.25 for LB-7.5-50 and 1.15 for SB-S3-20. The wind loading protocol was completed for LB-S5-50 and then the beam was loaded monotonically to a displacement ductility demand of 7.25, where strength loss was observed due to cover loss and concrete crushing in the beam end spans at shear stress demand of $3.5\sqrt{f'_c}$. If this failure did not occur, a bar rupture failure, as observed for SB-S2-20, would likely have occurred. Additional details are provided in the following subsections.

4.1. Observed Damage and Cracking

SB-S6-16 displayed splice failure before reaching the expected yield strength with horizontal cracks forming along the splice region (See Figure 4-1). Figure 4-2 shows the beam condition at the end of test with concrete spalling starting from the right side of the splice and then propagated towards the left side of the splice. Figure 4-3 shows the gap formed at the end of the splice due to bar slip.

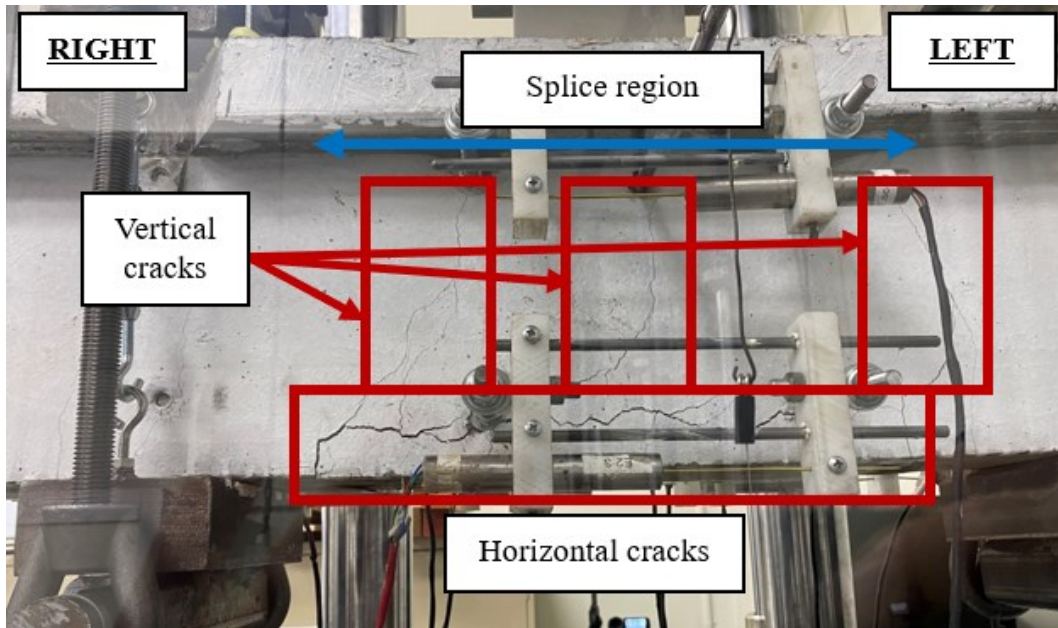


Figure 4-1: Horizontal cracks in the splice region of SB-S6-16

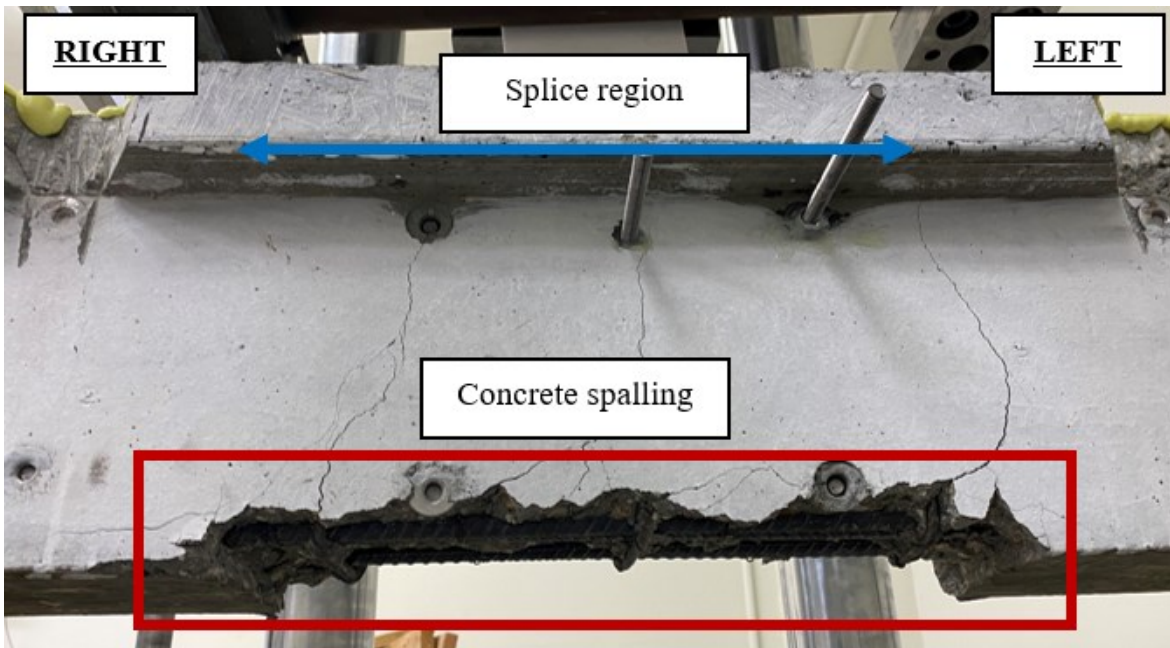


Figure 4-2: SB-S6-16 at the end of test

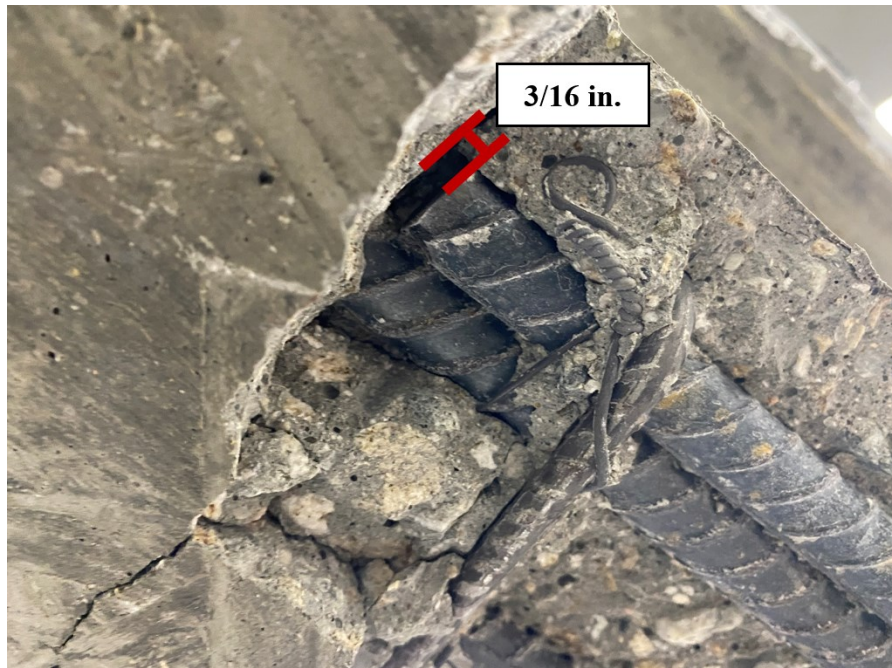


Figure 4-3: Slip at the end of spliced bars (SB-S6-16)

SB-S3-20 displayed splice failure at $2.5\Theta_y$ wall demand with vertical cracks forming along the splice region and followed by horizontal cracks (Figure 4-4). Figure 4-5 shows the amount of slip occurred in the splice which was 67% higher than SB-S6-16. Figure 4-6 displays the beam condition at the end of the test with concrete spalling over the splice length.

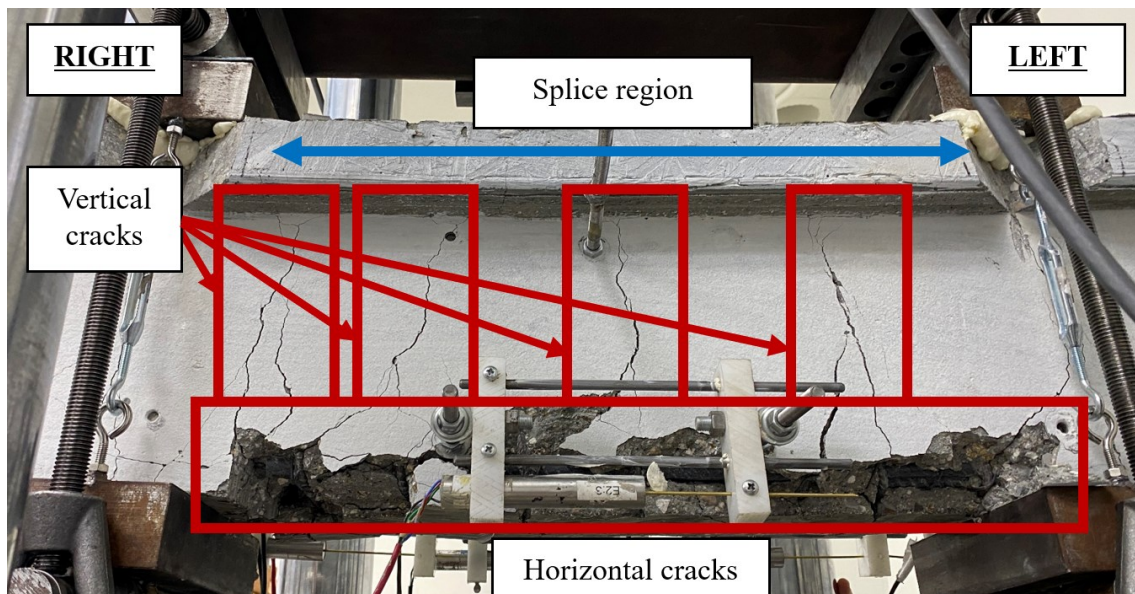


Figure 4-4: Horizontal cracks in the splice region of SB-S3-20

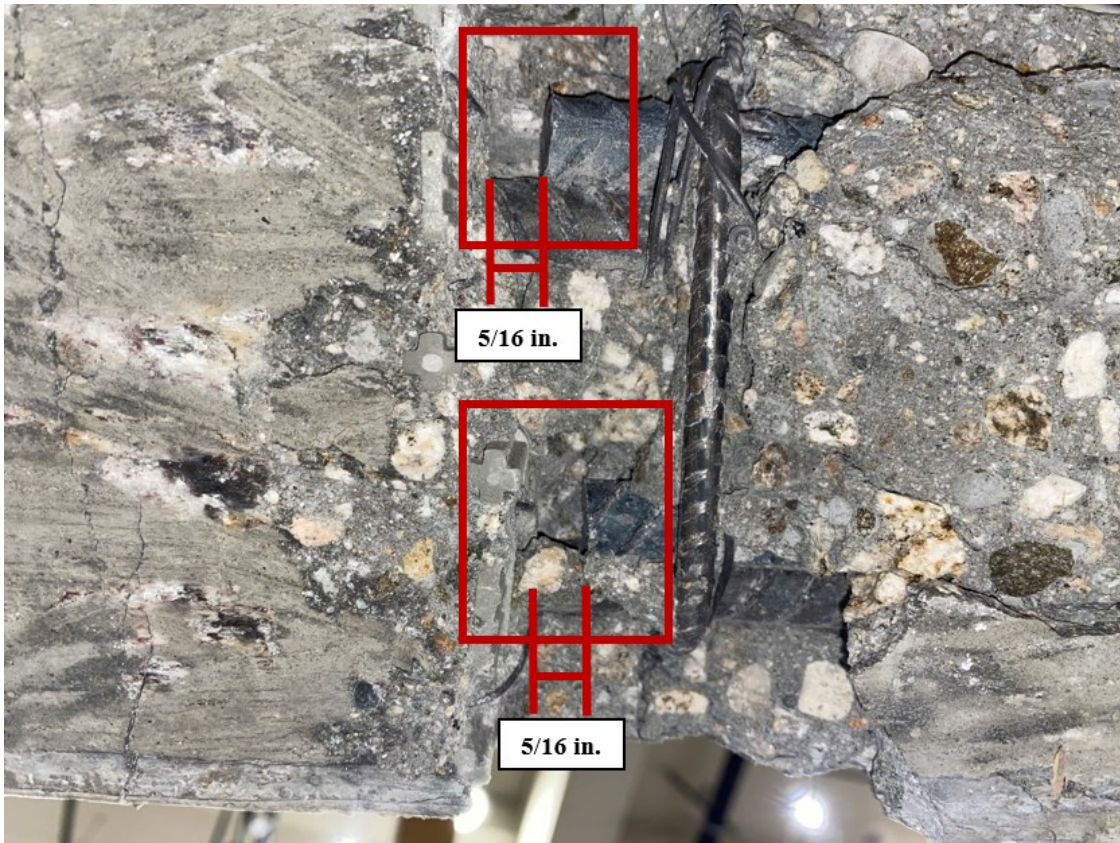


Figure 4-5: Slip at the end of splice bars (SB-S3-20)

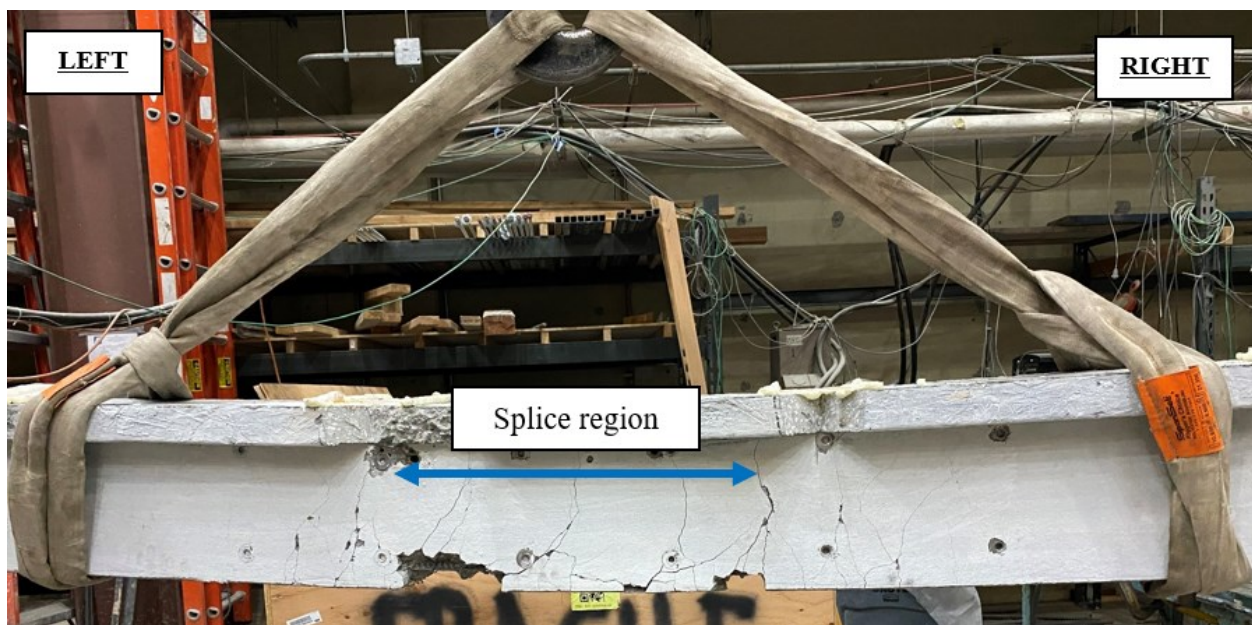


Figure 4-6: SB-S3-20 at the end of the test

SB-S2-20 displayed no damage in the splice region at the end of the wind-loading protocol (See Figure 4-7). Figure 4-8 shows minor horizontal cracks at the end of the splice due to minor slip when the splice was engaged; this is expected in spliced bars. No damage was observed in the splice region until the end of the wind-loading protocol.

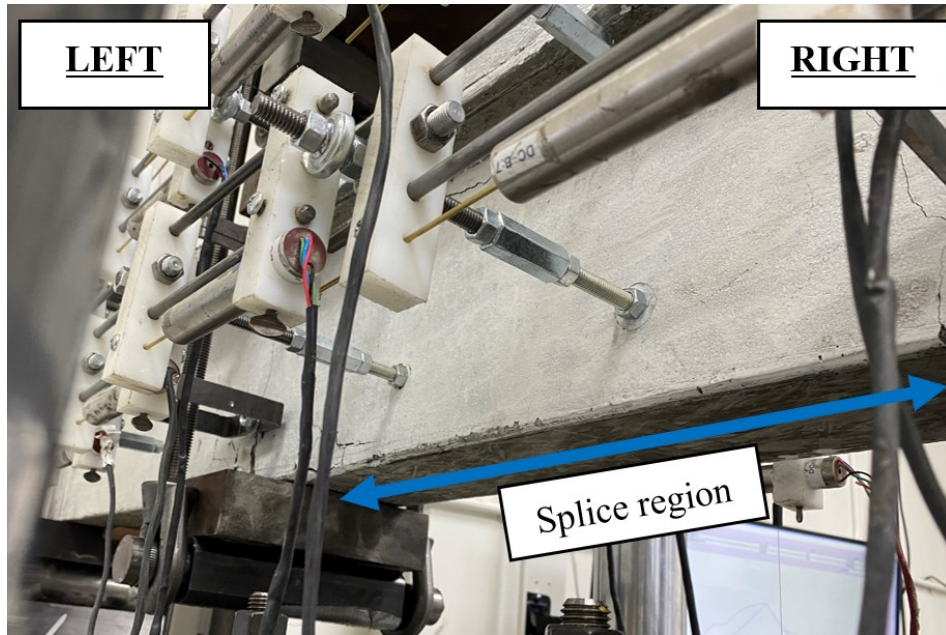


Figure 4-7: SB-S2-20 at the end of the wind-loading protocol

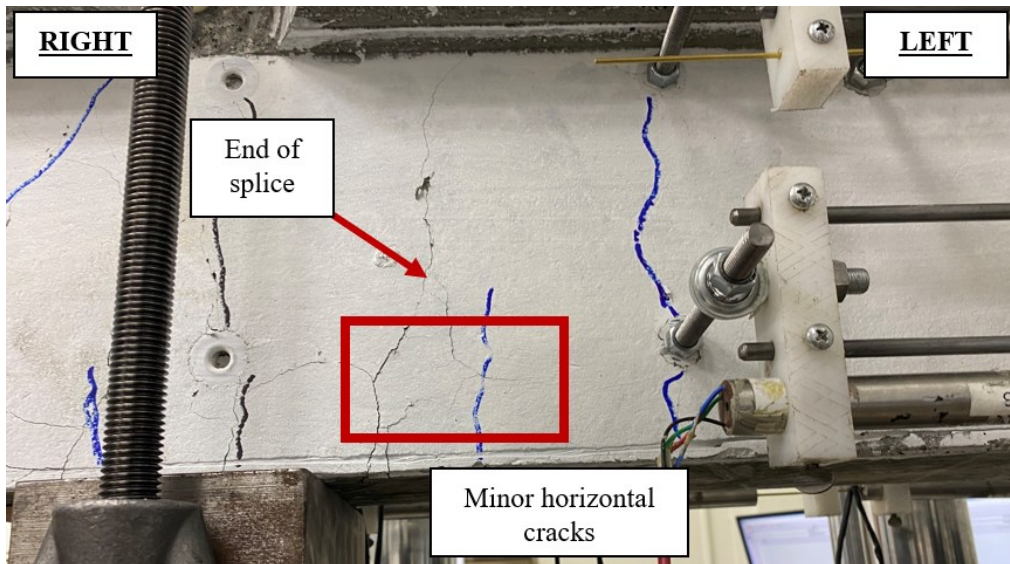


Figure 4-8: Minor horizontal cracks at ends of splice (SB-S2-20)

SB-S2-20 then underwent a seismic-loading protocol until failure. Figure 4-9 shows the large vertical cracks forming at the ends of the splice, where stirrups were located, after completion of the test. No splice failure was observed in this specimen; bar fracture occurred at a displacement ductility demand of 12 (Figure 4-10). Figure 4-11 shows the beam condition at the end of the test.

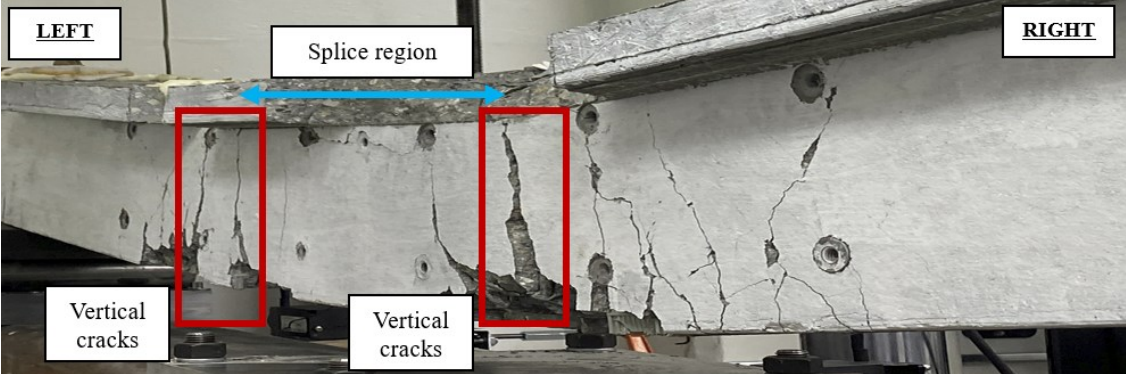


Figure 4-9: Large vertical cracks at splice ends of SB-S2-20

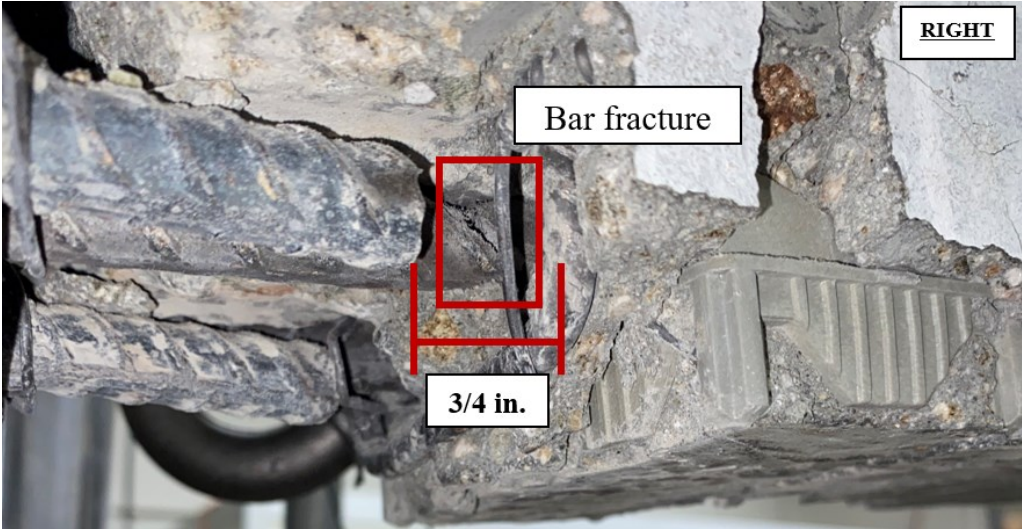


Figure 4-10: Bar fracture failure on SB-S2-20



Figure 4-11: SB-S2-20 at the end of the test

LB-S7.5-50 splice damage initiated at the ends of the splice where vertical cracks were observed. Subsequently, horizontal cracks were observed along the spliced bars at $2.5\Theta_y$ wall demand, indicative of splice slip (See Figure 4-12). This specimen displayed similar damage and cracks to SB-S3-20. Bar rupture was not observed until the end of the test (See Figure 4-13).

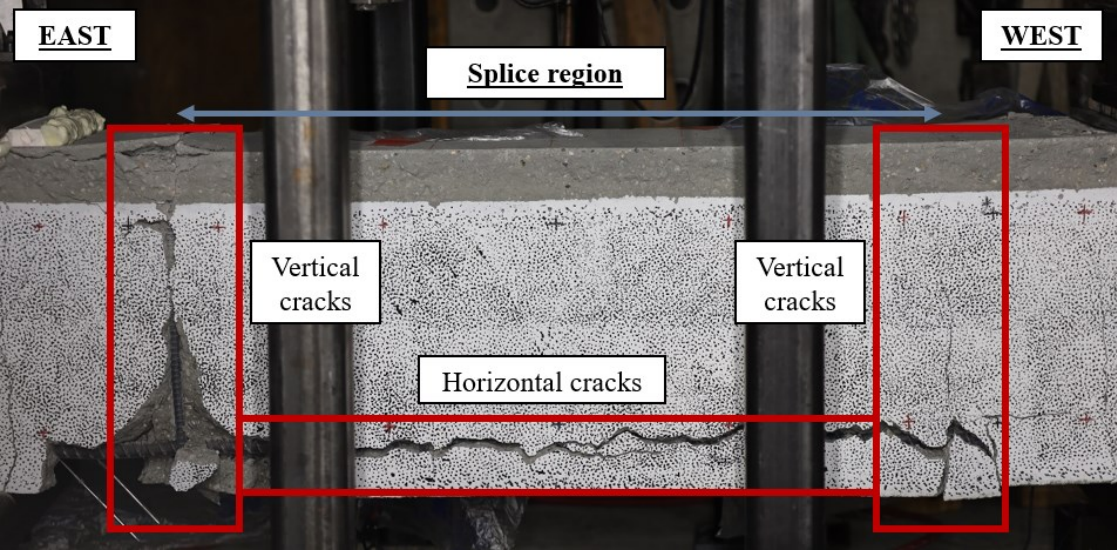


Figure 4-12: LB-S7.5-50 splice failure @4th cycle of $2.5\Theta_y$

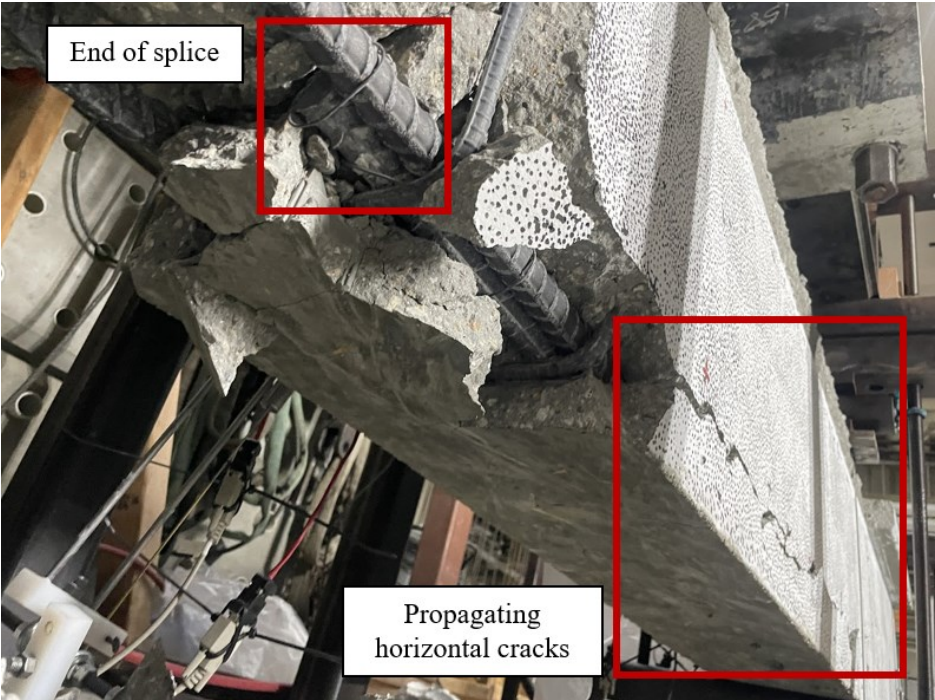


Figure 4-13: LB-S7.5-50 failure detail

A more detailed description of the progression of LB-S7.5-50 damage under the wind-loading protocol is displayed in Figure 4-14.

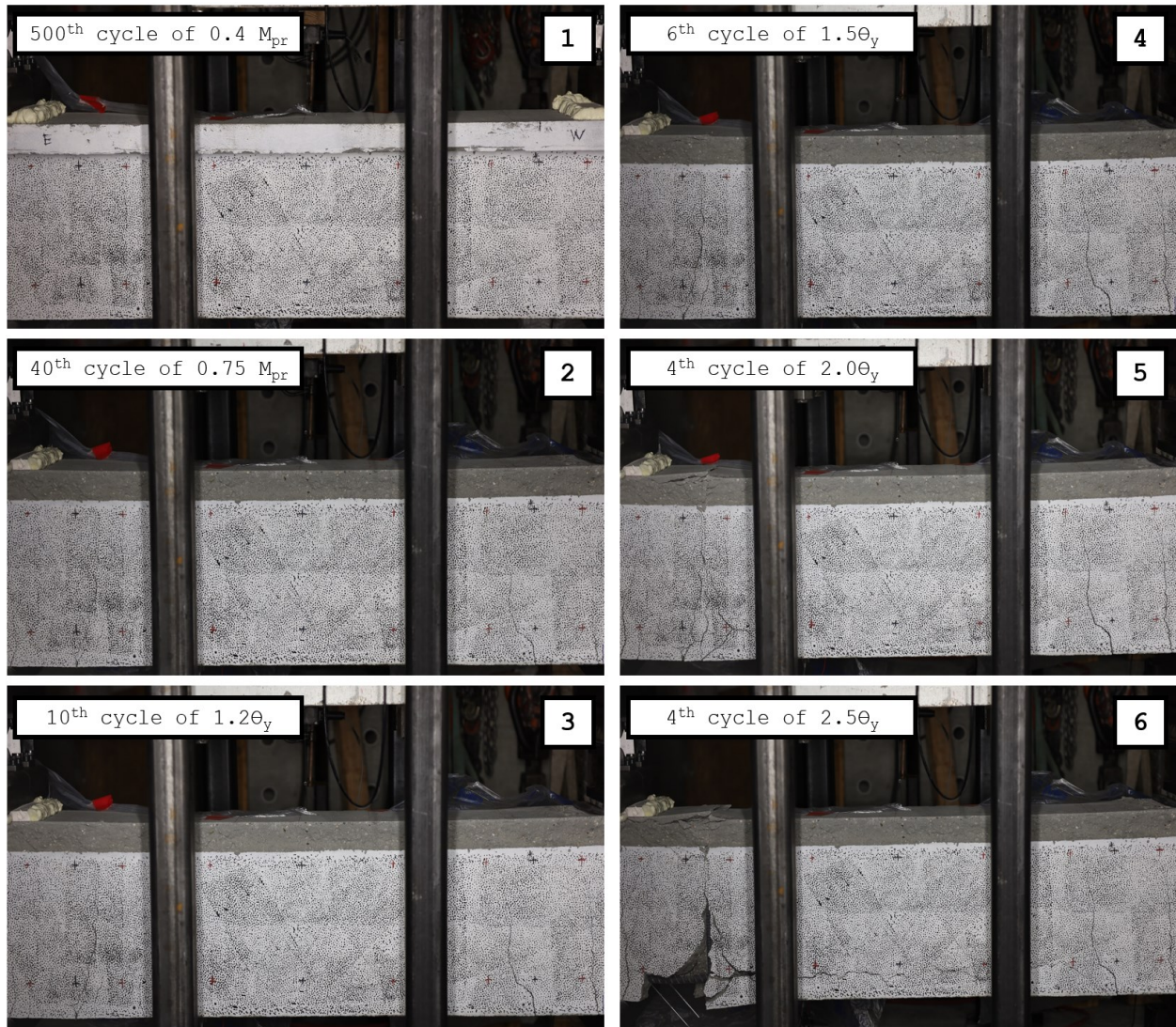


Figure 4-14: LB-S7.5-50 at the end of each loading stage (WLP)

LB-S5-50 exhibited similar cracks and damage patterns to SB-S2-20, with large vertical cracks forming at the ends of the splice, where stirrups were located (Figure 4-15). Minor horizontal cracks formed at the ends of the splice. No strength loss was observed at the end of the wind-loading protocol.

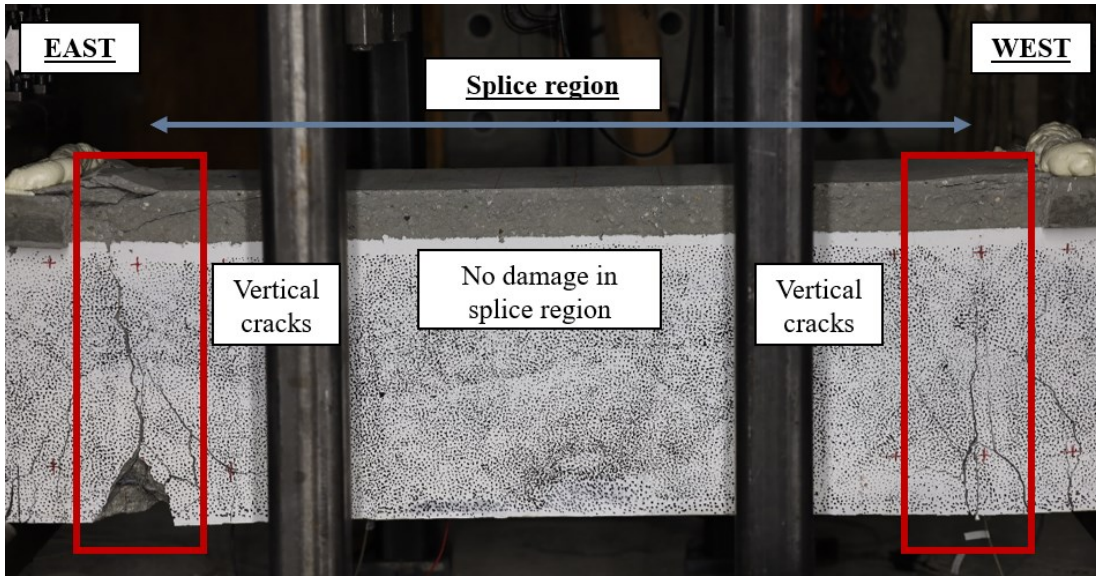


Figure 4-15: LB-S5-50 at the end of the wind-loading protocol

A monotonic push was performed instead of a seismic-loading protocol due to large residual displacement in the specimen (See Section 4.2). Figure 4-16 shows the aftermath of the monotonic push to a total midspan displacement of 7.4 inches. The test was stopped due to cover loss/concrete crushing just outside of the constant moment region where shear force was present. Even so, no splice failure occurred during the monotonic push for LB-S5-50; bar fracture failure would be expected in this specimen (similar to SB-S2-20) if no concrete crushing occurred.

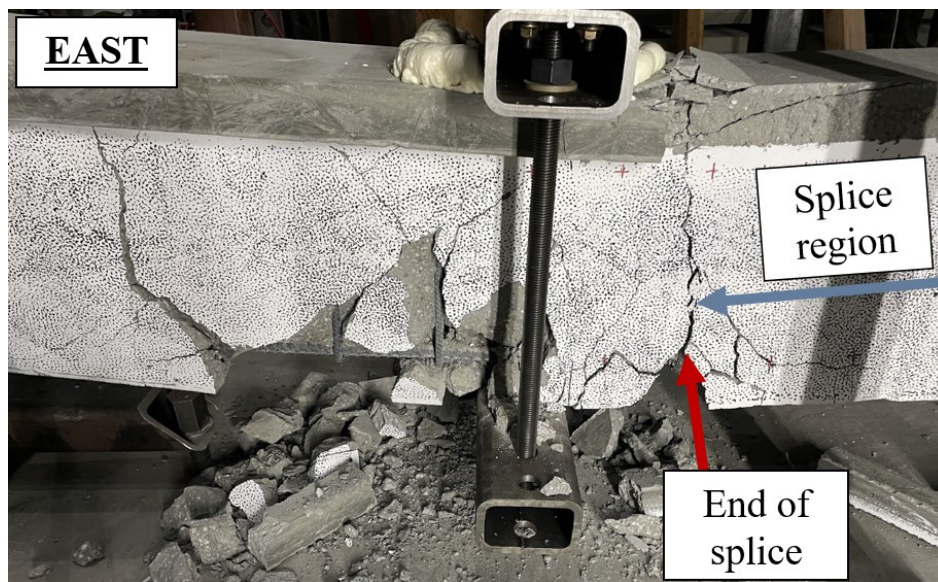


Figure 4-16: LB-S5-50 at the end of the monotonic push

A more detailed description of the progression of LB-S5-50 damage under the wind-loading protocol is displayed in Figure 4-17.

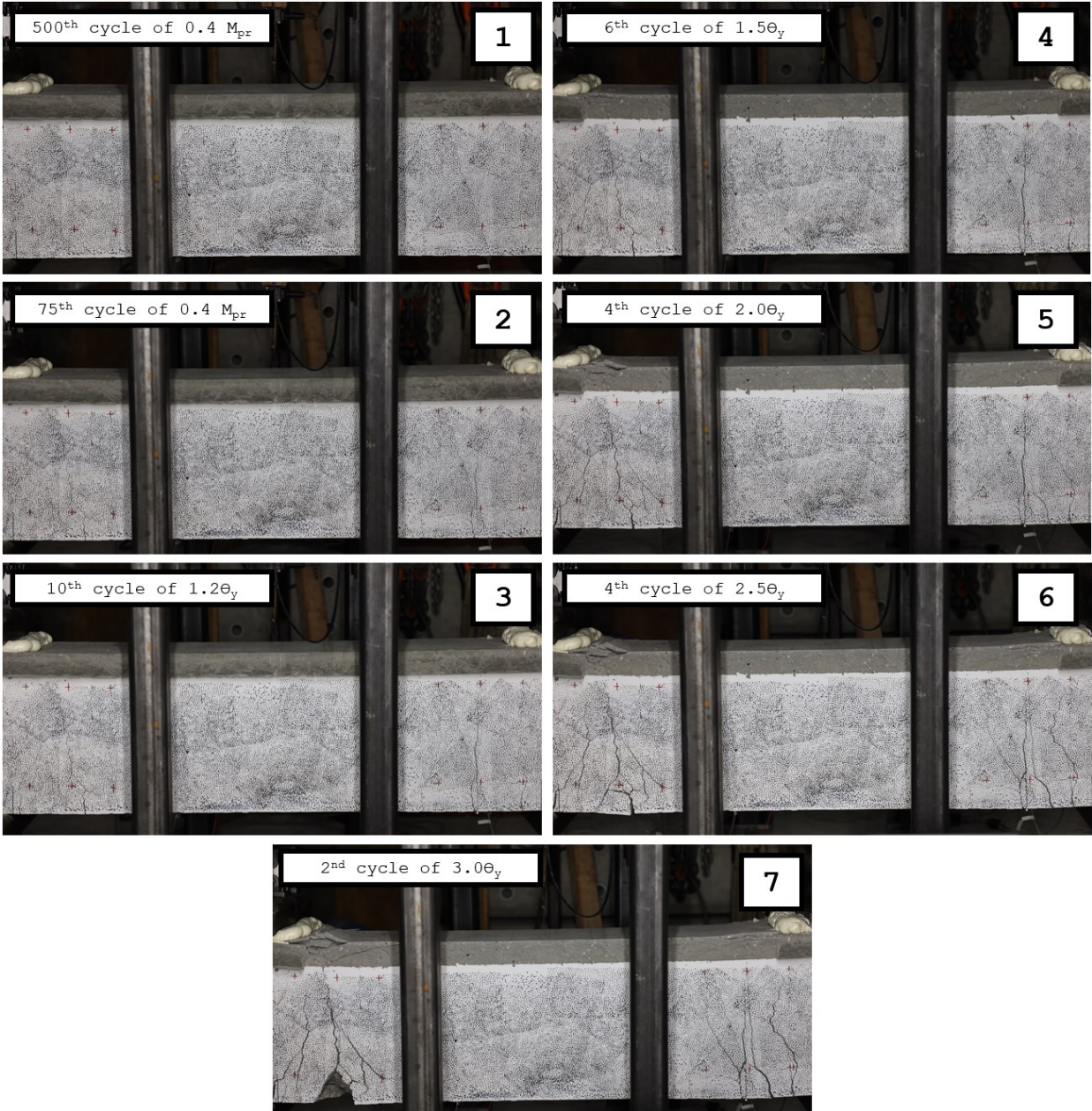


Figure 4-17: LB-S5-50 at the end of each loading stage (WLP)

4.2. Load-Deformation Responses

Predicted and experimental results for load (and moment within the splice region) versus total midspan displacement for the small and large beams are plotted in Figure 4-18 through Figure 4-19. The predicted relations are based on monotonic loading whereas the experiment relations are for the applied loading protocol. The midspan displacement at yield for SB-S3-20, SB-S2-20, LB-S7.5-50, and LB-S5-50 were larger than the predicted values given in Table 4-1, likely because of the cyclic loading protocol applied in the experiment with 500 cycles applied at 0.4 wall M_{pr} and 40 to 75 cycles at 0.75 wall M_{pr} (versus the predicted based on monotonic loading). The target displacement demands (See Table 3-3) were calculated based on the experimental yield displacement (See Table 4-1).

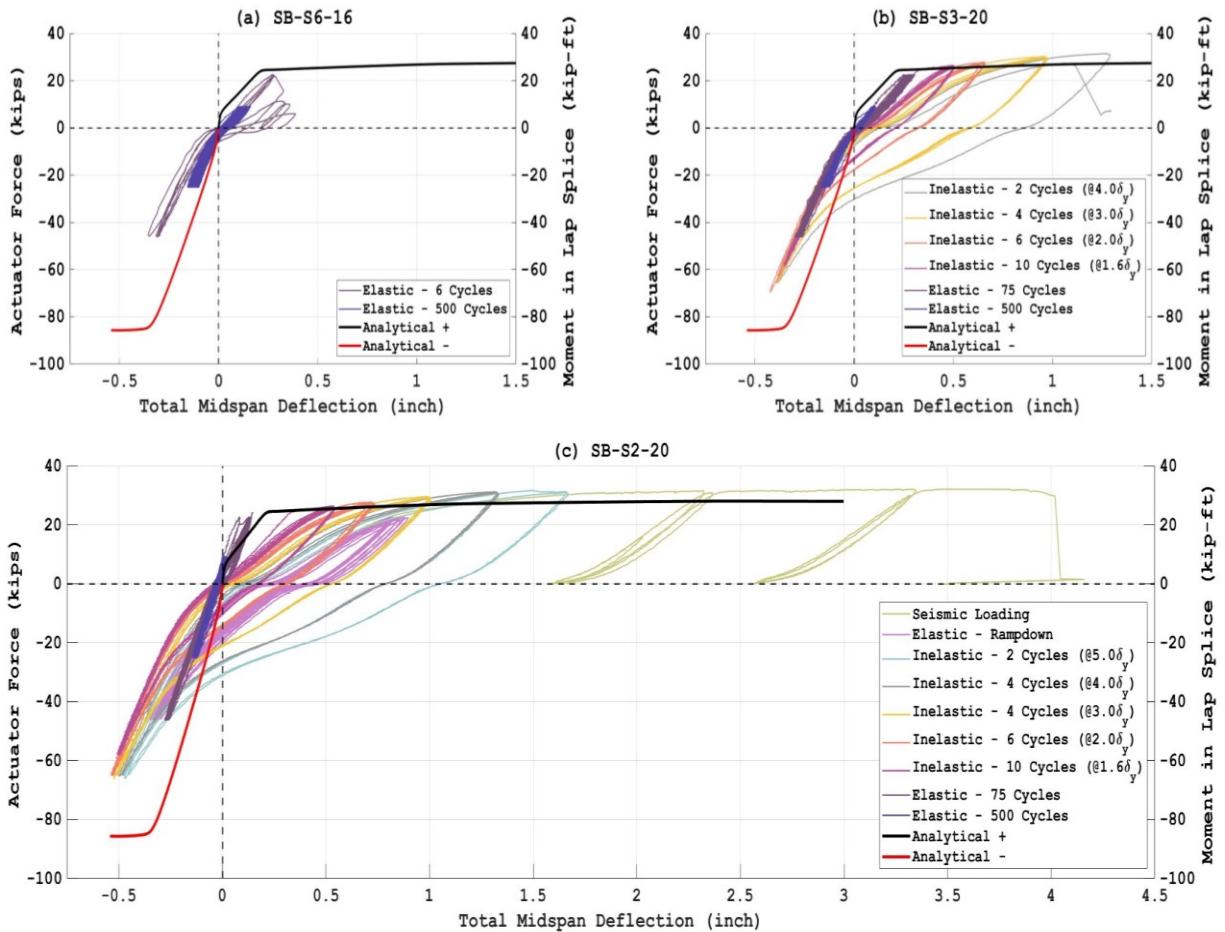


Figure 4-18: Load-Deformation responses of small beam test specimens

Figure 4-18(a) shows the failure of SB-S6-16 at the 3rd cycle of $0.75M_{pr}$ (for the wall) without reaching the expected yield strength. The observed strength degradation was 30% from the peak load at the 3rd cycle and 75% at the 6th cycle. During the 500 cycles at $0.4 M_{pr}$ (for the wall), even though the beam did not experience any strength loss, degradation of beam stiffness was observed due to repeated cyclic loading. Compared to SB-S3-20, SB-S6-16 had larger stiffness degradation due to the application of 500 cycles.

Figure 4-18(b) displays the failure of SB-S3-20 at the 2nd cycle of $2.5\Theta_y$ wall demand. The observed strength degradation was 84% from the peak load at the 2nd cycle. Stiffness degradation was present during the 500 cycles at $0.4 M_{pr}$ and 75 cycles at $0.75M_{pr}$.

During the application of the 500 cycles at $0.4M_{pr}$ and the 75 cycles at $0.75M_{pr}$ of SB-S2-20 (See Figure 4-18(c)), issues were observed at the simply supports (custom link was used that did not provide enough rotational capacity at the supports) that resulted in a higher stiffness than predicted, which resulted in slightly lower strain demands in the splice. To solve the issue, the roller supports were readjusted using steel cylinders clamped between two steel plates for the subsequent loading stages. SB-S2-20 did not show any strength loss throughout the wind-loading protocol and the ramp-down. The beam specimen was then subjected to seismic loading protocol: 2 cycles each at $7\delta_y$ and $10\delta_y$; 1 cycle at $12\delta_y$ (failure).

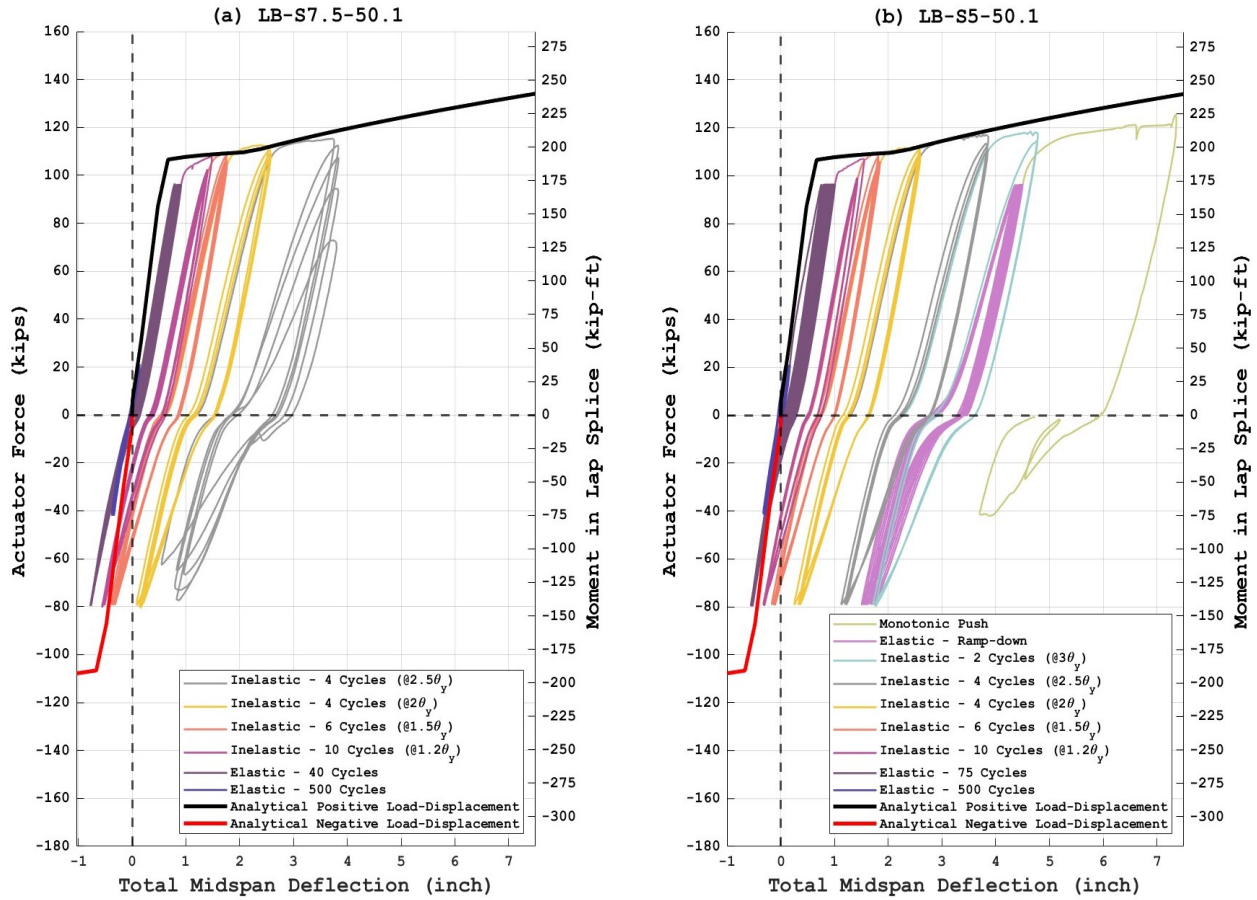


Figure 4-19: Load-Deformation responses of large beam test specimens

The results presented in Figure 4-19(a) indicate that LB-S7.5-50 failed during the 4th cycle of $2.5\theta_y$ (wall demand) or $3.81\delta_y$ of the beam ($\mu_\delta=3.81$). The failure resulted from stiffness degradation observed in subsequent cycles for the same peak loading. Observed strength degradation was 15% from the peak load for the 4th cycle and 38% during the 1st cycle of $3.0\theta_y$ wall demand.

The loading protocol was developed with 75 cycles at $0.75 M_{pr}$ of the wall; however, during LB-S7.5-50 test, only 40 cycles were applied because the rotation of the custom support link used on the spreader beam to test beam connection started generating tension loads on the beam (and the splice) (See Figure 4-20). This issue was identified because the beam started to yield at an actuator force that was less than the expected. To address this issue, the test setup was modified as

shown in Figure 3-14. Rather than to complete the 75 cycles at $0.75M_{pr}$ (apply another 35 cycles), based on discussions with the Project Advisory Committee (PAC), the testing was continued with the inelastic portion of the loading protocol. The support issue was not present during LB-S5-50 test because the test setup was modified.

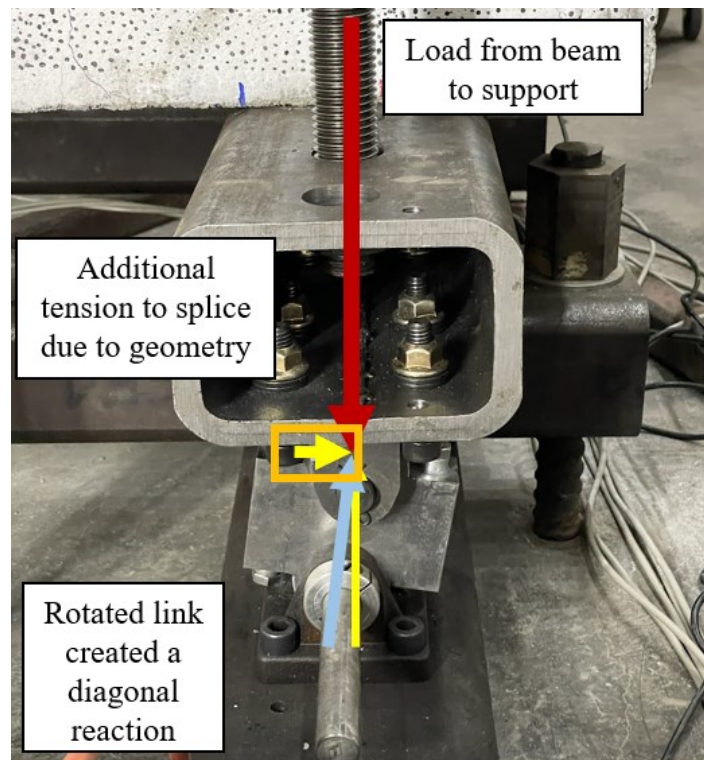


Figure 4-20: Custom link roller support issue

Additionally, during the cycles to $0.75M_{pr}$, both large beam flanges cracked and a portion of the flange near midspan spalled off on one side of the beam. The loss of a portion of the flange resulted in a slightly lower moment capacity for the experiments than predicted; however, the difference was only about 5%.

In Figure 4-19(b), LB-S5-50 showed no strength loss during the wind loading protocol, which included application of the ramp-down cycles. However, due to the residual tensile strain that remained in the splice (smaller compression strain applied in the splice induced larger residual tensile strain), the intended target strain range during the ramp-down portion of the loading

protocol were not achieved. Therefore, the ramp-down was stopped at the 6th cycle and a monotonic push was performed. The beam reached a midspan displacement value of 7.4 in. before large cover loss/concrete crushing occurred at a location outside of the constant moment region.

4.3. Moment-Curvature Responses

Results from pairs of LVDTs attached to the specimen were used to determine beam average curvature and rotation over the LVDT gauge length. The difference of the LVDT displacement readings between the top and bottom pair was divided by the vertical distance between the LVDTs (small beams = 8 in.; large beams = 12 in.) to obtain the average rotation in that LVDT span. This rotation was divided by the span of LVDT (small beams = 8 in.; large beams = 10 in.) to obtain the average curvature. Figure 4-21 through Figure 4-25 displayed the moment-curvature responses from each pair of LVDTs to the predicted values (monotonic loading) for all beam specimens. In the small beam test specimens, Pair 3 values were averaged from the pairs located in the front and back of the specimens. It is noted that the predicted curvature values ignore the contribution of slip to rotation and curvature.

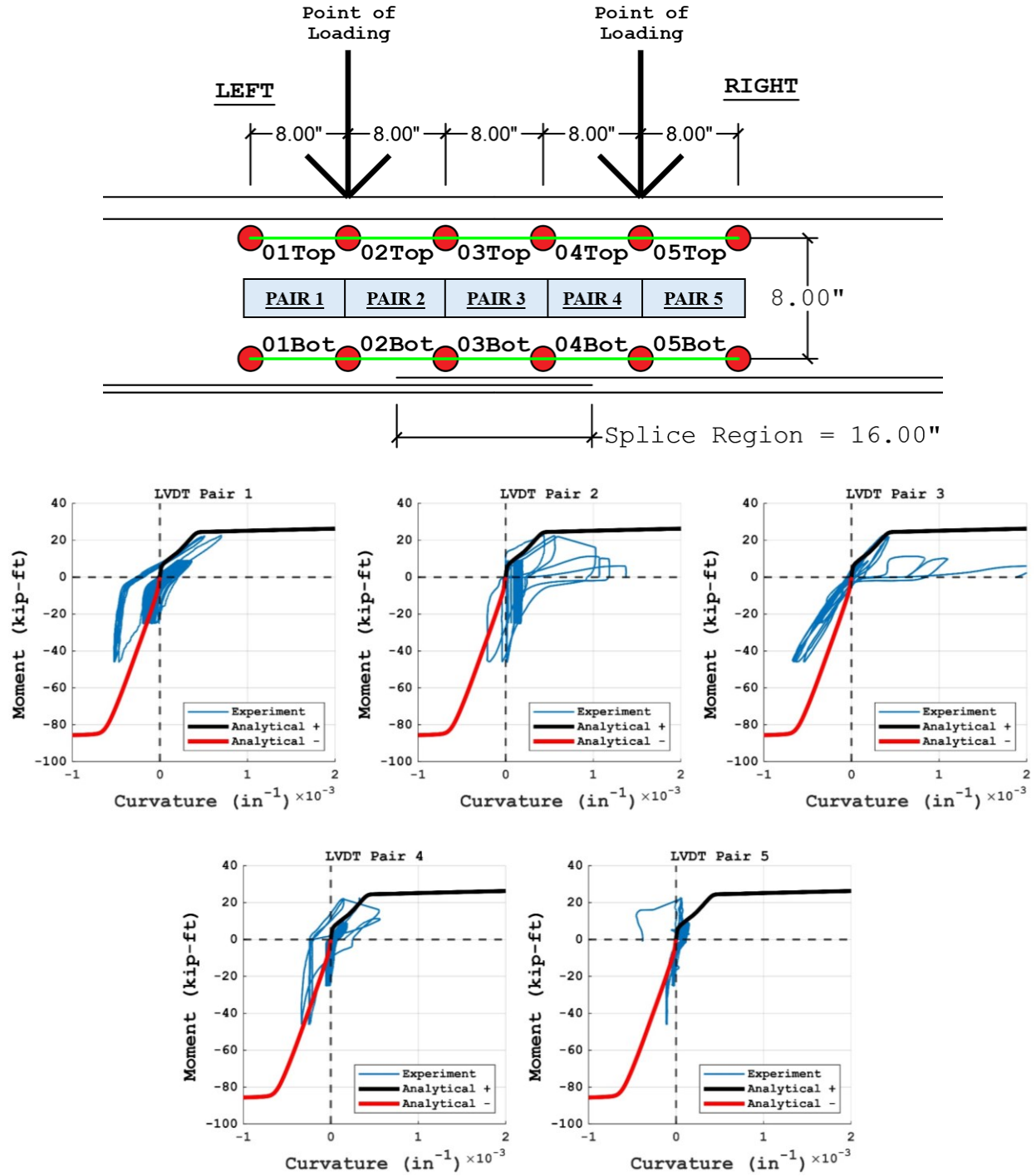


Figure 4-21: SB-S6-16 moment-curvature for each LVDT pair

SB-S6-16 moment-curvature relations determined from experimental data were similar to the predicted relations at the 500 cycles of $0.4 M_{pr}$. However, as noted above, the specimen failed at the 3rd cycle of $0.75 M_{pr}$, resulting in lower moment-curvature values than predicted.

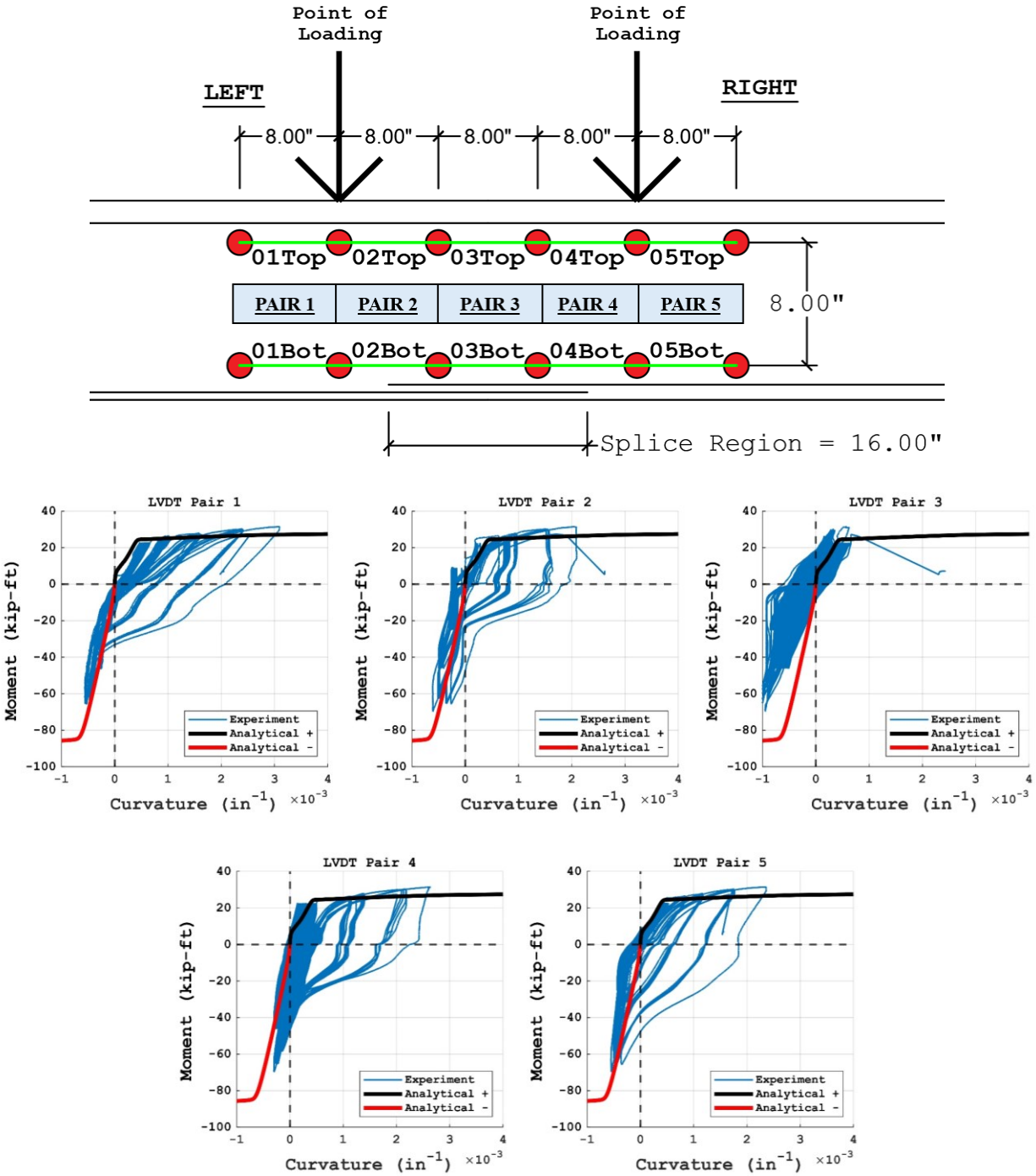


Figure 4-22: SB-S3-20 moment-curvature for each LVDT pair

Figure 4-22 shows that moment-curvature relations from Pairs 1, 2, 4, and 5 were similar to the predicted relations. Pair 3 showed smaller curvature relations as it was located at the middle of the splice where horizontal cracks formed only just before splice failure.

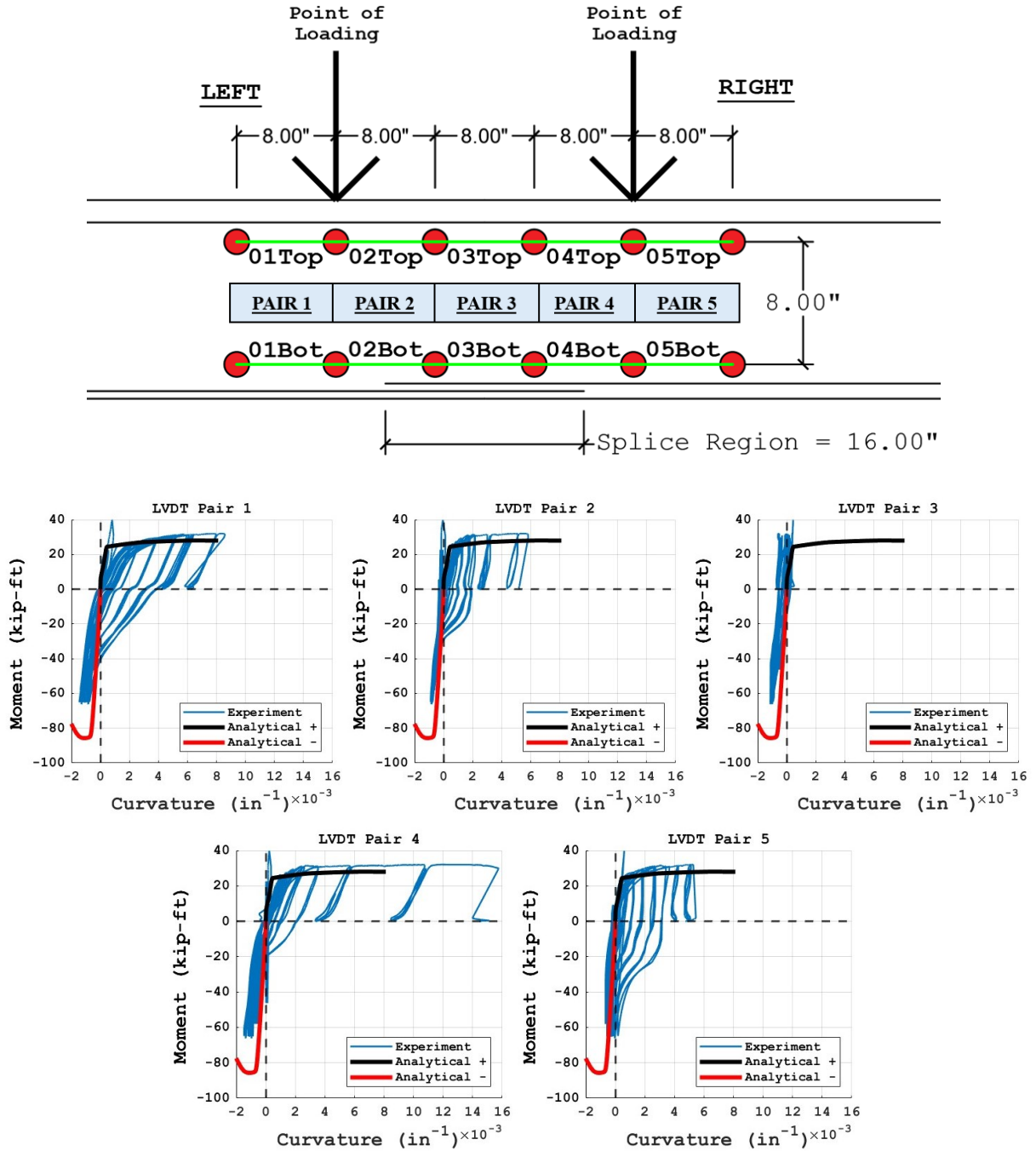


Figure 4-23: SB-S2-20 moment-curvature for each LVDT pair

In Figure 4-23, Pair 4 shows significantly higher curvature values than predicted; it was observed in Figure 4-10 that bar fracture occurred at Pair 4. Curvature values for Pairs 1, 2, and 5 were similar with predicted values. Pair 3, which was located at the middle of the splice region where damage was not observed, displayed smaller curvature values.

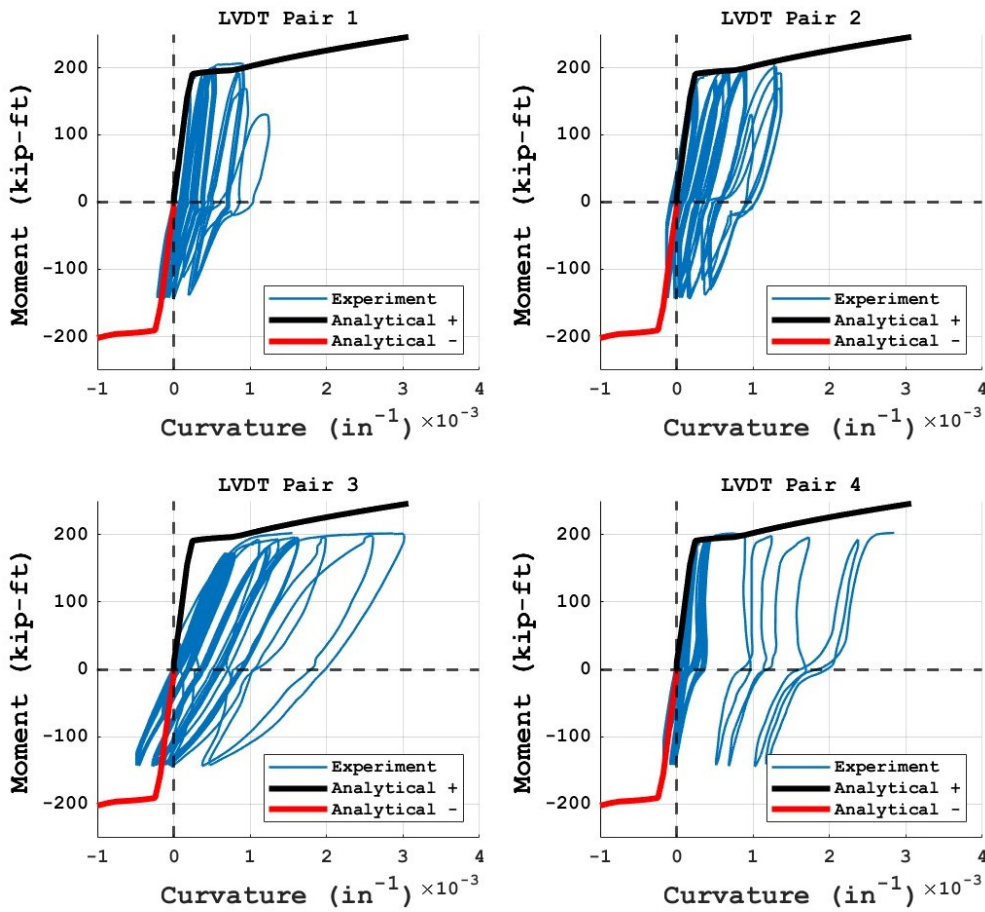
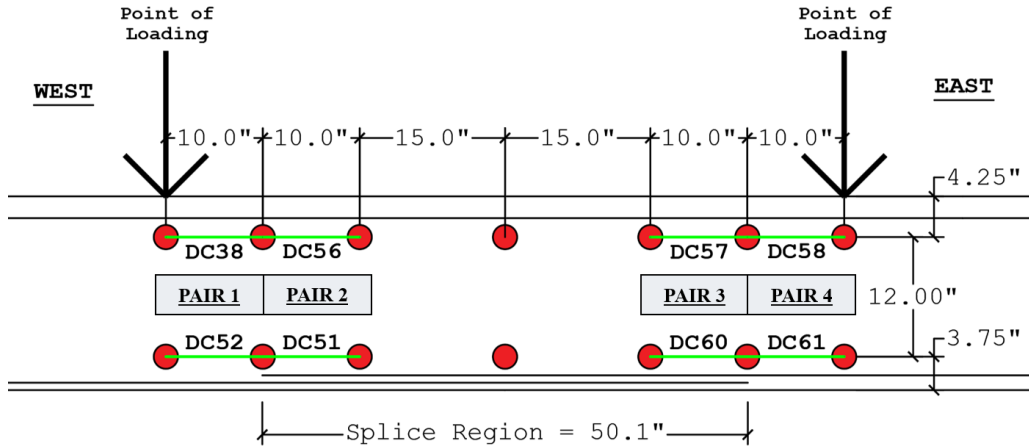


Figure 4-24: LB-S7.5-50 moment-curvature for each LVDT pair

In LB-S7.5-50, large cracks were observed on the east end of the splice (Pair 3 and Pair 4; See Figure 4-24) which resulted in larger curvature values than predicted. Curvature values of Pair 1 and Pair 2, where smaller cracks were observed, were similar to values for the predicted relations.

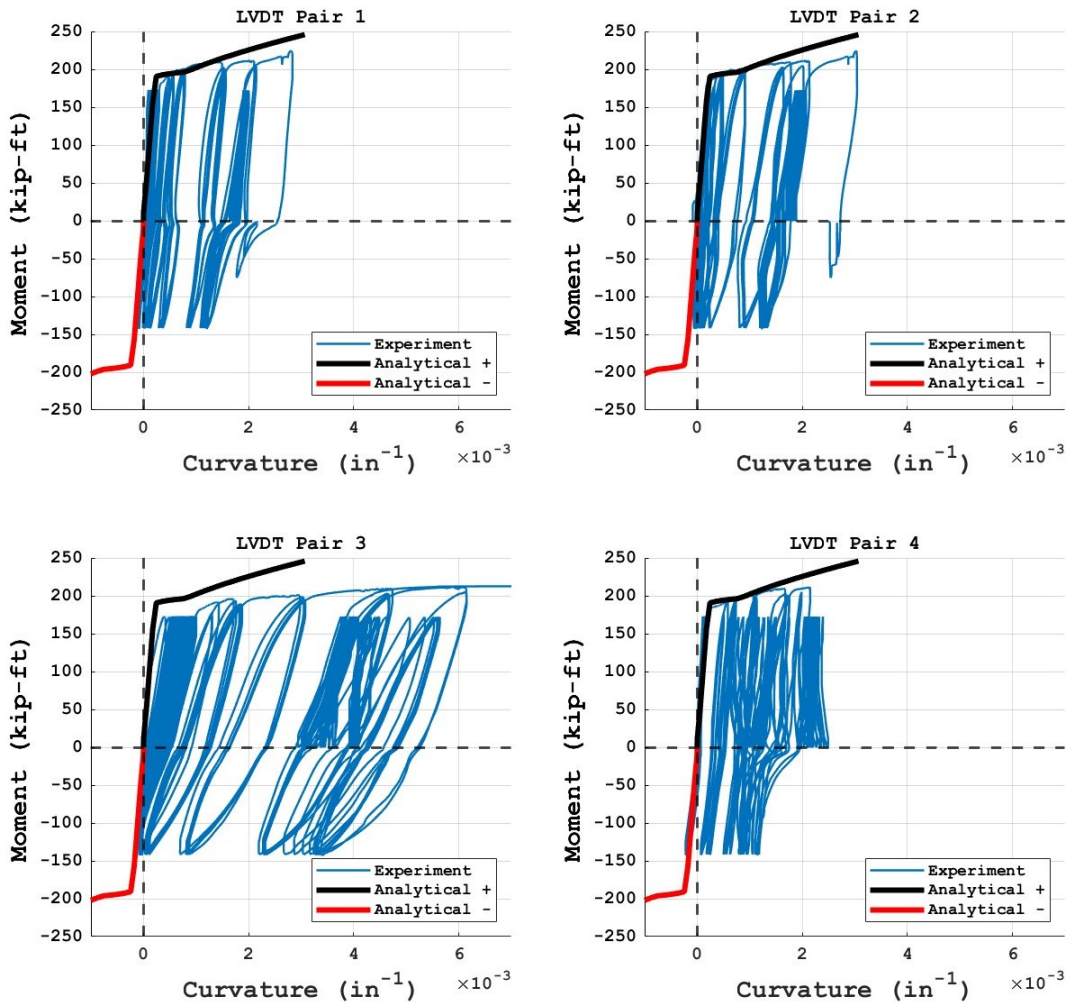
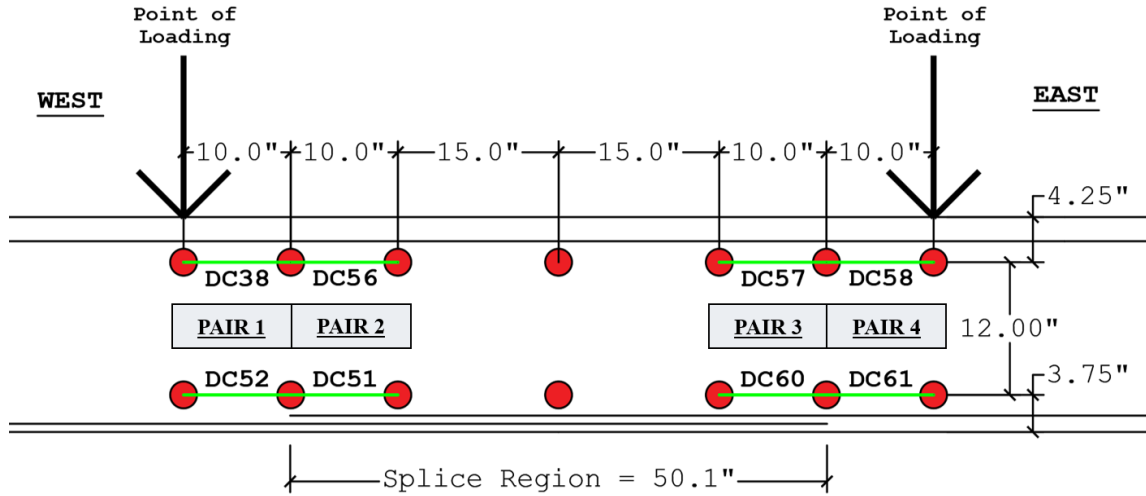


Figure 4-25: LB-S5-50 moment-curvature for each LVDT pair

In LB-S5-50, a large vertical crack was also observed at the east end of the splice (Pair 3 and Pair 4; See Figure 4-25); smaller cracks were observed at the west end of the splice (Pair 1

and Pair 2; See Figure 4-25). Pair 1 and 2 exhibited curvature values similar to values for the predicted relation. The large vertical crack formed just before Pair 4 attachment (See Figure 4-26), which resulted in the curvature values at this region being concentrated on Pair 3 instead of being distributed between Pair 3 and 4.

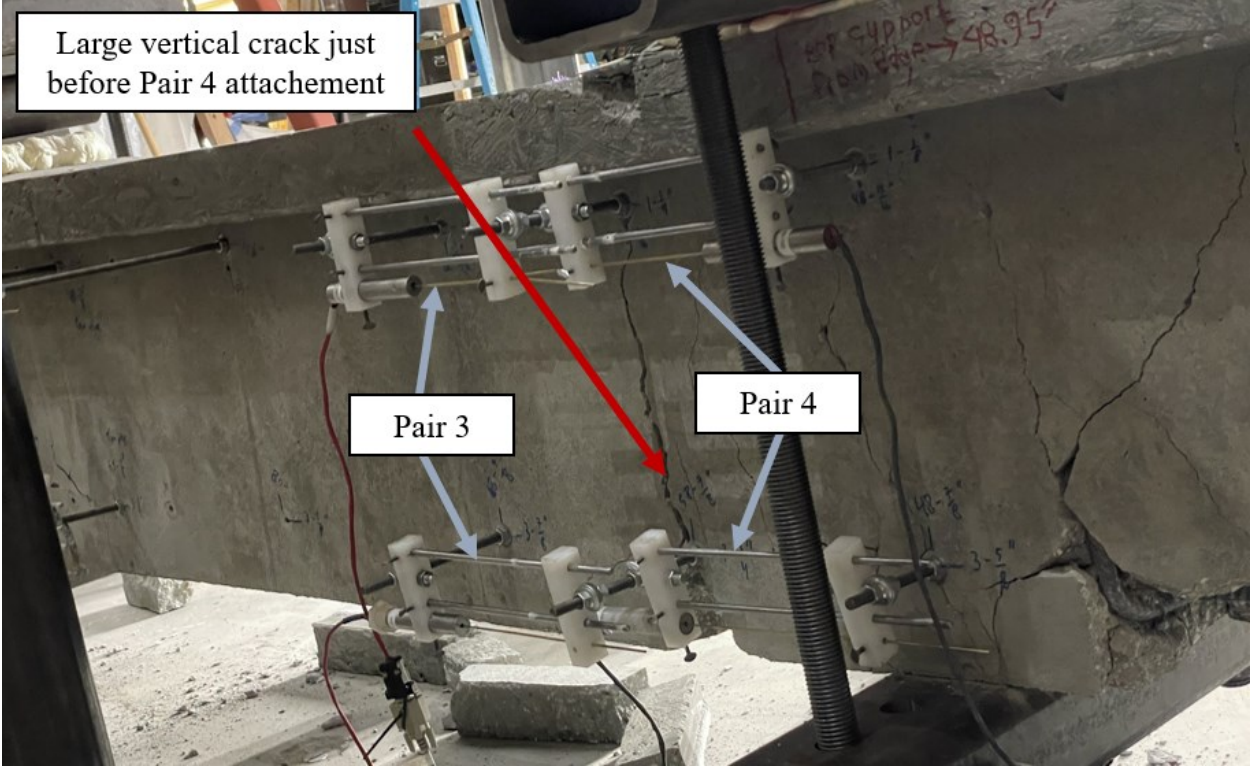


Figure 4-26: LB-S5-50 crack detail (LVDT: Pair 3 and 4)

4.4. Axial Growth

As discussed in the previous chapters, axial growth of the beam, due to concrete cracking and reinforcement yielding, was not restrained during testing. In this study, axial growth data were obtained from the large beam test specimens. Figure 4-27 shows the axial growth of the large beam relative to the total midspan displacement. It is observed that the axial growth occurred during the ramp-up cycles, where new cracks were observed to form as the magnitude of the applied load increased. The maximum values of axial growth in LB-S7.5-50 was 1.82 in. or 1.16% of the beam span (13 ft support-to-support), whereas LB-S5-50 exhibited larger axial growth (2.25 in. or 1.4% of the beam's span (13 ft support-to-support)) at the end of the wind-loading protocol and increased to 2.75 in. or 1.82% of the beam's span at the final load of the monotonic push.

In real buildings, some degree of axial restraint exists, e.g., due to engaging slabs between walls and gravity columns, and this axial restraint would affect the beam moment capacity, stiffness values, and crack widths (Anaraki, 2023). The presence of axial restraint preventing axial growth would produce axial compression in the beam and increase the moment capacity. However, as tested (without axial restraint), the test results should provide a conservative estimate of the splice length and detailing required to achieve the target performance.

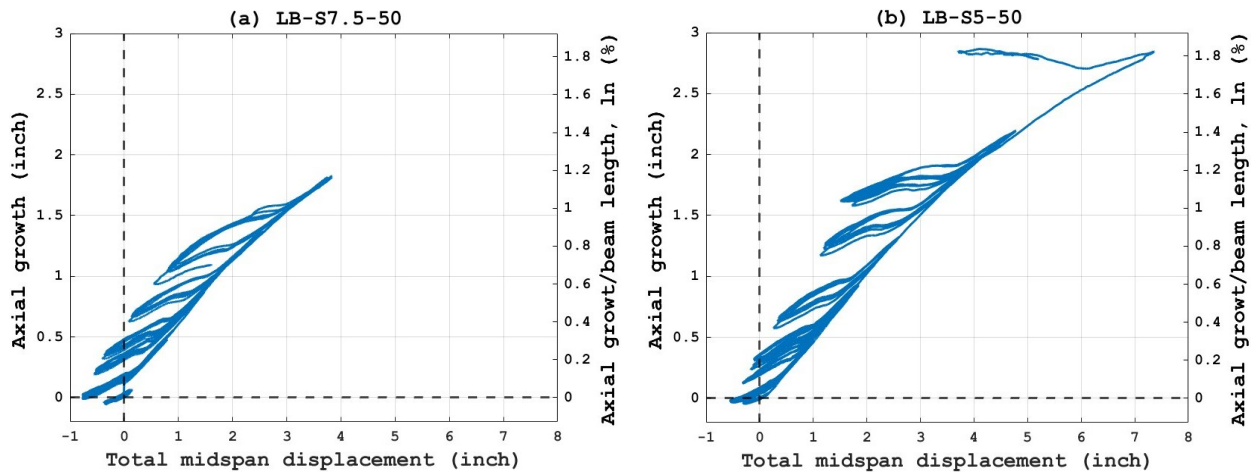


Figure 4-27: Axial growth on large beam test specimens

4.5. Digital Image Correlation (DIC) Results

As mentioned in Chapter 3, data to enable DIC was also collected during the tests for the large beams. The DIC was used to measure surface strains and crack patterns on the north face of the beam. Figure 4-28 presents processed data for Y-Y strain at $0.79M_{pr}^+$ ($0.93\epsilon_y$) demand between the 1st cycle and the 40th cycle. It is observed that, for the 1st cycle, horizontal cracks started to form at the end of splice and propagated towards the middle portion of the splice. The horizontal cracks increased in the middle of the splice between the 1st and the 40th cycle.

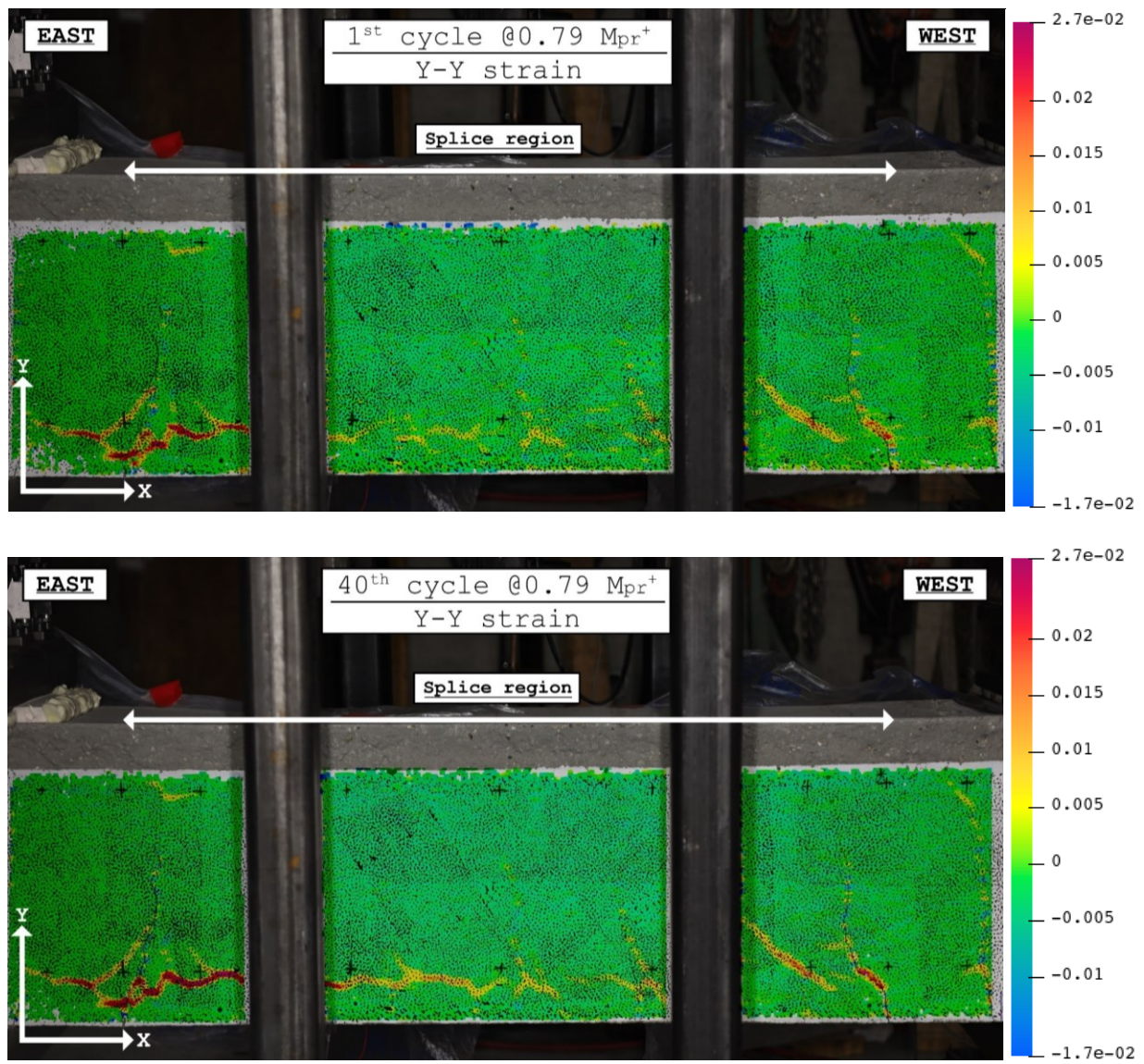


Figure 4-28: Y-Y surface strain at 0.75 wall M_{pr} demand (LB-S7.5-50)

Although the beam strength did not degrade during these cycles, crack widths and crack lengths increased due to the repeated cycling below the static yield stress, which is typical of fatigue behavior. Figure 4-29 presents results for X-X and Y-Y strains at $0.75M_{pr}$ demand. Large vertical cracks formed at the ends of the splice, and horizontal cracks formed at the ends of the splice and propagated towards the middle of the splice, as previously noted.

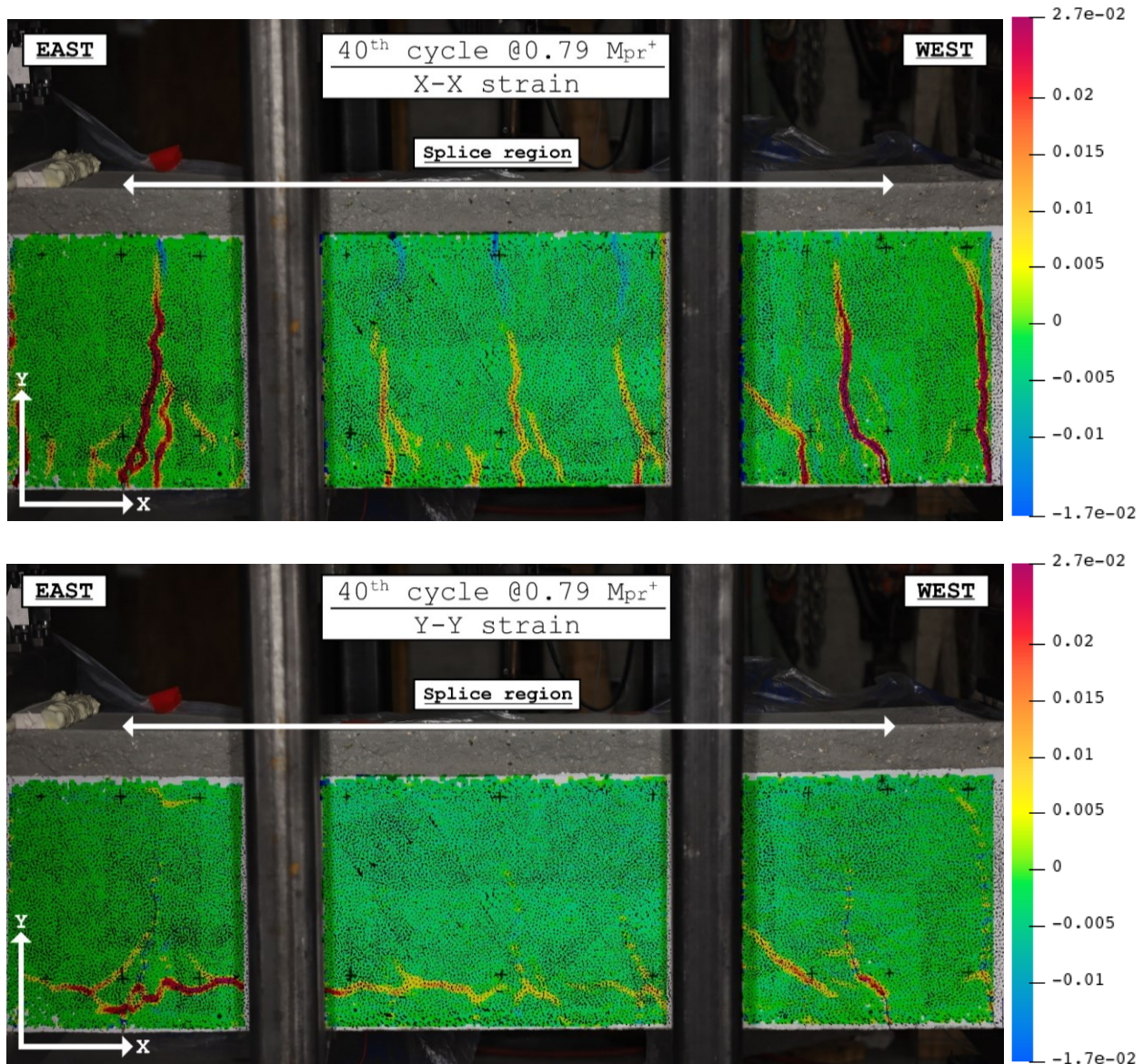


Figure 4-29: LB-S7.5-50 Surface strain and crack pattern from DIC (LB-S7.5-50)

Similar to LB-S7.5-50, DIC was performed on LB-S5-50 to display surface strains and crack patterns on the north face of the beam. Figure 4-30 presents X-X and Y-Y strains at $2.5\Theta_y$ inelastic demand. It was observed that vertical cracks occurred in the splice region (indicating flexural cracks) and minor horizontal cracks formed near the ends of the splices. The complete DIC results for each loading stage under the wind-loading protocol are presented in Appendix E.

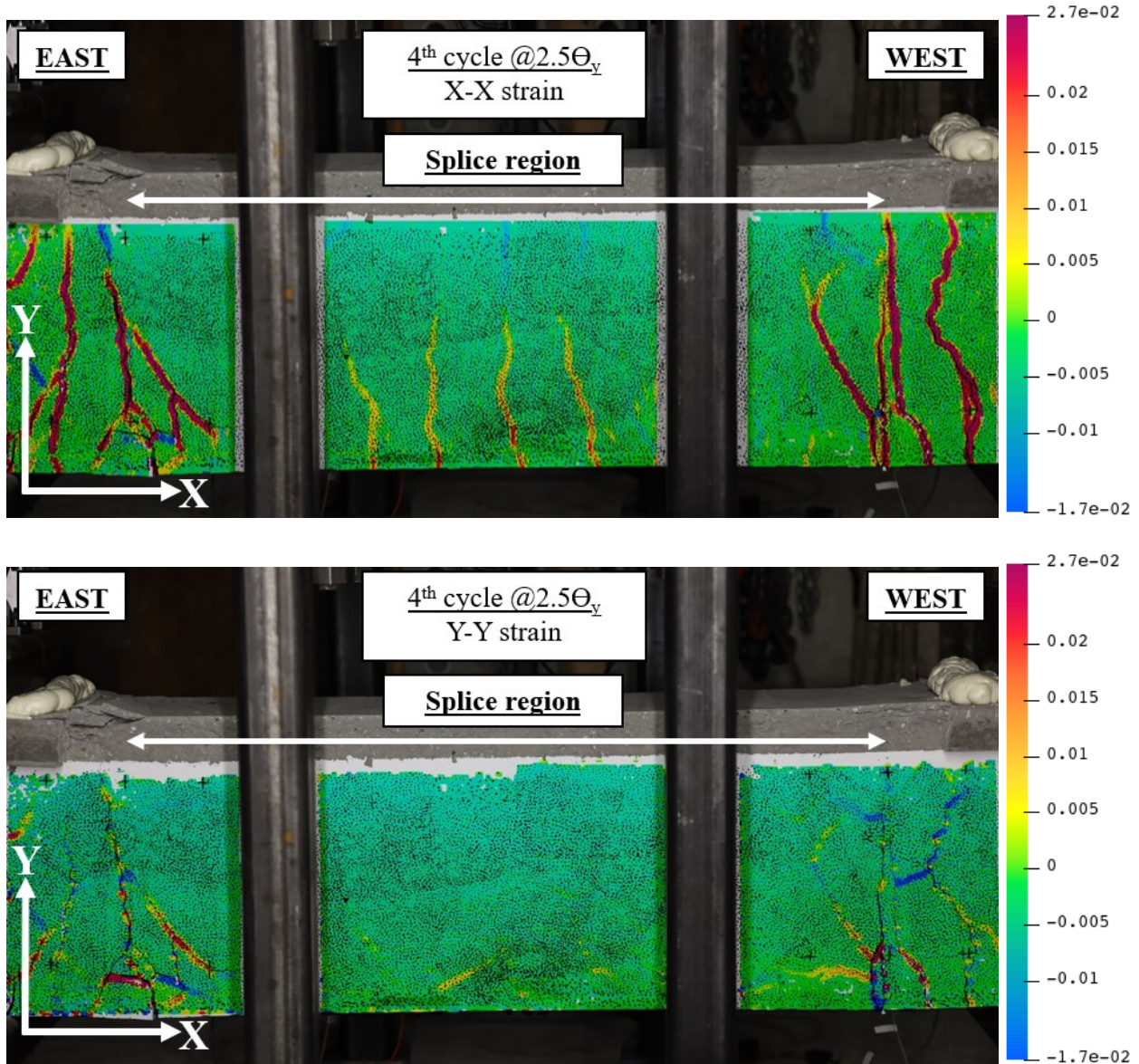


Figure 4-30: LB-S5-50 Surface strain and crack pattern from DIC (LB-S5-50)

5. Comparison of Beam Specimens

This chapter talks about the relation of the small beam and large beam tests results with previously done tests from other investigators. Recommendations of transverse reinforcement requirements are also included in the following subsections.

5.1. Rebar Diameter Size Factor in Lap Splice

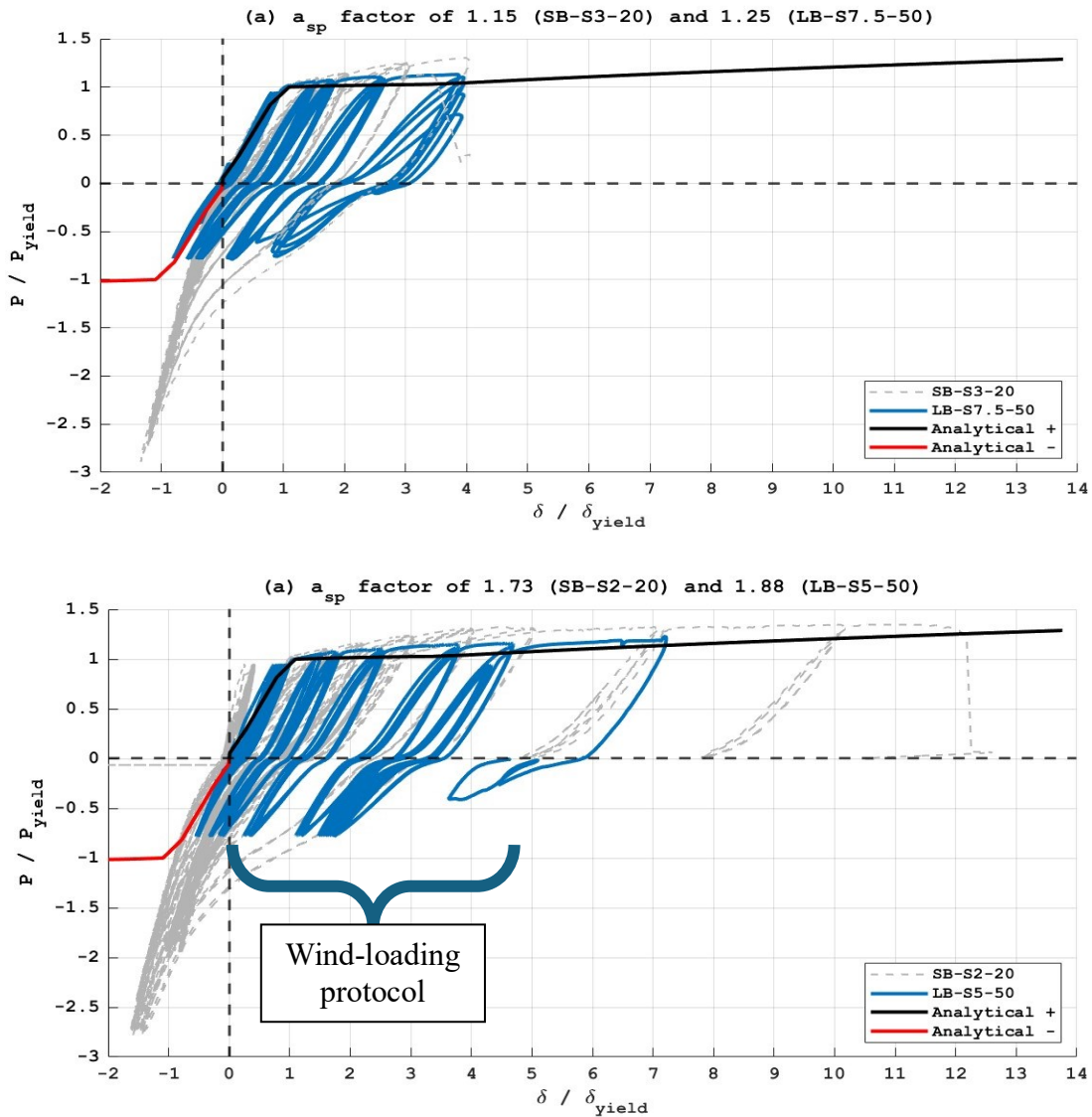


Figure 5-1: Small versus large beams normalized load-displacement curve

Comparisons between the small and large beams were made using normalized load-displacement curves. The goal was to determine if the results varied with rebar size, i.e., #4 for the

small beams and #8 for the large beams. From Figure 5-1, it was observed that the small and large beams produced similar behavior; SB-S3-20 and LB-S7.5-50 (a_{sp} factor of 1.15 and 1.25) failed at $2.5\Theta_y$ wall demand, whereas SB-S2-20 and LB-S5-50 (a_{sp} factor of 1.73 and 1.88) both were able to complete the wind-loading protocol and failed at modestly higher displacement ductility values during the seismic-loading protocol. The failure mode and crack patterns for the small and large beams were also similar. Therefore, based on the results, rebar diameter from #4 to #8 does not affect the strength or deformation capacity of the beams (splice), i.e., bar diameter is adequately accounted for in the expression for the splice length.

5.2. Recommendation of Transverse Reinforcement based on Confining Force

Spacing requirements for transverse reinforcement over the lap splice length required to develop inelastic behavior have been proposed by various investigators (see Section 2.4). In this study, the parameter a_{sp} was used to enable comparisons between beam tests with different stirrup bar diameter and stirrup spacing. Values of a_{sp} for various beam test programs, included the tests conducted in this study, along with summary test parameters and the strain ductility achieved over the length of the lap splice, are summarized in Table 5-1.

Table 5-1: a_{sp} values of beam test specimens

Stirrup Criterion	Spacing	l_s/s	a_{sp}	Strain Ductility
ACI Committee 408	10.50 in	4.8	0.89	≤ 1.0
Lukose et al. (1982)	5.00 in	10.0	1.88	5.0-5.5
Sivakumar et al. (1983)	7.30 in	6.9	1.29	≥ 1.0
MacKay et al. (1988)	6.70 in	7.5	1.40	≥ 1.0
Tocci et al. (1981)	5.20 in	9.6	1.81	≥ 1.0
SB-S6-16	6.00 in	2.7	0.46	≤ 1.0
SB-S3-20	3.00 in	6.7	1.15	6.2
SB-S2-20	2.00 in	10.0	1.73	16.5*
LB-S7.5-50	7.50 in	6.7	1.25	6.4
LB-S5-50	5.00 in	10.0	1.88	12.4**

*No splice failure. Strain was based on steel failure.

**No splice failure. Test was stopped before steel failure.

The results presented in Table 5-1 indicate that values of $a_{sp} \geq 1.0$ are needed to achieve bar yield (strain ductility ≥ 1.0). In some studies, ductility values (displacement or strain) were not reported; however, information was provided to indicate that spliced bars were loaded beyond the yield strain.

The a_{sp} values for SB-S2-20 and LB-S5-50 were similar to the a_{sp} value obtained for the recommended stirrup spacing by Lukose et al. (1982). However, significant differences in the maximum strain ductility values were reported by Lukose et al. (1982) and this study, likely because Lukose et al. (1982) applied almost double the number of inelastic cycles for their tests (48 cycles) and used smaller loading increments compared to the loading protocol used in this study. The lap splice lengths used in the Lukose et al. (1982) tests were also shorter than the ones used in this study, which reduced the concrete confining effect for the lap splice (MacKay et al., 1989).

Correlations between a_{sp} values and strain ductility (μ_ϵ) for the small and large beam specimens are shown in Figure 5-2.

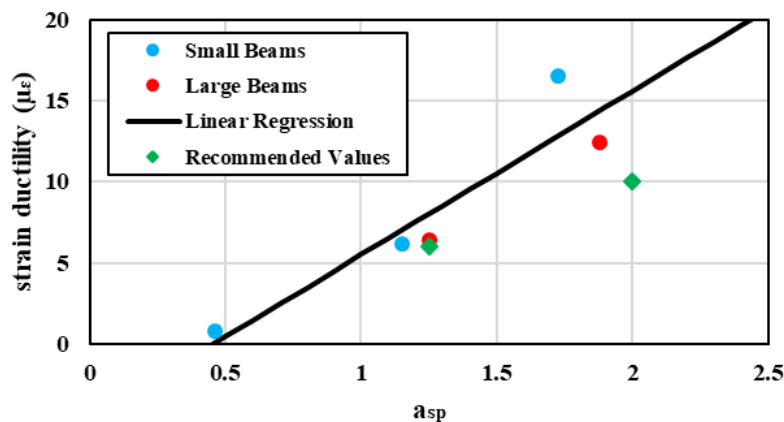


Figure 5-2: a_{sp} and μ_ϵ correlation for small and large beams

Based on the test results for the wind-loading protocol used (Figure 5-2), a_{sp} values greater than or equal to 1.25 and 2.0 are recommended for lap splices to achieve strain ductility demands ≤ 6 and ≥ 10 , which fall below the linear regression line as a conservative approach.

6. Summary and Conclusions

Three small and two large beams with tension lap splices were tested in the Structural Engineering Laboratory at the University of California, Los Angeles. These experiments were developed as a part of a study to investigate the performance of ordinary reinforced concrete walls under wind-loading protocols. The primary objective of this study was to investigate the nonlinear fatigue behavior of wall lap splices and to develop strength and detailing provisions that achieve a prescribed level of ductility without strength loss to support the implementation of Performance-Based Wind Design.

From these experiments, the following conclusions and recommendations for lap splices subjected to wind loading producing modest nonlinear fatigue demands were obtained:

1. Required transverse reinforcement (bar size and spacing) along the lap splice is related to the parameter a_{sp} , which is the ratio of the confining force provided by the transverse reinforcement along the splice length to the total yield force of the spliced longitudinal reinforcement. Values of a_{sp} for the small beam test specimens, i.e., SB-S6-16, SB-S3-20, and SB-S2-20, were 0.46, 1.15, and 1.88, respectively. Values of a_{sp} for the large beam test specimens, i.e., LB-S7.5-50 and LB-S5-50, were 1.25 and 1.88, respectively. Splice failure was observed for SB-S6-16 prior to reaching the yield strength (moment). SB-S3-20 and LB-S7.5-50, which have comparable a_{sp} values (1.15 and 1.25), displayed strength loss at a measured strain ductility of 6.2 and 6.4 ($2.5\Theta_y$ wall demand), whereas SB-S2-20 and LB-S5-50 (with comparable a_{sp} values of 1.73 and 1.88) displayed no strength loss during the wind-loading protocol. Subsequently, both SB-S2-20 and LB-S5-50 were loaded monotonically, and failure was observed at strain ductility values of 16.5 and 12.4, respectively. Based on these results, a value of $a_{sp} \geq 1.25$ is recommended for splices if strain ductility demands ≤ 6.0 , and

a value of $a_{sp} \geq 2.0$ is recommended for strain ductility demands ≥ 10.0 for fatigue capacity under the given wind-loading protocol.

2. To achieve adequate lap splice performance, the lap splice length required for ordinary walls according to ACI 318-19 Section 25.4.2.4 was multiplied by 1.25 to account for overstrength and strain-hardening of the longitudinal reinforcement under the nonlinear strain demands. This multiplier is not required in ACI 318-19 or ACI 318-25. It is noted that the multiplier of 1.25 is consistent with what is required for special walls in ACI 318-19 Section 18.10.2.3(b).
3. The results for the large and small beam tests were compared to determine if longitudinal reinforcement bar diameter affected strain ductility. Longitudinal bar diameters were #8 and #4 for the large and small beam tests, respectively. Based on this comparison, large and small beams with similar a_{sp} values and ACI 318-19 lap splice lengths multiplied by 1.25 achieved similar values of strain ductility. Therefore, for the range of parameters considered in this study and for the given loading protocol, longitudinal bar size did not affect the results.
4. Future tests of lap splices subjected to nonlinear strain demands under wind-loading might consider tests on beams with larger longitudinal bar diameters, e.g., #10 or #11, since these bar diameters are used in construction of taller core wall buildings.

For loading protocols with lower or higher peak demands, additional studies would be needed to determine the recommended lap splice length and requirements for transverse reinforcement.

Appendix A. Strength Calculation

Predicted Moment-Curvature

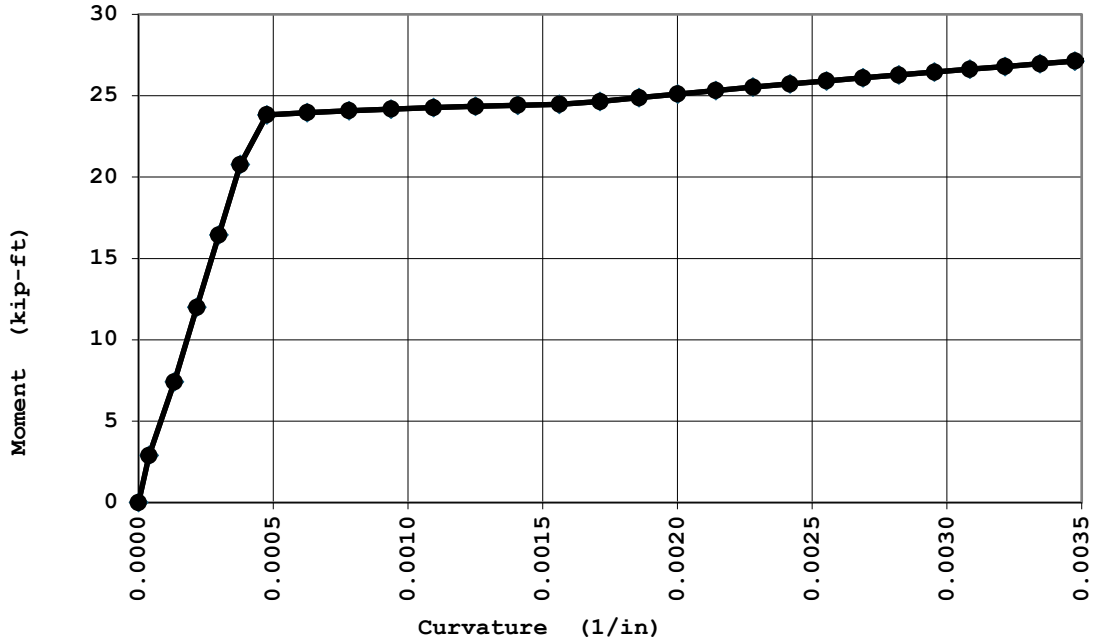


Figure A-1: Small beam positive bending analytical moment-curvature

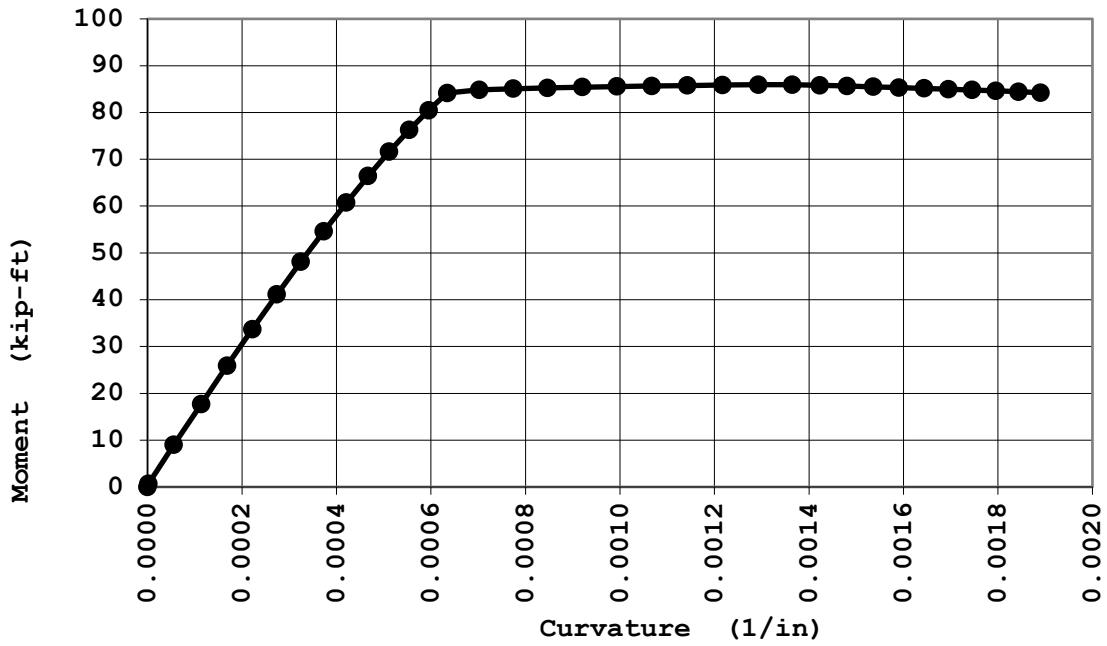


Figure A-2: Small beam negative bending analytical moment-curvature

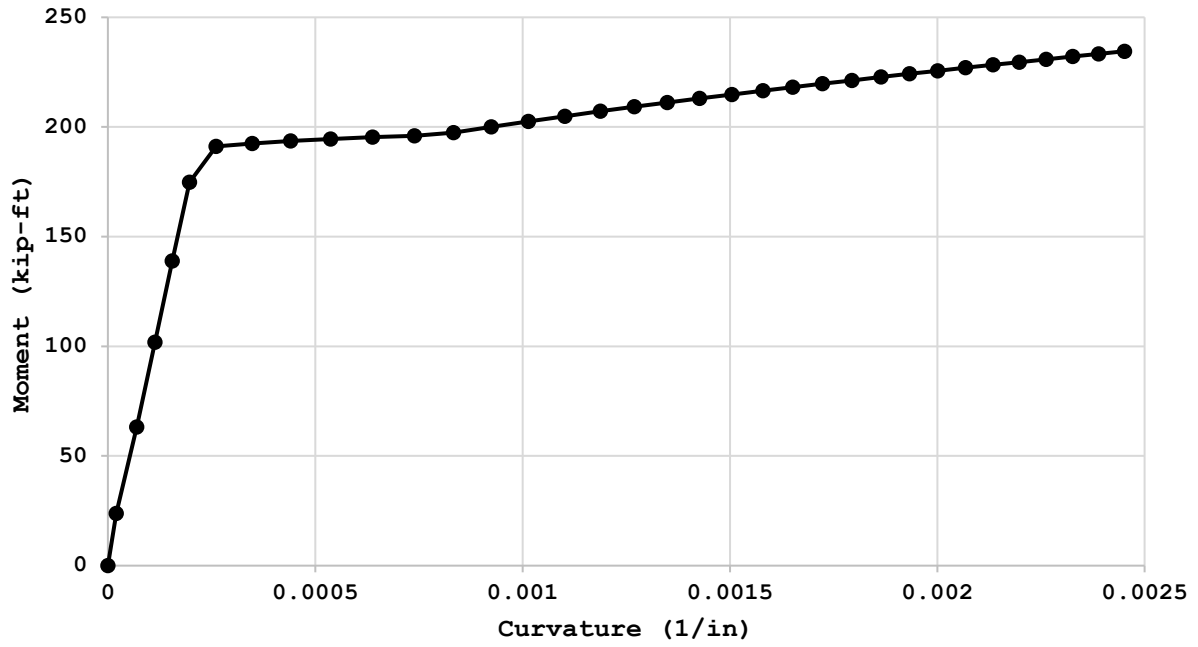


Figure A-3: Large beam positive bending analytical moment-curvature

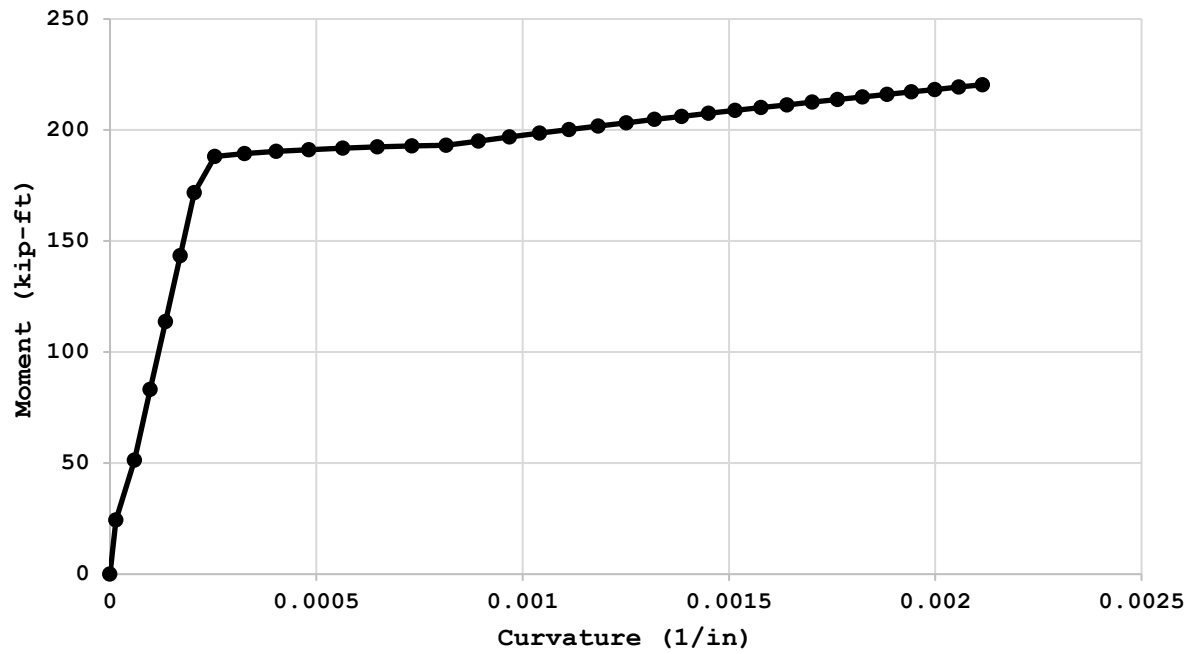


Figure A-4: Large beam negative bending analytical moment-curvature

Lap Splice Length

Development length (ACI 318-19 Section 25.4.2.4)

$$l_d = \left[\frac{3}{40} \frac{f_y}{\lambda \sqrt{f'_c}} \frac{\Psi_t \Psi_e \Psi_s \Psi_g}{\left(\frac{c_b + K_{tr}}{d_b} \right)} \right] d_b$$

$$K_{tr} = \frac{40A_{tr}}{sn}$$

- Small beam test specimens (SB-S6-16, SB-S3-20, SB-S2-20)

$$f_y = 80 \text{ ksi}$$

$$f'_c = 8 \text{ ksi (expected)}$$

$$d_b = 4/8" (\#4); d_t = 2/8" (\#2)$$

$$\Psi_t = 1.0; \Psi_e = 1.0; \Psi_s = 0.8; \Psi_g = 1.15$$

$$\lambda = 1.0$$

$$c_b = \min \left(c_c + d_t + 2d_t, \frac{b_w}{2} - c_c - d_t - 2d_t \right)$$

$$c_b = \min \left(\frac{3}{8} + \frac{2}{8} + \frac{2 \times 2}{8}, \frac{5}{2} - \frac{3}{8} - \frac{2}{8} - \frac{2 \times 2}{8} \right) = \min(1.125 \text{ in.}, 1.375 \text{ in.})$$

$$c_b = 1.125 \text{ in.}$$

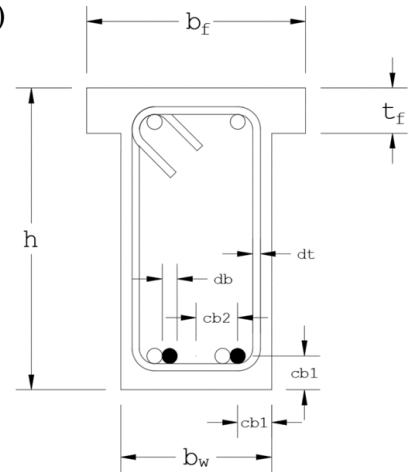
$$K_{tr} = \frac{40 \times 2 \times \frac{\pi}{4} \times \frac{1^2}{4}}{6 \text{ in.} \times 2} = 0.33$$

$$\frac{c_b + K_{tr}}{d_b} = \frac{1.125" + 0.33}{\frac{4}{8}} = 2.91 \geq 2.5$$

$$l_d = \left[\frac{3}{40} \frac{80000 \text{ psi}}{1.0 \times \sqrt{8000 \text{ psi}}} \frac{1.0 \times 1.0 \times 0.8 \times 1.15}{(2.5)} \right] \frac{4}{8} = 12.3 \text{ in.}$$

$$l_s (SB-S6-16) = 1.3 \times l_d = 16 \text{ in.}; \text{ ACI 318-19 Table 25.5.2.1}$$

$$l_s (SB-S3-20 \& SB-S2-20) = 1.25 \times 1.3 \times l_d = 20 \text{ in.}; \text{ ACI 318-19 Section 18.10.2.3(b)}$$



- Large beam test specimens (LB-S7.5-50, LB-S5.50)

$$f_y = 80 \text{ ksi}$$

$$f'_c = 8 \text{ ksi (expected)}$$

$$d_b = 1" \text{ (#8)}; d_t = 4/8" \text{ (#4)}$$

$$\Psi_t = 1.0; \Psi_e = 1.0; \Psi_s = 1.0; \Psi_g = 1.15$$

$$\lambda = 1.0$$

$$c_b = \min \left(c_c + d_t + 2d_t, \frac{b_w}{2} - c_c - d_t - 2d_t \right)$$

$$c_b = \min \left(\frac{3}{4} + \frac{2}{4} + \frac{2 \times 2}{4}, \frac{10}{2} - \frac{3}{4} - \frac{2}{4} - \frac{2 \times 2}{4} \right) = \min(2.25 \text{ in.}, 2.25 \text{ in.})$$

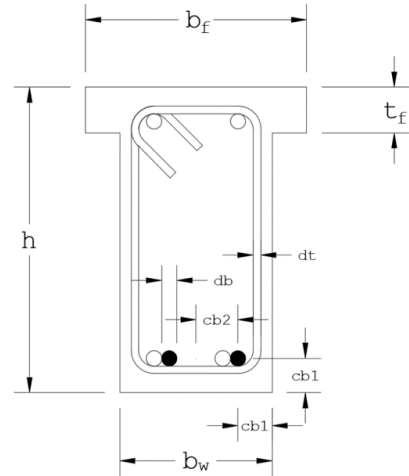
$$c_b = 2.25 \text{ in.}$$

$$K_{tr} = \frac{40 \times 2 \times \frac{\pi}{4} \times \frac{1^2}{2}}{7.5 \text{ in.} \times 2} = 1.05$$

$$\frac{c_b + K_{tr}}{d_b} = \frac{2.25" + 1.05}{1"} = 3.3 \geq 2.5$$

$$l_d = \left[\frac{3}{40} \frac{80000 \text{ psi}}{1.0 \times \sqrt{8000 \text{ psi}}} \frac{1.0 \times 1.0 \times 1.0 \times 1.15}{(2.5)} \right] 1 = 30.9 \text{ in.}$$

$$l_s \text{ (LB-S7.5-50 \& LB-S5-50)} = 1.25 \times 1.3 \times l_d = 50 \text{ in.; ACI 318-19 Section 18.10.2.3(b)}$$



a_{sp} factor

$$a_{sp} = \frac{A_{vsp} \times f_y}{A_{sl} \times f_{yl}}; \quad A_{vsp} = A_v \times \frac{l_s}{s}$$

- SB-S6-16

$$l_s = 16 \text{ in.}; \quad s = 6 \text{ in.}$$

$$A_{vsp} = 2 \times \frac{\pi}{4} \times 0.24^2 \times \frac{16 \text{ in.}}{6 \text{ in.}} = 0.24 \text{ in}^2$$

$$A_{sl} = 2 \times \frac{\pi}{4} \times \frac{1^2}{2} = 0.39 \text{ in}^2$$

$$a_{sp} = \frac{0.24 \text{ in}^2 \times 60 \text{ ksi}}{0.39 \text{ in}^2 \times 80 \text{ ksi}} = 0.46$$

- SB-S3-20

$$l_s = 20 \text{ in.}; \quad s = 3 \text{ in.}$$

$$A_{vsp} = 2 \times \frac{\pi}{4} \times 0.24^2 \times \frac{20 \text{ in.}}{3 \text{ in.}} = 0.6 \text{ in}^2$$

$$A_{sl} = 2 \times \frac{\pi}{4} \times \frac{1^2}{2} = 0.39 \text{ in}^2$$

$$a_{sp} = \frac{0.6 \text{ in}^2 \times 60 \text{ ksi}}{0.39 \text{ in}^2 \times 80 \text{ ksi}} = 1.15$$

- SB-S2-20

$$l_s = 20 \text{ in.}; \quad s = 2 \text{ in.}$$

$$A_{vsp} = 2 \times \frac{\pi}{4} \times 0.24^2 \times \frac{20 \text{ in.}}{2 \text{ in.}} = 0.9 \text{ in}^2$$

$$A_{sl} = 2 \times \frac{\pi}{4} \times \frac{1^2}{2} = 0.39 \text{ in}^2$$

$$a_{sp} = \frac{0.9 \text{ in}^2 \times 60 \text{ ksi}}{0.39 \text{ in}^2 \times 80 \text{ ksi}} = 1.73$$

- LB-S7.5-50

$$l_s = 50 \text{ in.}; \quad s = 7.5 \text{ in.}$$

$$A_{vsp} = 2 \times \frac{\pi}{4} \times 0.5^2 \times \frac{50 \text{ in.}}{7.5 \text{ in.}} = 2.62 \text{ in}^2$$

$$A_{sl} = 2 \times \frac{\pi}{4} \times 1^2 = 1.57 \text{ in}^2$$

$$a_{sp} = \frac{2.62 \text{ in}^2 \times 60 \text{ ksi}}{1.57 \text{ in}^2 \times 80 \text{ ksi}} = 1.25$$

- LB-S5-50

$$l_s = 50 \text{ in.}; \quad s = 5 \text{ in.}$$

$$A_{vsp} = 2 \times \frac{\pi}{4} \times 0.5^2 \times \frac{50 \text{ in.}}{5 \text{ in.}} = 3.93 \text{ in}^2$$

$$A_{sl} = 2 \times \frac{\pi}{4} \times 1^2 = 1.57 \text{ in}^2$$

$$a_{sp} = \frac{3.93 \text{ in}^2 \times 60 \text{ ksi}}{1.57 \text{ in}^2 \times 80 \text{ ksi}} = 1.88$$

Appendix B. Concrete Mix Design




Submittal Information		Mix Information	
Submittal Name	99594 - BEAMS UNDER WIND LOAD	Mix ID	40E2S86
Date Submitted	12/06/2021	Mix Name	0.40 W/C 6000 PSI 3/8" ADVA
Customer	COD - UCLA COLLEGE OF ENGINEERING	Compressive Strength (f'c)	6000 psi @ 28 Days
Project Name	99594 - BEAMS UNDER WIND LOAD	Aggregate Nominal Size	3/8" (9.5mm)
Project Location	UCLA	Air Entrained	<input type="checkbox"/>
Use	BEAMS UNDER WIND LOAD TEST		

Mix Properties							
Slump	8" ± 1"	Sack Content	10.2	94 lb/sack	Total Mass	3982	lb
Air	1%	Total Water	42.8	gal	Total Volume	26.99	ft ³
W/CM Ratio	0.37	Water/Sack	4.2	gal	Unit Weight	147.6	lb/ft ³

Group	Material Description	Supplier	Specific Gravity	Mass lb	Volume ft ³
Cement	TYPE II/V		3.15	961	4.889
Aggregate	SAN GABRIEL VALLEY / IRWINDALE 3/8" GRAVEL 3/8" G	SAN GABRIEL VALLEY / IRWINDALE	2.64	1061	6.441
	SAN GABRIEL VALLEY / IRWINDALE WASHED CONCRETE SAND WCS	SAN GABRIEL VALLEY / IRWINDALE	2.65	1599	9.670
Water	WATER		1	357	5.721
Admixture	GRACE ADVA SUP Dosage: 38.4 fl oz/yd ³ Range: fl oz/yd ³		1		
	Low Range Water Reducer WRDA 64 Dosage: 28.9 fl oz/yd ³ Range: fl oz/yd ³	GCP APPLIED TECHNOLOGIES	1		
Air	Air				0.270

Mix Notes
 WRDA 64 - Dosage Range: 2.0 - 5.0 ozs/cwt
 ADVA 195 - Dosage Range: 2.0 - 10.0 ozs/cwt
 RECOVER - Dosage Range: 0.0 - 6.0 ozs/cwt

Submittal Notes
 Note: This mix should be approved by the project's structural engineer or architect. Mix designed for CalPortland only. No substitutions or alternations may be made. Approval of this mix design carries the inclusion of CalPortland on the distribution list for all concrete test results.

Sincerely,

 Name/Title Brandon Coble / Quality Control Manager

Contact Brandon Coble
 Phone 626-691-2411
 Email bcoble@calportland.com



Digitally signed by David Hattaway
 Reason: I am approving this document
 Date: 2021.12.02 15:12:34-08'00'

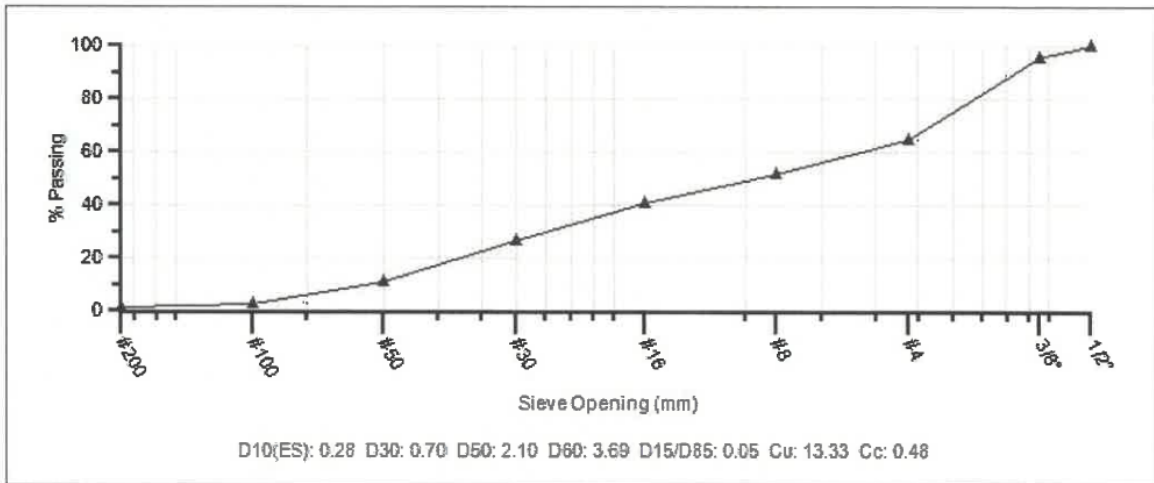


CALPORTLAND®

Combined Aggregate Blend Report

Mix ID 40E2S86	Nominal Max Size 3/8" (9.5mm)
Mix Name 0.40 W/C 6000 PSI 3/8" ADVA	Aggregate Volume 16.1
Design Strength (f'c) 6000 psi @ 28 Days	Coarse Aggregate % 40.0
Specification	Fine Aggregate % 60.0

Sieve/Test	Spec	Result	% Passing Gradations	
			Aggregate Type % Contribution	Coarse
			40.0	60.0
1/2" (12.5mm)		100.0	100.0	100.0
3/8" (9.5mm)		95.6	89.0	100.0
#4 (4.75mm)		64.6	16.0	97.0
#8 (2.36mm)		51.8	5.0	83.0
#16 (1.18mm)		40.8	3.0	66.0
#30 (.6mm)		26.8	2.4	43.0
#50 (.3mm)		10.9	1.8	17.0
#100 (.15mm)		2.9	1.2	4.0
#200 (75µm)		1.08	0.60	1.40





CATALINA PACIFIC
A CALPORTLAND Company
TRIAL BATCH RESULTS

Mix Design: 40E2S86
Proportioning: California Building Code
Water/Cementitious Ratio: 0.37

<u>Ingredients</u>	<u>Cu Yd Weights</u>	<u>Specific Gravities</u>	<u>Absolute Volume (Cu Ft)</u>
Cement Type II/V	961 lbs	3.15	4.89
Water (Design)	357.3 lbs	1.00	5.73
W C Sand Orca	1599 lbs	2.65	9.67
3/8" Gravel Durbin	1061 lbs	2.64	6.44
Entrapped Air 1.0%			<u>0.27</u>
<u>Admixtures:</u>			27.00
WRDA 64	25.7 ozs		
ADVA 195	34.2 ozs		

TESTING RESULTS (ASTM C 192)

Date Cast: May 6, 2019 Plastic Unit Weight: 142.2 pcf
Slump: 9.00" Air Content: 4.1%
Temperature: 66°/64°

COMPRESSIVE STRENGTH RESULTS (ASTM) C 39)

<u>Number</u>	<u>3 Days</u>	<u>7 Days</u>	<u>28 Days</u>	<u>56 Days</u>
1	5430 psi	6490 psi	7880 psi	8430 psi
2	5400 psi	6430 psi	7770 psi	8360 psi
3	5340 psi	6210 psi	7690 psi	8240 psi
Average	5390 psi	6380 psi	7780 psi	8340 psi

DRYING SHRINKAGE RESULTS (ASTM C 157 as modified by SEAOC)

Prism Size (ASTM C490): 4" x 4" x 11" (gage length = 10" ± 0.10")

<u>Total Age (Days)</u>	<u>Air Dry Age (Days)</u>	<u>Shrinkage Percentage</u>
7	0	0.000
14	7	0.029
21	14	0.036
28	21	0.040
35	28	0.048

Vulcan Materials Company

Western Division

Contractor: *CalPortland Company*

November 5, 2021

Project: *Various*

Plant: *Vulcan Materials / Durbin (SMARA# 91-19-0023)*

Material: *3/8" Pea Gravel (ASTM #8)*

Product Code: *28092*

This is to certify that Vulcan Materials Company, Western Division, Durbin, will supply 3/8" Pea Gravel to the above listed project and that this product will conform to Table 1 and the grading limits in section 6, of ASTM designation C33 - 18, except where indicated by an asterisk *. *Due to the natural effects of segregation and the effects of post-delivery handling, Vulcan Materials Company guarantees that its material will meet the specifications in this submittal at the point of delivery only, and when sampled in accordance with ASTM D75.*

Sieve Size	ASTM C33 Table 1	Percent Passing
12.5 mm (1/2")	100	100
9.5 mm (3/8")	85 - 100	83*
4.75 mm (No. 4)	10 - 30	11
2.36 mm (No. 8)	0 - 10	4
1.18 mm (No. 16)	0 - 5	1
75 um (No. 200)	0-1	0.8

Specific Gravity (SSD)	2.64
Absorption	1.1%

Table 4 - Non-eligible Weathering Region

	Method	Result	Spec.
Clay Lumps / Friable Particles*	C 142	0.0%	5.0 % Max.
Material Finer than #200	C 117	0.8%	1.0 % Max.
Coal and Lignite *	C 123	0.0%	1.0 % Max.
Abrasion (C) 500 rev.	C 131	30%	50 % Max.

* All other classes of concrete

Soundness	C88	2%	na
-----------	-----	----	----

Submitted by:



Jeff Pollard
Manager Technical Services
JP/je

VULCAN HEREBY EXCLUDES ALL WARRANTIES OF MERCHANTABILITY OR FITNESS FOR ANY PURPOSE, AND ALL OTHER WARRANTIES, EXPRESS OR IMPLIED, OF THE MATERIAL SOLD BY VULCAN TO BUYER HEREUNDER, OTHER THAN THE APPLICABLE EXPRESS WARRANTY SET FORTH ABOVE. VULCAN MAKES NO WARRANTY OR GUARANTEE OF FINISHED WORK WHATSOEVER, IN NO EVENT SHALL VULCAN BE LIABLE OR RESPONSIBLE FOR ANY INDIRECT, INCIDENTAL, CONSEQUENTIAL, SPECIAL, EXEMPLARY, LIQUIDATED OR PUNITIVE DAMAGES, INCLUDING, BUT NOT LIMITED TO, LOST PROFITS, WHETHER SUCH CLAIM IS BASED ON EXPRESS OR IMPLIED WARRANTY, CONTRACT, TORT (INCLUDING NEGLIGENCE) OR OTHERWISE, EVEN IF THE POSSIBILITY OF SUCH DAMAGES HAS BEEN DISCLOSED IN ADVANCE BY BUYER OR COULD HAVE BEEN REASONABLY FORESEEN.

Southern California Quality Control Department
16009 Foothill Boulevard • Irwindale, California 91706 • Telephone (626) 856-6190 • Fax (626) 969-2918
Please Note: Not Valid if Altered



Vulcan Materials Company

Western Division

Contractor: *CalPortland Company*

November 5, 2021

Project: *Various*

Plant: *Vulcan Materials / Durbin (SMARA# 91-19-0023)*

Material: *Washed Concrete Sand (WCS)*
Product Code: *31822*

This is to certify that Vulcan Materials Company, Western Division, Durbin, will supply Washed Concrete Sand (WCS) to the above listed project and that this product will conform to Table 1 and the grading limits in section 6, of ASTM designation C33 - 18. *Due to the natural effects of segregation and the effects of post-delivery handling, Vulcan Materials Company guarantees that its material will meet the specifications in this submittal at the point of delivery only, and when sampled in accordance with ASTM D75.*

Sieve Size		ASTM C33 Section 6	Percent Passing
9.5 mm	(3/8")	100	100
4.75 mm	(No. 4)	95 - 100	96
2.36 mm	(No. 8)	80 - 100	82
1.18 mm	(No. 16)	50 - 85	66
600 um	(No. 30)	25 - 60	46
300 um	(No. 50)	5 - 30	23
150 um	(No. 100)	0 - 10	8
75 um	(No. 200)	0 - 5 ^A	2.7

Specific Gravity(SSD)	2.65
Absorption	0.9%

	Method	Result	Spec.
Fineness Modulus (F.M.)	C 136	2.8	2.3 - 3.1
Soundness	C 88	3%	10 % Max.
Organic Impurities	C 40	lighter	lighter than standard

Table 1

	Method	Result	Spec.
Clay Lumps / Friable Particles	C 142	0.0%	3.0 % Max.
Coal and Lignite *	C 123	0.0%	1.0 % Max.

* All other concrete

Submitted by:



Jeff Pollard
Manager Technical Services
JP/je

VULCAN HEREBY EXCLUDES ALL WARRANTIES OF MERCHANTABILITY OR FITNESS FOR ANY PURPOSE, AND ALL OTHER WARRANTIES, EXPRESS OR IMPLIED, OF THE MATERIAL SOLD BY VULCAN TO BUYER HEREUNDER, OTHER THAN THE APPLICABLE EXPRESS WARRANTY STATED ABOVE. VULCAN MAKES NO WARRANTY OR GUARANTEE OF FINISHED WORK WHATSOEVER. IN NO EVENT SHALL VULCAN BE LIABLE OR RESPONSIBLE FOR ANY INDIRECT, INCIDENTAL, CONSEQUENTIAL, SPECIAL, EXEMPLARY, LIQUIDATED OR PUNITIVE DAMAGES, INCLUDING, BUT NOT LIMITED TO, LOST PROFITS, WHETHER SUCH CLAIM IS BASED ON EXPRESS OR IMPLIED WARRANTY, CONTRACT, TORT (INCLUDING NEGLIGENCE) OR OTHERWISE, EVEN IF THE POSSIBILITY OF SUCH DAMAGES HAS BEEN DISCLOSED IN ADVANCE BY BUYER OR COULD HAVE BEEN REASONABLY FORESEEN.

Southern California Quality Control Department
16009 Foothill Boulevard • Irwindale, California 91706 • Telephone (626) 856-6190 • Fax (626) 969-2918
Please Note: Not Valid if Altered





Manufacturer's Certification

Report Date: 3/8/2021

We hereby certify that CalPortland Type II/V Cement meets the standard requirements of ASTM C150 and AASHTO M85 specification for Type II and Type V cements, as well as Caltrans Standard Specification Sec. 90-1.02B(2). Reported are the average chemical and physical data for the month indicated below.

Month: February, 2021

Riverside Type II / V Cement

Source: Oro Grande, CA, USA

Chemical Properties	ASTM C150 and AASHTO M85 Requirements		Analysis	IPA	Limestone
	Type II	Type V	Results	Analysis	Analysis
Silicon dioxide (SiO ₂), %	---	---	20.5	11.6	7.5
Aluminum oxide (Al ₂ O ₃), max, %	6.0	---	4.1	2.9	0.6
Ferric oxide (Fe ₂ O ₃), max, %	6.0	---	3.8	1.5	0.3
Calcium oxide (CaO), %	---	---	63.9	44.6	50.5
Magnesium oxide (MgO), max, %	6.0	6.0	1.5	0.9	0.4
Sulfur trioxide (SO ₃), max, %	3.0	2.3	2.5	0.2	0.2
Loss on ignition (LOI), max, %	3.5	3.5	2.6		
Insoluble residue (IR), max, %	1.5	1.5	1.1		Base
Alkalies (Na ₂ O+0.658*K ₂ O), %	---	---	0.46		Cement
Tricalcium silicate (C ₃ S), %	---	---	59		61
Dicalcium silicate (C ₂ S), %	---	---	13		14
Tricalcium aluminate (C ₃ A), max, %	8	5	4		5
Tetracalcium aluminoferrite (C ₄ AF), %	---	---	12		12
C ₄ AF + 2(C ₃ A), max, %	---	25	20		
CO ₂ , %	---	---	1.4		
Limestone addition, max, %	5.0	5.0	3.4		
IPA addition, max, %	5.0	5.0	0.5		
CaCO ₃ in Limestone, min, %	70	70	92		
Physical Properties					
Air content of mortar, max, volume %	12	12	7		
Blaine Fineness, min, m ² /kg	260	260	398		
Autoclave expansion, max, %	0.80	0.80	-0.02		
Compressive Strength, min					
3 Day, MPa	10.0	8.0	28.6		
3 Day, psi	1450	1160	4150		
7 Day, MPa	17.0	15.0	36.4		
7 Day, psi	2470	2180	5280		
28 Day (from previous month), MPa	---	21.0	44.0		
28 Day (from previous month), psi	---	3050	6380		
Vicat Setting Time, min-max, minutes	45 - 375	45 - 375	92		
C1038 expansion, max, %	0.020	0.020	0.005		

Apparatus and methods used in this laboratory have been audited by the Cement and Concrete Reference Laboratory of the National Institute of Standards and Technology. A copy of the report detailing their findings is available upon request. Major oxides are analyzed in accordance with ASTM C114.

Note 1: ASTM C150, Table 1, Note D, It is permissible to exceed the values in the table for SO₃ content, provided it has been demonstrated by ASTM C1038 that the cement with the increased SO₃ will not develop expansion exceeding 0.020% at 14 days.

Note 2: Complies with Caltrans Specification Sec 90-1.02B(2).

Bob Sylvia - Chief Chemist

Appendix C. Steel Reinforcements Certified Mill Test Report

CMC Rebar West												San Bernardino, CA	
Item Bundle Check List				Session: 033373		Fab Shop: San Bernardino, CA		Fab Date: 10/21/2021					
				Run: 162343		Shift: 1st Shift		Caption: LOAD #5488					
SRQV				Job Name: SBD CASH NON TAXABLE		Job: 8824930002		Description: UCLA ENGINEERING DONATION					
				Customer: SBD CASH SALE		Release: 1		Ship Date: 10/25/2021					
				LOAD #5488									
Tag	Load	Color / Shape	Quantity	Size	Length	Mark	Shape	Lbs	Grade	Coating	BC	Page / Item	CL / Tag
Bent													
9		Black ◊ Black ▲	30	8	6-03	8A01	0TMB	501	80	Blk	B	1 / 2	1 / 2
Straight													
8		Black ◊ Black ▲	7	8	60-00			1,121	80	Blk	ST	1 / 1	1 / 1
10		Black ◊ Black ▲	5	7	60-00			613	80	Blk	ST	1 / 3	2 / 1
11		Black ◊ Black ▲	5	5	60-00			313	80	Blk	ST	1 / 4	3 / 1
12		Black ◊ Black ▲	50	4	60-00			2,004	80	Blk	ST	1 / 5	4 / 1
13		Black ◊ Black ▲	45	4	60-00			1,804	80	Blk	ST	1 / 5	4 / 2
			Total Rebar Tags: 6		Longest Length: 60-00			Total Weight:		6,356 Lbs			

v20.01.148

Thursday, October 21, 2021 1:36:56 PM
 ©2021 aSa UNAUTHORIZED REPRODUCTION PROHIBITED

Page 1 of 2

CMC Rebar West												San Bernardino, CA	
Item Bundle Check List				Session: 033373		Fab Shop: San Bernardino, CA		Fab Date: 10/21/2021					
				Run: 162343		Shift: 1st Shift		Caption: LOAD #5488					
SRQV				Job Name: SBD CASH NON TAXABLE		Job: 8824930002		Description: UCLA ENGINEERING DONATION					
				Customer: SBD CASH SALE		Release: 1		Ship Date: 10/25/2021					
				LOAD #5488									
Tag	Load	Color / Shape	Quantity	UM	Item	Description	Lbs						
Miscellaneous Items													
7		Black ◊ Black ▲	60	Pcs	EL25D6	COUPLER, LENTON D6 TERMINATOR #6	78						
			Total Miscellaneous Tags: 1		Total Weight:			78 Lbs					

v20.01.148

Thursday, October 21, 2021 1:36:56 PM
 ©2021 aSa UNAUTHORIZED REPRODUCTION PROHIBITED

Page 2 of 2



**STRAIGHT BILL OF LADING-SHORT FORM
ORIGINAL-NON NEGOTIABLE**

74440995

74440995

SHIPMENT NO.(BOL) : 74440995 DATE AND TIME : 10/25/2021 12:46:07 SHIP FROM : CMC Rebar CA San Bernardino Truck 5425 Industrial Parkway San Bernardino, CA 92407-1803 USA Contact Phone No. : Fax No. :	CARRIER'S NAME: Enrique Avendano TRUCK/UNIT No: CMC INCO TERMS: CPT San Bernardino SHIP TO: 3131318 CMC Rebar San Bernardino Cash/ 5425 Industrial Pkwy San Bernardino, CA 92407-1803 USA Contact Phone No. :9999999999 Fax No. :	SEAL NUMBER : TRAILER/RAILCAR No: SOLD TO: 3131316 CMC Rebar San Bernardino Cash 5425 Industrial Pkwy San Bernardino, CA 92407-1803 USA Contact Phone No. :9999999999 Fax No. :
---	---	--

NONRECOURSE - Subject to Section 7 of Conditions, if this shipment is to be delivered to the consignee without recourse on the consignor, the consignor shall sign the following statement: The carrier shall not make delivery of this shipment without payment of freight and all other lawful charges. The carrier shall not be entitled to recover from the consignor in the event of non-payment.

Consignor's Signature : Rick Jenkins

Carrier understands that Shipper will only be liable for payment for property directly tendered by Shipper to Carrier and Shipper will only accept an invoice or request for payment if received within 90 days from the date of shipment.

BOL INSTRUCTIONS:

NOTES/SPECIAL INSTRUCTIONS:

Additional Instructions :

Material Details

Delivery	Cust PO	Ctrl Cd	Rel No.	Release Description	Dwg #	Material Description	PCS	Weight LB
PROJECT: R/8824930002 LS								
4943302		SRQV	1	UCLA ENGINEERING DONATION		PROD STK REBAR 25MM (#8) 550/80	1622 LB	1,622
4943302		SRQV	1	UCLA ENGINEERING DONATION		Rebar Black 80/550		4,734
4943302		SRQV	1	UCLA ENGINEERING DONATION		TERMINATOR, LENTON 08	60 EA	54
Total Weight								6,410

RECEIVED, subject to the classifications in effect on the date of the issue of the Bill of Lading, the property described above, in apparent good order, except as noted (contents of packages unknown), marked, consigned, and destined as indicated below, which said carrier (the word carrier being understood throughout this contract as meaning any person or corporation in possession of the property under the contract) agrees to carry to its usual place of delivery at said destination, if on its route, otherwise to deliver to another carrier on the route to said destination. It is mutually agreed, as to each carrier of all or any said property over all or any portion of said route to destination, and as to each party at any time interested in all or any of said property, that every service to be performed hereunder shall be subject to all the terms and conditions of the Uniform Domestic Straight Bill of Lading set forth (1) in Official, Southern, Western and Illinois Freight Classifications in effect on the date hereof, if this is a rail or a rail-water shipment, or (2) in the applicable motor carrier classification or tariff if this is a motor carrier shipment. Shipper hereby certifies that he is familiar with all the terms and conditions of the said bill of lading, including those on the back thereof, set forth in the classification or tariff which governs the transportation of this shipment and the said terms and conditions are hereby agreed to by the shipper and accepted for himself and his assigns. This is to certify that the above articles are properly describe by name and are packed and marked and are in proper condition for transportation according to regulations by the Interstate Commerce Commission. * If the shipment moves between two ports by a carrier by water, the law requires that the bill of lading shall state whether it is "carrier's or shipper's weight." * Shipper's imprints in lieu of stamp; not a part of Bill of Lading approved by the Interstate Commerce Commission. NOTE: Where the rate is dependent on value, shippers are required to state specifically in writing the agreed or declared value of property. The agreed or declared value of the property is hereby specifically state by the shipper to be not exceeding. WARNING: This product can expose you to chemicals which are known to the State of California to cause cancer, birth defects or other reproductive harm. For more information go to www.P65Warnings.ca.gov. Note: In the case of Customer Pick Up, the Ship To address indicated above has been provided by the entity identified in the Sold To field above (#Customer#) and Customer is solely responsible for transporting the property described above from the CMC facility to Customer#s designated Ship To address. Alternatively, if Customer does not provide a Ship To Address, the Ship To Address above will reflect the CMC facility.

DRIVER'S SIGNATURE/AGENT : _____

NOTICE TO RECEIVERS :Please check each item on this shipping bill carefully. CMC will not be responsible for any exceptions to goods unless notified within twenty four hours and noted on this document.

RECEIVED BY : _____ DATE: _____ TIME: _____



CMC STEEL TEXAS
1 STEEL MILL DRIVE
SEGUN TX 78155-7510

CERTIFIED MILL TEST REPORT
For additional copies call

We hereby certify that the test results presented here
are accurate and conform to the reported grade specification

Rolande A Davila
Rolande A Davila
Quality Assurance Manager

HEAT NO.: 3102853 SECTION: REBAR 13MM (#4) 60" A706-80 GRADE: ROLL DATE: 01/17/2021 MELT DATE: 01/07/2021 Cert. No.: 83556591 / 102853A652	S O L D T O	CMC CA San Bernardino Industrial Parkway San Bernardino CA US 92407-1803	S H I P T O	CMC REBAR SAN BERNARDINO 5425 Industrial Parkway San Bernardino CA US 92407-1803 909-713-1130	Delivery#: 83556591 BOL#: 74311689 CUST POW: CUST P/N: DLVRY LBS / HEAT: 5772,000 LB DLVRY PCS / HEAT: 144 EA
---	----------------------------	---	----------------------------	---	--

Characteristic	Value	Characteristic	Value	Characteristic	Value
C	0.27%	Tensile to Yield ratio test1	1.28		
Mn	1.27%	Bend Test 1	Passed		
P	0.012%	Bend Test Diameter	1.500IN		
S	0.030%				
Si	0.26%				
Cu	0.28%				
Cr	0.09%				
Ni	0.10%				
Mo	0.035%				
V	0.103%				
Cb	0.001%				
Sn	0.010%				
Al	0.002%				
N	0.0216%				
Carbon Eq A706	0.50%				
Yield Strength test 1	89.6ksi				
Tensile Strength test 1	114.9ksi				
Elongation test 1	14%				
Elongation Gage Lgth test 1	8IN				

The Following is true of the material represented by this MTR:
 *Material is fully killed
 *100% melted and rolled in the USA
 *EN10204:2004 3.1 compliant
 *Contains no weld repair
 *Contains no Mercury contamination
 *Manufactured in accordance with the latest version of the plant quality manual
 *Meets the "Buy America" requirements of 23 CFR635.410, 49 CFR 681
 *Warning: This product can expose you to chemicals which are known to the State of California to cause cancer, birth defects or other reproductive harm. For more information go to www.P65Warnings.ca.gov

REMARKS :



CMC STEEL ARIZONA
11444 E. GERMAN RD.
MESA AZ 85212-9700

CERTIFIED MILL TEST REPORT
For additional copies call
830-372-8771

Jacob Seizer
Jacob Seizer - CMC Steel

We hereby certify that the test results presented here
are accurate and conform to the reported grade specification

Quality Assurance Manager

EAT NO.: 4112750
SECTION: REBAR 16MM (#5) 60"0"
615/A706-80
RADE: ASTM A615 & A706 GR80 Dual Gr
OLL DATE: 10/15/2021
ELT DATE: 10/15/2021
ert. No.: 83630552 / 112750F928

S	CMC CA San Bernardino	S	CMC REBAR SAN BERNARDINO	Delivery#: 83630552 BOL#: 74434035 CUST PO#: CUST PIN: DLVRY LBS / HEAT: 18399.000 LB DLVRY PCS / HEAT: 294 EA
O	Industrial Parkway San Bernardino CA US 92407-1803	H	5425 Industrial Parkway San Bernardino CA US 92407-1803	
L		I		
D		P		
T		T		
O		O		

Characteristic	Value	Characteristic	Value	Characteristic	Value
C	0.28%	Elongation test 1	12%	The Following is true of the material represented by this MTR: *Material is fully killed *100% melted and rolled in the USA *EN10204:2004 3.1 compliant *Contains no weld repair *Contains no Mercury contamination *Manufactured in accordance with the latest version of the plant quality manual *Meets the "Buy America" requirements of 23 CFR635.410, 49 CFR 661 *Warning: This product can expose you to chemicals which are known to the State of California to cause cancer, birth defects or other reproductive harm. For more information go to www.P65Warnings.ca.gov	
Min	1.22%	Elongation Gage Lgth test 1	8IN		
P	0.012%	Tensile to Yield ratio test1	1.32		
S	0.028%	Bend Test 1	Passed		
Si	0.20%	Rebar Deformation Avg. Spaci	0.415IN		
Cu	0.32%	Rebar Deformation Avg. Heigh	0.041IN		
Cr	0.19%	Rebar Deformation Max. Gap	0.124IN		
Ni	0.12%	Bend Test Diameter	1.875IN		
Mo	0.068%	Strain at Peak Stress test 1	8.8%		
V	0.016%				
Cb	0.000%				
Sn	0.011%				
Al	0.002%				
N	0.0138%				
Carbon Eq A706	0.52%				
Yield Strength test 1	85.1ksi				
Yield Strength test 1 (metric)	587MPa				
Tensile Strength test 1	111.9ksi				
Tensile Strength 1 (metric)	772MPa				


MARKS :



CMC STEEL TEXAS
1 STEEL MILL DRIVE
SEGUN TX 78155-7510

CERTIFIED MILL TEST REPORT
For additional copies call

We hereby certify that the test results presented here
are accurate and conform to the reported grade specification


Rolanda A. Davila
Quality Assurance Manager

HEAT NO.: 3107727
SECTION: REBAR 22MM (#7) 60'0" A706-80
GRADE: A706-16 Grade 550 (80)
ROLL DATE: 08/04/2021
MELT DATE: 07/30/2021
Cert. No.: 83618107 / 107727A870

S O L D
CMC CA San Bernardino
Industrial Parkway
San Bernardino CA
US 92407-1803

S H I P
CMC REBAR SAN BERNARDINO
5425 Industrial Parkway
San Bernardino CA
US 92407-1803
909-713-1130

Delivery#: 83618107
BOL#: 74414074
CUST PO#:
CUST P/N:
DLVRY LBS / HEAT: 12264.000 LB
DLVRY PCS / HEAT: 100 EA

Characteristic	Value	Characteristic	Value	Characteristic	Value
C	0.29%	Tensile to Yield ratio test 1	1.28		
Min	1.36%	Bend Test 1	Passed		
P	0.013%	Bend Test Diameter	4.375IN		
S	0.037%				
Si	0.21%				
Cu	0.37%				
Cr	0.09%				
Ni	0.09%				
Mo	0.026%				
V	0.099%				
Cb	0.001%				
Sn	0.010%				
Al	0.001%				
N	0.0341%				
Carbon Eq A706	0.53%				
Yield Strength test 1	93.2ksi				
Tensile Strength test 1	119.3ksi				
Elongation Gage Lgth test 1	13%				
Elongation Gage Lgth test 1	8IN				

The Following is true of the material represented by this MTR:
 *Material is fully killed
 *100% melted and rolled in the USA
 *EN10204 2004 3 1 compliant
 *Contains no weld repair
 *Contains no Mercury contamination
 *Manufactured in accordance with the latest version of the plant quality manual
 *Meets the "Buy America" requirements of 23 CFR635.410, 49 CFR 661
 *Warning: This product can expose you to chemicals which are known to the State of California to cause cancer, birth defects or other reproductive harm. For more information go to www.P85Warnings.ca.gov

REMARKS :



CMC STEEL TEXAS
1 STEEL MILL DRIVE
SEGUIN TX 78155-7510

CERTIFIED MILL TEST REPORT
For additional copies call

We hereby certify that the test results presented here
are accurate and conform to the reported grade specification

Quality Assurance Manager

Rolande A Davila
Rolande A Davila

HEAT NO.: 3107727
SECTION: REBAR 22MM (#7) 60"0" A706-80
GRADE: A706-16 Grade 550 (80)
ROLL DATE: 08/04/2021
MELT DATE: 07/30/2021
Cert. No.: 83618107 / 107727A870

S	CMC CA San Bernardino Industrial Parkway San Bernardino CA US 92407-1803	S	CMC REBAR SAN BERNARDINO 5425 Industrial Parkway San Bernardino CA US 92407-1803 909-713-1130	Delivery#: 83618107 BOL#: 74414074 CUST PO#: CUST PIN: DLVRY LBS / HEAT: 12264.000 LB DLVRY PCS / HEAT: 100 EA
O		H		
L		I		
D		P		
T		T		
O		O		

Characteristic	Value	Characteristic	Value	Characteristic	Value
C	0.29%	Tensile to Yield ratio test1	1.28		
Min	1.36%	Bend Test 1	Passed		
P	0.013%	Bend Test Diameter	4.375IN		
S	0.037%				
Si	0.21%				
Cu	0.37%				
Cr	0.09%				
NI	0.09%				
Mn	0.026%				
V	0.099%				
Cb	0.001%				
Sn	0.010%				
Al	0.001%				
N	0.0341%				
Carbon Eq A706	0.53%				
Yield Strength test 1	93.2ksi				
Tensile Strength test 1	119.3ksi				
Elongation test 1	13%				
Elongation Gage Lgth test 1	8IN				

The Following is true of the material represented by this MTR:
 *Material is fully killed
 *100% melted and rolled in the USA
 *EN10204 2004 3 1 compliant
 *Contains no weld repair
 *Contains no Mercury contamination
 *Manufactured in accordance with the latest version of the plant quality manual
 *Meets the "Buy America" requirements of 23 CFR635.410, 49 CFR 661
 *Warning: This product can expose you to chemicals which are known to the State of California to cause cancer, birth defects or other reproductive harm. For more information go to www.P65Warnings.ca.gov

REMARKS :



CMC STEEL TEXAS
1 STEEL MILL DRIVE
SEGUN TX 78155-7510

CERTIFIED MILL TEST REPORT
For additional copies call

We hereby certify that the test results presented here
are accurate and conform to the reported grade specification

Rolando A Devilla
Rolando A Devilla
Quality Assurance Manager

HEAT NO.: 3107663
SECTION: REBAR 25MM (#8) 60" A706-80
GRADE:
ROLL DATE: 08/02/2021
MELT DATE: 07/27/2021
Cert. No.: 83583854 / 107663A871

S CMC CA San Bernardino
O Industrial Parkway
L San Bernardino CA
D US 92407-1803

S CMC REBAR SAN BERNARDINO
H 5425 Industrial Parkway
I San Bernardino CA
P US 92407-1803
T 909-713-1130

Delivery#: 83583854
BOL#: 74356185
CUST PO#:
CUST P/N:
DLVRY LBS / HEAT: 24352.000 LB
DLVRY PCS / HEAT: 152 EA

Characteristic	Value	Characteristic	Value	Characteristic	Value
C	0.26%	Tensile to Yield ratio test1	1.33		
Min	1.34%	Bend Test 1	Passed		
P	0.012%	Bend Test Diameter	5.000IN		
S	0.027%				
Si	0.19%				
Cu	0.32%				
Cr	0.13%				
Ni	0.09%				
Mo	0.025%				
V	0.108%				
Cb	0.001%				
Sn	0.009%				
Al	0.002%				
N	0.0181%				
Carbon Eq A706	0.50%				
Yield Strength test 1	88.6ksi				
Tensile Strength test 1	118.0ksi				
Elongation test 1	14%				
Elongation Gage Lgth test 1	8IN				

The Following is true of the material represented by this MTR:
 *Material is fully killed
 *100% melted and rolled in the USA
 *EN10204:2004 3.1 compliant
 *Contains no weld repair
 *Contains no Mercury contamination
 *Manufactured in accordance with the latest version of the plant quality manual
 *Meets the "Buy America" requirements of 23 CFR835.410, 49 CFR 691
 *Warning: This product can expose you to chemicals which are known to the State of California to cause cancer, birth defects or other reproductive harm. For more information go to www.P65Warnings.ca.gov

REMARKS :

Appendix D. LVDTs and Wire Potentiometers Readings

LVDTs (SB-S6-16)

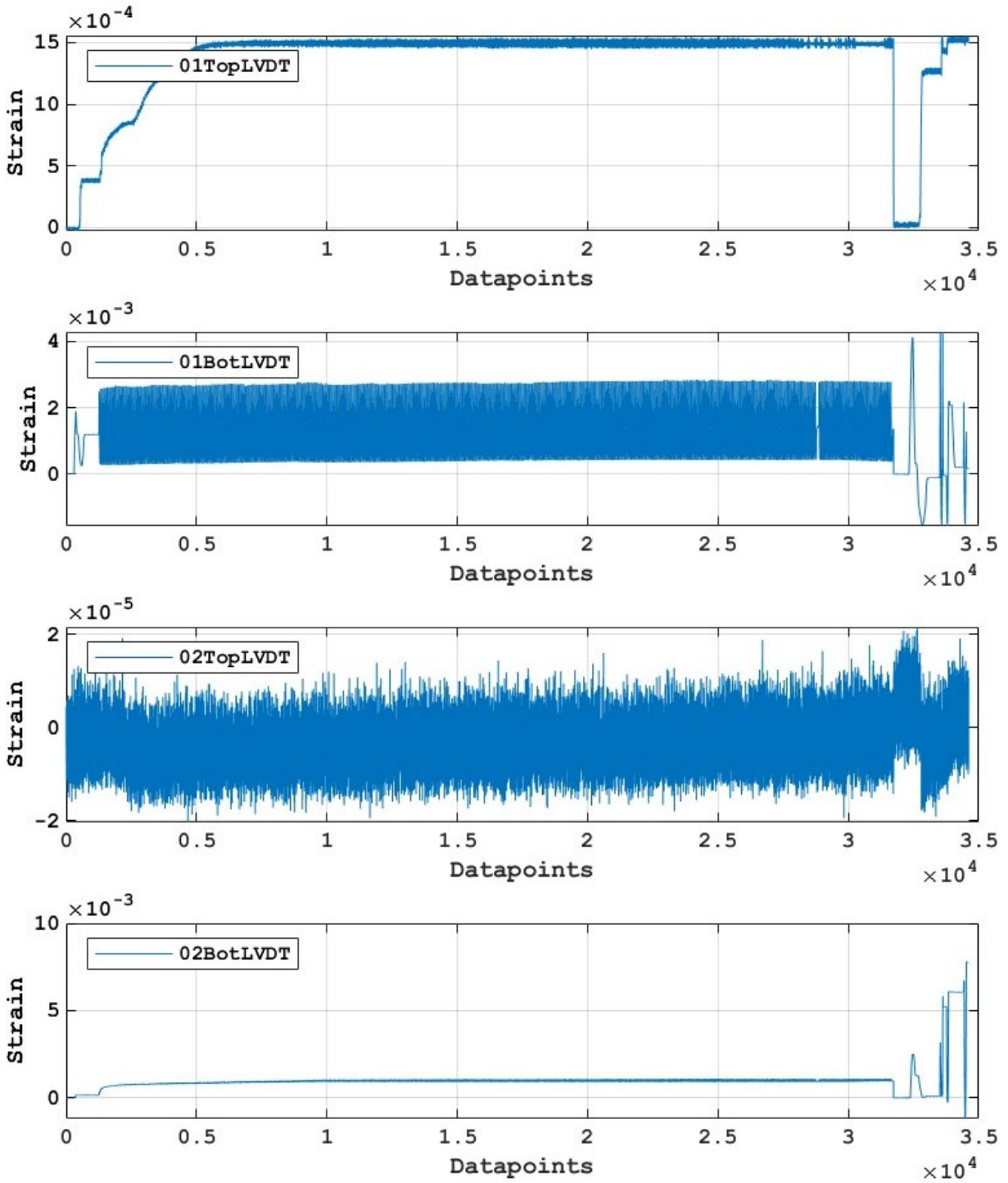


Figure D-1: 01 and 02 LVDT readings (SB-S6-16)

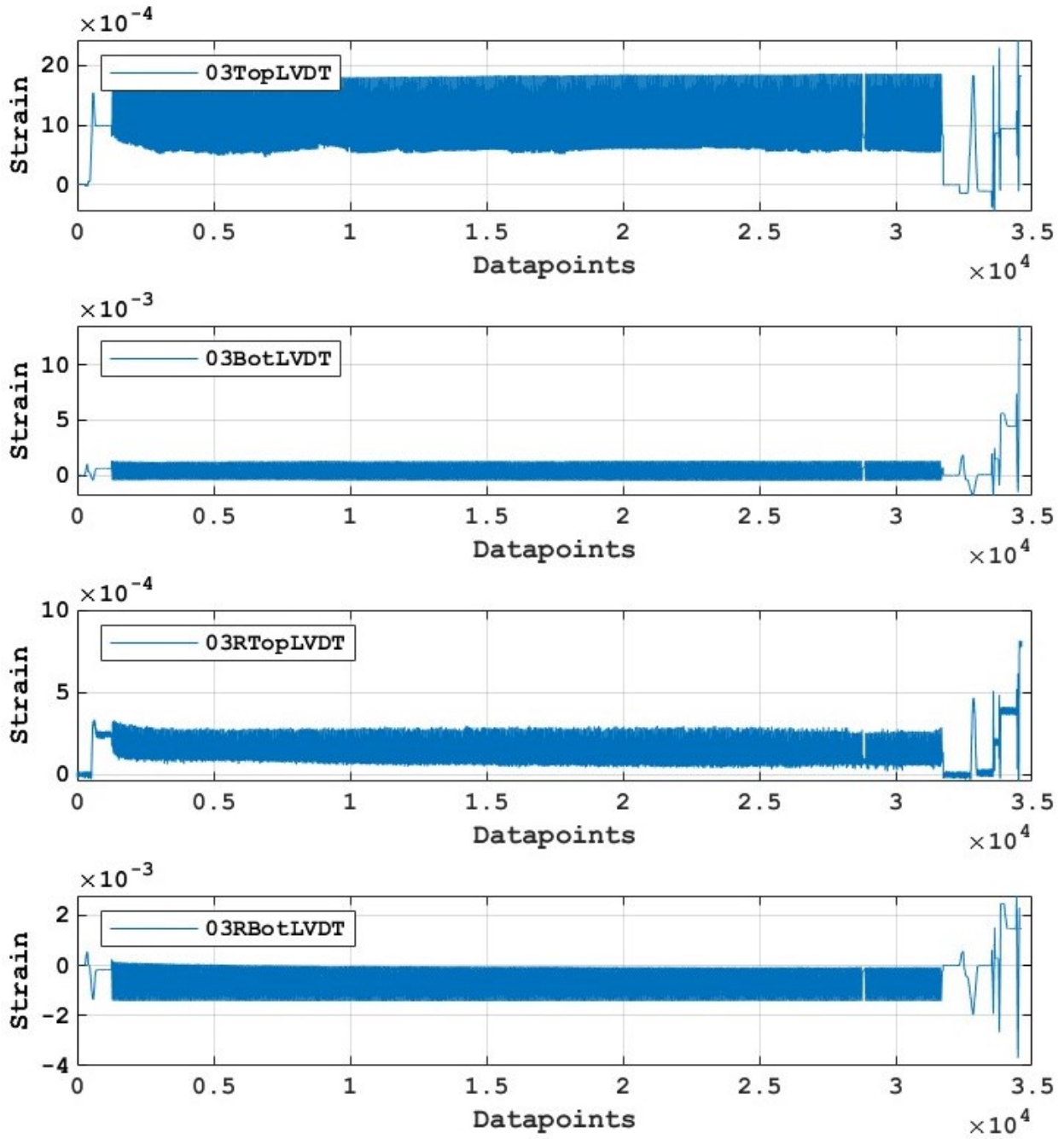


Figure D-2: 03 and 03R LVDT readings (SB-S6-16)

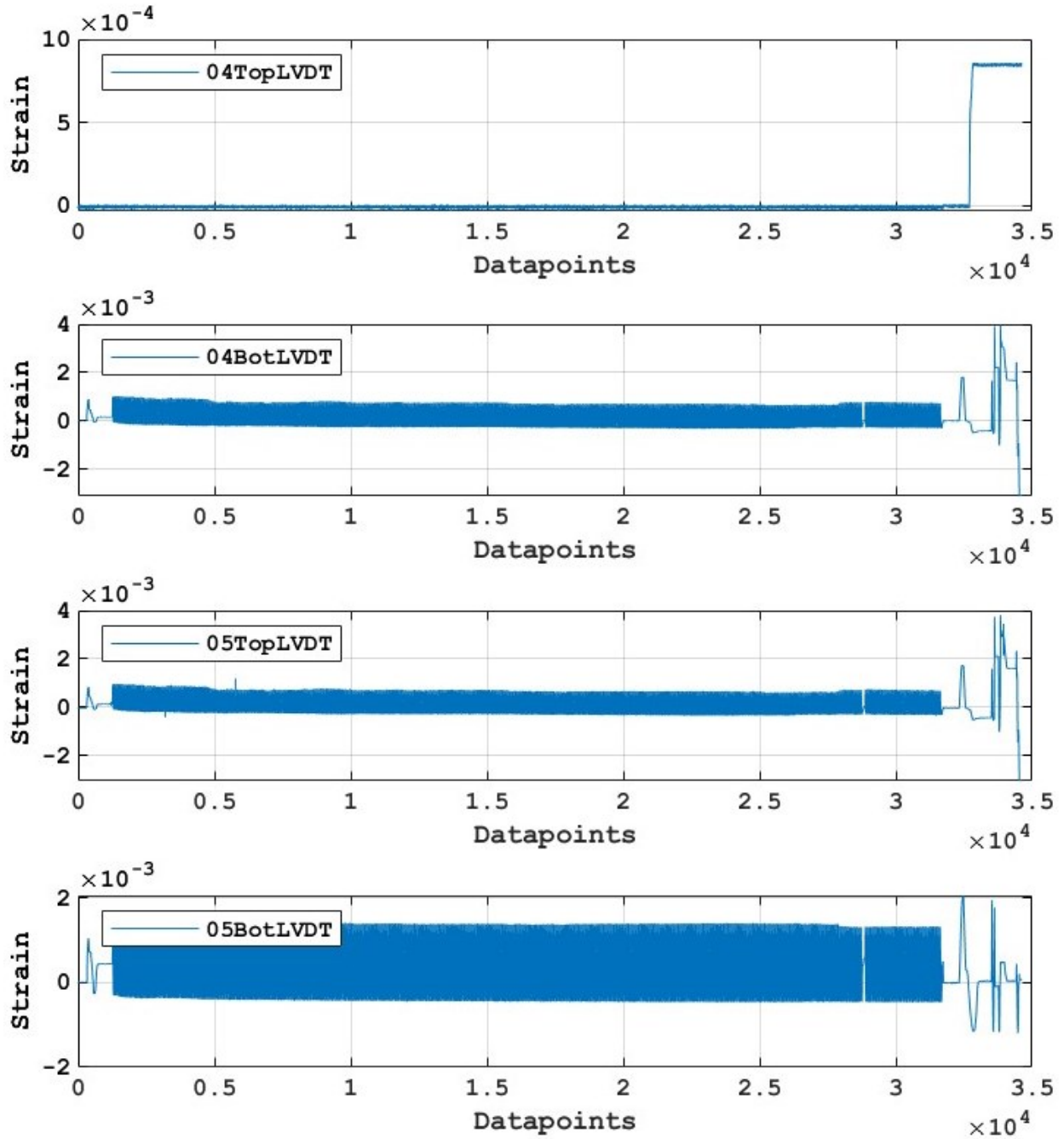


Figure D-3: 04 and 05 LVDT readings (SB-S6-16)

WIRE POTENTIOMETERS (SB-S6-16)

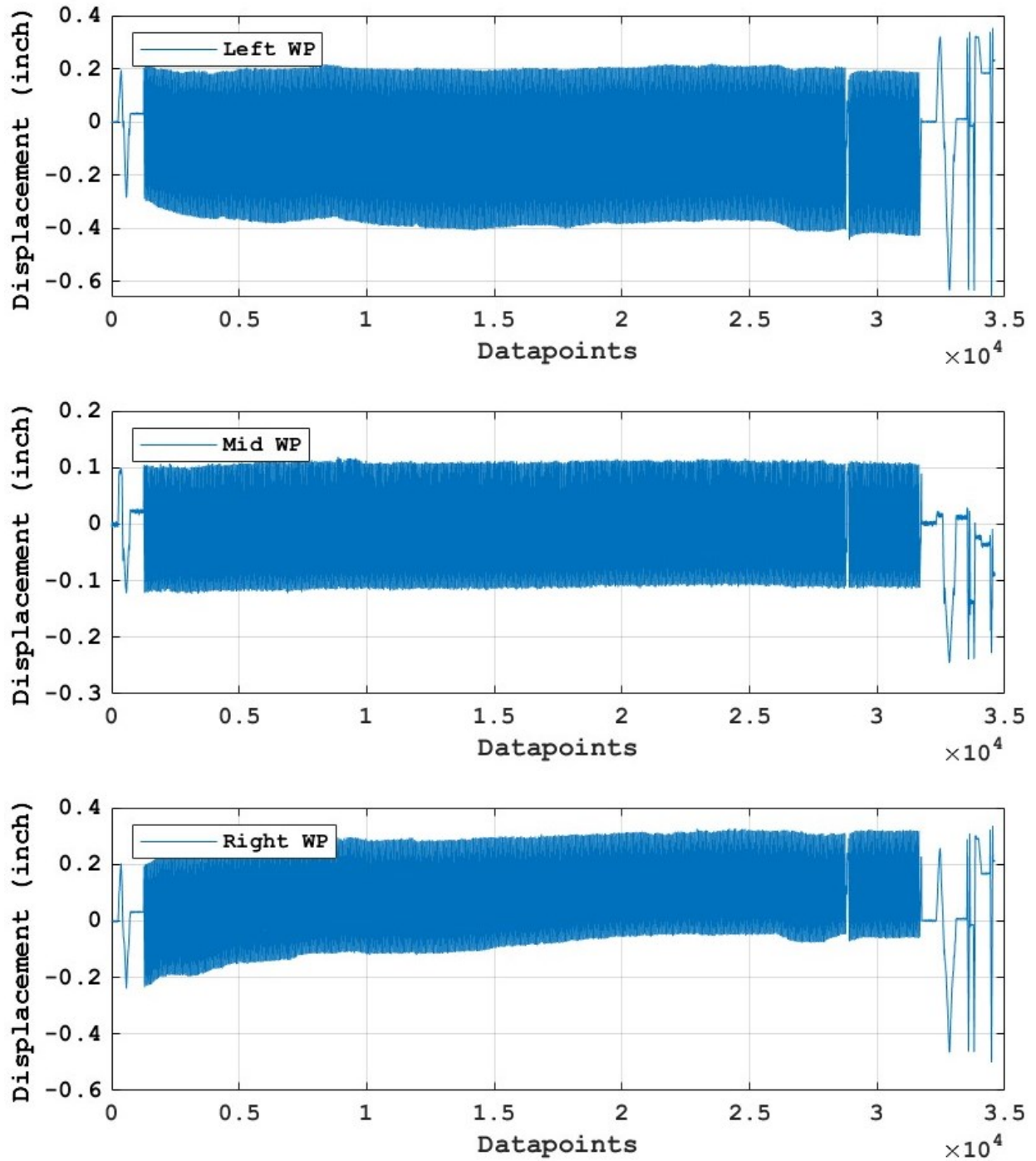


Figure D-4: Wire potentiometers readings (SB-S6-16)

LVDTs (SB-S3-20)

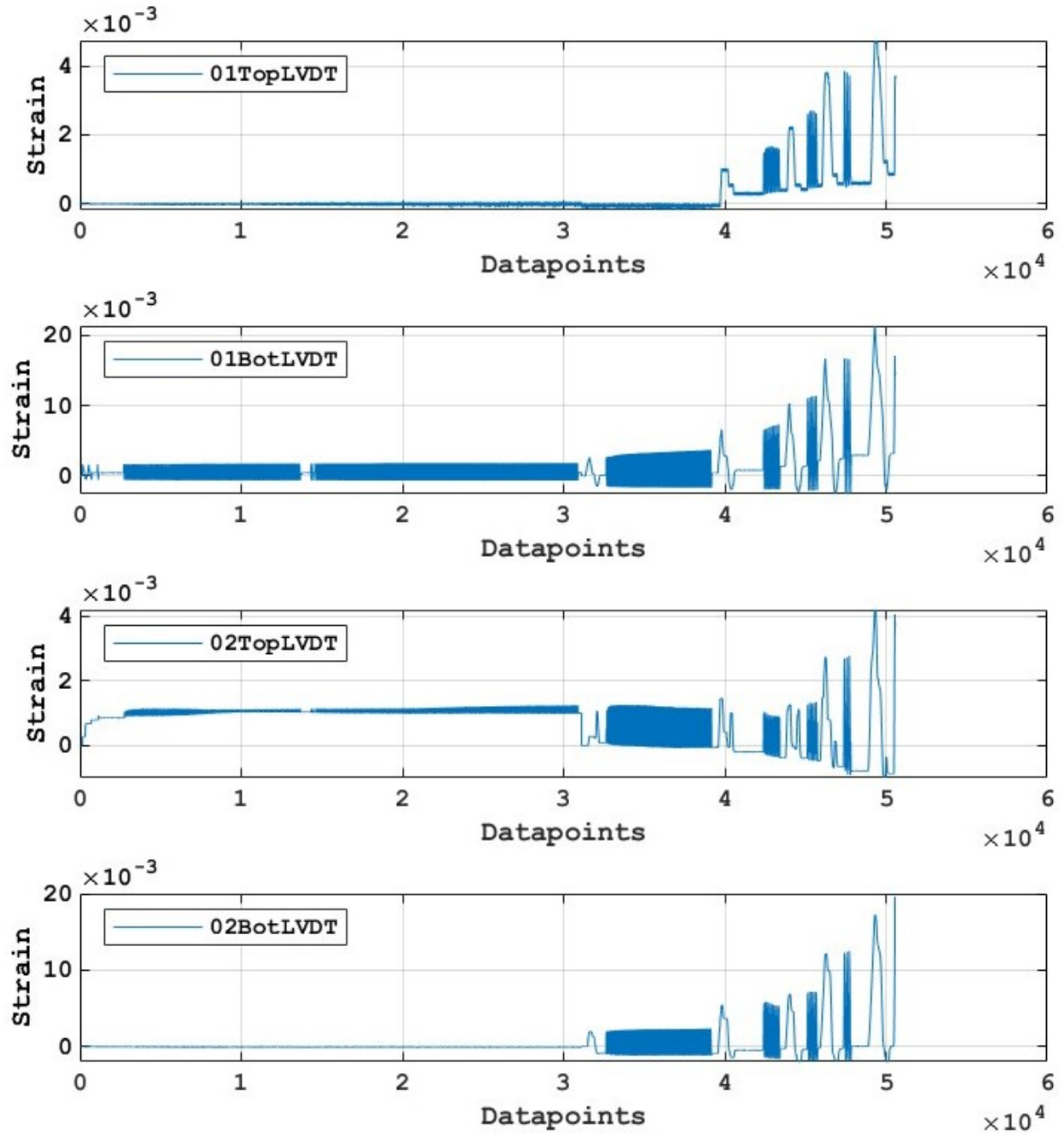


Figure D-5: 01 and 02 LVDT readings (SB-S3-20)

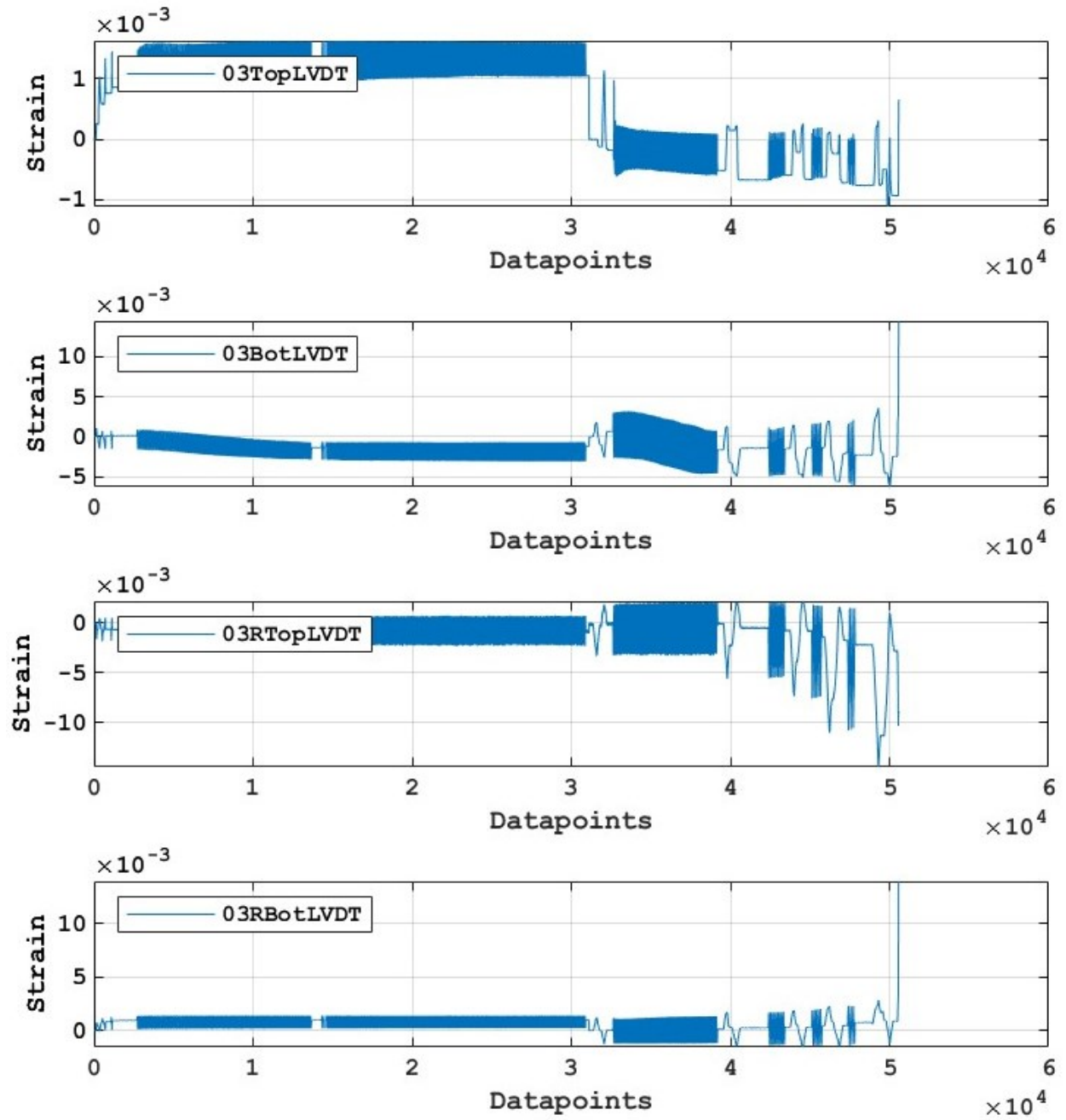


Figure D-6: 03 and 03R LVDT readings (SB-S3-20)

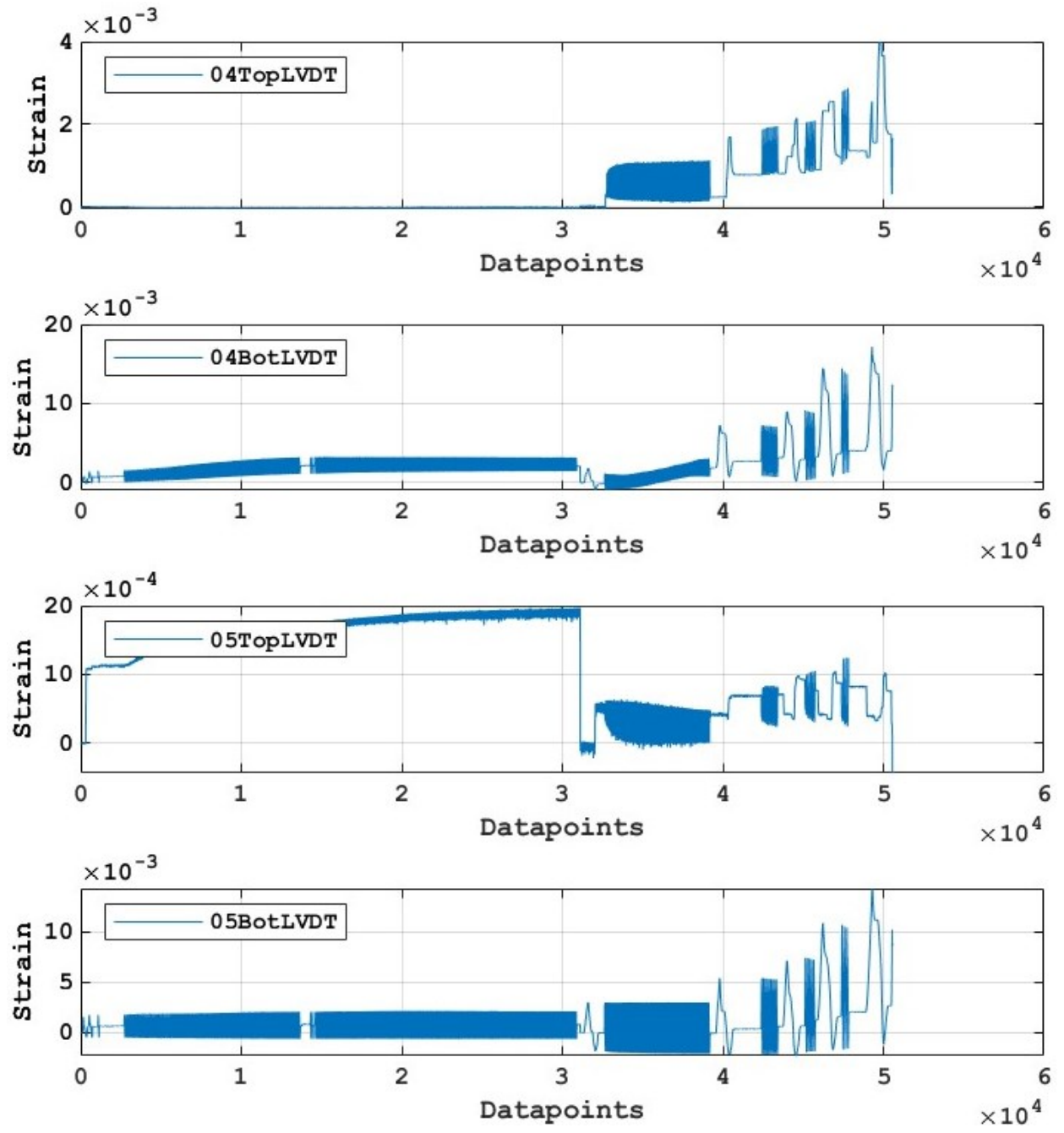


Figure D-7: 04 and 05 LVDT readings (SB-S3-20)

WIRE POTENTIOMETERS (SB-S3-20)

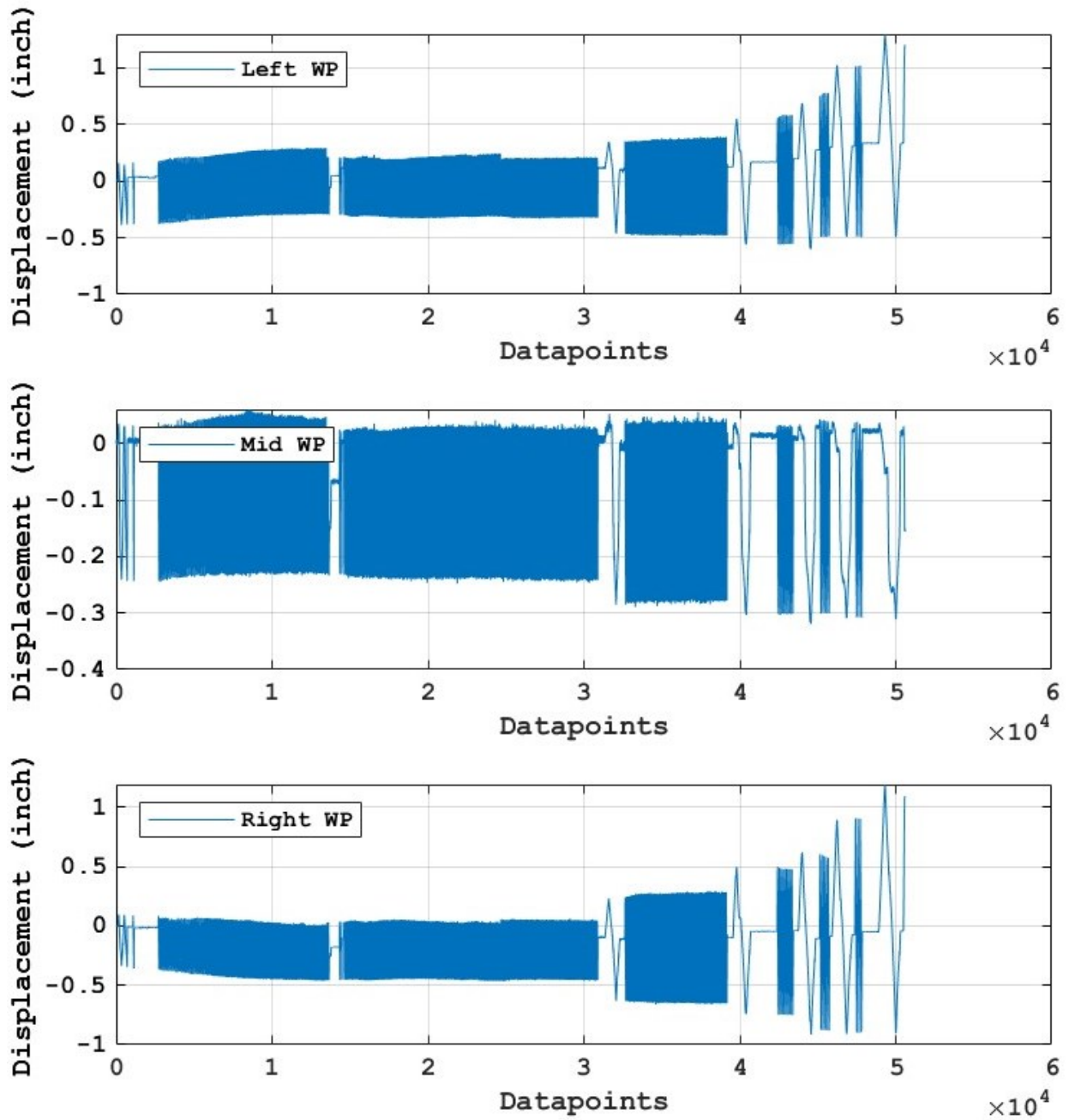


Figure D-8: Wire potentiometers readings (SB-S3-20)

LVDTs (SB-S2-20)

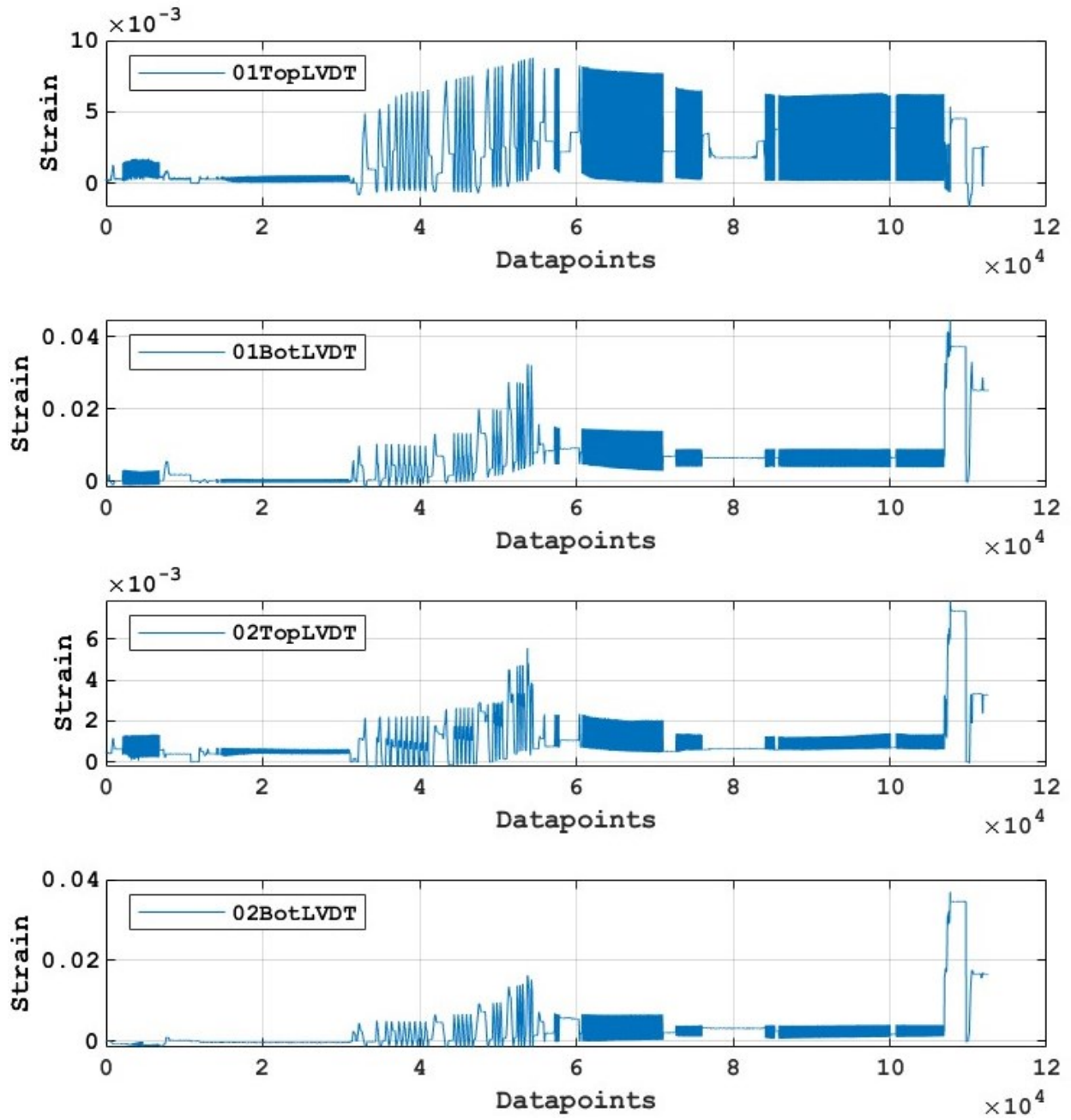


Figure D-9: 01 and 02 LVDT readings (SB-S2-20)

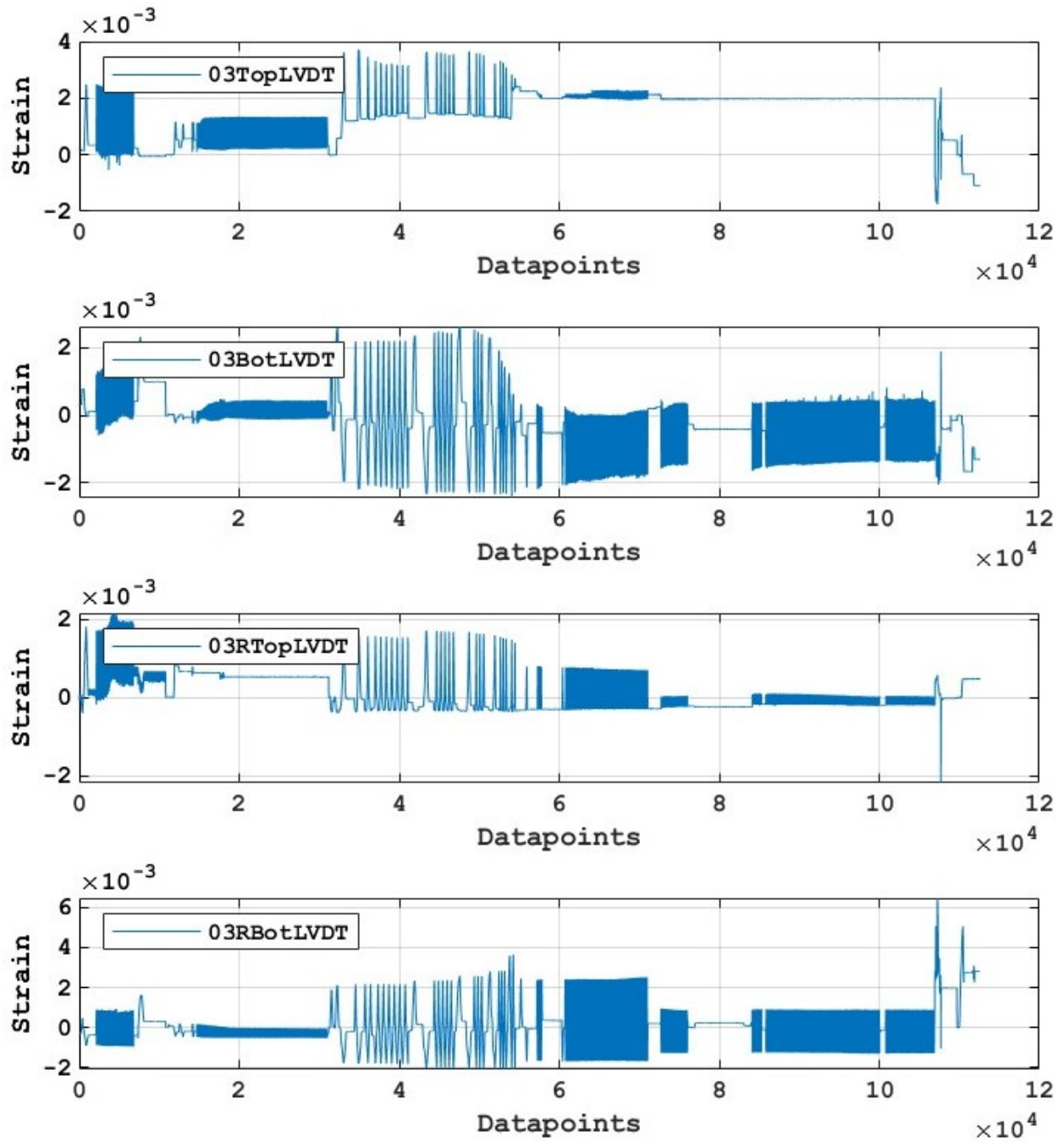


Figure D-10: 03 and 03R LVDT readings (SB-S3-20)

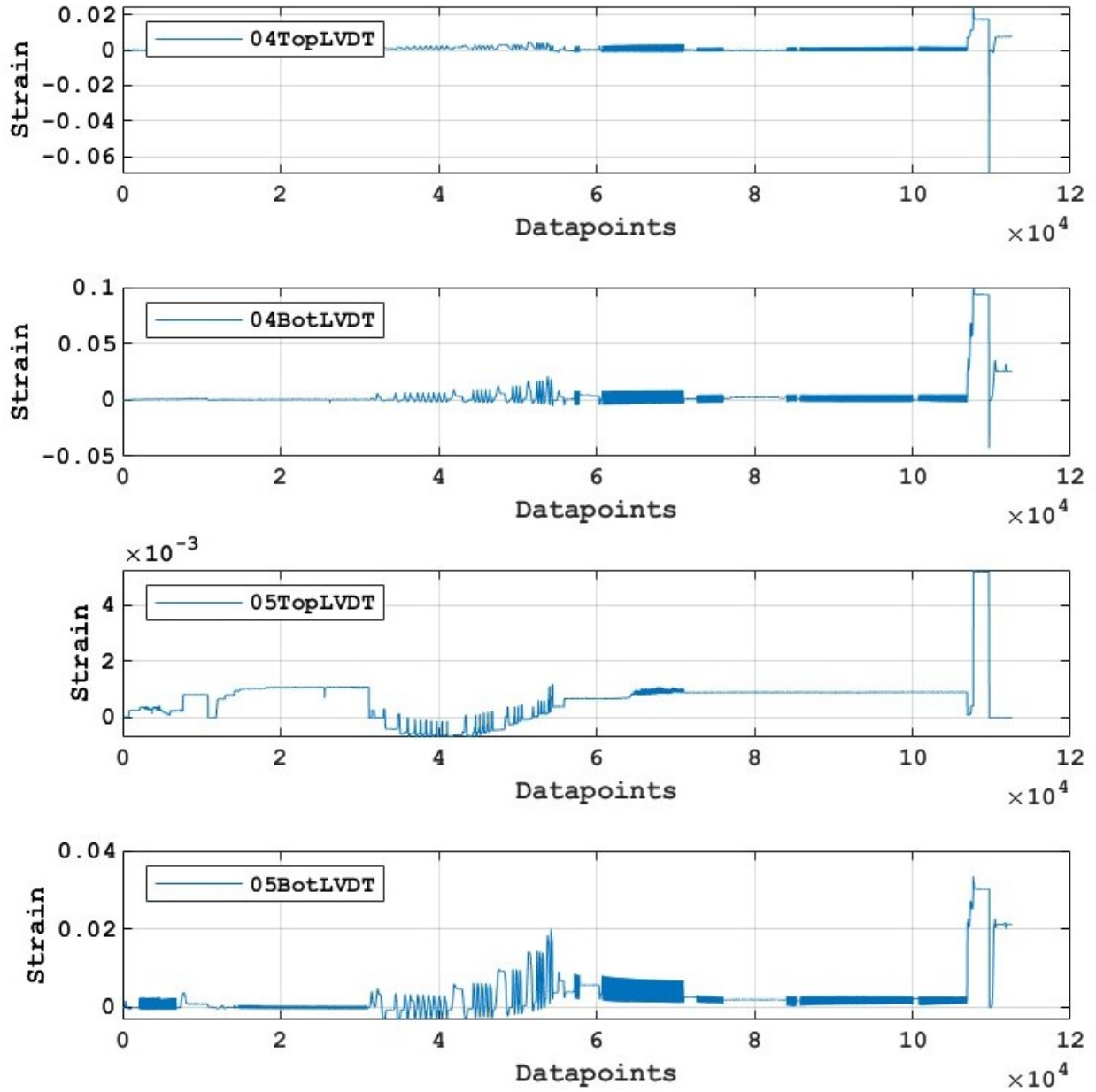


Figure D-11: 04 and 05 LVDT readings (SB-S2-20)

WIRE POTENTIOMETERS (SB-S2-20)

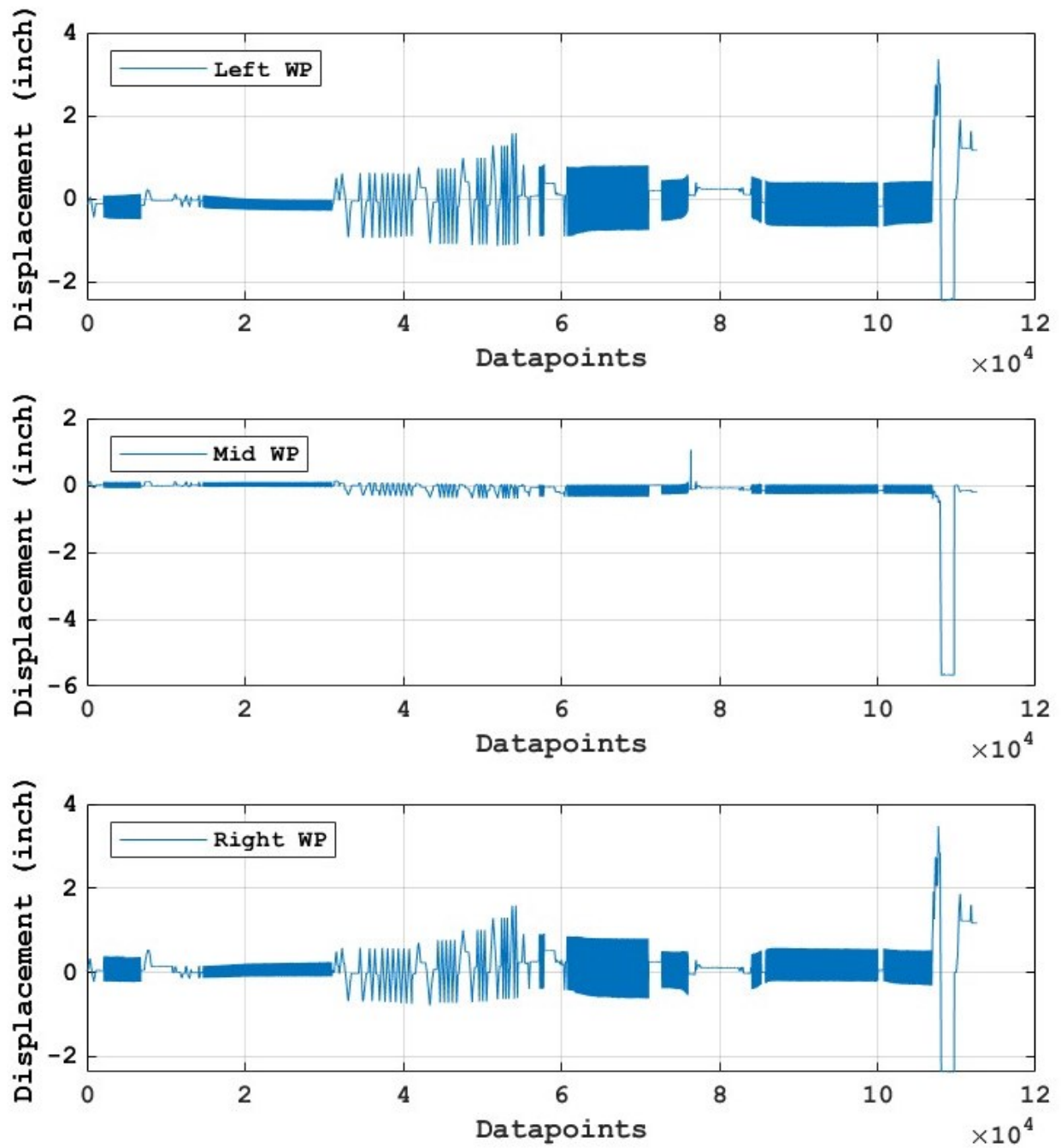


Figure D-12: Wire potentiometers readings (SB-S2-20)

WEST SIDE LVDTs (LB-S7.5-50)

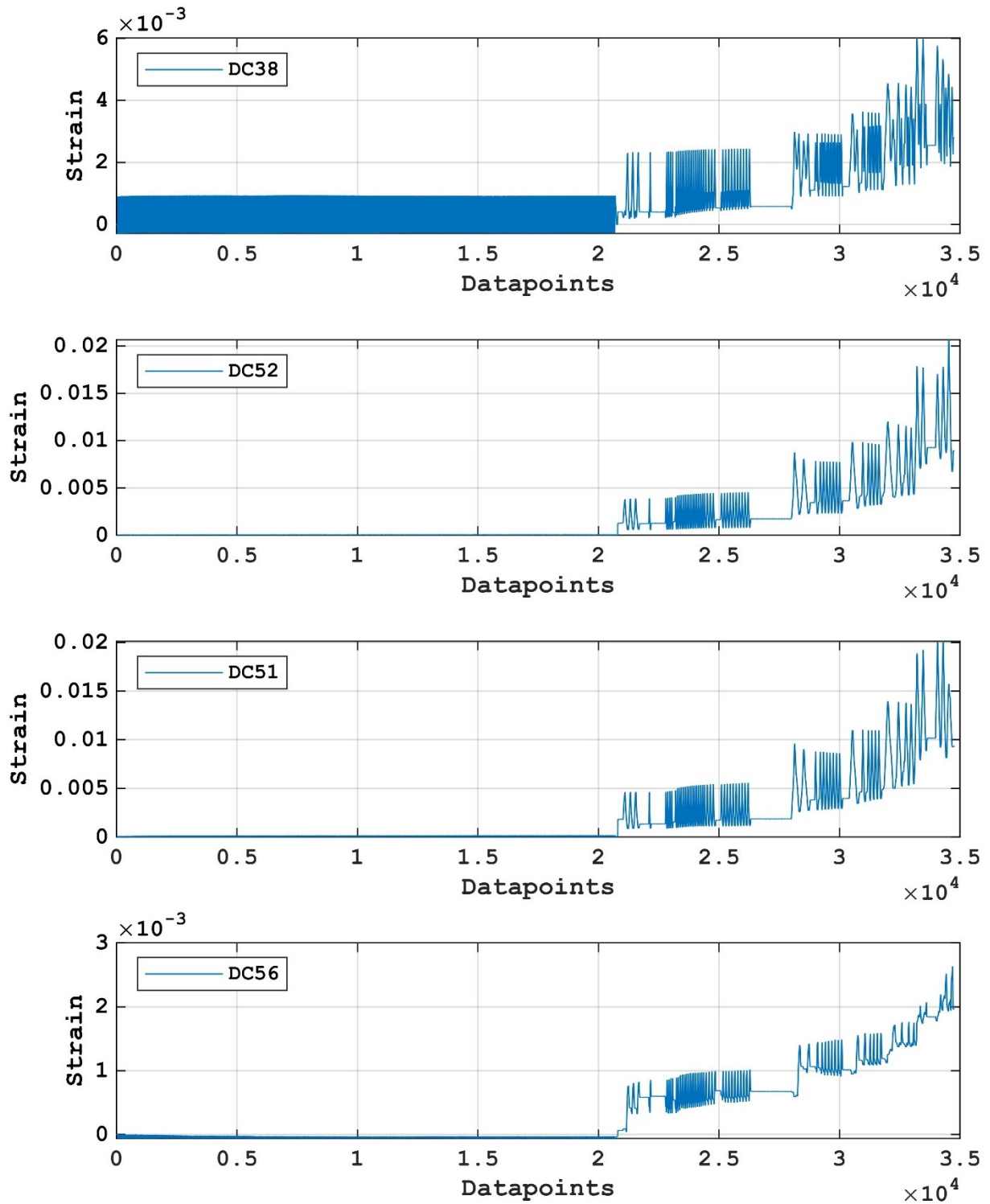


Figure D-13: West side LVTD readings (LB-S7.5-50)

EAST SIDE LVDTs (LB-S7.5-50)

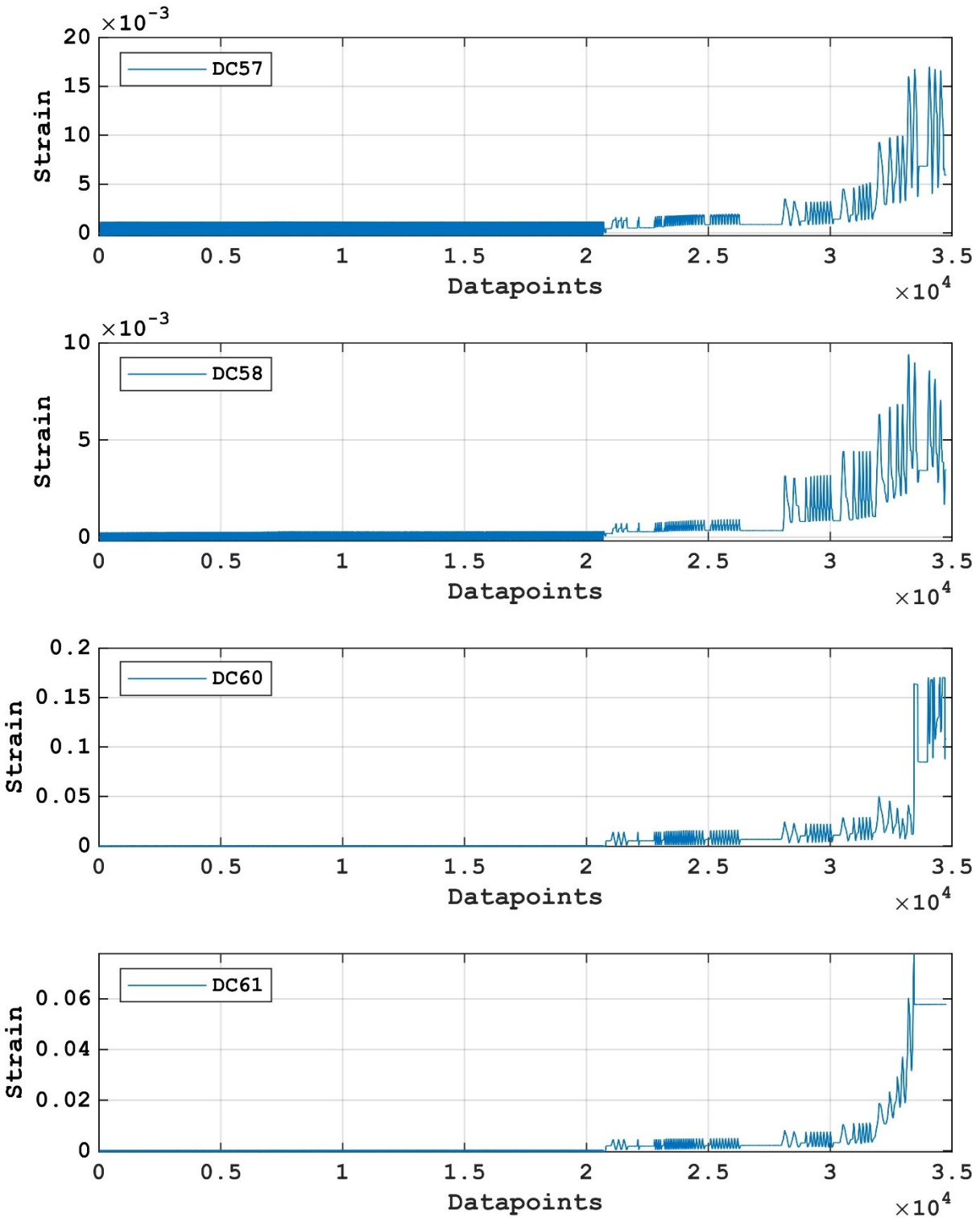


Figure D-14: East side LVTD readings (LB-S7.5-50)

WIRE POTENTIOMETERS (LB-S7.5-50)

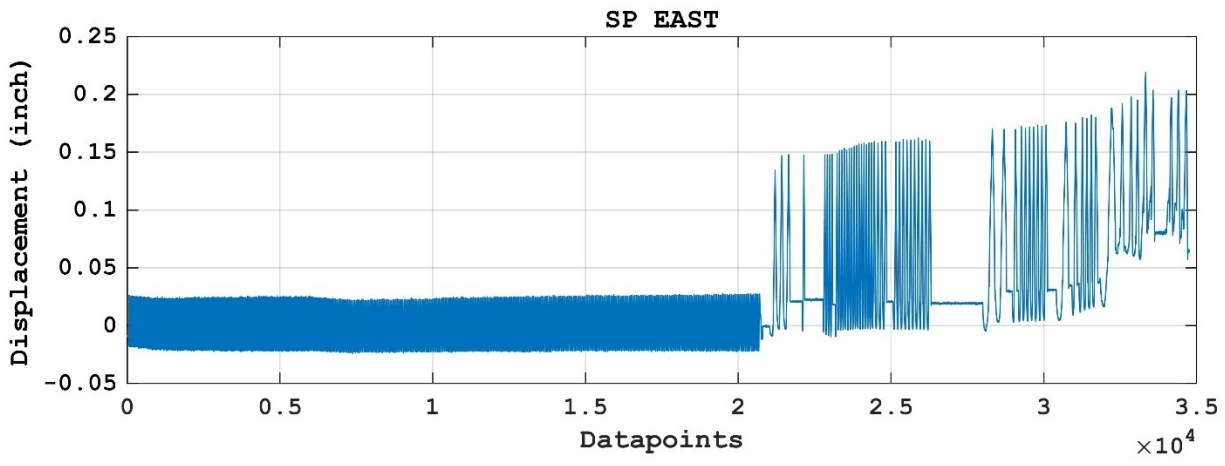
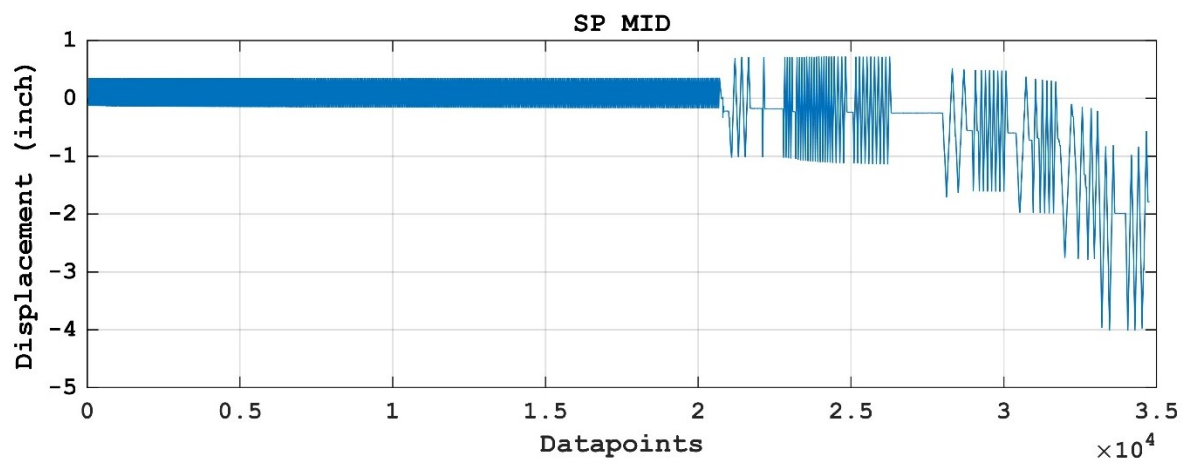
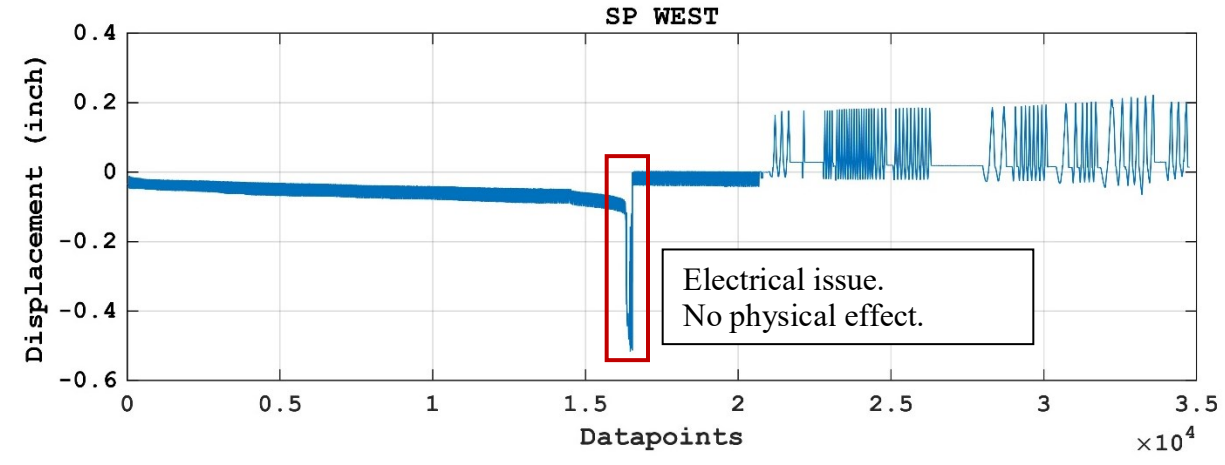


Figure D-15: Wire potentiometers readings (LB-S7.5-50)

WEST SIDE LVDTs (LB-S5-50)

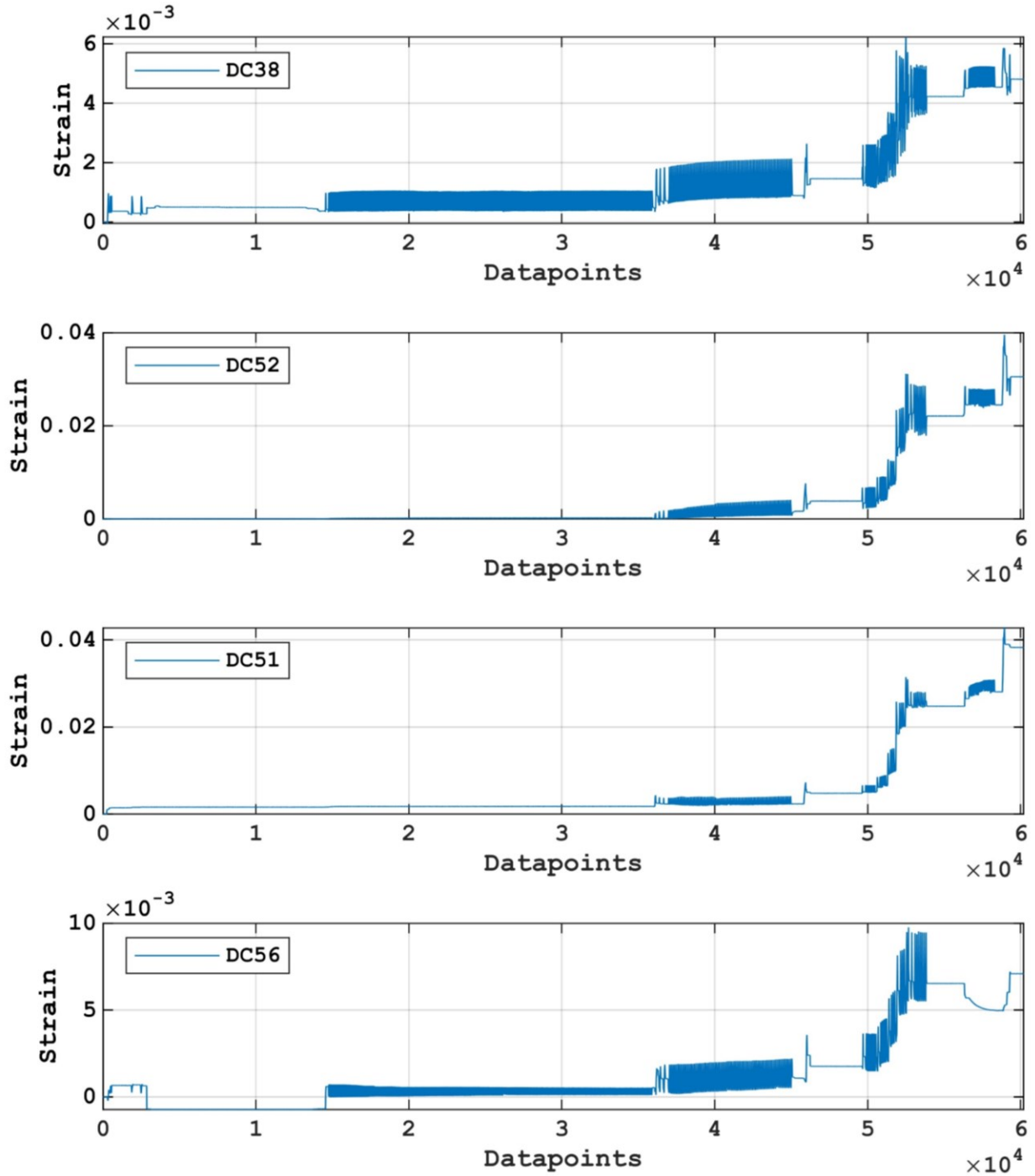


Figure D-16: West side LVTD readings (LB-S5-50)

EAST SIDE LVDTs (LB-S5-50)

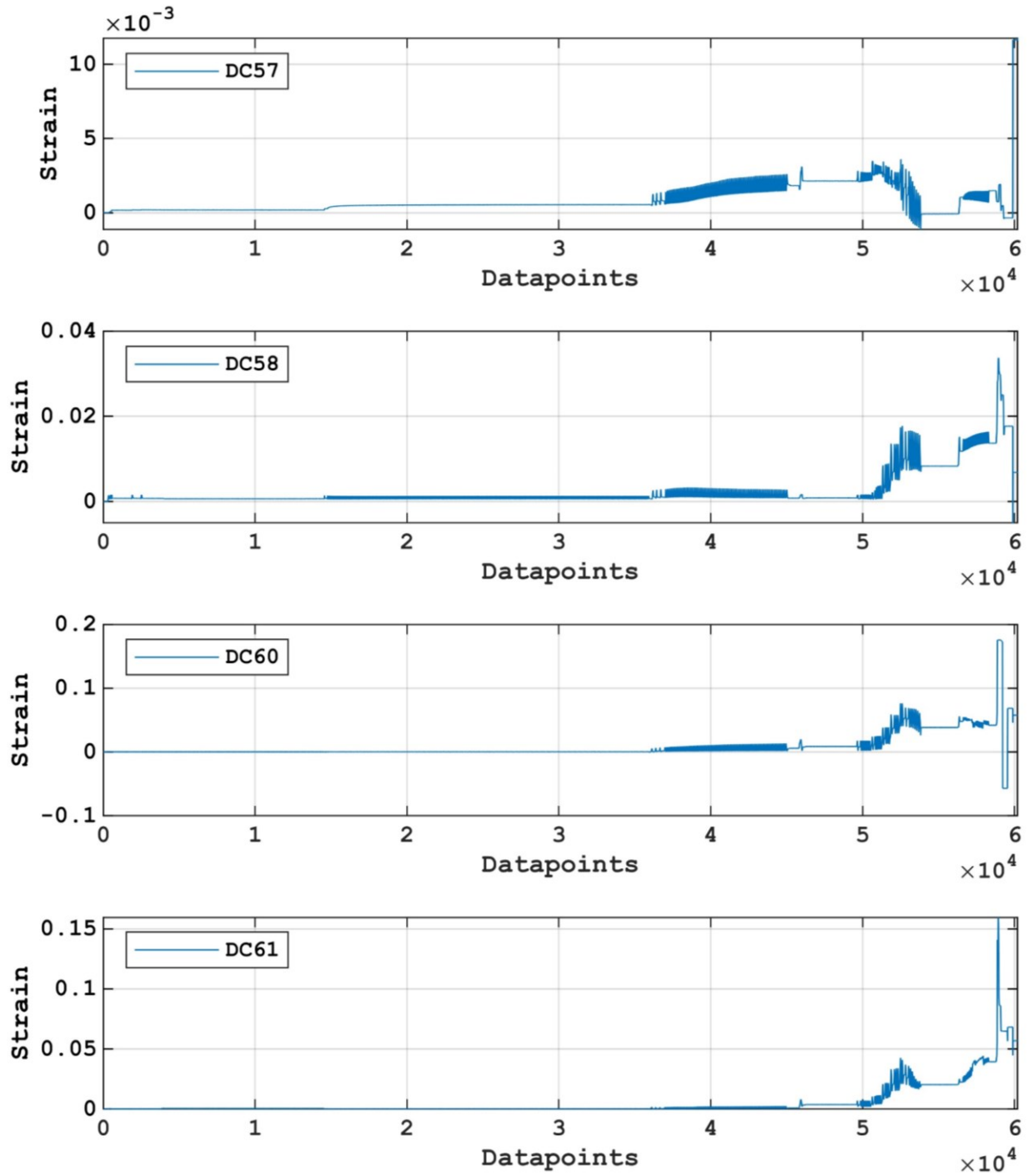


Figure D-17: East side LVTD readings (LB-S5-50)

WIRE POTENTIOMETERS (LB-S5-50)

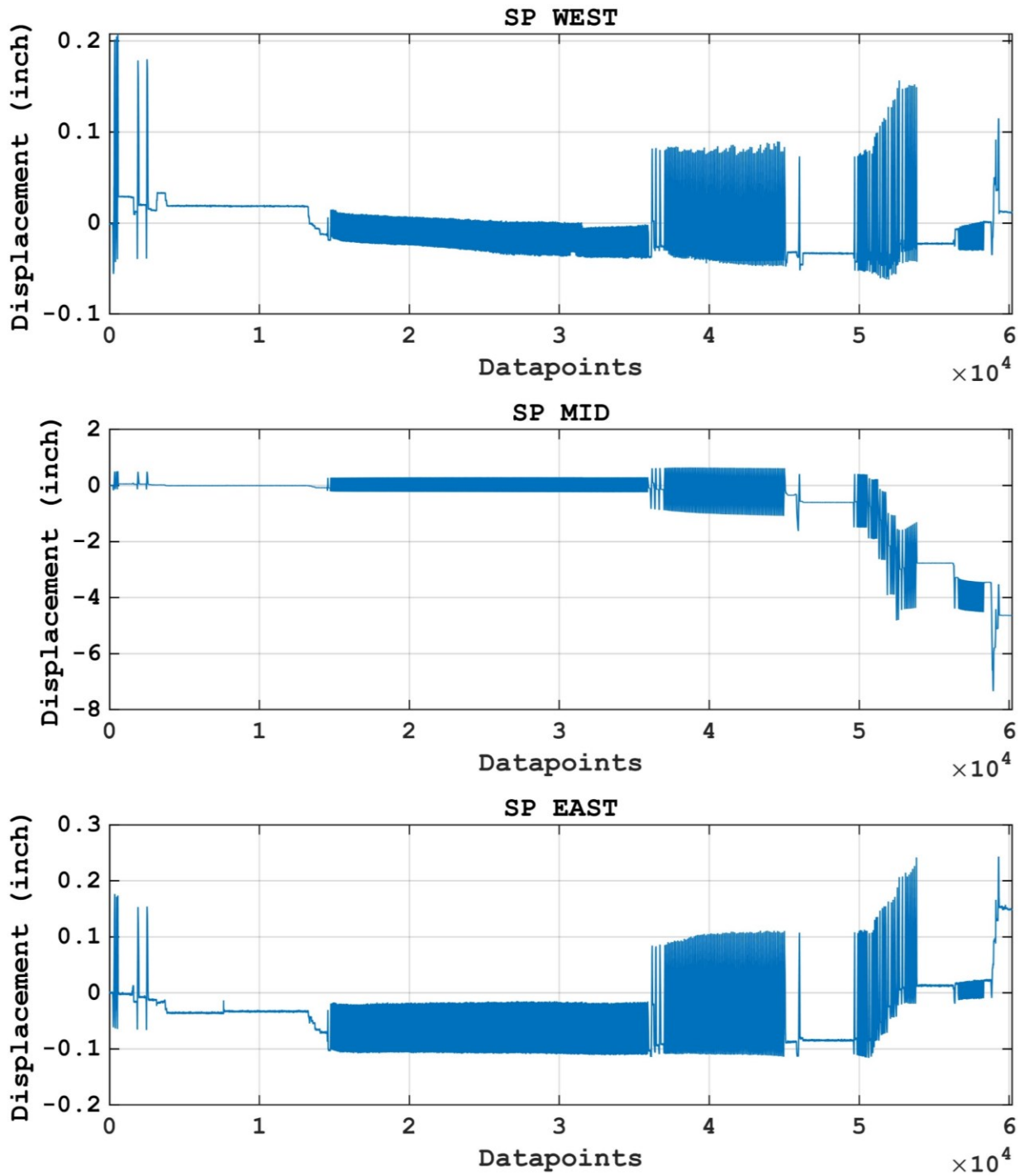


Figure D-18: Wire potentiometers readings (LB-S5-50)

Appendix E. Digital Image Correlation (DIC) Results

LB-S7.5-50

Stage 1: 500 Cycles @ $0.18M_{pr}^+$ and @ $0.32M_{pr}^-$

100th Cycle

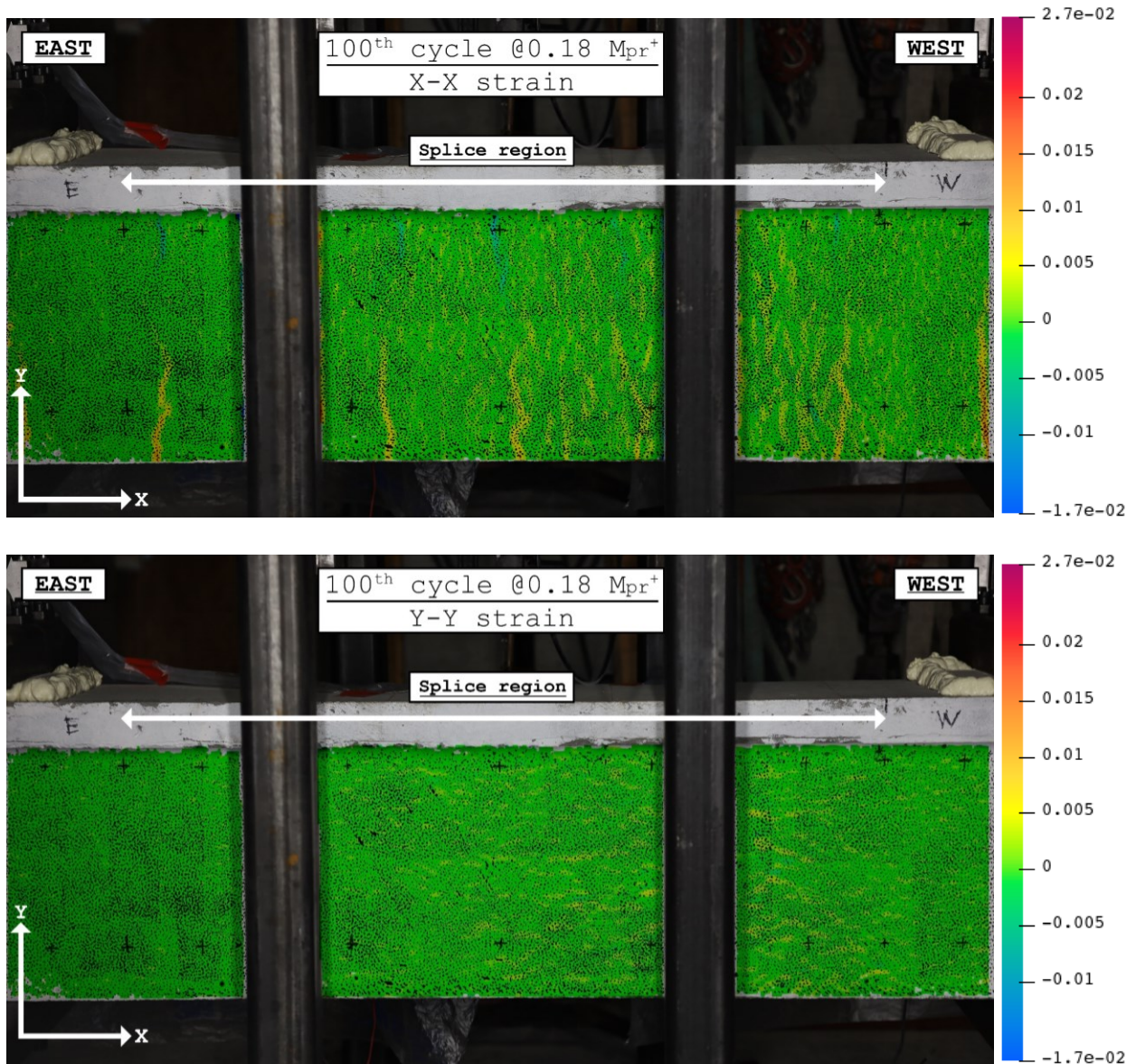


Figure E-1: (LB-S7.5-50) Stage 1-100th cycle @ $0.18M_{pr}^+$ DIC results

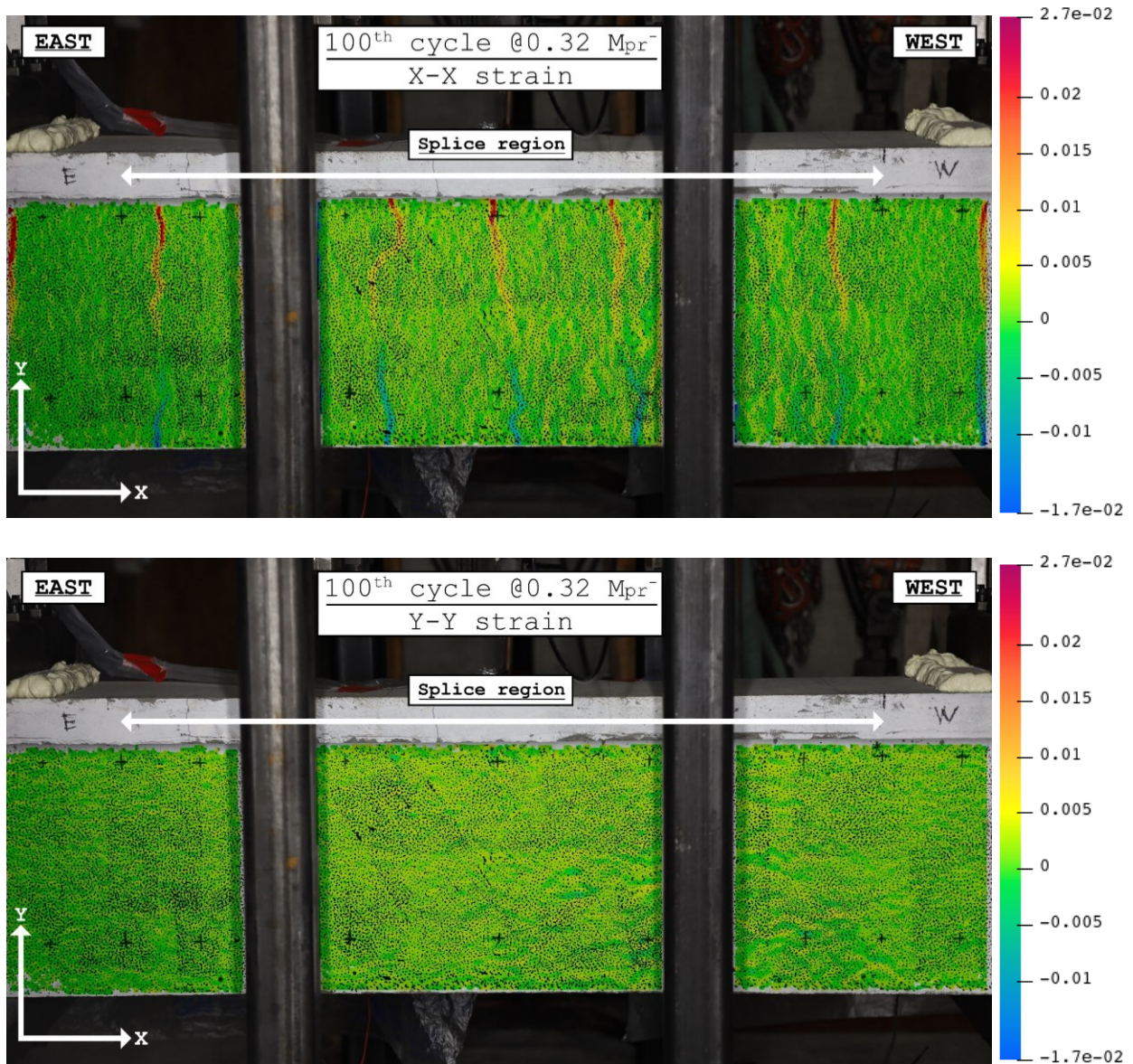


Figure E-2: (LB-S7.5-50) Stage 1-100th cycle @0.32M_{pr} DIC results

200th Cycle

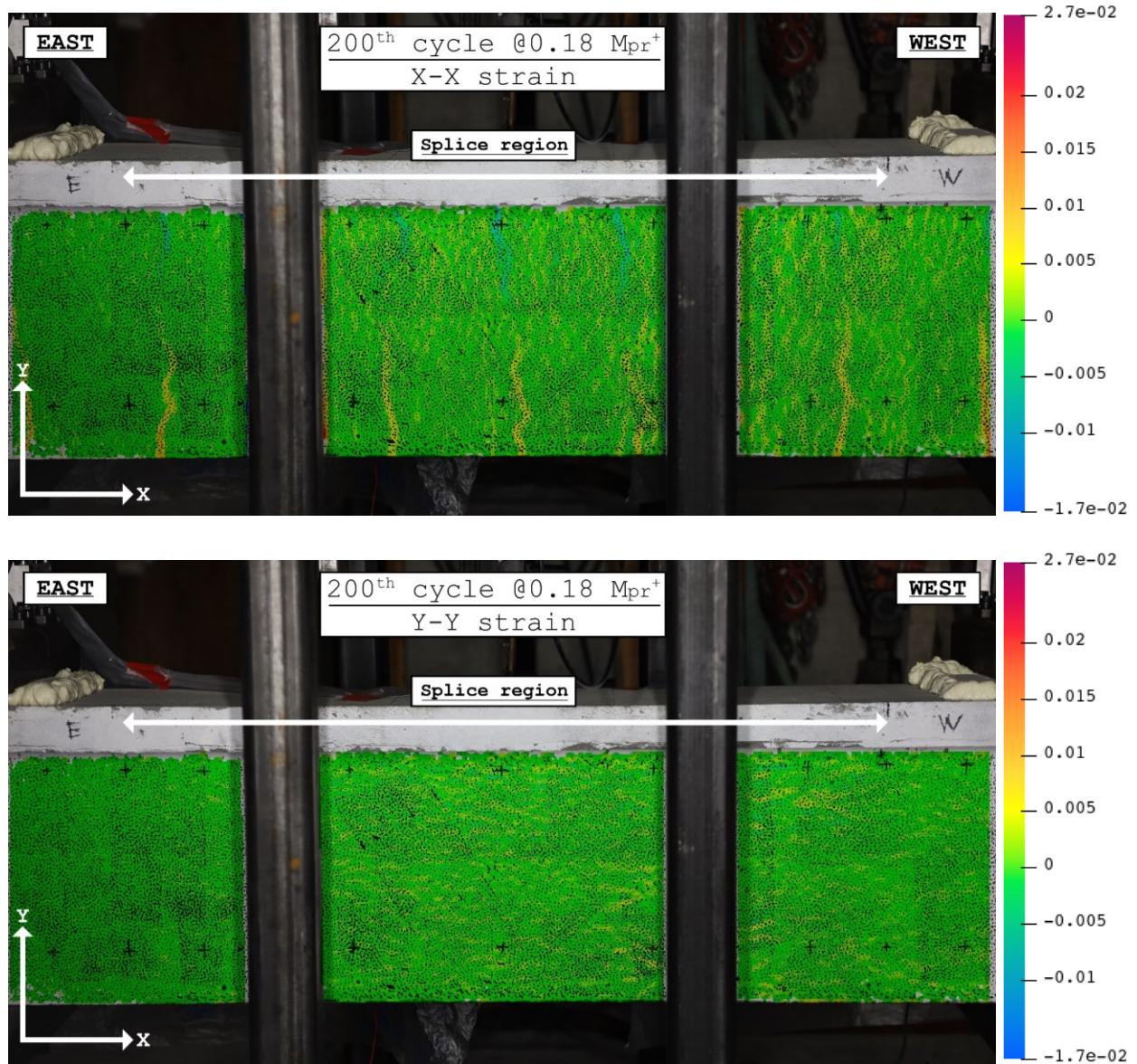


Figure E-3: (LB-S7.5-50) Stage 1-200th cycle @0.18M_{pr}⁺ DIC results

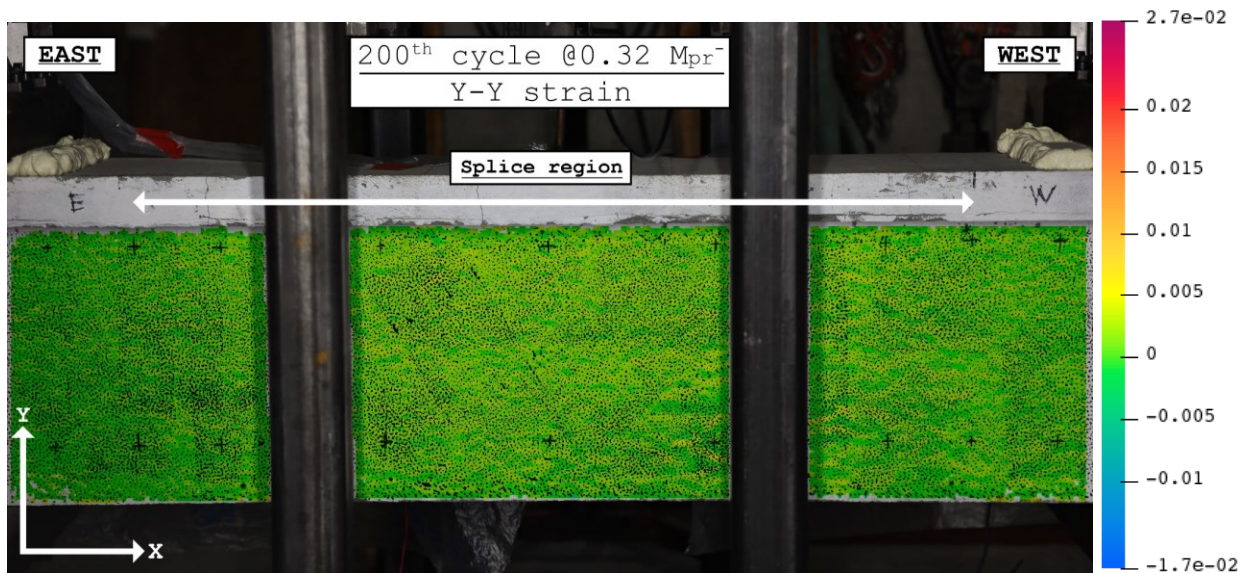
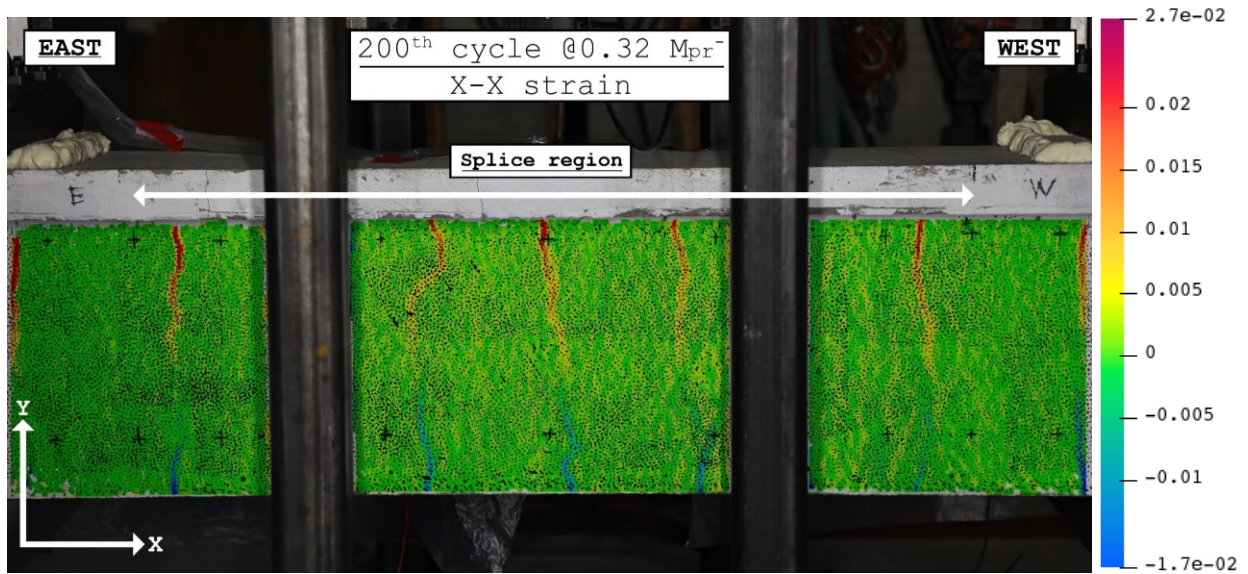


Figure E-4: (LB-S7.5-50) Stage 1-200th cycle @0.32M_{pr}⁻ DIC results

500th Cycle

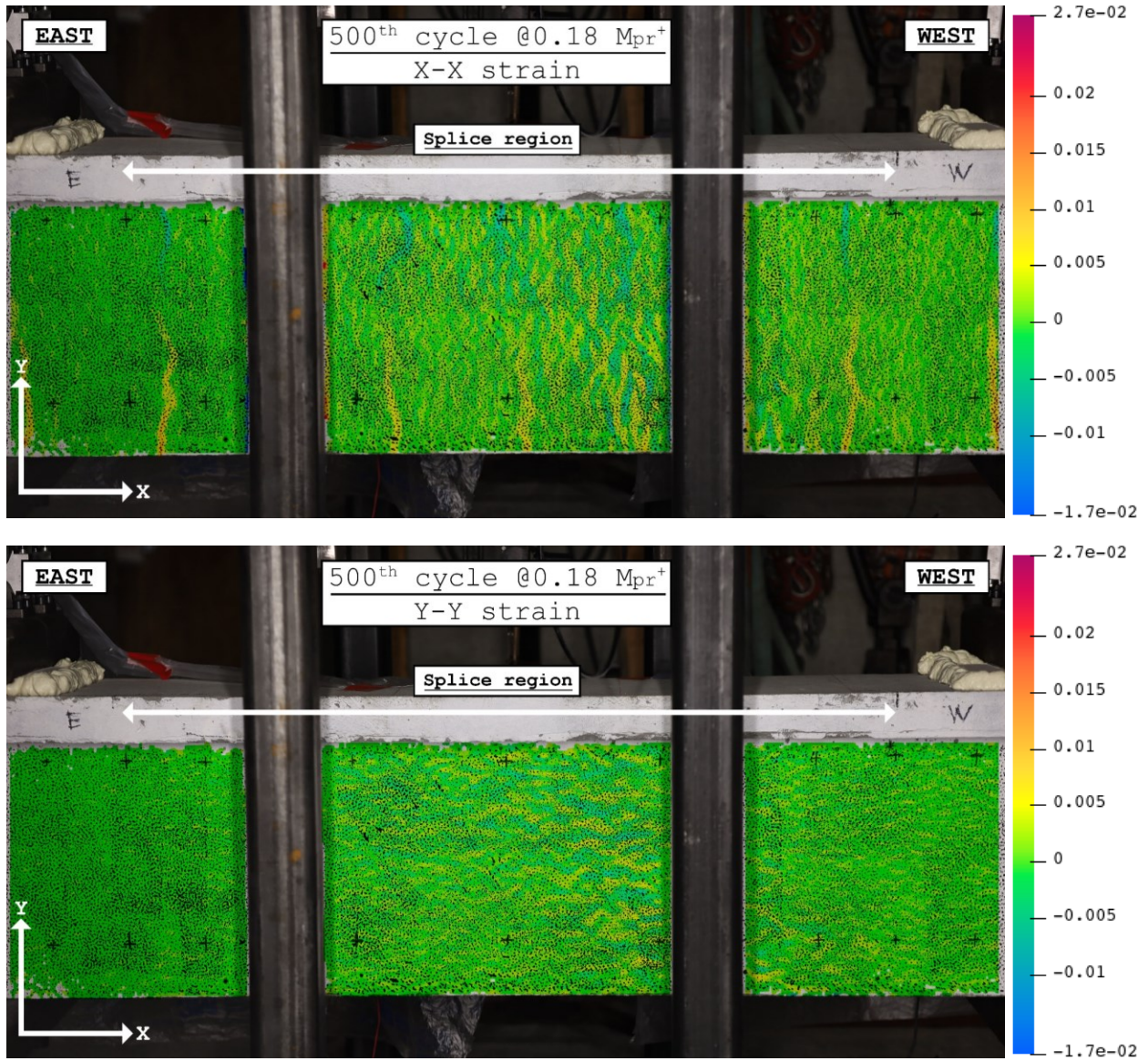


Figure E-5: (LB-S7.5-50) Stage 1-500th cycle @0.18M_{pr}⁺ DIC results

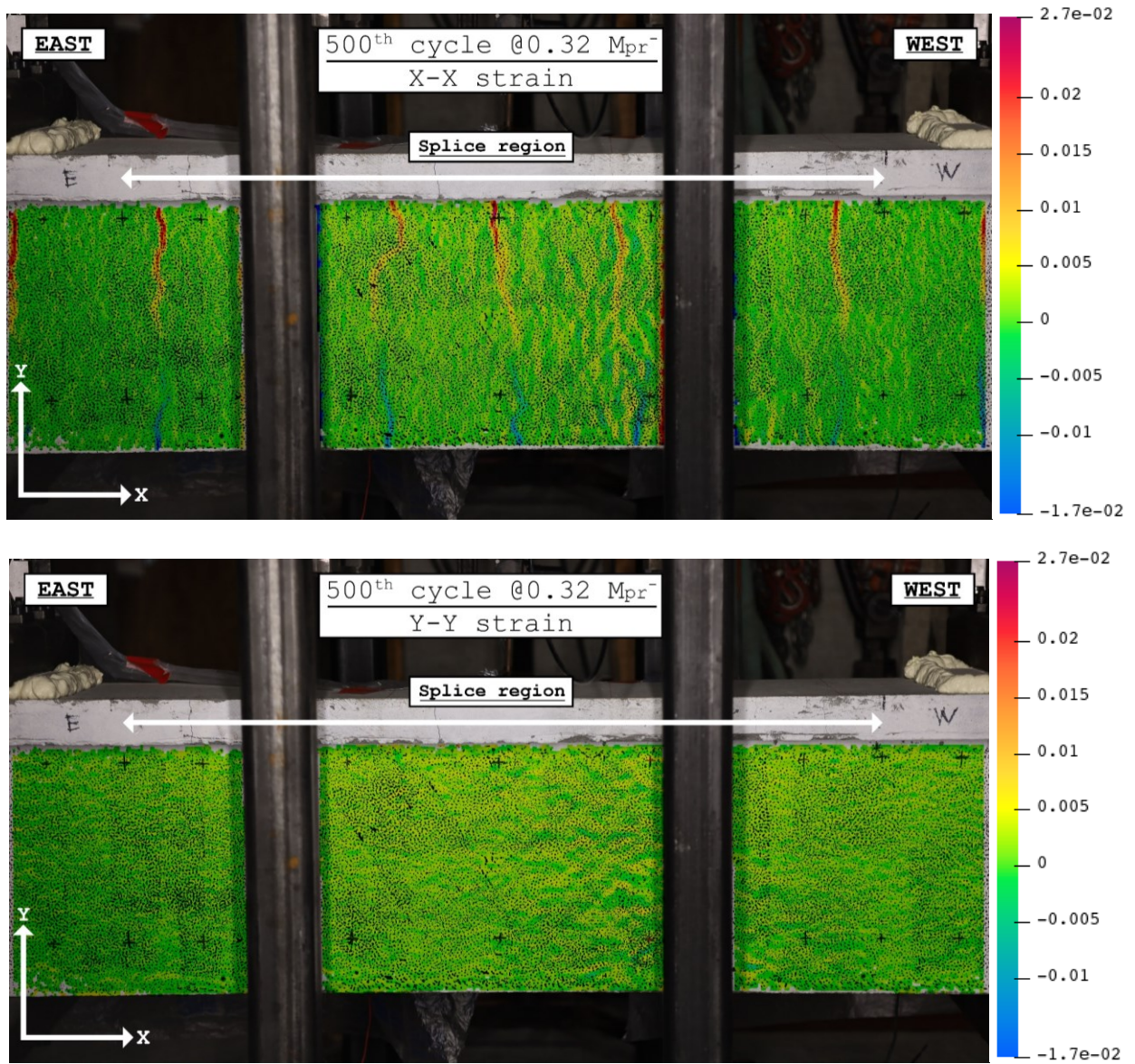


Figure E-6: (LB-S7.5-50) Stage 1-500th cycle @0.32M_{pr} DIC results

Stage 2: 40 Cycles @0.79M_{pr}⁺ and @0.63M_{pr}⁻

40th Cycle

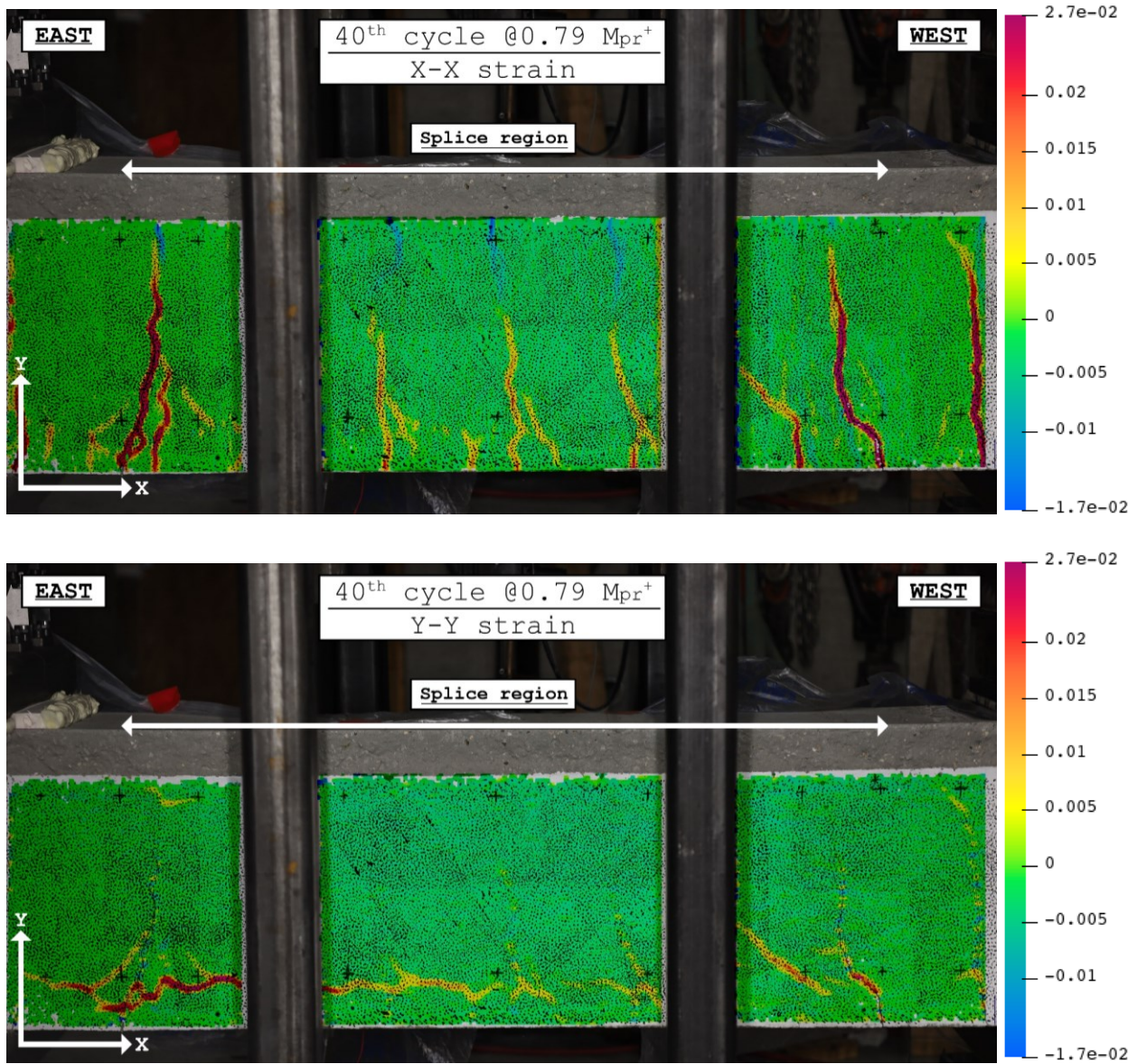


Figure E-7: (LB-S7.5-50) Stage 2-40th cycle @0.79M_{pr}⁺ DIC results

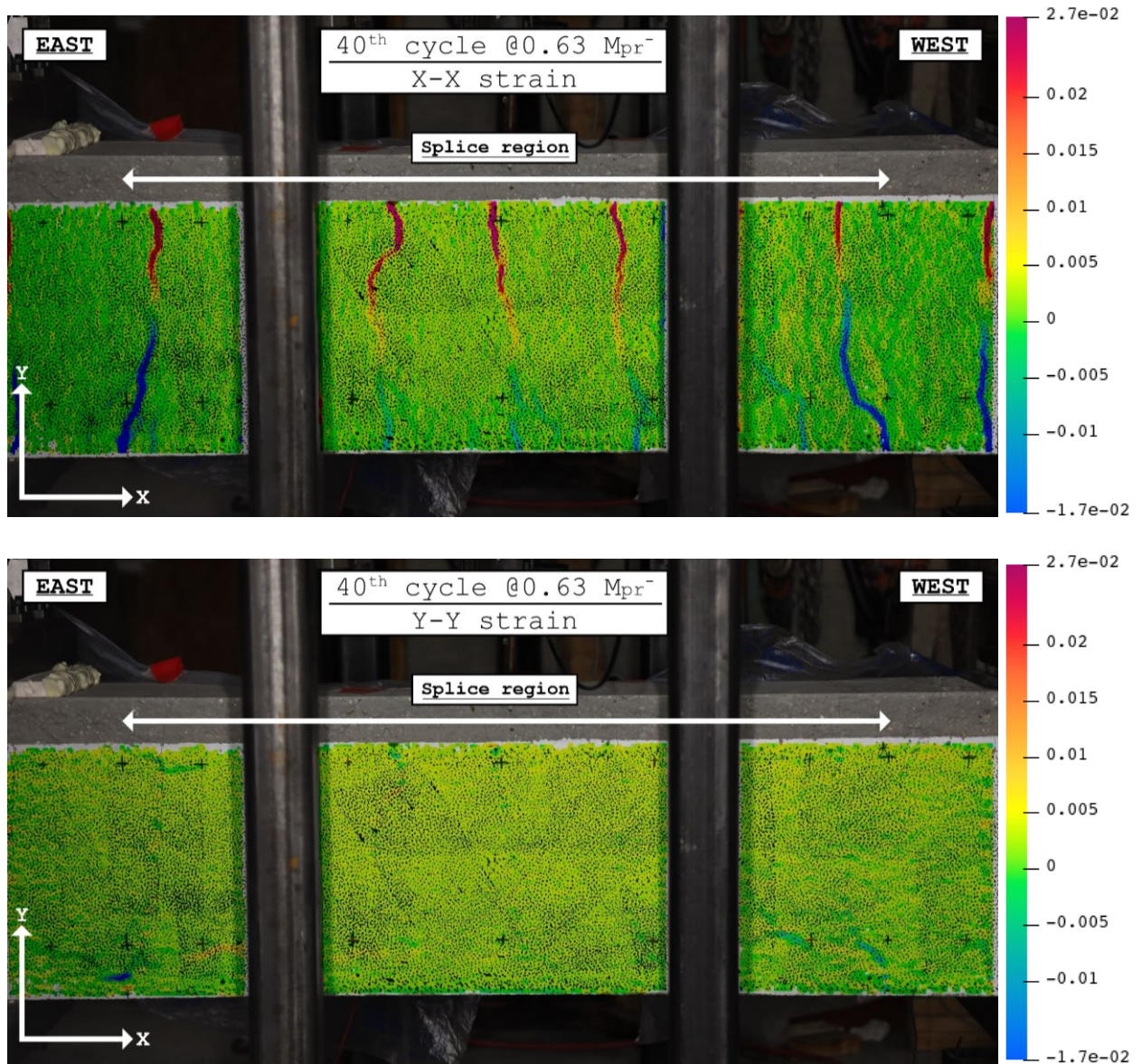


Figure E-8: (LB-S7.5-50) Stage 2-40th cycle @0.63M_{pr} DIC results

Stage 3: 10 Cycles @ $1.38\delta_y$ and @ $0.63M_{pr}$

10th Cycle

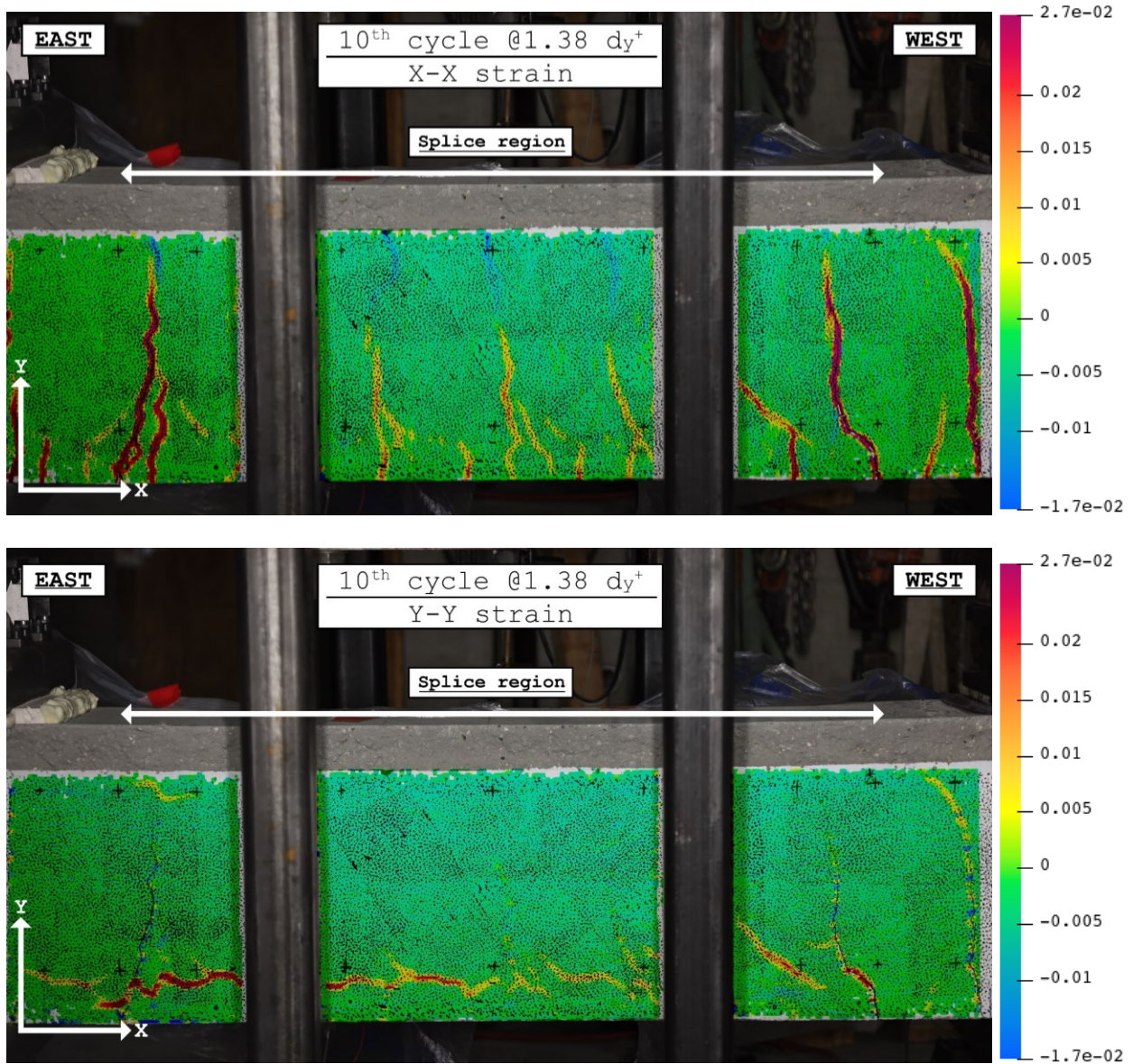


Figure E-9: (LB-S7.5-50) Stage 3-10th cycle @ $1.38\delta_y$ DIC results

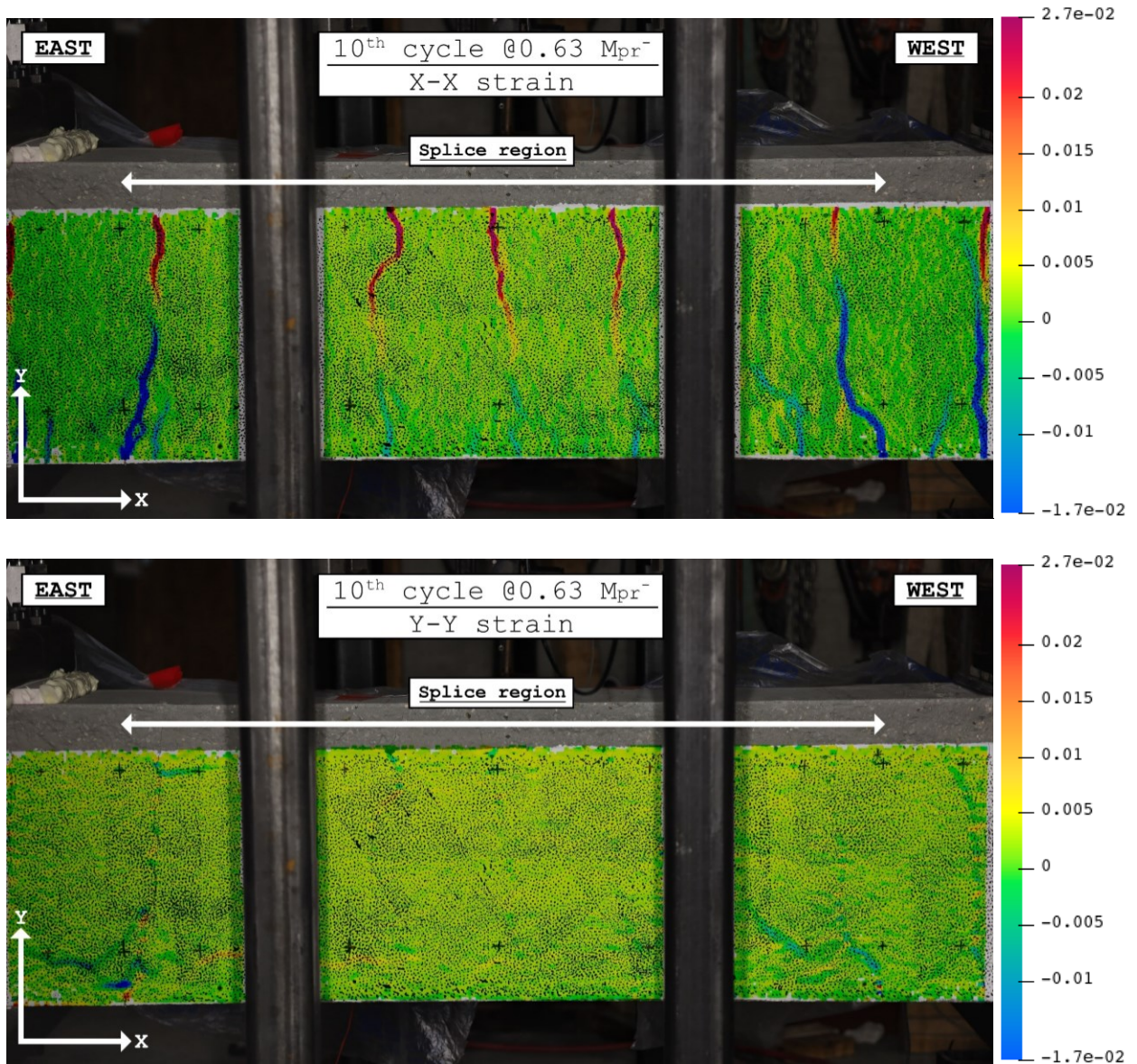


Figure E-10: (LB-S7.5-50) Stage 3-10th cycle @ $0.63M_{pr}$ DIC results

Stage 4: 6 Cycles @ $1.77\delta_y$ and @ $0.63M_{pr}$

6th Cycle

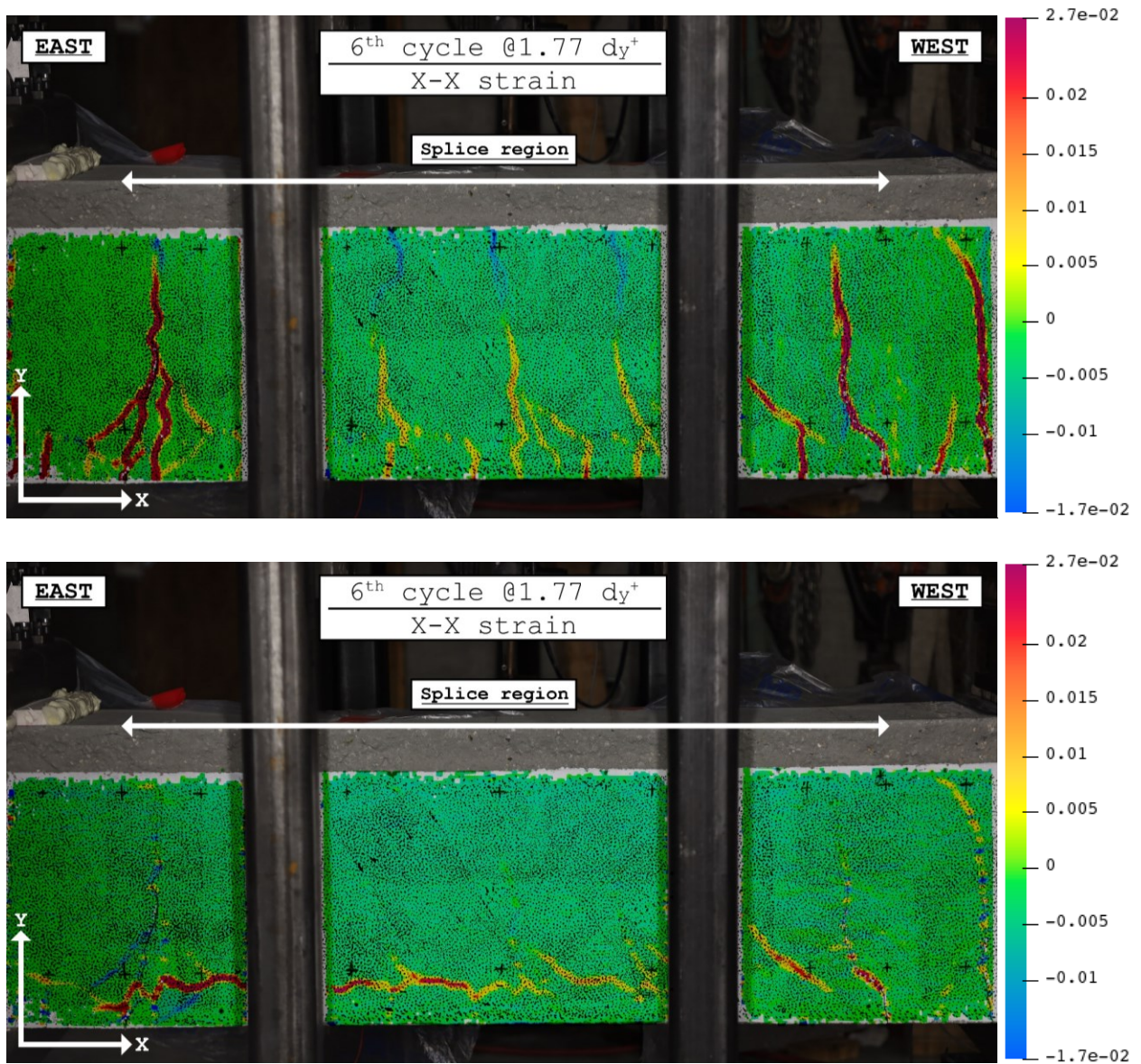


Figure E-11: (LB-S7.5-50) Stage 4-6th cycle @ $1.77\delta_y^+$ DIC results

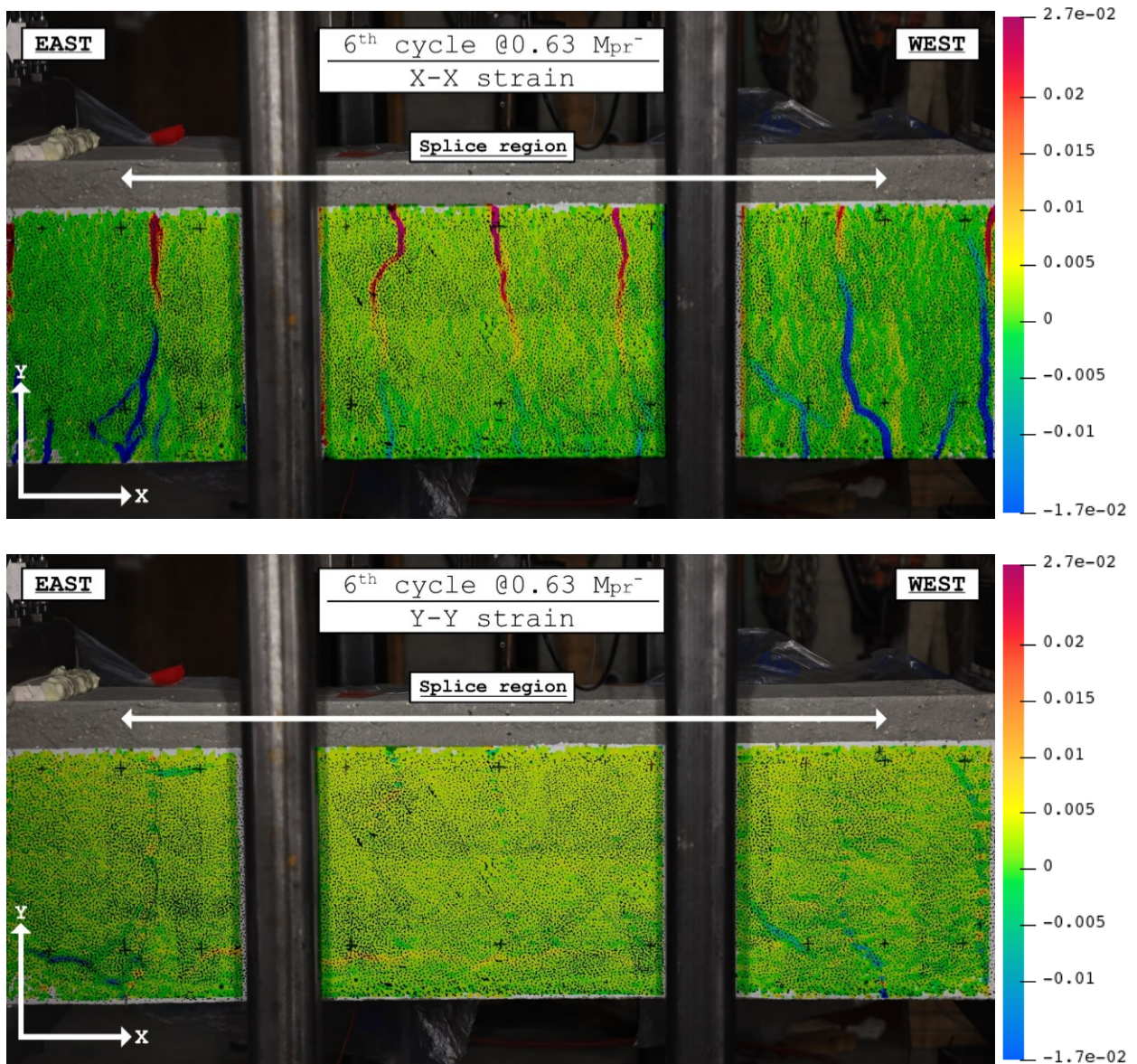


Figure E-12: (LB-S7.5-50) Stage 4-6th cycle @ 0.63M_{pr}⁻ DIC results

Stage 5: 4 Cycles @ $2.55\delta_y$ and @ $0.63M_{pr}$

4th Cycle

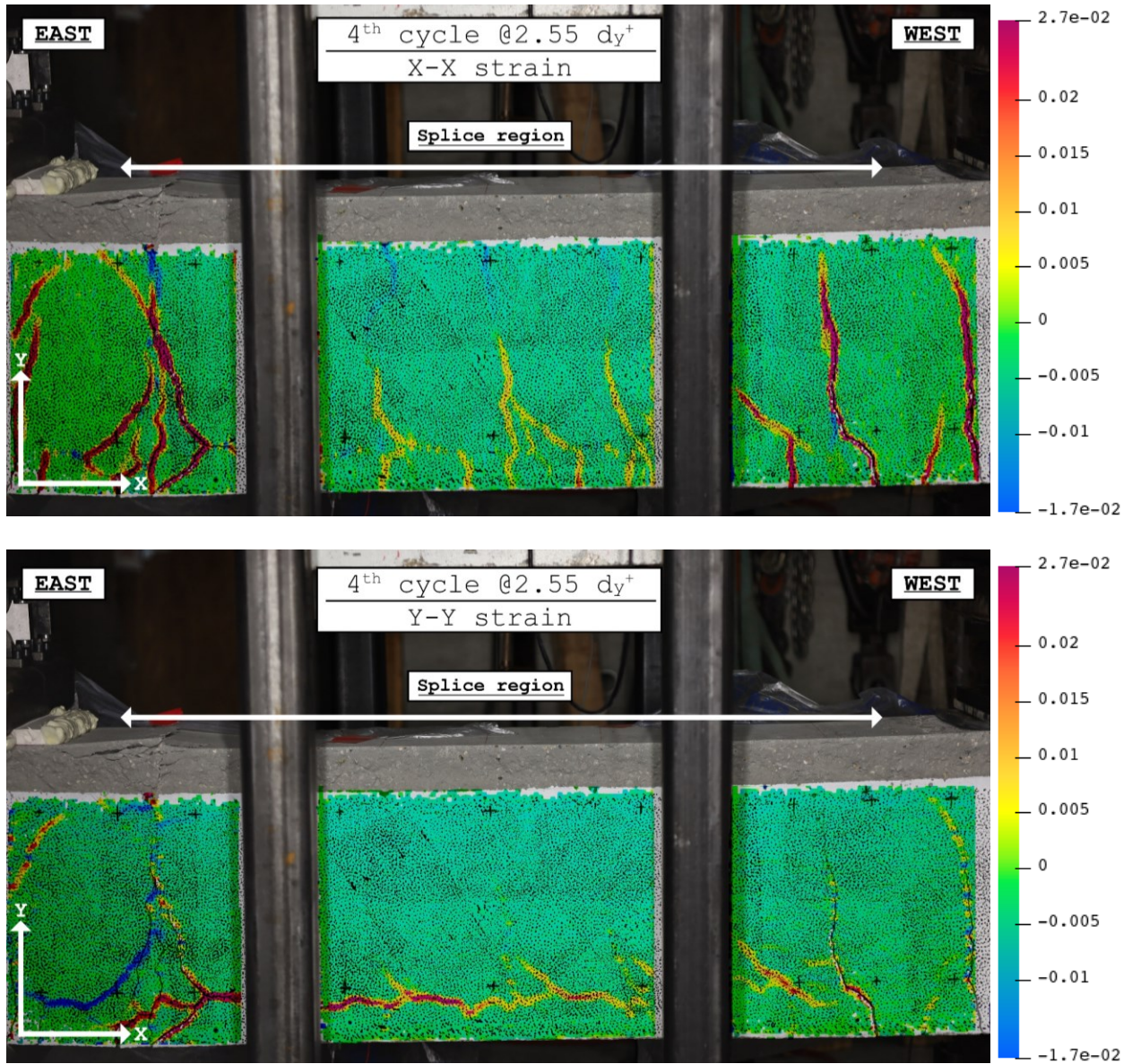


Figure E-13: (LB-S7.5-50) Stage 5-4th cycle @ $2.55\delta_y$ DIC results

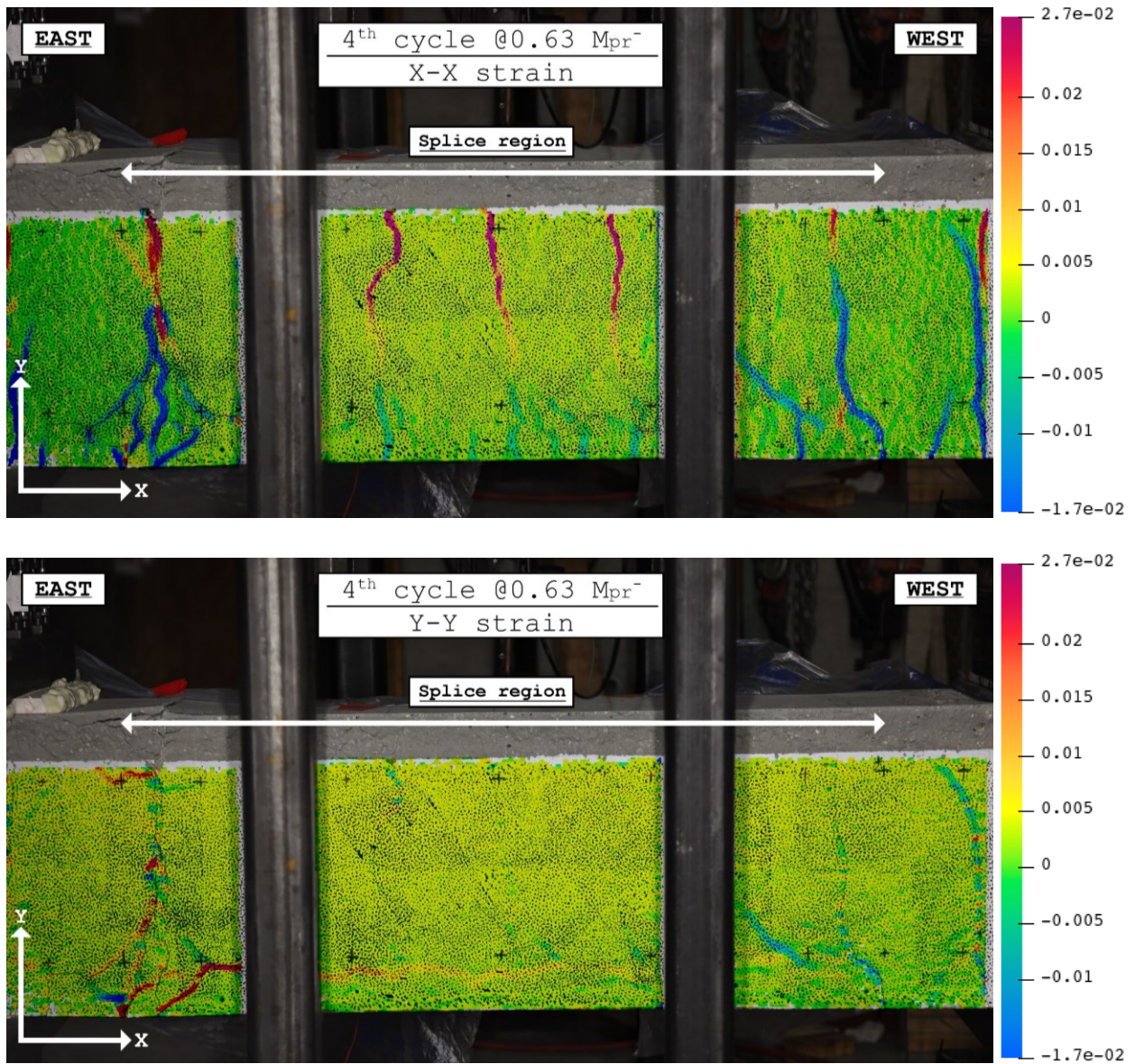


Figure E-14: (LB-S7.5-50) Stage 5-4th cycle @ 0.63M_{pr}⁻ DIC results

Stage 6: 4 Cycles @ $3.81\delta_y$ and @ $0.63M_{pr}$

4th Cycle

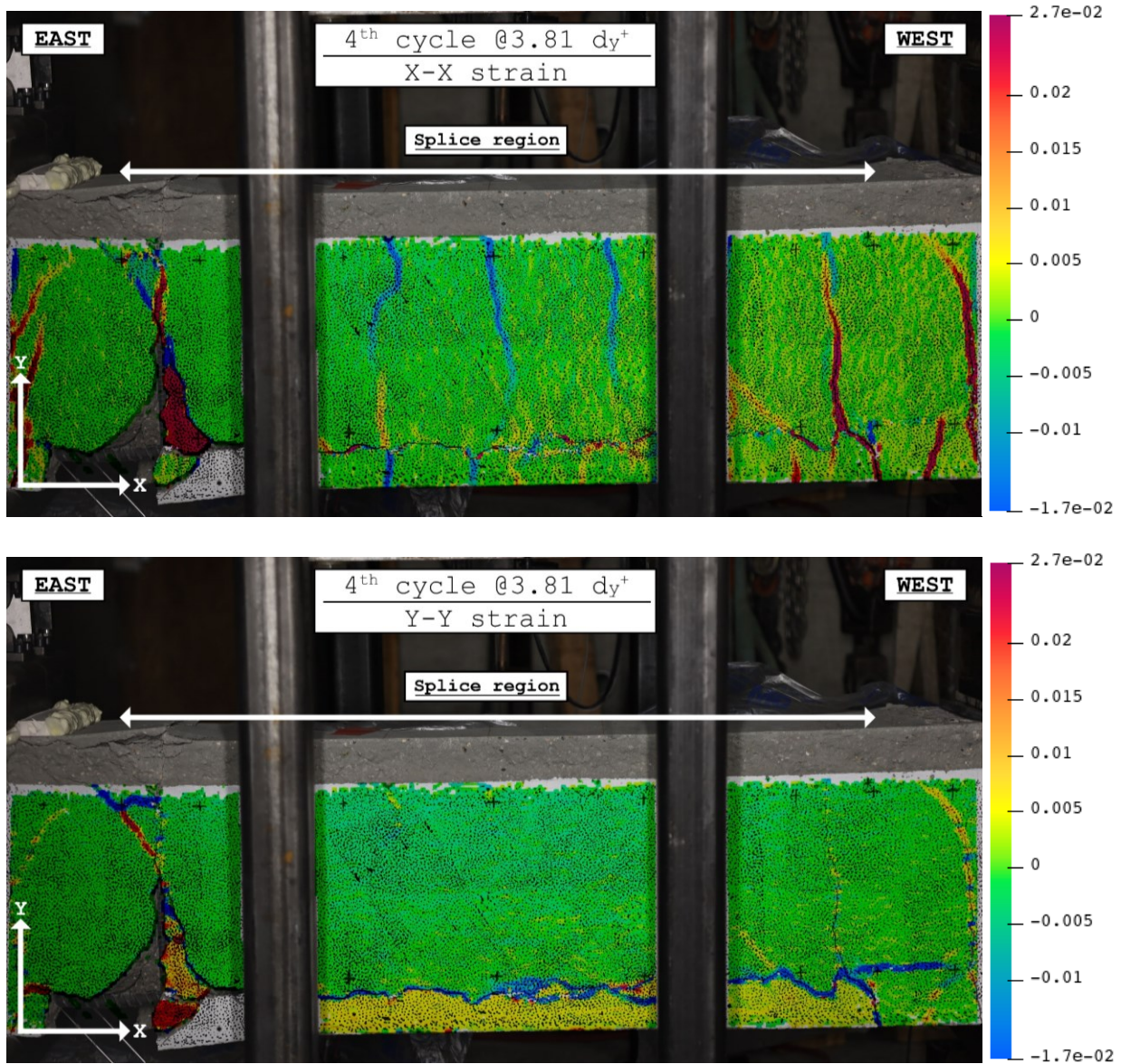


Figure E-15: (LB-S7.5-50) Stage 6-4th cycle @ $3.81\delta_y$ DIC results

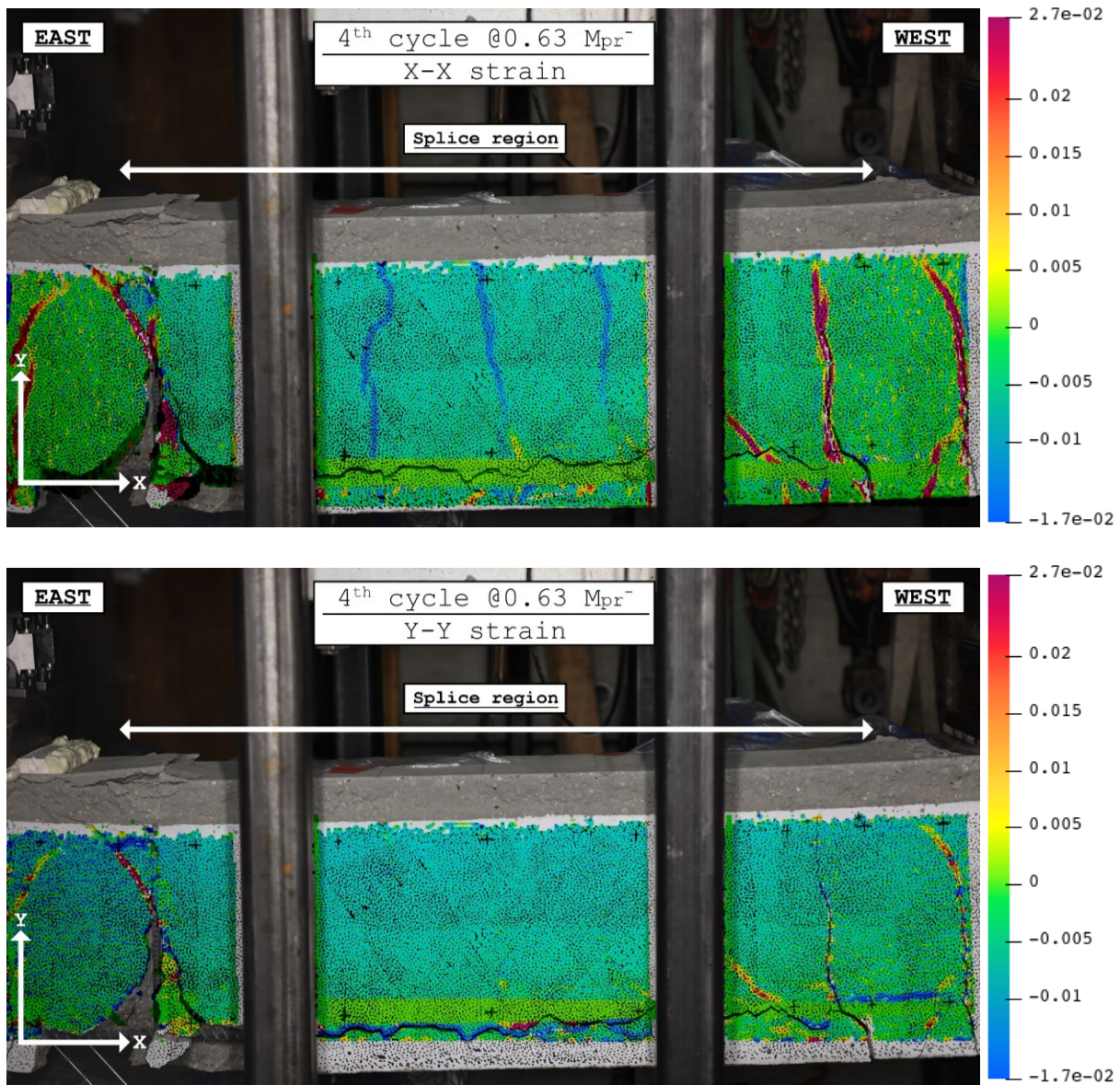


Figure E-16: (LB-S7.5-50) Stage 6-4th cycle @ 0.63 Mpr^{-1} DIC results

LB-S5-50

Stage 1: 500 Cycles @ $0.18M_{pr+}$ and @ $0.32M_{pr-}$

100th Cycle

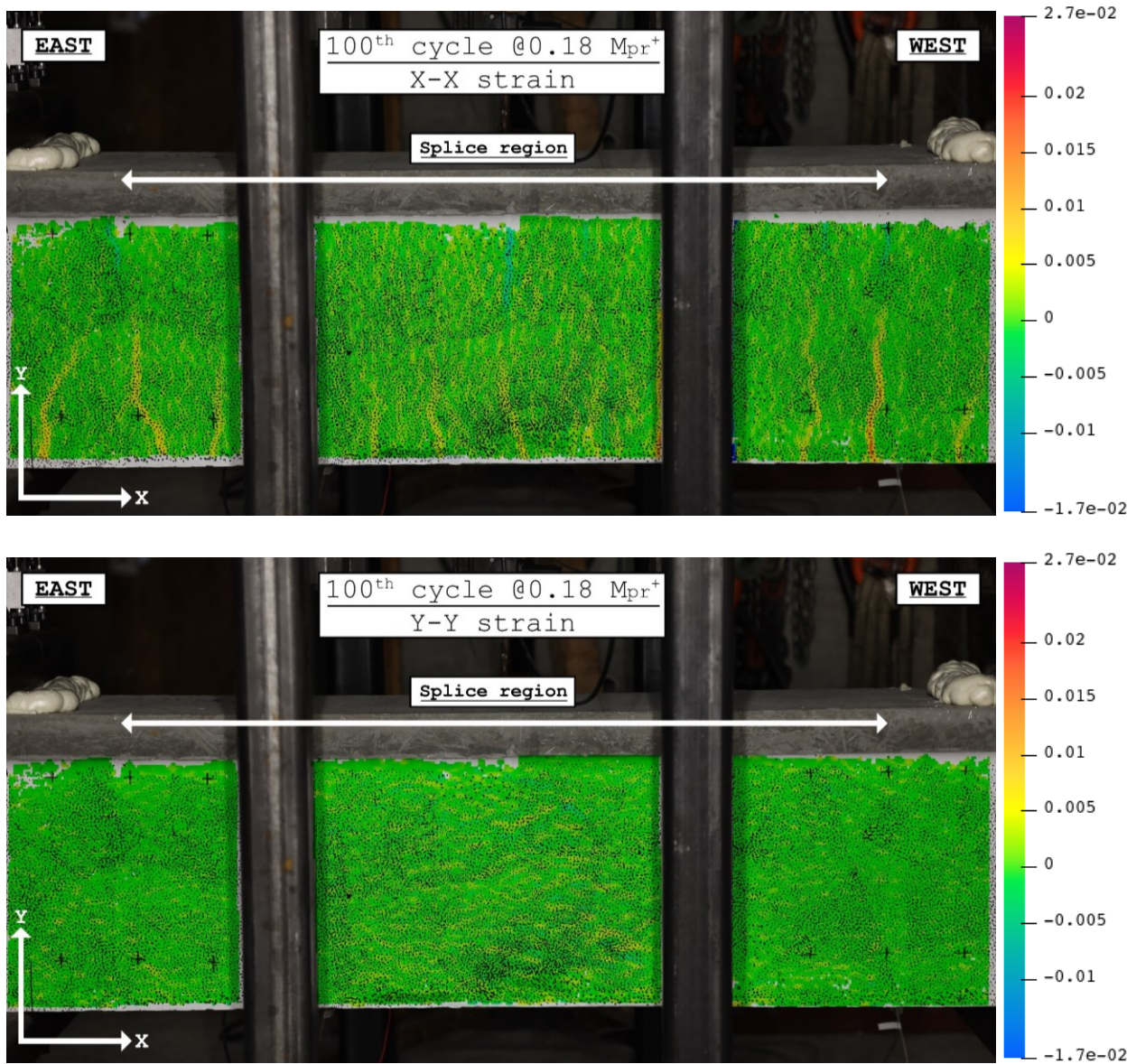


Figure E-17: (LB-S5-50) Stage 1-100th cycle @ $0.18M_{pr+}$ DIC results

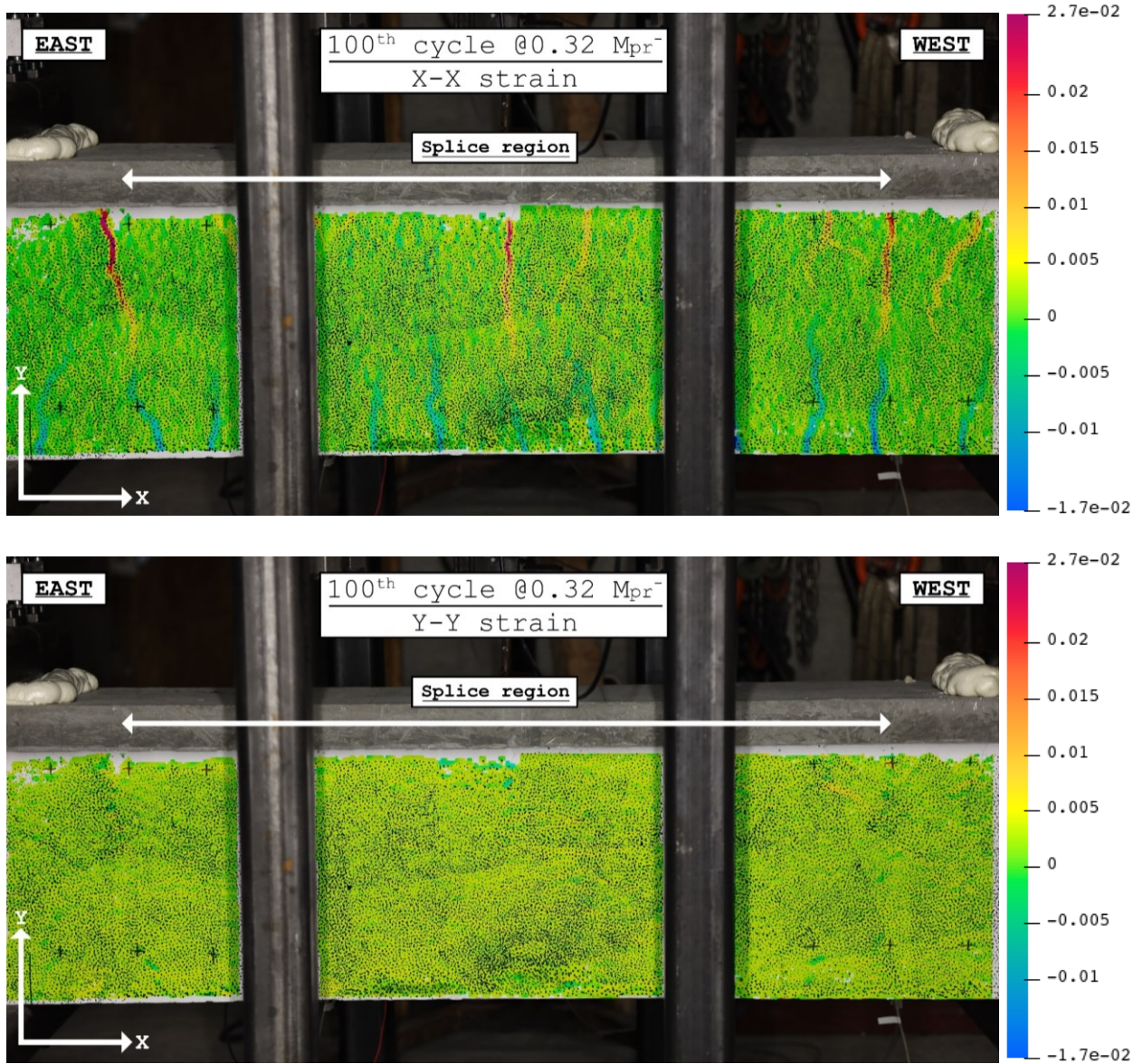


Figure E-18: (LB-S5-50) Stage 1-100th cycle @ 0.32 Mpr^{-1} DIC results

200th Cycle

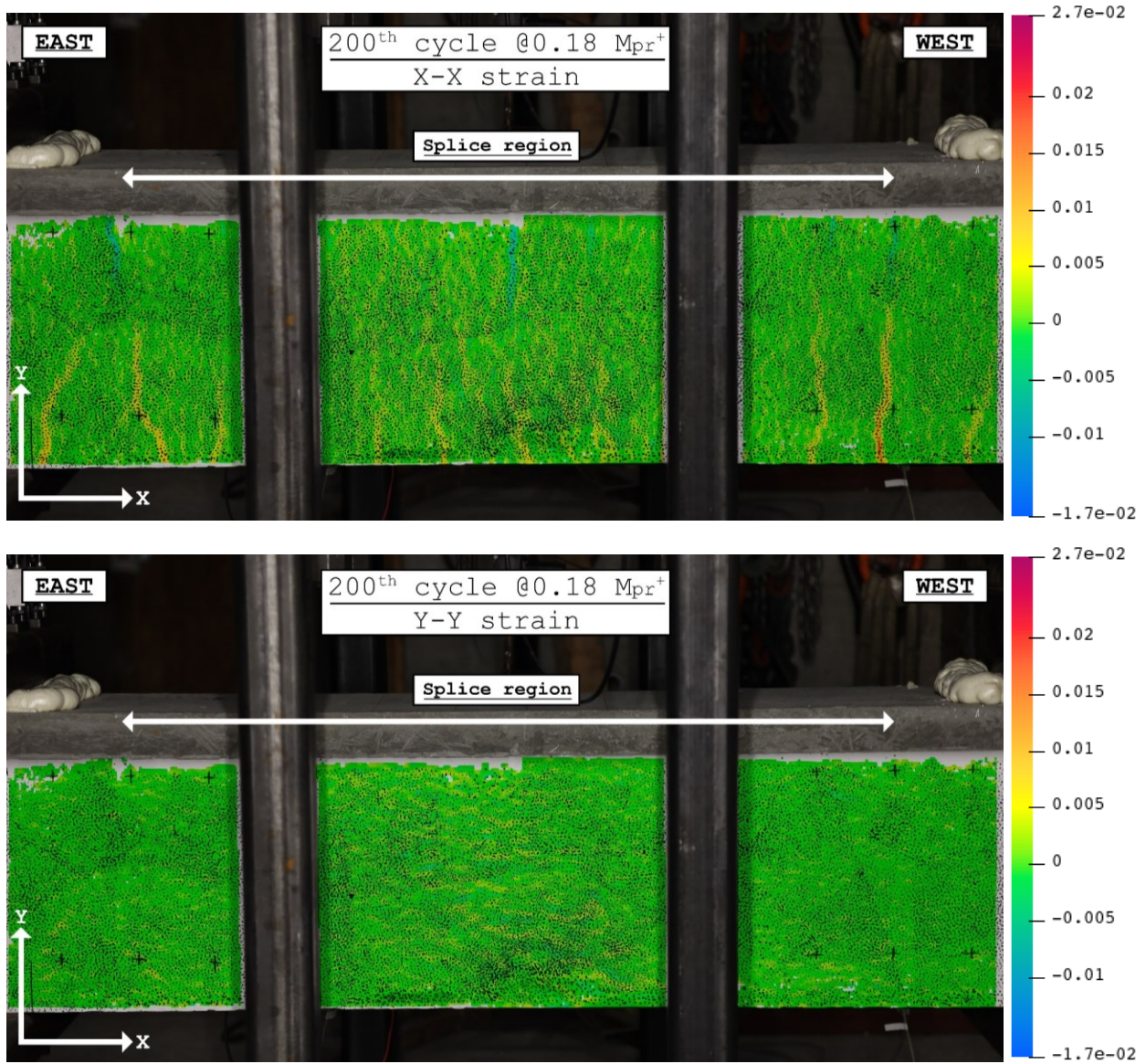


Figure E-19: (LB-S5-50) Stage 1-200th cycle @0.18M_{pr}⁺ DIC results

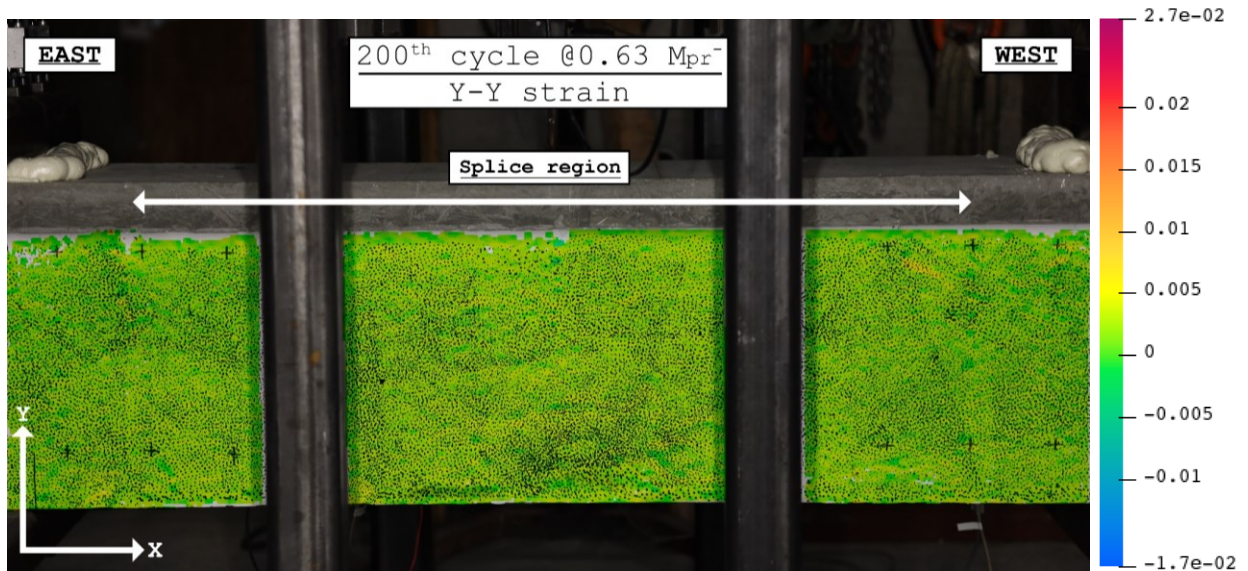
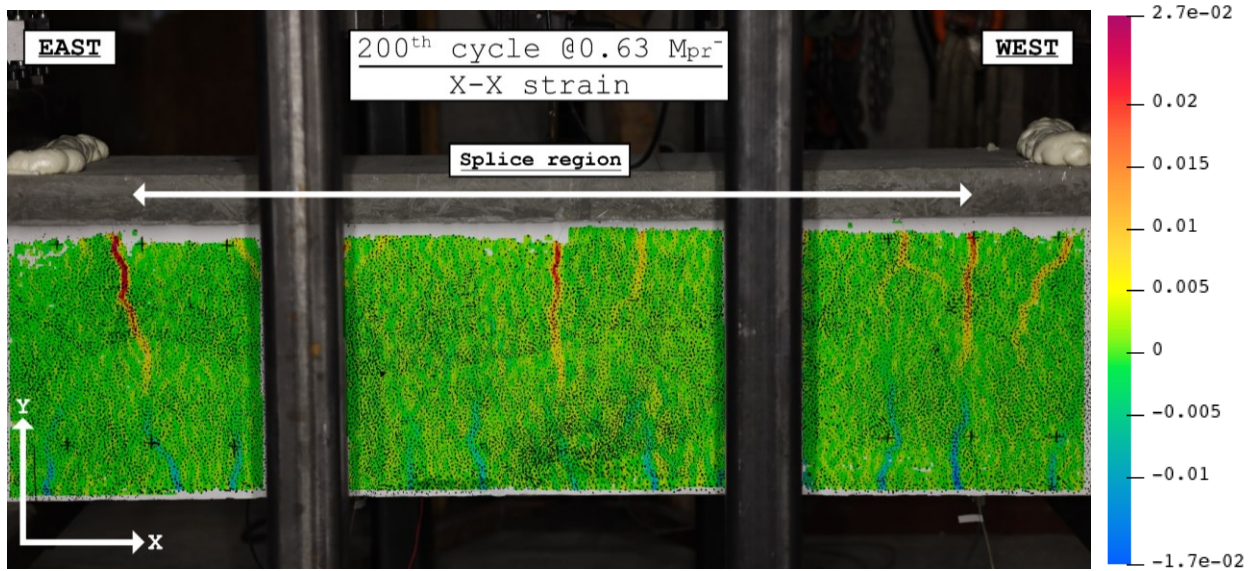


Figure E-20: (LB-S5-50) Stage 1-200th cycle @0.32M_{pr}⁻ DIC results

500th Cycle

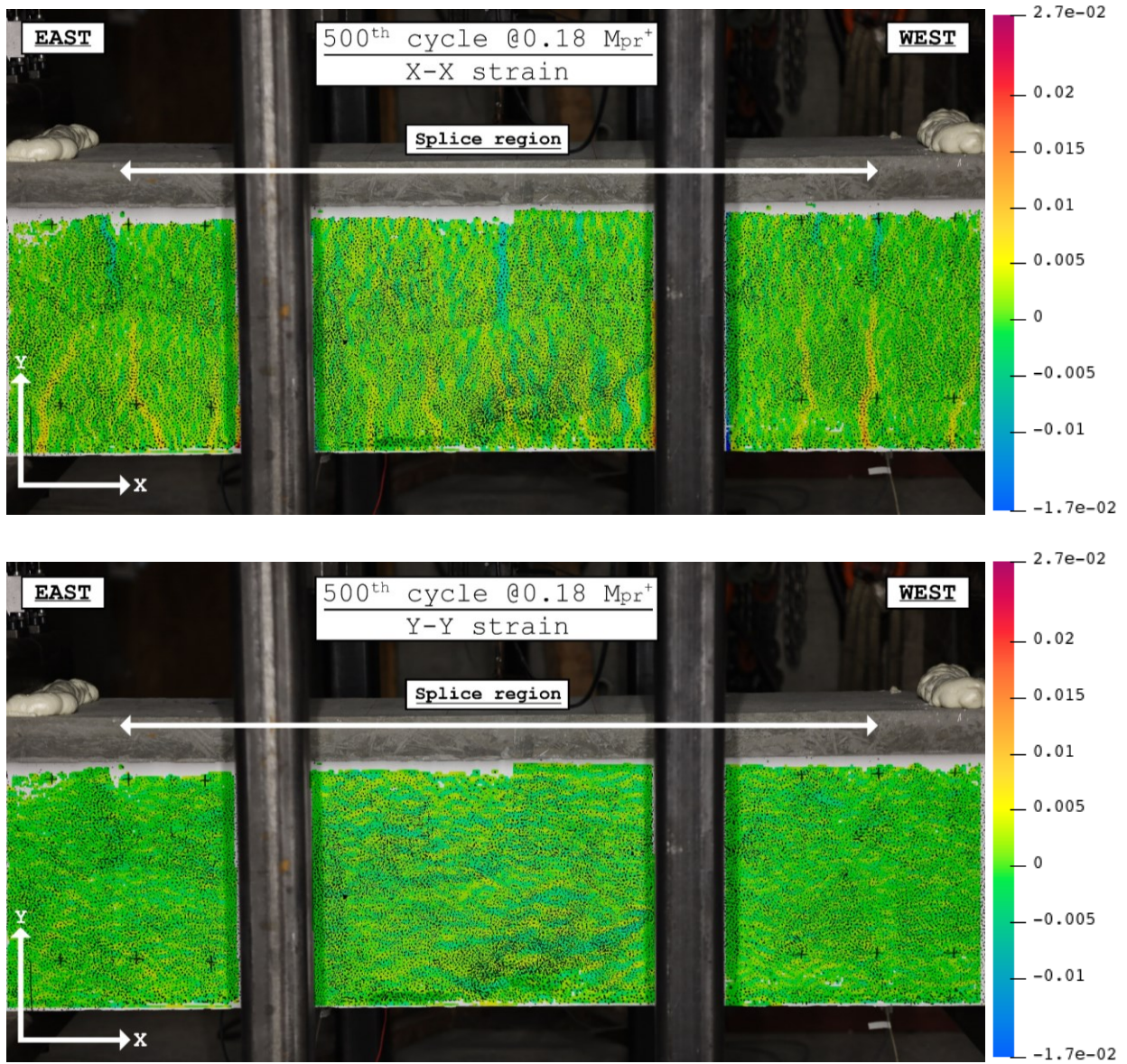


Figure E-21: (LB-S5-50) Stage 1-500th cycle @0.18M_{pr}⁺ DIC results

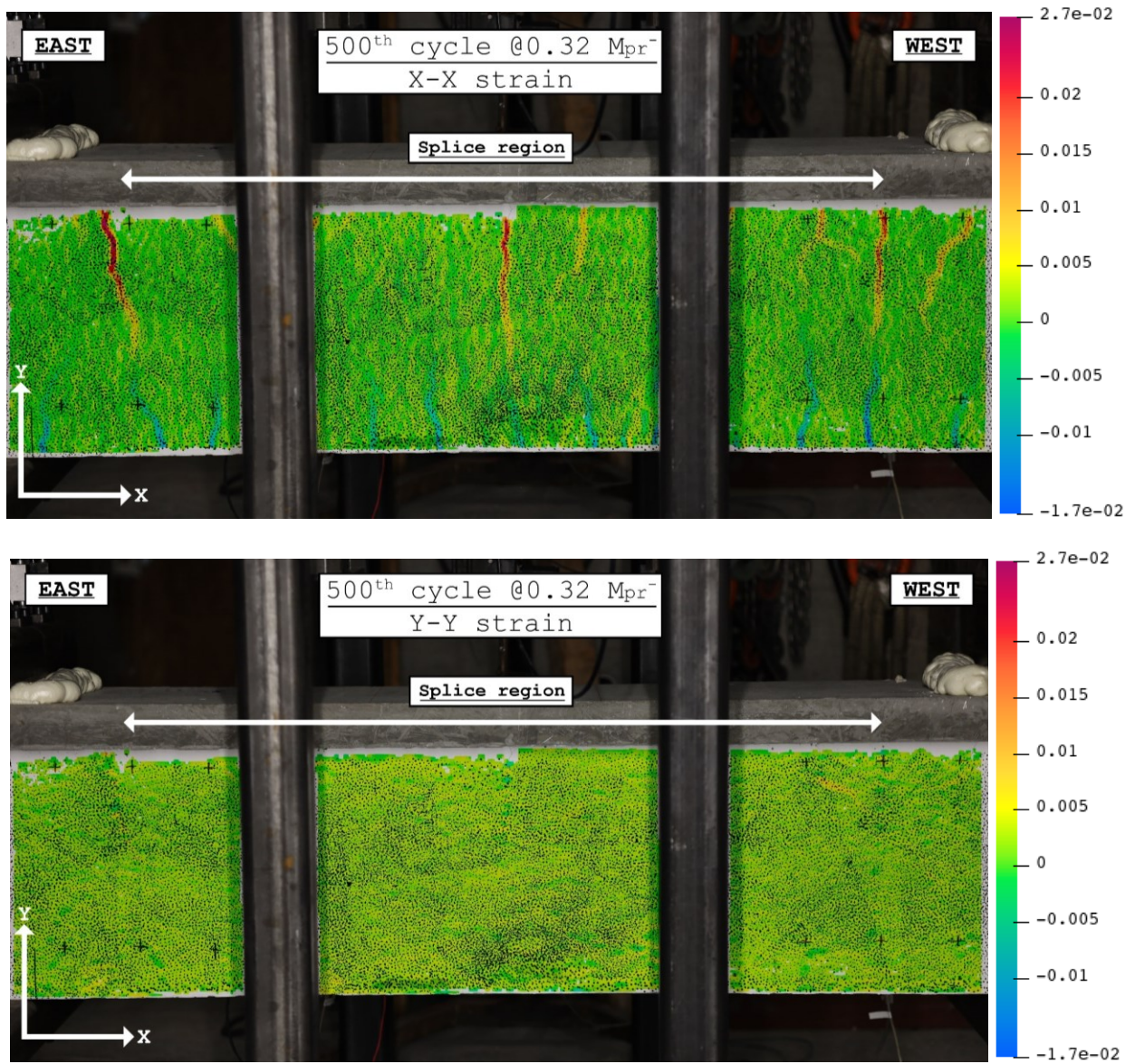


Figure E-22: (LB-S5-50) Stage 1-500th cycle @0.32M_{pr}⁻¹ DIC results

Stage 2: 75 Cycles @0.79M_{pr}⁺ and @0.63M_{pr}⁻

75th Cycle

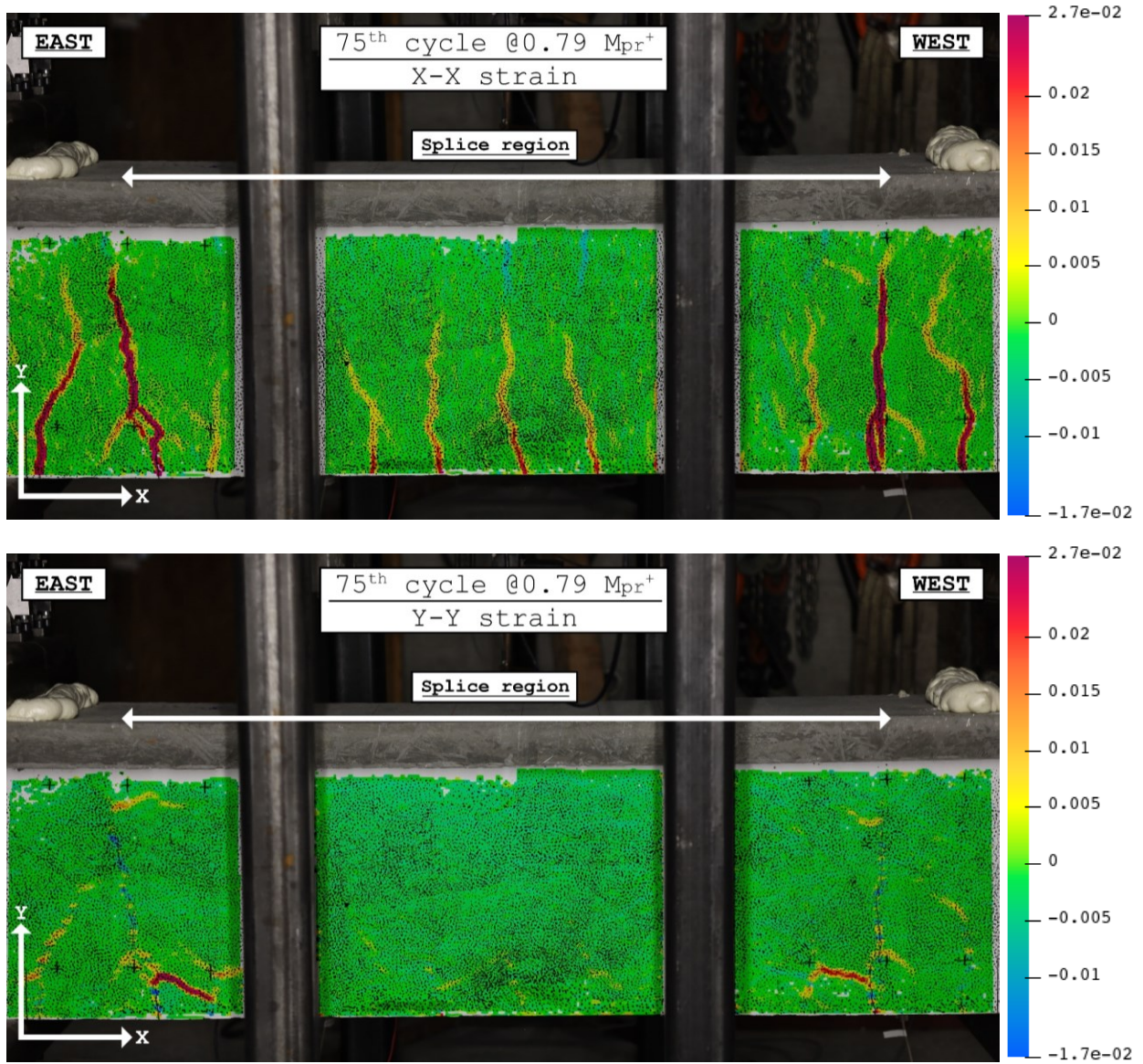


Figure E-23: (LB-S5-50) Stage 2-75th cycle @0.79M_{pr}⁺ DIC results

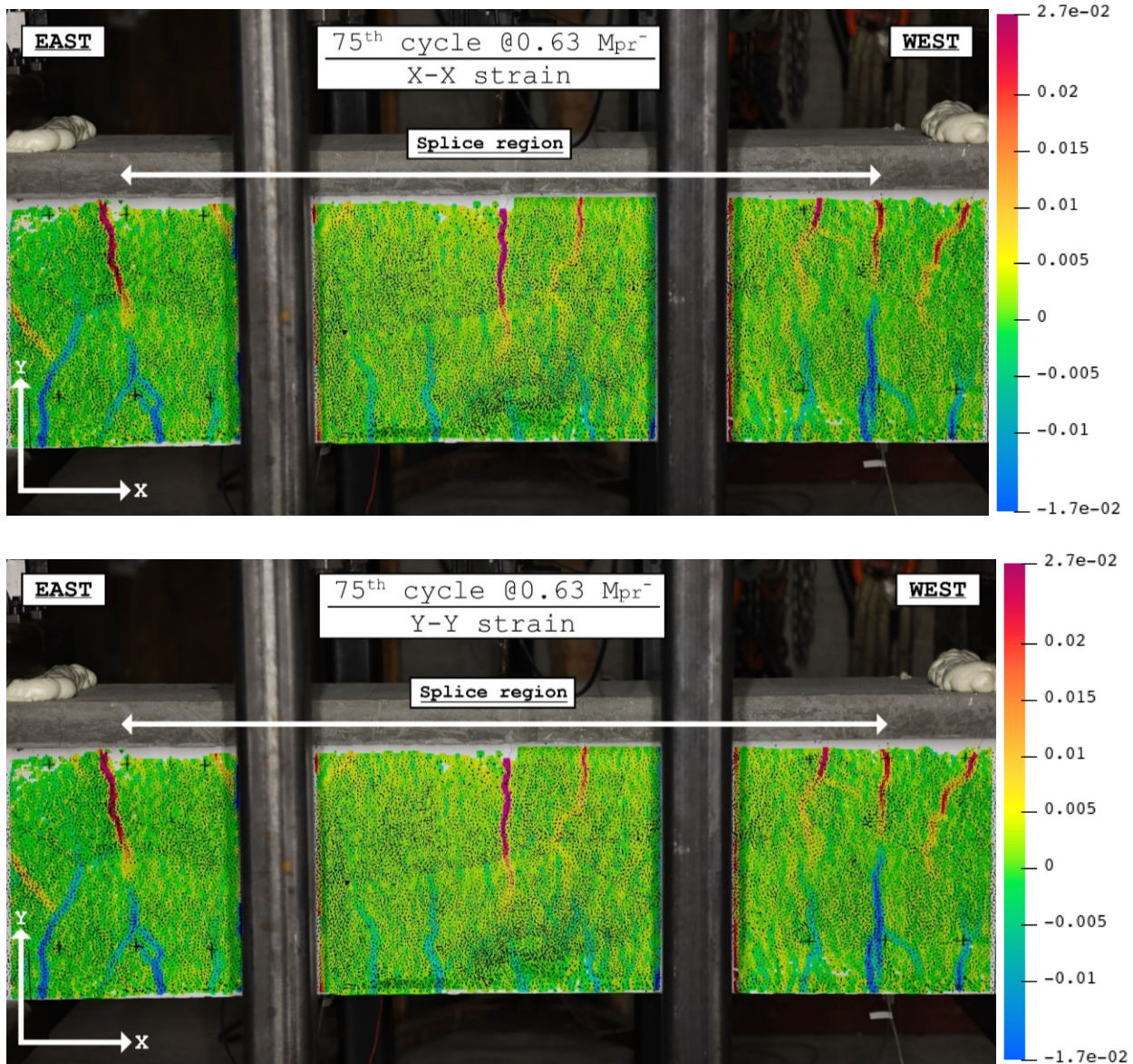


Figure E-24: (LB-S5-50) Stage 2-75th cycle @0.63M_{pr} DIC results

Stage 3: 10 Cycles @ $1.38\delta_y$ and @ $0.63M_{pr}$

10th Cycle

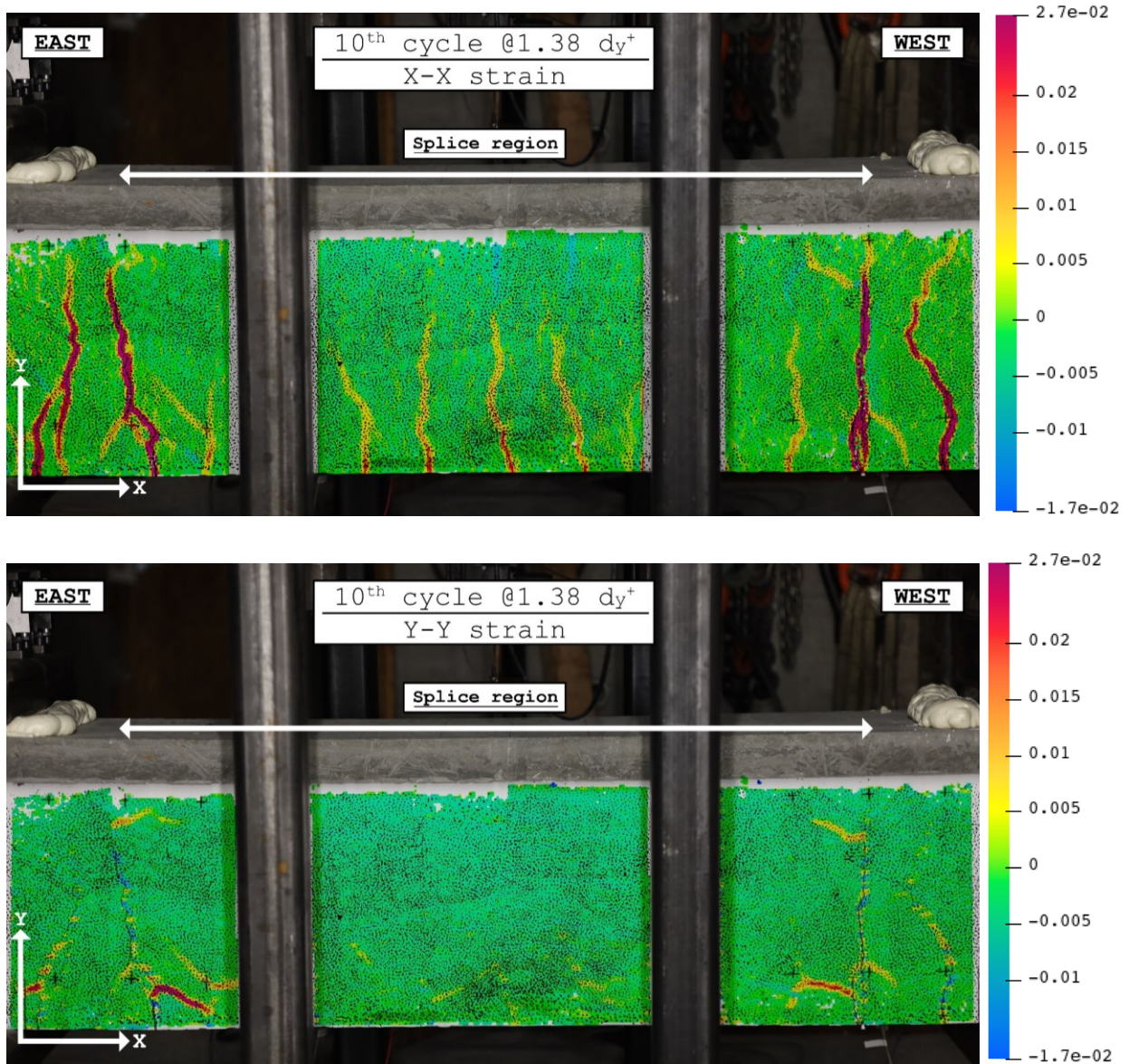


Figure E-25: (LB-S5-50) Stage 3-10th cycle @ $1.38\delta_y$ DIC results

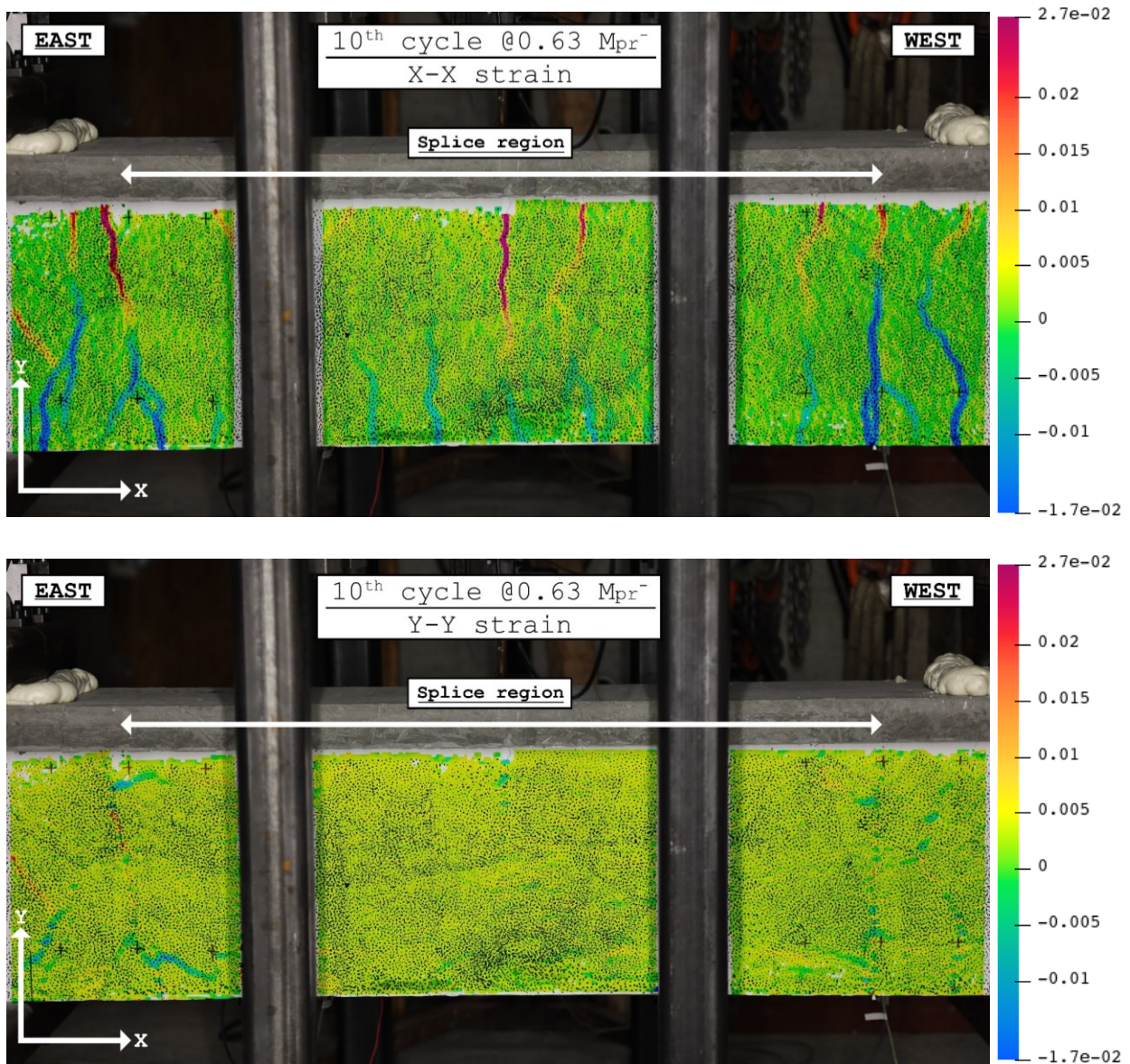


Figure E-26: (LB-S5-50) Stage 3-10th cycle @0.63M_{pr} DIC results

Stage 4: 6 Cycles @ $1.77\delta_y$ and @ $0.63M_{pr}$

6th Cycle

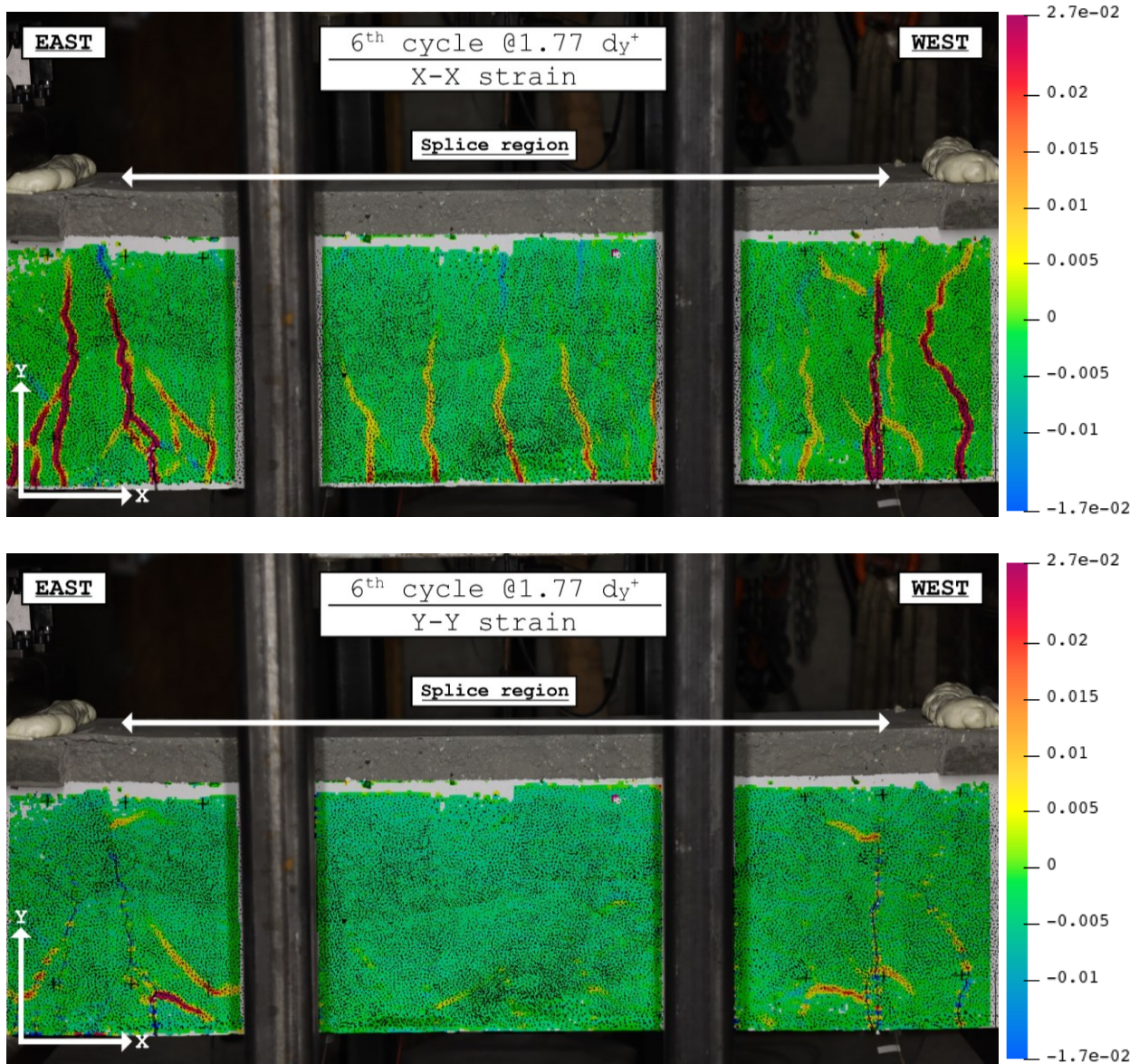


Figure E-27: (LB-S5-50) Stage 4-6th cycle @ $1.77\delta_y$ DIC results

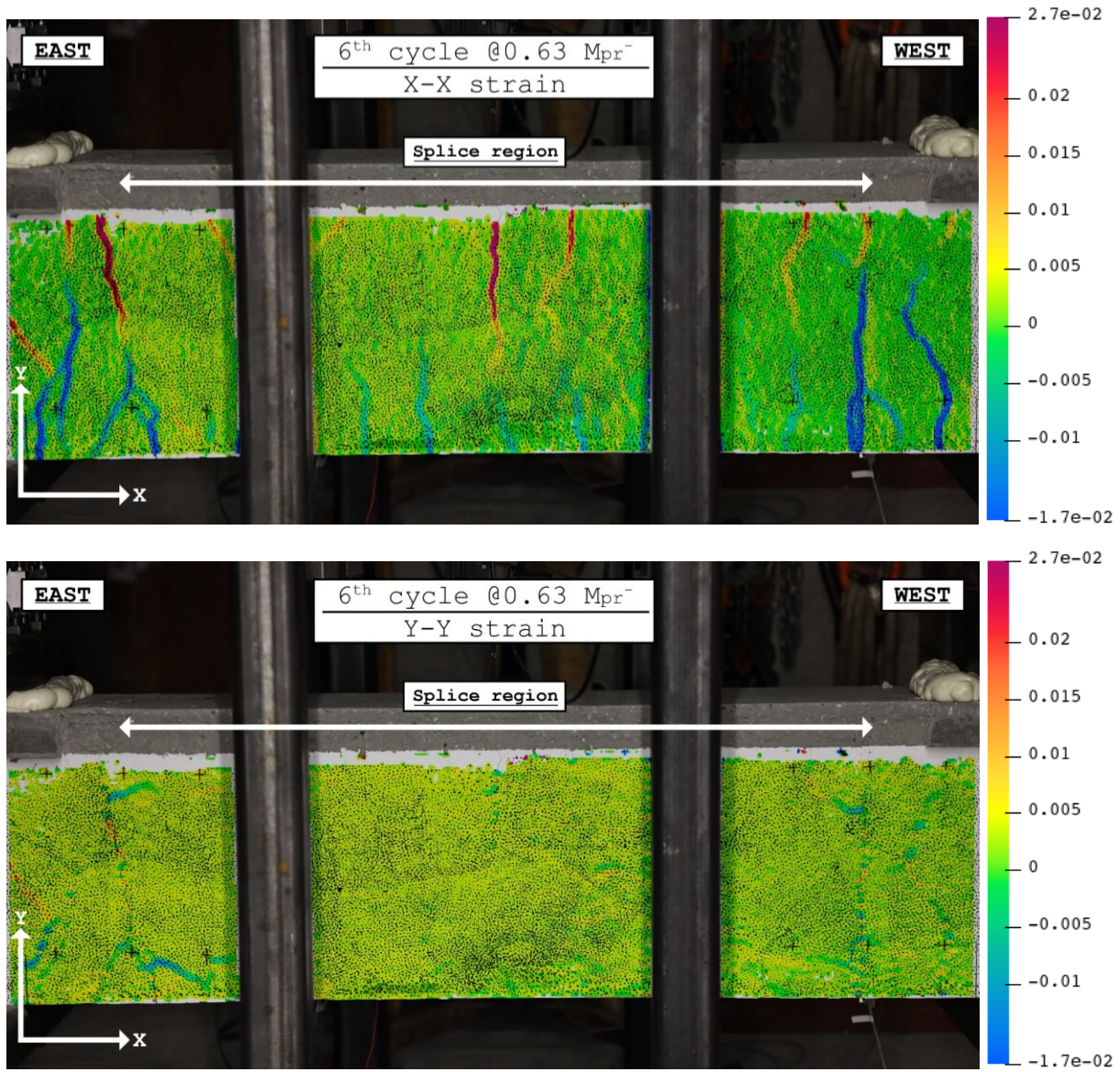


Figure E-28: (LB-S5-50) Stage 4-6th cycle @ 0.63M_{pr}⁻¹ DIC results

Stage 5: 4 Cycles @ $2.55\delta_y$ and @ $0.63M_{pr}$

4th Cycle

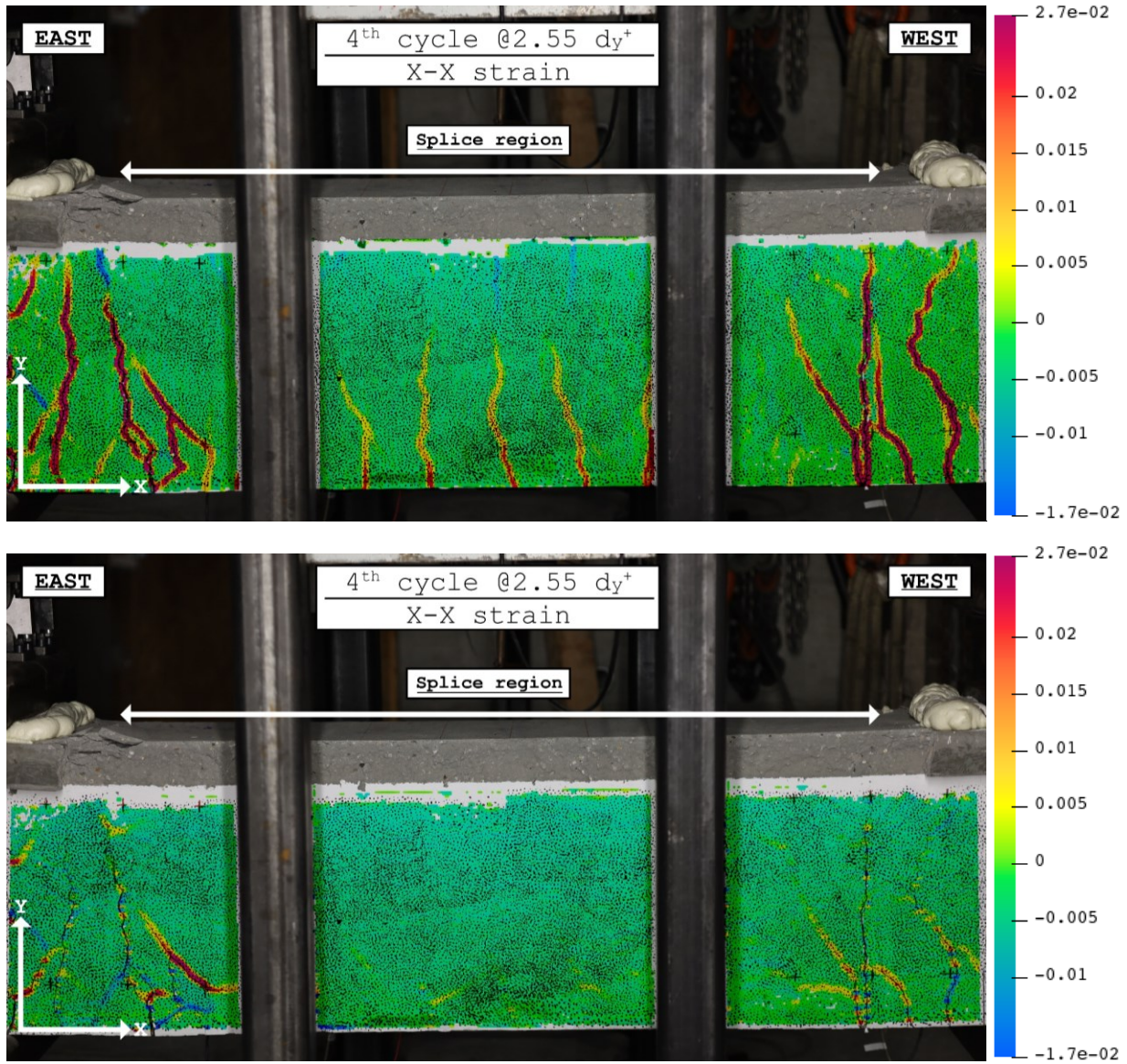


Figure E-29: (LB-S5-50) Stage 5-4th cycle @ $2.55\delta_y^+$ DIC results

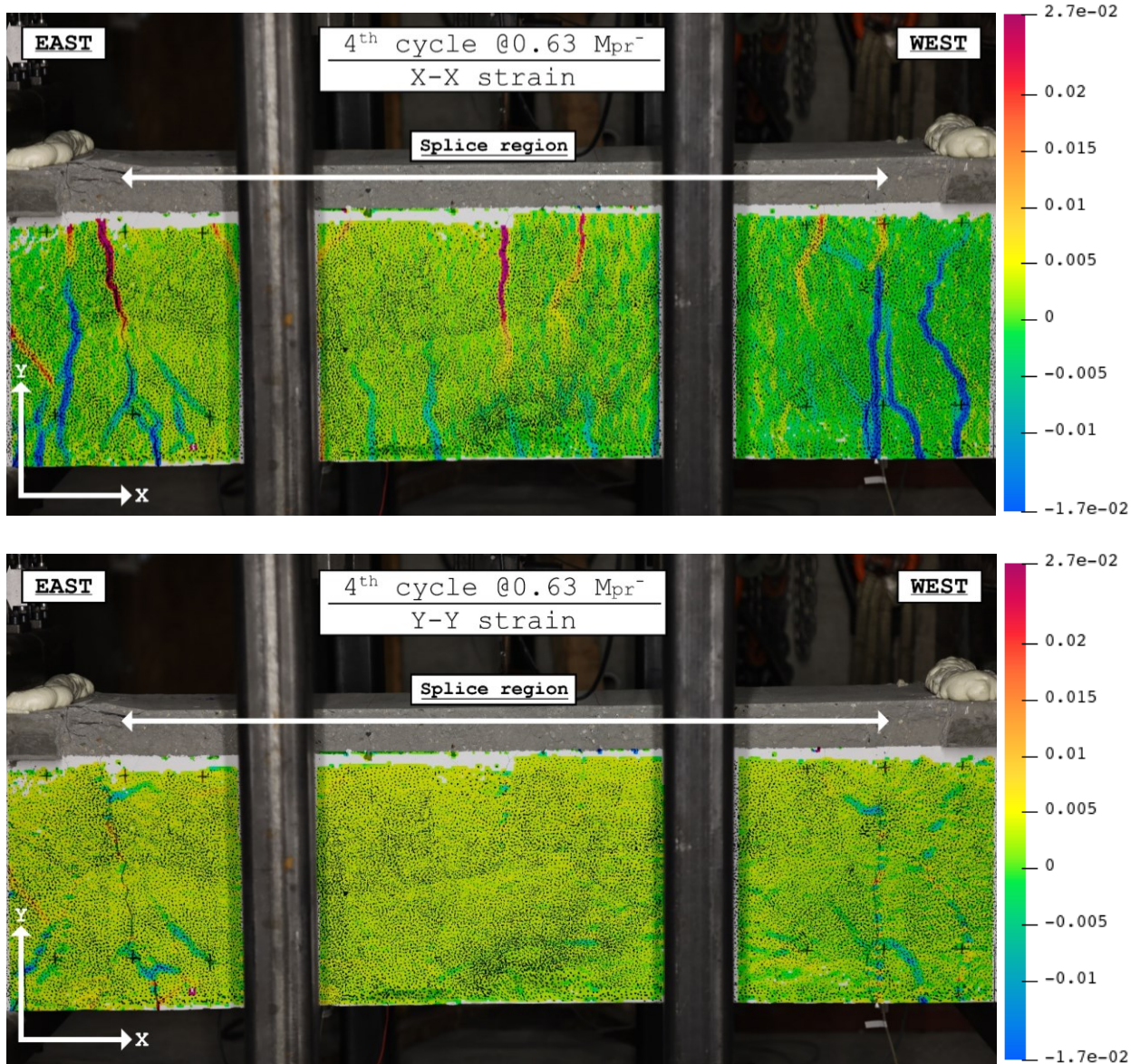


Figure E-30: (LB-S5-50) Stage 5-4th cycle @ 0.63 Mpr^{-1} DIC results

Stage 6: 4 Cycles @ $3.81\delta_y$ and @ $0.63M_{pr}$

4th Cycle

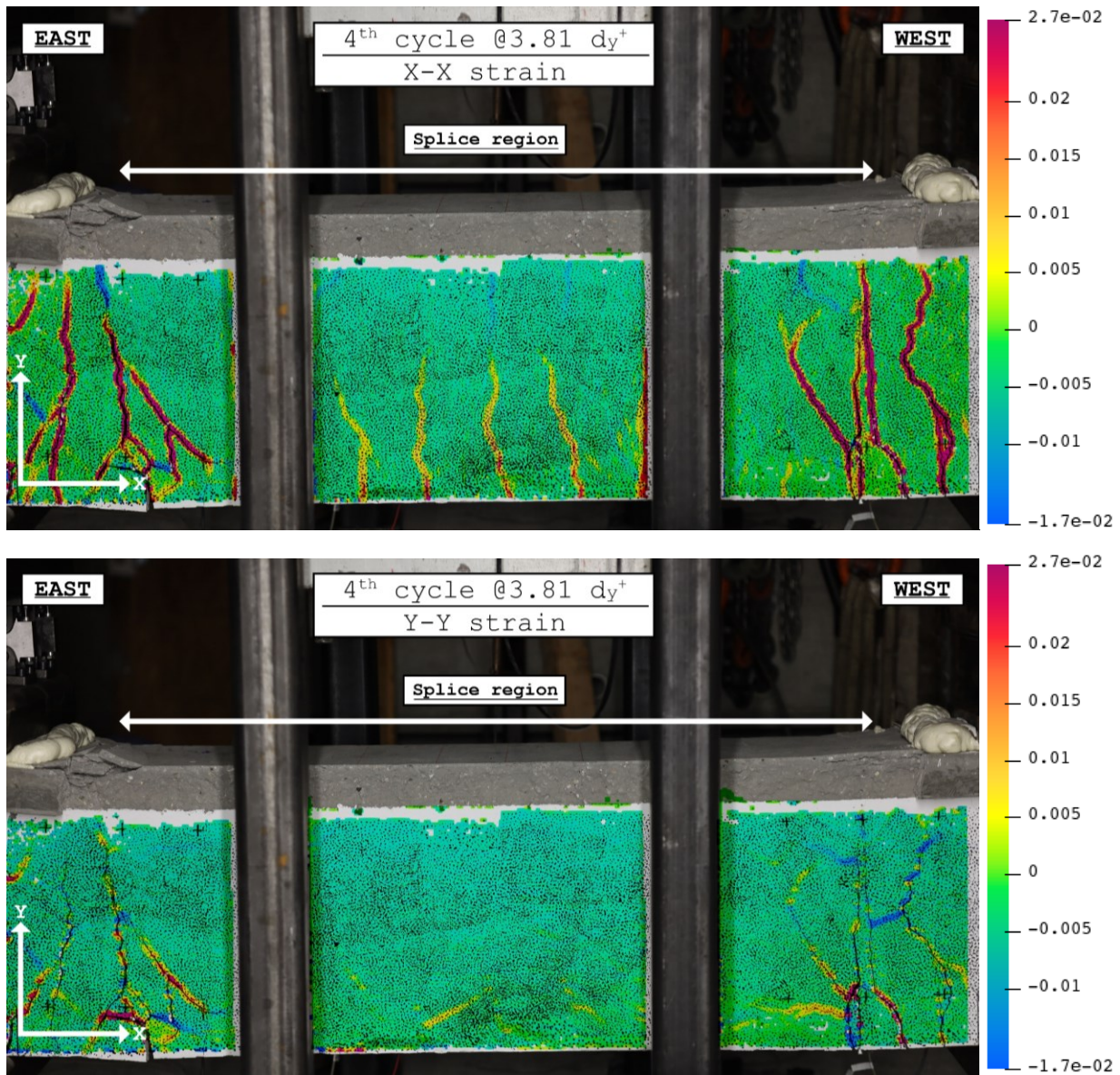


Figure E-31: (LB-S5-50) Stage 6-4th cycle @ $3.81\delta_y$ DIC results

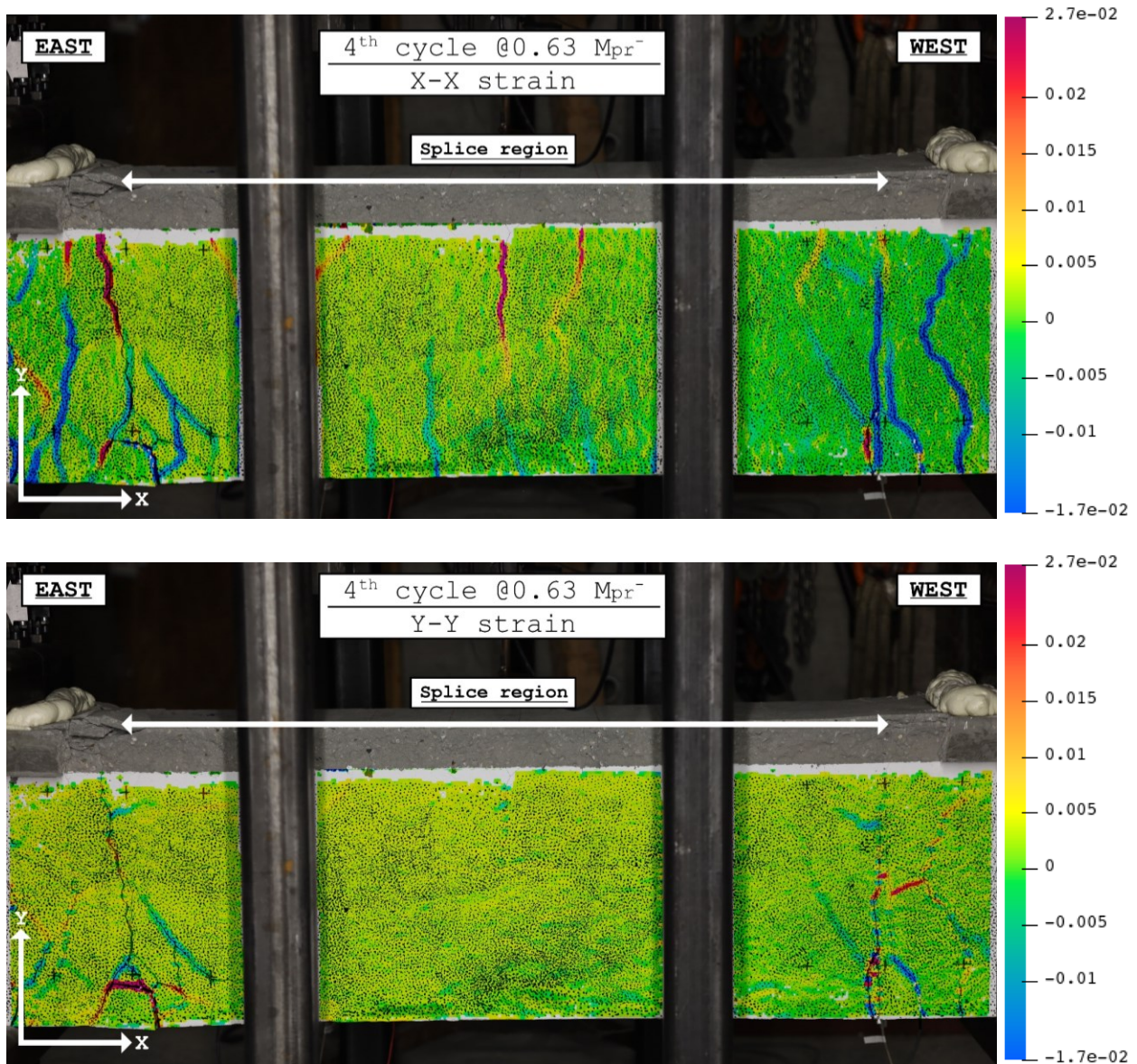


Figure E-32: (LB-S5-50) Stage 6-4th cycle @ $0.63M_{pr}$ DIC results

Stage 7: 2 Cycles @ $4.71\delta_y$ and @ $0.63M_{pr}$

2th Cycle

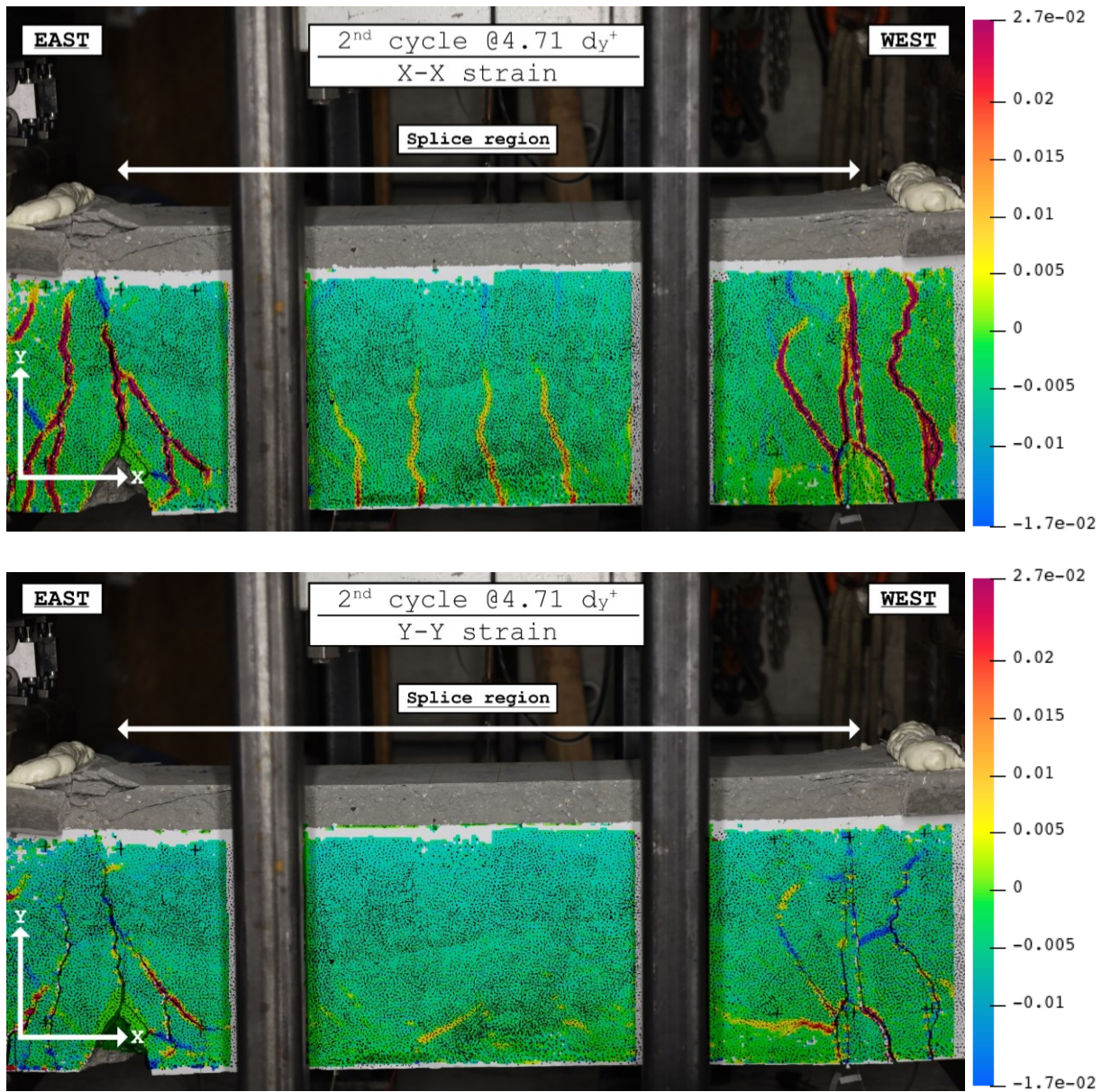


Figure E-33: (LB-S5-50) Stage 7-2nd cycle @ $4.71\delta_y^+$ DIC results

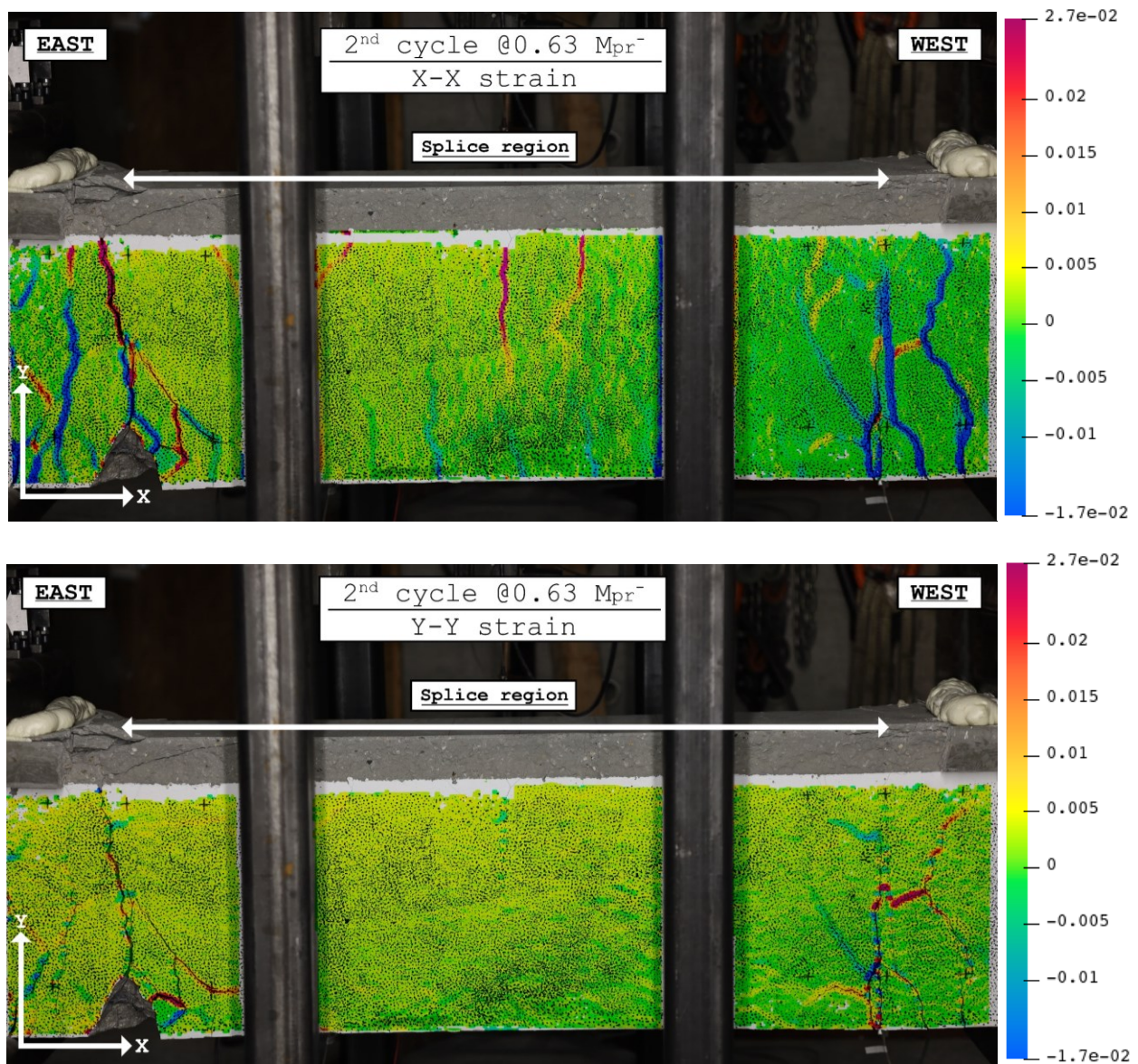


Figure E-34: (LB-S5-50) Stage 7-2nd cycle @0.63M_{pr} DIC results

References

- Aas-Jakobsen, K. (1970). *Fatigue of Concrete Beams and Columns*. Tapir.
<https://books.google.com/books?id=2McQNAAACAAJ>
- Abdullah, S. A., Wallace, J. W., Aswegan, K., & Klemencic, R. (2020). *Experimental Study of Concrete Coupling Beams Subjected to Wind and Seismic Loading Protocols* (2020/01). Department of Civil & Environmental Engineering at University of California, Los Angeles.
- ACI 215R. (1974). Considerations for Design of Concrete Structures Subjected to Fatigue Loading. *ACI Journal Proceedings*, 71(3). <https://doi.org/10.14359/11172>
- ACI 408.2R. (2012). *408.2R-12 Report on Bond of Steel Reinforcing Bars Under Cyclic Loads* (408.2R-12).
- Afseth, J. G. (1993). High cycle (fatigue) resistance of reinforced concrete beams with lap splices. *Canadian Journal of Civil Engineering*, 20(4), 642–649. <https://doi.org/10.1139/193-081>
- Alyousef, R. (2016). *The Fatigue Behaviour of Tension Lap Spliced Reinforced Concrete Beams Strengthened with Fibre Reinforced Polymer Wrapping*. University of Waterloo.
- American Society of Civil Engineers. (2019). *Prestandard for Performance-Based Wind Design*. American Society of Civil Engineers. <https://doi.org/10.1061/9780784482186>
- American Society of Civil Engineers. (2021). *Minimum Design Loads and Associated Criteria for Buildings and Other Structures* (7th ed.). American Society of Civil Engineers.
<https://doi.org/10.1061/9780784415788>
- Anaraki, K. K. (2023). *Influence of Coupling Beam Axial Restraint on Analysis and Design of Reinforced Concrete Coupled Walls*. University of California, Los Angeles.
- Eligehausen, R., Popov, E. P., & Bertero, Vite. V. (1983). *Local Bond Stress-Slip Relationships of Deformed Bars Under Generalized Excitations* (UCB/EERC-83/23).
- Hibbeler, R. C. (2017). *Mechanics of materials* (Tenth edition). Pearson.
- Khatri, D. (2016, December). Fatigue Analysis of Concrete Structures. *Structure Magazine*.

- LATBSDC. (2023). *An Alternative Procedure for Seismic Analysis and Design of Tall Buildings*. Los Angeles Tall Buildings Structural Design Council.
- Lukose, K., Gergely, P., & White, R. N. (1982). Behavior of Reinforced Concrete Lapped Splices for Inelastic Cyclic Loading. *ACI Journal Proceedings*, 79(5). <https://doi.org/10.14359/10912>
- MacGregor, J. G., Nuttall, N., & Jhamb, I. C. (1971). Fatigue Strength of Hot Rolled Deformed Reinforcing Bars. *ACI Journal Proceedings*, 68(3). <https://doi.org/10.14359/11303>
- MacKay, B., Schmidt, D., & Rezansoff, T. (1989). Effectiveness of concrete confinement on lap splice performance in concrete beams under reversed inelastic loading. *Canadian Journal of Civil Engineering*, 16(1), 36–44. <https://doi.org/10.1139/l89-005>
- Moss, D. S. (1980). *Aerial Fatigue of High-Yield Reinforcing Bars in Air* (TRRL SR622 Monograph). Article TRRL SR622 Monograph. <https://trid.trb.org/View/163798>
- Scott, D. (2023). *Advancement in Performance-Based Wind Design: Workshop Report* (NIST GCR 23-045-upd1; p. NIST GCR 23-045-upd1). National Institute of Standards and Technology. <https://doi.org/10.6028/NIST.GCR.23-045-upd1>
- Sivakumar, B. ; G., P. ; White, R. N. (2005). Suggestions for the Design of R/C Lapped Splices for Seismic Loading. *318Reference*, 21(16).
- Sparling, B., & Rezansoff, T. (1986). The effect of confinement on lap splices in reversed cyclic loading. *Canadian Journal of Civil Engineering*, 13(6), 681–692. <https://doi.org/10.1139/l86-103>
- Tepfers, R. (1973). *A Theory of Bond Applied to Overlapped Tensile Reinforcement Splices for Deformed Bars*. Chalmers University of Technology Division of Concrete Structure.
- Tocci, A. D. (1981). *The Behavior and Strength of Lapped Splices in Reinforced Concrete Beams Subjected to Cyclic Loading*. Cornell University. <https://books.google.com/books?id=WGZUAAAAYAAJ>
- Unal, M. E., Wallace, J. W., Abdullah, S. A., Kim, S., & Kolozvari, K. (2024). *Testing of Lap Splices in Reinforced Concrete Beams and Structural Walls under Wind Loading Protocols*. 18th World Conference on Earthquake Engineering, Milan, Italy.

Wascheidt, H. (1965). *On the Fatigue Strength of Embedded Concrete Reinforcing Steel (Zur Frage der Dauerschwingfestigkeit von Betonstählen im einbetonierten Zustand)*. Technical University of Aachen.

Zacaruk, J. A. (1990). *Performance of Large size Reinforced Concrete Beams containing a Lap Splice Subjected to Fatigue Loads*. University of Saskatchewan.